

## INFORMATION TO USERS

This reproduction was made from a copy of a document sent to us for microfilming. While the most advanced technology has been used to photograph and reproduce this document, the quality of the reproduction is heavily dependent upon the quality of the material submitted.

The following explanation of techniques is provided to help clarify markings or notations which may appear on this reproduction.

1. The sign or "target" for pages apparently lacking from the document photographed is "Missing Page(s)". If it was possible to obtain the missing page(s) or section, they are spliced into the film along with adjacent pages. This may have necessitated cutting through an image and duplicating adjacent pages to assure complete continuity.
2. When an image on the film is obliterated with a round black mark, it is an indication of either blurred copy because of movement during exposure, duplicate copy, or copyrighted materials that should not have been filmed. For blurred pages, a good image of the page can be found in the adjacent frame. If copyrighted materials were deleted, a target note will appear listing the pages in the adjacent frame.
3. When a map, drawing or chart, etc., is part of the material being photographed, a definite method of "sectioning" the material has been followed. It is customary to begin filming at the upper left hand corner of a large sheet and to continue from left to right in equal sections with small overlaps. If necessary, sectioning is continued again—beginning below the first row and continuing on until complete.
4. For illustrations that cannot be satisfactorily reproduced by xerographic means, photographic prints can be purchased at additional cost and inserted into your xerographic copy. These prints are available upon request from the Dissertations Customer Services Department.
5. Some pages in any document may have indistinct print. In all cases the best available copy has been filmed.

University  
Microfilms  
International  
300 N. Zeeb Road  
Ann Arbor, MI 48106

8321387

**King, James Michael**

**HYDROGEOLOGY AND NUMERICAL MODELING OF THE FLAMBEAU MINE  
SITE, RUSK COUNTY, WISCONSIN**

*Indiana University*

**PH.D. 1983**

**University  
Microfilms  
International**

300 N. Zeeb Road, Ann Arbor, MI 48106

**Copyright 1983**

**by**

**King, James Michael**

**All Rights Reserved**

HYDROGEOLOGY AND NUMERICAL MODELING  
of the  
FLAMBEAU MINE SITE, RUSK COUNTY, WISCONSIN

By  
James M. King

Submitted to the Graduate School  
in partial fulfillment of the requirements for the degree  
Doctor of Philosophy  
in the Department of Geology,  
Indiana University

July 1983

This thesis is accepted by the Faculty of the Graduate School in partial fulfillment of the requirements for the degree of Doctor of Philosophy in the Department of Geology, Indiana University.

*Noel C. Krothe*

---

Noel C. Krothe, Chairman

*Daniel P. Maki*

---

Daniel P. Maki, Mathematics

*Haydn H. Murray*

---

Haydn H. Murray

*David G. Towell*

---

David G. Towell

*Bryson D. Trexler, Jr.*

---

Bryson D. Trexler, Jr.



Hydrogeology and Numerical Modeling  
of the Flambeau Mine Site,  
Rusk County, Wisconsin

By James M. King

©1983

James M. King

ALL RIGHTS RESERVED

## TABLE OF CONTENTS

List of Figures	vi
List of Tables	x
Acknowledgements	xii
Abstract	xiii
CHAPTER I: INTRODUCTION	1
Historical Development of the Study	1
Purpose and Scope of the Study	4
Previous Investigations	6
- Geologic Studies	6
- Hydrogeologic Studies	7
- Numerical Modeling	8
Description of Study Area	9
- Location	9
- Physiography	11
- Climate	16
- Land Use	20
- Proposed Mining Operation	22
CHAPTER II: BEDROCK GEOLOGY	27
Introduction	27
Precambrian Rocks	27
The Ore Deposit	33
Precambrian Surface	35
Paleozoic Deposits	36
CHAPTER III: SURFICIAL GEOLOGY	38
Introduction	38
Mine Site	38
Waste-Containment Area	45
CHAPTER IV: SURFACE-WATER HYDROLOGY	55
Introduction	55
Pit-Area Hydrology	61
Waste-Containment Area Hydrology	66
Wetlands	68
CHAPTER V: HYDROLOGIC BUDGET	75
Introduction	75

Major Budget Components and their Measurement	77
- Precipitation	77
- Evapotranspiration	78
- Runoff	81
Ground-Water Recharge	83
Validation of Budget Values	99
CHAPTER VI: HYDROGEOLOGY	104
Occurrence of Ground Water	104
Availability of Ground Water	106
Aquifer Characteristics	108
- Modified Packer and other Field Methods	114
- Laboratory Determination of K	118
- Pumping Tests	122
- Estimation of Hydraulic Parameters from Drilling Logs	127
Hydrostratigraphic Units	128
Ground-Water Movement	130
- Mine Area	131
- Waste-Containment Area	136
CHAPTER VII: SIMULATION OF GROUND-WATER SYSTEMS	140
Introduction	140
Types of Ground-Water Flow Models	141
Model Selection	146
Finite-Difference Mathematics and Numerical Considerations	148
- Finite-Difference Analogs	148
- Matrix Solution Methods	160
- Sources of Error in Numerical Modeling	165
Description of Two-Dimensional Model	168
- General Model Features	168
- Theoretical Development	169
- Boundary and Initial Conditions	175
- Model Input/Output	177
CHAPTER VIII: SIMULATION OF THE PROPOSED OPEN-PIT MINE	179
Model Development Objectives	179
Modifications to the Two-Dimensional Model	180

- Modifications to Print Flow Rates at Constant-Head Nodes	180
- Modifications to Print Evapotran- spiration Rates	181
- Miscellaneous Modifications	181
Steady-State Simulation of the Existing System	181
- General Discussion	181
- Steady-State Input Data	184
- Boundary Conditions	189
- Model Calibration	191
Steady-State Stress Simulations	200
- General Discussion	200
- Large Open Pit - Interior Drainage System	200
- Large Open Pit - Perimeter Slurry Wall	215
- Direct-Ship Pit - Interior Drainage System	221
- Direct-Ship Pit - Dewatering with Wells	226
- Direct-Ship Pit - Perimeter Slurry Wall	235
CHAPTER IX: SIMULATION OF THE PROPOSED WASTE-CONTAINMENT AREA	242
Model Development Objectives	242
Steady-State Simulation of the Existing System	243
- General Discussion	243
- Steady-State Input Data	243
- Boundary Conditions	248
- Model Calibration	249
Steady-State Stress Simulations	256
- General Discussion	256
- Containment Structure - Undisturbed Soil Bottom	260
- Containment Structure - Saproli- te Bottom Seal	274
CHAPTER X: CONCLUDING REMARKS	285
Summary of Study and Findings	285
Realization of Study Objectives	289
- Testing of Remedial Methods	290
- Recommendations for Additional Data	291
Comments on Transient Simulations	293
REFERENCES CITED	295

APPENDIX I:	Unified Soil Classification and Descriptions of Common Soil Types near the Flambeau Mine Site	304
APPENDIX II:	General Hydrologic Budget and Estimates of Natural Ground-water Recharge	308
APPENDIX III:	Estimates of Transmissivity and Hydraulic Conductivity from Soil-Boring Logs	314

## LIST OF FIGURES

Figure

1	Locations of the proposed mine pit and waste-containment structure at the Flambeau mine site near Ladysmith, Wisconsin.....	10
2	Areal distribution of prominent surface features in the vicinity of the Flambeau mine site.....	14
3	TOP: Plan view of the proposed Flambeau mine pit showing the extent of the excavation after 3, 4, and 12 years. BOTTOM: Cross section of the pit showing estimated depths for the same time periods.....	23
4	Plan view of the proposed waste-containment structure 1.2 mi south of the mine area.....	25
5	Map of Precambrian lithologies in the vicinity of the Flambeau deposit.....	29
6	Locations of known massive sulfide ore bodies in the Middle Precambrian of northern Wisconsin and their relation to the metavolcanic belt.....	30
7	Lithologic map of the immediate mine area.....	34
8	Areal distribution of granular outwash material and fine-grained glacial till in the vicinity of the proposed Flambeau mine pit.....	40
9	The areal distribution of surficial soils at the mine site and waste-containment area.....	46
10	East-west cross section through the waste-containment area.....	47
11	North-south (B) and northwest-southeast (C) cross sections through the waste-containment area.....	48
12	Sand zones near the surface of the disposal structure site as defined by shallow soil borings.....	50

13	Extents and thicknesses of the intermediate and lower outwash zones at the disposal structure site.....	51
14	The Chippewa River drainage basin and its relation to the Flambeau River, Rusk County, and the project area.....	56
15	Comparison of average monthly precipitation and discharge of the Flambeau River.....	58
16	Local drainage basins in the vicinity of the proposed mine pit.....	63
17	Surface-drainage features within the southern study area.....	67
18	Basic hydrologic characteristics of wetlands....	72
19	Distribution of features affecting ground-water recharge near the open-pit location.....	90
20	Distribution of features affecting ground-water recharge in the waste-containment area....	91
21	Comparison of average monthly fluctuations in ground-water levels and estimated recharge in the pit area.....	94
22	Comparison of average monthly fluctuations in ground-water levels and estimated recharge in the waste-containment area.....	95
23	Network of water-level observation stations at the mine site.....	109
24	Network of water-level observation stations in the waste-containment area.....	110
25	Average configuration of the water table in the area of the mine pit based on water levels from 1970-80, topography, and wetlands.....	132
26	Average configuration of the water table in the waste-containment area based on shallow wells, piezometers, topography, and wetlands....	137
27	Geometrical interpretation of forward, backward, and central finite-difference analogs.....	152
28	Finite-difference computational cell for a regular grid showing the common 5-point star used in deriving derivative analogs.....	155

29	Finite-difference grid of the mine site showing the distribution of hydrologic boundaries used in the simulations.....	185
30	Steady-state head distribution in the mine area generated by the model after calibration.....	195
31	Areal distribution of hydraulic conductivity resulting from the calibration of the mine-pit model.....	197
32	Schematic representation of the method used to approximate the seepage face and its effects on surrounding flow gradients.....	204
33	Simulated steady-state distribution of hydraulic head due to the 3-year mine pit with internal drainage facilities.....	207
34	Simulated steady-state distribution of hydraulic head due to the 4-year mine pit with internal drainage facilities.....	210
35	Simulated steady-state distribution of hydraulic head due to the final mine pit with internal drainage facilities.....	213
36	Simulated steady-state distribution of hydraulic head due to a low-conductivity slurry wall around the large open pit.....	217
37	Changes in hydraulic head caused by encircling the large pit with a slurry wall.....	218
38	Simulated steady-state head distribution due to an internally drained direct-ship pit.....	224
39	Changes in hydraulic head due to an internally drained direct-ship pit.....	225
40	Simulated steady-state head distribution due to partially dewatering the area of the direct-ship pit with 10 wells discharging at a combined rate of 16.9 gpm.....	230
41	Average saturated thickness of water-bearing materials at steady-state due to dewatering in the area of the direct-ship pit.....	232
42	Simulated steady-state head distribution due to a low-conductivity slurry wall around the direct-ship mine pit.....	237



43	Changes in hydraulic head caused by encircling the direct-ship pit with a slurry wall...	238
44	Finite-difference grid of the waste-containment area showing the distribution of hydrologic boundaries used in the simulations.....	245
45	Steady-state head distribution in the waste-containment area generated by the model after calibration.....	253
46	Simulated steady-state head distribution in the waste-containment area for a natural-soil bottom and 25 ft of saturated waste.....	266
47	Simulated steady-state head distribution in the waste-containment area for a natural-soil bottom and 50 ft of saturated waste.....	271
48	Simulated steady-state head distribution in the waste-containment area for a lined impoundment with 25 ft of saturated waste.....	282

## LIST OF TABLES

Table

1	Mean monthly precipitation and temperatures at the Flambeau project area near Ladysmith.....	19
2	Currently designated land uses within the Flambeau project area.....	21
3	Discharge data for small steams draining the area of the proposed open pit.....	65
4	Discharge data for streams draining the area of the proposed waste-disposal structure.....	65
5	Annual rates of evapotranspiration, runoff, and recharge for each of the four area categories identified in the Flambeau project area.....	92
6	Recharge data for the mine and waste-containment areas based on the water-budget rates in Table 5...	102
7	Summary of field hydraulic conductivities by general material type for the open-pit and waste-containment areas.....	117
8	Summary of laboratory hydraulic conductivities of samples from the waste-containment area.....	121
9	Summary of hydraulic properties determined from low-discharge pumping tests conducted near the open-pit location in 1971 and 1972.....	124
10	Steady-state ground-water budget for the natural pit area determined from mass-balance computations by the model.....	199
11	Steady-state ground-water budget for the pit area resulting from the final pit with an internal seepage-collection system.....	214
12	Steady-state ground-water budget for the pit area resulting from the installation of a low-conductivity slurry wall around the mine pit.....	220
13	Steady-state ground-water budget of the mine area for the direct-ship pit with an internal seepage-collection system.....	227

14	Discharges, drawdowns, and steady-state heads at individual dewatering wells near the direct-ship pit.....	231
15	Steady-state ground-water budget of the mine area for the direct-ship pit with dewatering wells..	234
16	Steady-state ground-water budget of the mine area for the direct-ship pit enclosed by a slurry wall.....	240
17	Steady-state ground-water budget for the unstressed waste-containment area determined from mass-balance computations in the model.....	255
18	Steady-state ground-water budget for the waste-containment area with a natural-soil bottom and 25 ft of saturated waste within the disposal structure.....	269
19	Steady-state ground-water budget for the waste-containment area with a natural-soil bottom and 50 ft of saturated waste within the disposal structure.....	273
20	Estimated initial seepage rates for various combinations of liner and waste thicknesses computed with Equation 51 for saturated conditions.....	279

## ACKNOWLEDGEMENTS

First and foremost, I extend my gratitude to Kennecott Minerals Company of Salt Lake City for their generous financial support which made this study possible. Special recognition is merited by Bryson D. Trexler, Jr., for his assistance and avid personal interest in my work.

Special thanks are in order for Noel C. Krothe for his guidance and the gracious (and nearly continuous) use of his office for much of the computer work. I also wish to thank Dr. Krothe, Haydn Murray, David Towell, Daniel Maki, and Bryson Trexler for their critical review of the paper and their helpful editorial comments.

I must also acknowledge the efforts of Gerald Bradshaw, formerly of the Flambeau Mining Corporation at Ladysmith, for drafting many of the large plates, and of Charles Faust and Bill Miller of GeoTrans, Inc., for their advice during the early stages of this project.

Finally, I express my deepest gratitude to my wife, Jo, for her moral and logistical support during these past three years.

HYDROGEOLOGY AND NUMERICAL MODELING  
of the  
FLAMBEAU MINE SITE, RUSK COUNTY, WISCONSIN

By James M. King

Abstract. In 1970 Kennecott Minerals Company announced the discovery of the Flambeau deposit, a 4- to 6-million ton massive copper/zinc sulfide body southwest of Ladysmith in northwest Wisconsin. The company proposes to mine the deposit through both surface and underground mining.

Ground water in the project area occurs primarily within the Pleistocene till and outwash deposits and a thin Upper Cambrian sandstone that overlie the Precambrian basement. The hydrologic study was thus limited to these sediments. Following a detailed study of the local ground-water systems, two-dimensional numerical flow models of the mine site and an associated diked tailings-disposal structure were constructed to assist in mine management and hydrologic-impact evaluation. Both sites were modeled as unconfined aquifers with the Flambeau River as the major ground-water sink. Data limitations restricted all subsequent simulative work to the steady-state case.

Simulations of the mine site were carried out for the large open pit originally proposed and for a smaller direct-

ship pit. Both pit geometries were simulated for cases representing 1) an interior seepage-collection system and 2) enclosing the pits by a low-conductivity slurry wall. The outcomes of simulations for each pit type were generally the same for both water-control options except results for the large pit were of greater magnitude and extent. Simulations with an interior collection system indicated the diversion of flow from the Flambeau River to the pits and the creation of cones of depression around them. The expansion of the cones was effectively halted by fine-grained glacial deposits to the east. Predicted steady-state rates of seepage into the pits ranged from 25 to 45 gpm. Simulations of the encircling slurry wall indicated it could cause minor ground-water mounding on its up-gradient (east) side and head losses west and northwest of the mine. These effects result from the obstruction of subsurface flow and the loss of recharge through the area occupied by the excavation. Large simulated head changes were confined to within several hundred feet of the slurry wall. The use of dewatering wells to control seepage into the direct-ship pit was also simulated. The optimal dewatering scheme consisted of 10 wells with a combined discharge of less than 17 gpm. The low pumping rate suggests that dewatering methods more suited for low-transmissivity soils would be more effective.

Simulations of the waste-disposal impoundment were less satisfactory due to data and model limitations which precluded the consideration of unsaturated flow in soils above the water table. In the three simulations attempted, water losses from

the structure were represented in the model by increases in areal recharge. The first two cases assumed that tailings and waste rock would be placed directly on the natural land surface inside the perimeter dike. The predicted maximum rates of water loss from the structure at steady state were 72 gpm for a saturated waste thickness of 25 ft and 140 gpm for a 50-ft thickness. Both simulations indicated slight ground-water mounding around the structure, especially to the north. The results also suggested that surface seepage could occur at the outer base of the perimeter dike along all sides of the structure. The final case called for lining the impoundment with compacted saprolite to reduce seepage. This simulation was unsatisfactory because of the prominent role that unsaturated flow would play under these circumstances. A simulation was attempted by assuming a 25-ft saturated waste thickness, a 5-ft liner, and that unsaturated conditions would prevail beneath the western part of the structure where the water table is deeper. The steady-state rate of water loss predicted by the model for these conditions was 36 gpm with mounding most evident on the north side of the structure.

## CHAPTER I

### INTRODUCTION

#### Historical Development of the Study

Kennecott Copper Corporation began prospecting for non-ferrous massive sulfides (greater than 50 percent sulfides by weight) in central Wisconsin as early as 1950, prompted by the discovery of native copper and chalcocite ores on the Upper Peninsula of Michigan. Subsequent exploration westward along strike into Wisconsin, however, was unsuccessful and further exploration in the state lagged until 1966 when an early account of copper staining on samples from a dug well (Hotchkiss and others, 1915) renewed Kennecott's interest in northwestern Wisconsin. Early exploration in this area consisted chiefly of conventional field and aeromagnetic surveys and some drilling. Though these techniques proved unsuccessful in locating base-metal deposits, the prevalence of iron sulfides in the exploration area was sufficiently encouraging to justify the use of improved airborne geophysical methods in 1967 which focused attention on a belt of high-conductivity anomalies southwest of the City of Ladysmith in Rusk County. Follow-up ground surveys delineated a highly conductive area within this belt about 0.6 mi (1.0 km) southwest of the city along the east bank of the Flambeau River. Test drilling in this zone in November 1968 confirmed the presence of massive



copper sulfides (Schwenk, 1977), marking the first important copper discovery in Wisconsin.

Public announcement of the Flambeau discovery late in 1970 led to heightened exploration in the region by numerous other companies. These intense search programs yielded four additional massive sulfide deposits aligned in an east-west direction from the Ladysmith area 110 mi (177 km) eastward across north-central Wisconsin. First, Kennecott located the Thornapple and Schoolhouse deposits, relatively small copper and zinc bodies northwest and southwest of the Flambeau find, respectively. Neither deposit has yet been drilled for ore evaluation. In 1974, the Noranda Exploration Company announced its discovery of the 2.2-million ton Pelican River zinc/copper deposit about 100 mi (160 km) east of Ladysmith near Rhineland. In 1976, Exxon announced the finding of a 70-million ton zinc/copper body about 25 mi (40 km) east-southeast of Rhineland at Crandon. The Crandon deposit is believed to be among the 10 largest massive sulfide bodies in the United States (Paydirt, 1979).

From the announcement of the initial discovery until the mid 1970's, much of Kennecott's technical effort at the Flambeau site was aimed at developmental planning and environmental monitoring. The site monitoring was conducted largely through the company's local subsidiary in Ladysmith, the Flambeau Mining Corporation (abbreviated "FMC" throughout this paper). Physical data from the monitoring and numerous site investigations formed the basis for the company's application to the

Wisconsin Department of Natural Resources in 1976 for approval to begin mining. Local approval required for permitting was withheld, however, because of strong opposition by environmental groups which felt that existing state mining regulations were inadequate for insuring environmentally acceptable operation of the mine. From this opposition to the proposed mine and from the rapid statewide expansion of mine-related activities accompanying the Flambeau discovery, there evolved a movement to develop more comprehensive state mining regulations. Development of the Flambeau site was thus forestalled throughout the mid 1970's to early 1980's pending the drafting of a new mining code. Kennecott continued its hydrologic and environmental surveillance while awaiting and participating in the development of the regulations. Though the code was issued in May of 1982, current downward trends in the copper market may postpone indefinitely any attempt to develop the site, though monitoring of hydrologic conditions in the area continues.

An issue central to the local opposition to the Flambeau mine is its potential to produce effects detrimental to local water resources. A large part of the concern focused on possible ground-water problems, since the City of Ladysmith and rural residents in the vicinity rely on ground-water supplies. While it is expected that construction of a mine and its attendant facilities will have some hydrologic consequences, it has been difficult to determine the magnitude and extent of potential effects using conventional techniques due to the

complexities and uncertainties of the subsurface environment. In response to this situation, Kennecott Minerals Company in late 1979 authorized the development of digital flow models to characterize the ground-water systems at the proposed mine site and at an associated mine-waste disposal area, the two locations where hydrologic impacts are of most concern. The chief motivations for using computer models are their flexibility to simulate a diverse array of hydrologic conditions and mining effects, and the ease with which they can be modified to account for new information and changing site conditions.

#### Purpose and Scope of the Study

The primary purpose of this study was to refine existing geologic and hydrogeologic information for the Flambeau site and use it to devise ground-water flow models capable of predicting the response of local flow systems to stresses imposed by the mining operation. Depending on the type of operation finally established, responses could include a decline in ground-water levels from dewatering or other types of large-scale withdrawals, and increased or decreased heads in some locales due to the alteration of natural recharge/discharge patterns and the obstruction of ground-water flow. The intent of the study was in part to determine if such impacts will accompany the mining operation and, if so, to ascertain their extent and magnitude so that appropriate design changes and

monitoring procedures for detecting, reducing and(or) eliminating adverse effects can be implemented if needed. If necessary, the models will also allow the effectiveness of various schemes for controlling these effects to be tested.

A third important purpose of the study is really a by-product of the modeling process. Modeling of a flow system provides a framework for organizing information and often improves insight into a system's behavior by allowing the simultaneous interaction of many properties and processes to be examined in such a way that the relative importance of each may be determined. The organization of data and knowledge of the variables to which a system is most responsive assist in site studies by pointing out where and what types of hydrogeologic data necessary for accurate site characterization are deficient.

The Flambeau study encompasses only the physical flow system in the vicinities of the mine and tailings-disposal areas. An assessment of impacts on surface- and ground-water quality is not included, though the results of the physical modeling may be used conjunctively with a large body of existing water-quality data to mount future water-chemistry investigations. Hydrogeologic aspects of the project area examined in the course of this study were the occurrence and movement of ground water within the mantle of glacial and Cambrian sediments overlying the Precambrian rocks at the sites, recharge and discharge characteristics, the areal distributions of hydraulic parameters of the flow systems, a general hydro-

logic budget, and the relationship between surface and ground water.

## Previous Investigations

### Geologic Studies

The geology of north-central Wisconsin has been given special attention in the literature since its economic potential was made known by the discovery of nonferrous massive sulfides. Hotchkiss and others (1915) first alluded to this potential early in this century. The most recent comprehensive geologic mapping in Wisconsin was conducted by Dutton and Bradley (1970) who describe lithologies, geophysical properties, and mineral commodities of earth materials in the state. This work was followed by Dutton (1971) who cited parts of central and northern Wisconsin as favorable locales for massive sulfide occurrences because of this area's similarity to sulfide-bearing Archean greenstone belts of Canada north of Lake Superior. Other papers describing Precambrian stratigraphy and massive sulfide occurrences in Wisconsin are Myers (1974), Sims (1976), Stacey and others (1976), LaBerge and Mudrey (1979), and Mudrey (1979).

The most detailed geologic studies focusing on the Flambeau site proper are largely in the form of unpublished consultant and internal staff reports resulting from on-site investigations. These include Soil Testing Services of Wisconsin (1972a, 1972b, 1973, 1975, 1976a, 1976b, 1976c), May

(1971, 1973a, 1973b), and Cahow (1973), most of which deal with the surficial deposits at the mine site and disposal area. Publicly available summaries of most of this data are Wisconsin Department of Natural Resources, Bureau of Environmental Impact (1975) and FMC (1976), which are the preliminary environmental report and mining permit application, respectively. These two documents contain essentially the same information. The most notable publications on the Flambeau deposit are by Schwenk (1977), in which the geophysical methods employed in discovering the ore deposit are outlined, and May (1977), who describes in detail the structure and mineralogy of the deposit.

#### Hydrogeologic Studies

No scientific papers on the hydrology and hydrogeology of the Flambeau project area currently exist. The site vicinity has been included in less-detailed, larger-scale investigations and reports dealing with the hydrology of all or parts of the encompassing Chippewa River basin (Young and Hindall, 1972), the ground-water resources of the upper Mississippi-valley region (Bloyd, 1975), potential yields from outwash and sandstone aquifers in Wisconsin (Borman, 1971a; 1971b), and the surface-water resources of Rusk County (Sather and others, 1971). A great deal of site-specific hydrologic and hydrogeologic data from consultant and staff reports (e.g., Harshbarger, 1971; and Passavant, 1971) is available in Wisconsin Department of Natural Resources (1975) and FMC (1976).

### Numerical Modeling

Stallman (1956) was the earliest user of numerical methods to analyze hydrologic information. This classic paper describes a finite-difference technique for analyzing regional water levels to define aquifer properties. Some of the first published uses of numerical computer models to solve hydrologic problems are Remson and others (1965) and Pinder and Bredehoeft (1968). These workers used finite-difference analogs and Gauss-Seidel iteration and the alternating-direction implicit (ADI) solution scheme, respectively, to simulate groundwater flow in two dimensions. Later, Bredehoeft and Pinder (1970) devised a quasi-three-dimensional numerical model to simulate flow in multiaquifer systems using finite-difference analogs and an iterative ADI procedure.

By the early 1970's, interest in numerical models began to spread rapidly, prompted by several landmark publications. One of these, Prickett and Lonquist (1971), listed simple and easily useable program codes for two- and three-dimensional simulations of water-table, confined, and semi-confined systems, thus giving essentially every interested professional access to numerical models. That same year, Remson and others (1971) published their classical text detailing the application of numerical theory to ground-water hydrology.

Trescott (1975), Trescott and others (1976), and Trescott and Larson (1976) are three- and two-dimensional model codes, respectively, published by the U. S. Geological Survey. The publication of these codes represented another notable advance

in making reliable models available for general use and these programs are perhaps the most widely used in this county at the present time. They are well documented and have been verified by numerous applications to real problems.

Recently, several useful publications treating numerical modeling at the introductory level have been released. Mercer and Faust (1981) is a brief survey of basic modeling concepts and applications. Wang and Anderson (1982) is a basic text which details and demonstrates finite-difference and finite-element methods, various matrix solution techniques, and elementary solute-transport modeling.

Recent simulative work with some bearing on the Flambeau study are Bair (1980) and Bair and Parizek (1981). Both of these papers describe efforts to simulate the effects of open-pit anthracite mining in eastern Pennsylvania using a modified version of the U. S. Geological Survey two-dimensional model (Trescott and others, 1976).

## Description of Study Area

### Location

The Flambeau massive sulfide deposit is located in northwestern Wisconsin about 185 mi (298 km) northwest of Madison and 48 mi (77 km) northeast of Eau Claire (Figure 1). More specifically, the ore body is approximately 0.6 mi (1.0 km) southwest of Ladysmith, the seat of Rusk County, at  $45^{\circ}26'30''$  North latitude and  $91^{\circ}07'05''$  West longitude. The associated



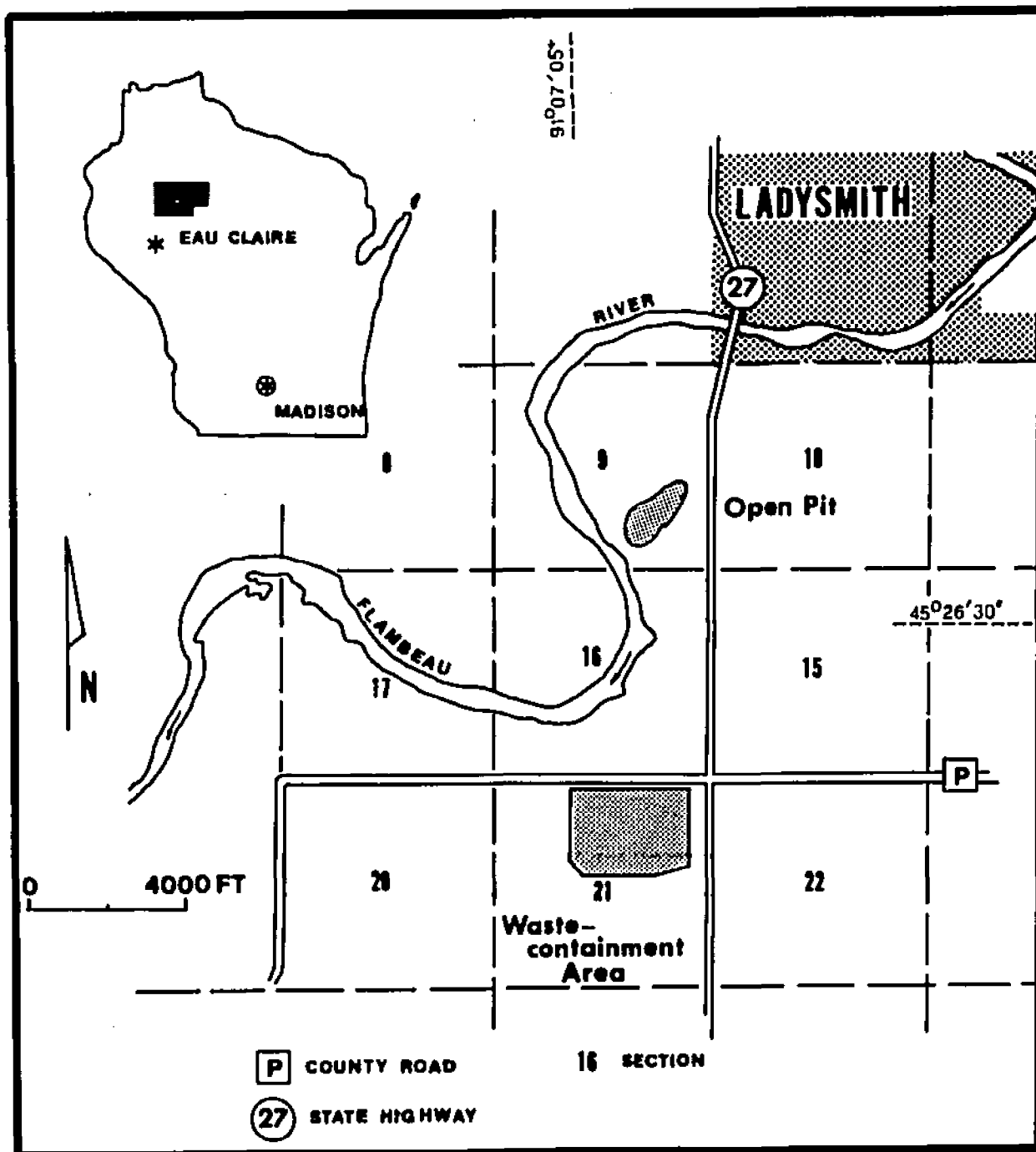


FIGURE 1. Locations of the proposed mine pit and waste-containment structure at the Flambeau mine site near Ladysmith, Wisconsin.

waste impoundment will be constructed 1.2 mi (1.9 km) south of the ore deposit at 45°25'00" North latitude and approximately the same longitude. The 2,750 acres (1,113 ha) presently controlled by the Flambeau Mining Corporation occur within sections 9, 10, 16, 17, 20, and 21 of T34N, R6W, as shown in Figure 1 and on the Ladysmith and Thornapple 7.5-minute quadrangles. The ore body is in the southeast quarter of Section 9 and the waste-containment structure will be located in the northern half of Section 21.

#### Physiography

The mine site is near the southwestern edge of what Martin (1916) termed the Northern Highland geographical province, a gently arched upland erosional surface of beveled Precambrian rocks within the area commonly known as the Canadian Shield. The Northern Highland province occurs in the southern part of a center of uplift called the Superior Upland geologic province which forms a southern extension of the Shield. The southern boundary of the Northern Highland area is approximated by the eroded margin of Paleozoic sediments which once covered all Precambrian rocks in this area. Erosion following the lower Paleozoic uplift of the Wisconsin arch removed the younger strata, exposing the Precambrian igneous and metamorphic sequences which were later obscured beneath a veneer of unconsolidated Pleistocene deposits.

Few bedrock exposures are known to exist in the area of the mine site and landforms in the locality are not signifi-

cantly influenced by the bedrock. Excluding the post-glacial valley of the Flambeau River, nearly all local landforms are constructional, having been formed by the deposition of glacial materials during the Woodfordian substage of the Wisconsinan stage in Pleistocene time (Cahow, 1973). Destructional climatic processes have only moderately altered the landscape since the ice retreated from the area. Though large areas of low relief exist, much of the locality is undulating to somewhat hilly with flat areas occupying the floors of poorly drained depressions. Steep slopes are more typically restricted to the outside banks of meanders on the Flambeau River. Elevations near the proposed open pit range from less than 1090 ft msl (mean sea level datum) near the river to over 1155 in the southwest part of Section 9, giving a total relief of more than 65 ft (20 m). Slopes are generally gentle to steep, ranging from less than 2 to over 9 percent. The waste-containment area is typically much flatter with a total relief of about 22 ft (6.7 m) and slopes on the order of 2 percent or less. Surface drainage throughout both the mine site and the waste area is generally to the west and northwest.

According to Cahow (1973), the mine locality is transitional between predominantly stagnant-ice features to the west and active-ice landforms to the east. Much of Rusk County east of the Flambeau River is characterized by flat to gently undulating topography and drumlinoid or fluted ground-moraine features. Areas in which these features occur are characterized by northeast-trending, poorly developed drumlins separated

by shallow and poorly drained linear depressions (Figure 2). These features are most prominent east of Highway 27 and south of the waste-disposal area where streams and wetlands display an obvious parallelism.

Discontinuous stagnant-ice features occur with increasing frequency from east to west across the southern portion of the FMC holdings. These features are not common east of the Flambeau River but dominate the topography east and south-east of Ladysmith and in the vicinity of the disposal area. These features consist chiefly of small, discontinuous eskers located northwest and south of the proposed waste area and east of the ore body and Highway 27, and linear gravel ridges near the disposal site's northwest corner. The eskers are composed largely of irregularly stratified gravel and are regarded as subglacial accumulations deposited within tunnel valleys eroded by meltwater streams flowing beneath the ice mass. The linear sand and gravel ridges appear to be ice-contact features deposited along the edge of a stagnant ice mass that occupied what is now a large wetland area within sections 20 and 21 (Cahow, 1973).

Perhaps the most distinctive examples of stagnant-ice topography are the tracts of small, steep-sided hills and intervening closed depressions collectively termed hummocky stagnation (knob-and-kettle) moraine. This type of terrain is extant west of the Flambeau River across from the pit area and west of the waste-impoundment site. These areas are composed of sediment that was contained within or upon extensive

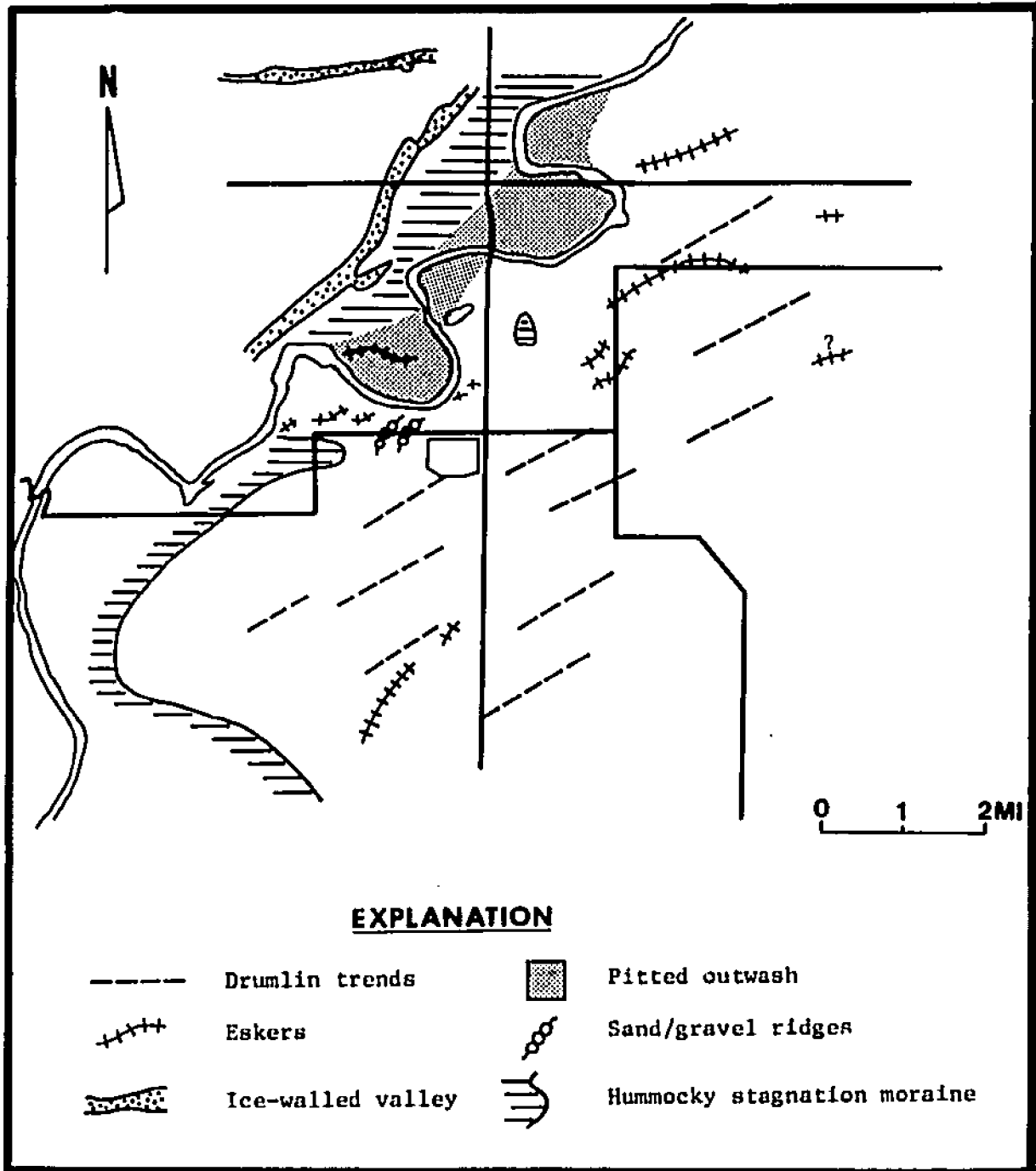


FIGURE 2. Areal distribution of prominent surface features in the vicinity of the Flambeau mine site (from Cahow, 1973).

ice masses and which was later deposited between them as the ice slowly wasted into separate blocks (Cahow, 1973).

Areas within meander cores of the Flambeau River, including the western portion of the pit area, are characterized by Cahow (1973) as pitted outwash features resulting from the deposition of coarsely granular materials over irregularly shaped ice masses by the Flambeau swollen with meltwater (Figure 2). He hypothesized that the stagnant ice masses did not melt until after the Flambeau had become entrenched, with the depressions and pits created by subsequent wasting of the buried ice blocks. In some areas the pitted outwash exhibits enough relief to be morphologically indistinguishable from adjoining areas of hummocky stagnation moraine composed of finer-grained till.

The Flambeau River is the most prominent drainage feature in the area. It flows diagonally from the northeast corner of Rusk County to a meandering reach near Ladysmith and across the west edge of the project area before turning southwestward to its confluence with the Chippewa River, a major tributary of the Mississippi River. Meandering streams typically have well-developed flood plains, but this segment of the Flambeau has virtually none that is topographically evident. Its valley is asymmetrical in cross section with steep undercut slopes on the outsides of meanders and gentle, low-relief slip-off slopes inside of them. Cahow (1973) noted that the meanders near Ladysmith are so disproportionately large with respect to the Flambeau's present discharge that their radii of curv-

ature are greater than those of meanders near the mouth of the Chippewa River. The meanders appear to have formed after outwash deposition had ceased and the ice margin had receded from the immediate area, but while the Flambeau was still discharging large quantities of meltwater. If this hypothesis is valid, the course and morphology of the Flambeau River have undergone only minor post-glacial modification.

### Climate

The climate of northern Wisconsin is classified as the cool-summer subtype of the temperate continental climatic category, according to the modified Köppen classification system (Trewartha, 1968). This land-controlled climatic regime is more severe than the warm-summer phase typical of much of the lower midwest. It is characterized by cold winters with a durable snow cover and warm to hot summers. Fall and spring are brief transitional seasons and are composites of winter and summer characteristics.

Summers in the temperate-continental, cool-summer phase are moderately warm and humid for a few months but are of relatively short duration. Summer mid-day temperatures are likely to be warm to hot during maximum insolation and cool when overcast conditions prevail. Hot spells are usually mild and ephemeral; summer cold spells associated with polar air masses are more common since the cool-summer regime is closer to the tracks of summer cyclones. Summer is generally

the season of maximum precipitation (see Table 1), though winters are by no means dry. The period of greatest rainfall thus corresponds to the period of maximum air temperatures, an arrangement favorable for nonconiferous vegetation, which is completely dormant during winter months. Summer precipitation occurs largely as convectional showers which are less areally extensive, of shorter duration, and more intense than winter rains and snows. Many showers occur as spotty, pelting rains which promote rapid surface runoff. The growing season, defined as the number of days between the last freeze in the spring and the first freeze in the fall, averages about 125 days (Sather and others, 1971). The date of the last freezing temperature in the spring is usually between May 20 and 30, while the first freeze of each fall typically occurs between September 10 and 20.

Winter is the dominant season in the temperate-continental climate, though the severity of winter weather varies greatly from year to year. No other climate is known to have such rapid, nonperiodic weather changes during the winter and large temperature changes frequently occur within short periods of time. Winter precipitation, occurring chiefly as snow, is primarily of frontal and cyclonic origin. Annual snowfall in the project area ranges from 43 to 50 ins (109 to 127 cm), and a durable snow cover may remain from mid-December to early April (Sather and others, 1971).

Local meteorological records from 1965 through 1980 indicate that the average annual temperature at Ladysmith is



42.1<sup>o</sup>F (5.6<sup>o</sup>C). January, the coldest month, averages 8.6<sup>o</sup>F (-13<sup>o</sup>C) while average temperatures in July and August, the warmest months, are respectively 68.3 and 65.4<sup>o</sup>F (20.2 and 18.6<sup>o</sup>C) for the period of record (Table 1). There are typically 180 days per year when the minimum daily air temperature is at or less than 32<sup>o</sup>F (0<sup>o</sup>C) (U. S. Environ. Data Serv., 1968), 43 days with minimum air temperatures at or below 0<sup>o</sup>F (-17.8<sup>o</sup>C), and two days with maximum temperatures at or above 90<sup>o</sup>F (32.2<sup>o</sup>C) (Wiscon. Statistical Reporting Serv., 1967; based on data from 1951 through 1960). Respective minimum and maximum temperatures of -40 and 95<sup>o</sup>F (-40 and 35<sup>o</sup>C) have been recorded at the mine site during the 15-year period from 1965 through 1980. The mean air temperature normally drops below the freezing mark in late November, at which time ice begins forming on lakes and streams (Sather and others, 1971).

For the 57 years of record through 1980, local precipitation averaged 31.42 ins (798 mm) (NOAA, 1981), though recent yearly totals as high as 49.12 ins (1,248 mm) and as low as 18.89 ins (480 mm) were measured in 1968 and 1976, respectively. About 60 percent of the annual rainfall occurs from May through September, while the period from December through February typically has the lowest precipitation (see Table 1 and Figure 15 on page 58 ). Data from 1951 through 1960 indicate that about 63 days each year have 0.1 ins (2.5 mm) or more of rainfall and 0.5 ins (12.7 mm) or more occurs on an average of 19 days (Wiscon. Statistical Reporting Serv., 1967).

TABLE 1. Mean monthly precipitation and temperatures at the Flambeau project area near Ladysmith.

<u>Month</u>	<u>Precipitation</u> <sup>1</sup>	<u>Temperature</u> <sup>2</sup>
January	1.00 ins	8.6 °F
February	0.77	14.9
March	1.70	27.5
April	2.48	43.2
May	3.63	55.4
June	4.95	63.4
July	4.25	68.3
August	4.01	65.4
September	3.69	56.8
October	2.20	47.1
November	1.60	31.3
December	1.14	18.0
Annual Average	31.42 ins	42.1 °F

<sup>1</sup> NOAA (1981)

<sup>2</sup> Ladysmith Ranger Station and on-site measurements from 1965 through 1980

An interpolation of wind data from Minneapolis and Wausau (Wisconsin) was done by the Flambeau Mining Corporation (FMC, 1976) to approximate long-term wind patterns in the Ladysmith area. This analysis showed that prevailing winds are westerly from late fall through early spring and southerly to westerly during the remainder of the year. April and May are usually the windiest months; July and August are the calmest. Wind velocities of 25 to 35 mph (40 to 56 km/hr) and gusts to 50 mph (80 km/hr) are not uncommon during periods of changing weather, particularly in the spring and fall (Sather and others, 1971). Wind velocities measured from April through October at Ladysmith show that the highest average velocity of 11 mph (18 km/hr) occurs in May and the lowest, 8 mph (13 km/hr), occurs in August (FMC, 1976).

#### Land Use

The 2,750 acres (1,113 ha) controlled by the Flambeau Mining Corporation include varied uses for single-family residential, industrial, commercial, institutional, forestry, and open-space purposes. Some agricultural land has been turned to pasture or recently cultivated while other fields, forests, and wetlands have been left relatively undisturbed in recent years (Wiscon. Dept. of Natural Res., 1975).

In the absence of a county-wide land-use plan, current zoning classifications are interpreted to indicate possible future land uses. Present zoning classifications on the com-

TABLE 2. Currently designated land uses within the Flambeau project area (from Wiscon. Dept. of Natural Res., 1975).

---



---

ZONING	ACREAGE	PERCENT
Agricultural	2,077	75.5
Industrial	221	8.0
Residential	171	6.2
Resource Conservation	160	5.8
Forestry	116	4.2
Commercial	5	0.2
	Total	99.9 %

---

pany's holdings are provided in Table 2.

There is presently little recreational use of the area near the mine site except for some canoeing and fishing on the Flambeau River and hunting and trapping in upland areas. Ultimate land-use plans for the abandoned mine pit, which will encompass an area of about 55 acres (22 ha), presently call for the establishment of a lake, although a firm decision regarding this reclamation plan has not yet been made.

It is anticipated that only 312 acres (126 ha), or about 11 percent of the project area, will be used directly during mining operations, including the open pit and the 156-acre (63-ha) waste-containment impoundment. The remaining acreage has been acquired to maintain noise and visual screening and will continue in its present use throughout the operation.

### Proposed Mining Operation

The ore deposit will be mined by conventional open-pit methods over an initial 11- to 12-year period (FMC, 1976). Pit excavation will result in a series of horizontal benches 35 ft (11 m) high and overall slopes of  $35^{\circ}$  (Figure 3). The operation will advance northeastward from the initial workings near the Flambeau River, producing an estimated 1,000 tons (900 metric tons) of ore per day. After three years of operation, the pit will be approximately 1,800 ft (550 m) in length along strike and 1,000 ft (305 m) in width at its widest point (Figure 3). After about five years, the pit will have attained its maximum dimensions of 2,400 ft (730 m) along strike, a width of 1,000 ft (305 m) at its western end, and a total area of 55 acres (22 ha). At the end of 11 years, the pit will reach its maximum depth of 285 ft (87 m). It is anticipated that mining will then continue via a two-compartment production shaft sunk 830 ft (253 m) into the footwall of the ore body from the bottom of the pit. The underground operation will employ cut-and-fill stoping to minimize subsidence and hanging-wall incompetency and may continue for another 11 years. Daily ore production during the underground phase is estimated at 1,400 tons (1,270 metric tons). The ore will be concentrated at processing facilities southeast of the pit. When operations cease, it is presently contemplated that the pit will be allowed to refill with ground water or a combination of ground water and surface water to an elevation of about 1092 ft, forming a 55-acre (22-ha) lake with a maxi-

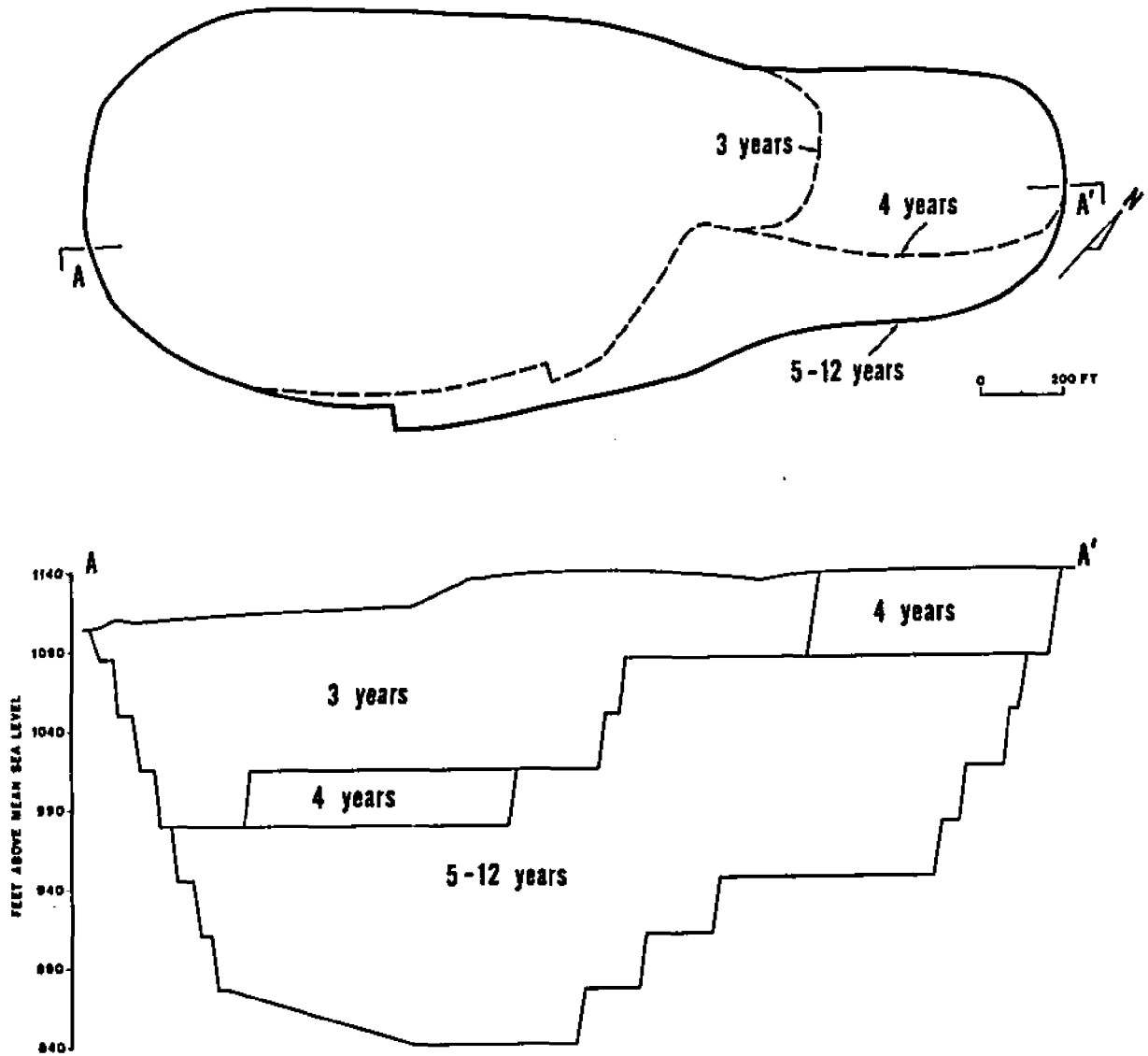


FIGURE 3. TOP: Plan view of the proposed Flambeau mine pit showing the extent of the excavation after 3, 4, and 12 years. BOTTOM: Cross section of the pit showing estimated depths for the same time periods (from unpubl. data, Kennecott Minerals Co.; based on 365 days per year at 1,000 tons per day).

mum depth of 240 ft (73 m).

An estimated  $1.23 \times 10^6$  yds<sup>3</sup> ( $9.42 \times 10^5$  m<sup>3</sup>) of topsoil, glacial material, waste rock, and saprolite will be removed during the course of mining operations (FMC, 1976). Approximately 48 percent of this volume will be reused at the site to construct haul roads, a flood dike between the pit and the river, and the dike walls of the waste-containment structure. Remaining topsoil, subsoil, and saprolite will be stored in segregated stockpiles north of County Road P between the pit and the disposal area for use during reclamation. Remaining waste rock, especially pyritic materials, will be placed in the waste structure.

The 156-acre (63-ha) waste-containment structure (figures 1 and 4) will be 1.2 mi (1.9 km) south of the mine pit and will receive daily an estimated 840 tons (762 metric tons) of tailings from the ore-processing facilities southeast of the pit and 4,120 tons (3,737 metric tons) of waste rock during the 11-year open-pit operation. A total of  $2.62 \times 10^6$  tons ( $2.37 \times 10^6$  metric tons) of tailings will be produced during that time. The subsequent 11-year underground operation is expected to generate an additional  $2.89 \times 10^6$  tons ( $2.62 \times 10^6$  metric tons) of tailings at an average daily rate of 860 tons (780 metric tons). Some of the waste rock from the mine, along with some topsoil and subsoil stripped from the pit area during initial preparations, will be used to construct the containment dike. The dike enclosing the disposal area will have a 40-ft (12-m) core of compacted, nearly impervious saprolite

Peripheral ring-feed system

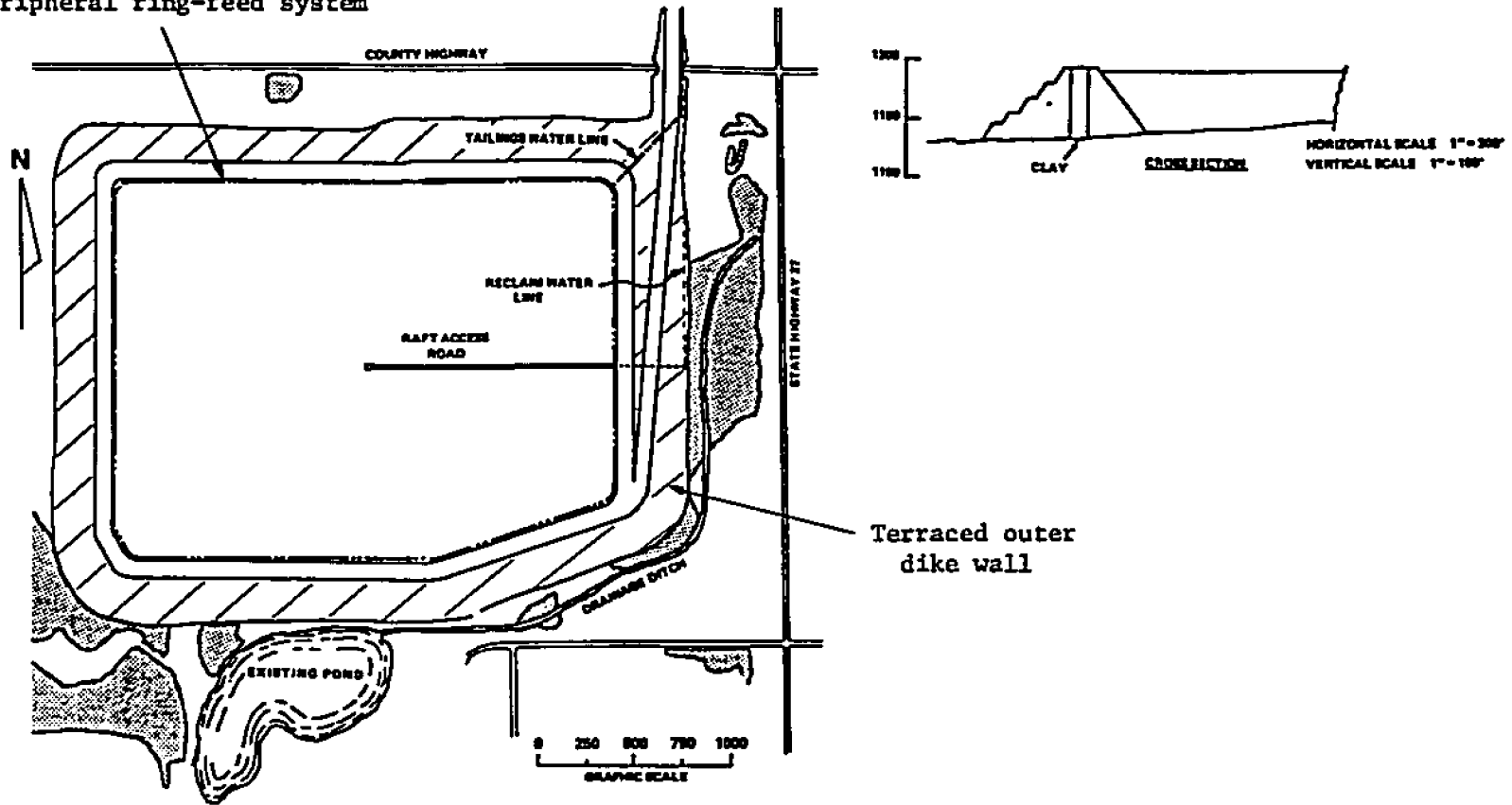


FIGURE 4. Plan view of the proposed waste-containment structure 1.2 mi south of the mine area. The cross section (above right) illustrates the construction of clay saprolite cores within the dike walls of the structure (modified from FMC, 1976).



from the pit excavation. Dike elevations will be continuously increased throughout the mining operation, maintaining 35-degree slopes that will be stabilized with vegetation. Tailings from the ore-processing plant will be transported as a slurry to the impoundment via a pipeline and will be discharged into the structure through a peripheral distribution system installed within the dike perimeter. Upon closing of the mine, the waste-disposal structure will be capped with compacted saprolite and subsoil from the stockpile area and haul roads, and then vegetated.

## CHAPTER II

### BEDROCK GEOLOGY

#### Introduction

The bedrock in the Flambeau project area plays an important role in characterizing the local ground-water flow system. Consolidated Paleozoic sediments in the area often act as isolated aquifers and the Precambrian rocks form the lower bound for the more hydrologically active Paleozoic and Pleistocene deposits which overlie it. An accurate description of the consolidated materials is thus paramount to defining their hydrologic properties.

#### Precambrian Rocks

Approximately 93,000 mi<sup>2</sup> (241,000 km<sup>2</sup>) of northern Minnesota, Wisconsin, and Michigan lie within the Superior Upland province of the Canadian Shield where dominant lithologies include Precambrian gneisses, mixed volcanic suites and greenstones, igneous intrusives, and metasediments. All rocks in the Shield area were structurally deformed during Precambrian time by folding and faulting, but there has been little tectonic activity since the Cambrian Period and the Shield is now regarded as one of the most geologically stable areas of the continent (Wiscon. Dept. of Natural Res., 1975).

The Precambrian basement in Rusk County near Ladysmith

consists of deformed and slightly to intensely metamorphosed volcanics and sediments of the late Middle Precambrian Penokean complex (Figure 5). In their unaltered, pre-metamorphic state, these rocks consisted of submarine volcanic flows, ash layers and other pyroclastic accumulations, and volcanogenic sediments ranging in composition from basalt to rhyolite. Lithologic units are generally steeply dipping, moderately to highly schistose, and strike northeastward. Within many rock sequences, regional metamorphism has locally produced upper-greenschist to lower amphibolite mineral suites collectively termed "greenstones". These greenstone belts are surrounded and penetrated by large granitic to gabbroic intrusives, though those of granodioritic to tonalitic composition are most common. The intrusives were emplaced at the end of the Penokean orogeny from 1.75 to 1.8 billion years ago (Dutton, 1976). The crystalline rocks are typically covered by a veneer of Pleistocene glacial material and, farther south and west, by increasing thicknesses of Paleozoic sediments. Exposures of Precambrian rock are rare in the region due to the mantle of Paleozoic and Pleistocene materials, though some are evident along valleys of streams and rivers. The only exposure reported in the project area is that of a highly foliated and intermediate metavolcanic rock beneath the Cambrian sandstone in Section 16 along the banks of Meadowbrook Creek south of the ore deposit (Cahow, 1973).

The ore body is situated at the western extremity of the Flambeau volcanic belt (Myers, 1974) which consists of an un-

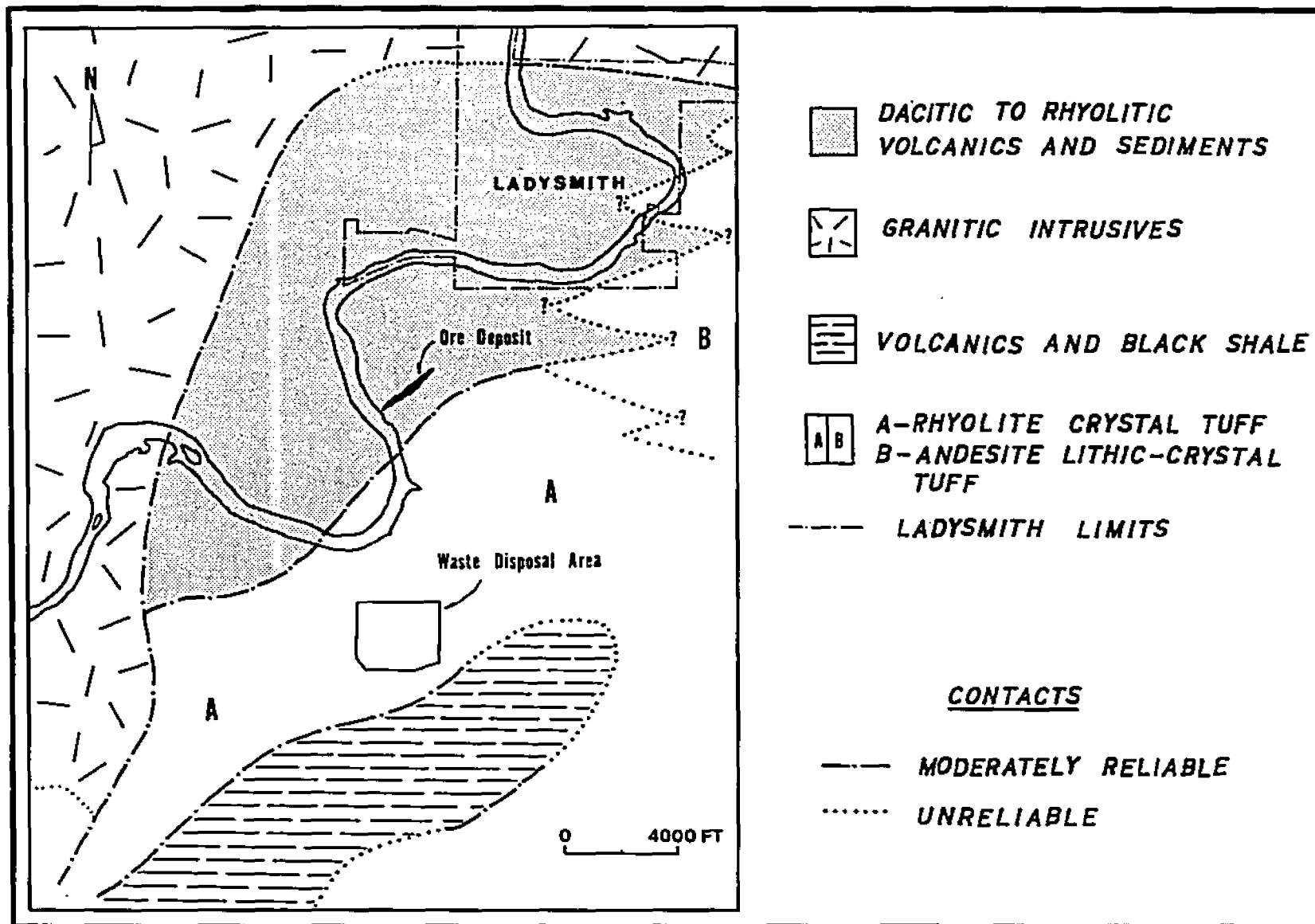
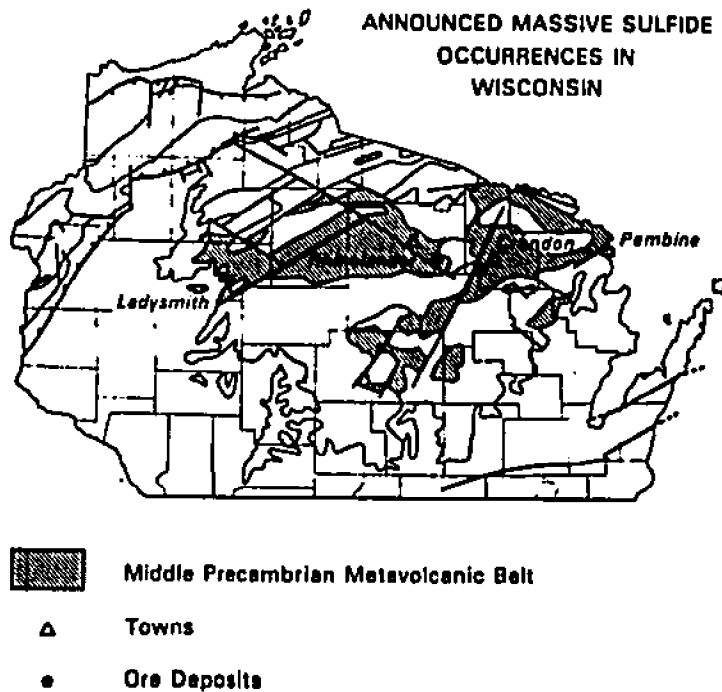


FIGURE 5. Map of Precambrian lithologies in the vicinity of the Flambeau deposit (from unpubl. data, FMC).



**FIGURE 6.** Locations of known massive sulfide ore bodies in the Middle Precambrian of northern Wisconsin and their relation to the metavolcanic belt (after Mudrey, 1979).

known thickness of highly schistose, alternating, intermediate to felsic (dacitic to rhyodacitic) volcanic breccias and tuffs with interbedded volcanoclastics (Figure 6). This sequence has generally been metamorphosed to andalusite grade (FMC, 1976). In the waste-containment area, the original bedrock units are thought to have been rhyolite crystal tuffs that were metamorphosed to phyllites and quartz-augen and quartz-sericite schists (Figure 5). The irregular greenstone belt is about 70 mi (113 km) wide and reaches 220 mi (350 km) east-northeastward across the state to the Michigan border where it is lost beneath younger units. Rocks of this belt, which

contain all presently known massive sulfide deposits of economic importance in Wisconsin, have been isotopically dated (Pb/Pb on galena) by the U. S. Geological Survey at ages ranging from 1.820 to 1.835 billion years (Stacey and others, 1976; Sims, 1976). The age of the Flambeau deposit was determined to be 1.820 billion years. North of the belt in the study area, large tonalite intrusives or series of intrusives underlie much of the Flambeau River valley and truncate known mineralized metavolcanics southwest of Ladysmith. To the east along regional strike, the felsic metavolcanics interfinger with and grade into more intermediate (andesitic) metavolcanics. South of the greenstone belt, the metavolcanics are more sedimentary in nature and grade into graphitic schists interbedded with intermediate flows, rhyolitic tuffs, and diabase sills.

Precambrian structural features in northern Wisconsin are chiefly the result of the Penokean orogeny and possibly two other deformational episodes of lesser intensity (Myers, 1974). The Flambeau volcanics are thought to lie within an overturned northeast-trending limb of a Penokean-age isoclinal fold dipping steeply to the northwest. Other than this feature, only crenulations, small faults, and minor drag folding have been documented in the vicinity of the deposit. Fault breccias and clay gouge have been noted during field studies and appear to be associated with several high-angle strike-slip faults that trend north-northwest. The orientation and dip of these faults is not clear at present, though several

may have relative displacements of as much as 30 ft (9 m). The dominant fabric of the Precambrian rocks is schistosity which is parallel or subparallel to the primary bedding. The schistosity dips northwestward and observed lineations plunge  $80^{\circ}$  to the northeast along strike (May, 1977).

During late Precambrian time, the folded Flambeau volcanics in the vicinity of the ore deposit were intensely decomposed by subaerial weathering. This alteration produced a gray, white, or bluish-green silt- and clay-rich saprolite on the Precambrian surface (May, 1977). This episode of intense weathering was probably synchronous with the supergene enrichment of the massive sulfides. In general, the saprolite is thickest adjacent to, and particularly north of, the mineralized zone and thins rapidly away from it. Evidence suggests it extends westward beneath and beyond the Flambeau River (May, 1973b) and southward into the area of the disposal site. The saprolite is best preserved beneath outliers of an unnamed Cambrian sandstone and attains thicknesses of 7 to 20 ft (2 to 6 m) beneath the Cambrian/Precambrian unconformity. The saprolite is composed almost entirely of micron-sized chlorite particles with subordinate amounts of quartz and other micaceous minerals, and grades downward into fresher rock. It appears to be particularly well-developed in quartz-deficient, plagioclase-rich rocks such as the actinolite schists.

### The Ore Deposit

The polymetallic ore deposit is a light-gray, fine-grained, and well-foliated body with near vertical orientation and tabular geometry (May, 1977). Several satellitic bodies of massive sulfide parallel the main ore deposit along its southern side (Figure 7). The ore body lies conformably within a pyritized quartz-sericite schist ore horizon with a footwall on the south composed of actinolite and chlorite phyllites, quartz-augen schist, and actinolite and andalusite-biotite schists. The hanging wall on the north consists of well-foliated andalusite-biotite schist. The ore horizon is thought to have originated from a rhyolitic lapilli tuff and is intimately associated with lenses of metachert. As defined through diamond drilling, the ore body is approximately 50 ft (15 m) wide, 2,400 ft (730 m) long, and 800 ft (245 m) deep. It strikes N45°E and dips steeply northwestward at approximately 70°.

The volume of ore contained within the schistose ore horizon is estimated at 4 to 6 million tons (3.6 to 5.4 million metric tons) averaging 3.5 to 4 percent copper as chalcopyrite, chalcocite, and bornite with some zinc present as sphalerite. Smaller values of gold, silver, and lead are also present. Primary sulfide minerals of economic significance are chalcopyrite and sphalerite. The mineralized zone is considered unique due to its 50- to 150-ft (15- to 45-m) thick zone of supergene enrichment which extends westward beneath but not across the Flambeau River. Within this en-



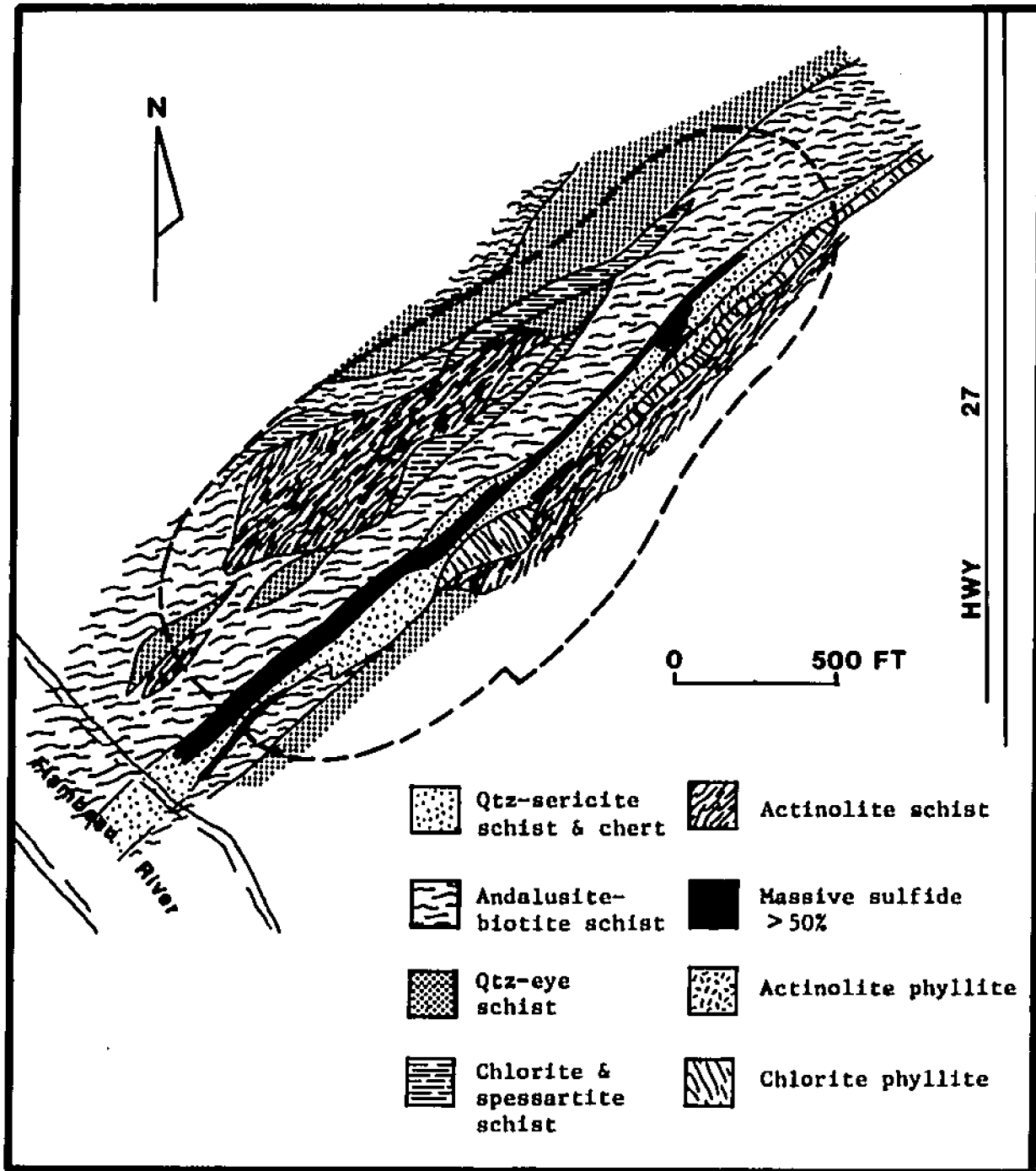


FIGURE 7. Lithologic map of the immediate mine area (the hanging wall is to the north); from FMC, 1976.

riched zone, secondary bornite and chalcocite are the sulfides of chief economic interest. The reader is directed to Dutton (1971) and May (1977) for detailed treatments of mineralogic data for the ore deposit and surrounding rocks.

### Precambrian Surface

A detailed examination of the Precambrian surface, including the saprolite, is warranted because of its hydrologic significance. Plates 2 and 3 are maps of this surface in the pit and waste-containment areas, respectively, as delineated by numerous diamond drill holes and soil borings. Elevation control was more abundant within the proposed pit perimeter where past exploration activities were concentrated.

The ore horizon and associated units, particularly the metachert over its west end, are more silicic than surrounding rocks and were more resistant to erosion occurring before the deposition of Paleozoic sediments. This characteristic led to the development of a gentle northeast-trending feature of slight positive relief on the Precambrian surface in the pit area (Plate 2). The surface immediately adjacent to the ore horizon consists of a northeast-trending ridge from which the surface descends rather steeply to the northwest and southeast. To the northwest, the surface slopes on the order of 4 to 5 percent with a change in elevation of about 80 ft (25 m). These relief patterns are suggestive of an ancestral Flambeau River valley and, indeed, the surface near the mineralized zone appears to exhibit relict drainage features

which radiate from the central high area of the ridge. The most prominent of these features trend to the northeast at the east end of the proposed pit and to the southwest along the southern edge of the pit perimeter. The greatest Precambrian surface elevation of 1095 occurs very near the mineralized zone and mostly in the western half of the pit where 10 to 15 ft (3 to 5 m) of leached metachert have added to that area's erosional resistance. Post-Precambrian fluvial erosion appears to have removed the resistant chert cap and, in some areas, the Cambrian sandstone over the ore zone.

Precambrian topography in the waste-containment area is less well-documented (Plate 3) since it is of lesser importance with respect to the mining operation. Data are especially sparse to the east and northeast. Scattered drilling data show a surface with some 65 ft (20 m) of relief which slopes to the north and south at 3 and 6 percent grades, respectively, from a ridge-like feature terminating near what will be the southeast corner of the containment structure. As in the pit area, the slopes to the north and south could be indicative of a relict drainage system.

### Paleozoic Deposits

Resting unconformably on the Precambrian surface in some parts of the project area are thin outliers of relatively flat-lying Upper Cambrian sandstone (May, 1977). This undifferentiated unit is typically a clean, well-sorted, fine- to medium-grained, friable quartzite with numerous thick clay

partings and a thin basal conglomerate. Limited mechanical analyses suggest the sandstone coarsens to the northeast and also with depth near the center of the proposed pit. The unit overlies all but the western end of the mineralized zone (plates 1 and 5) and attains thicknesses from less than 5 ft (1.5 m) at its periphery to more than 30 ft (9 m) northeast of the pit's center. The sandstone may have a maximum lateral extent of more than 500 ft (150 m) on either side of the ore deposit. May (1973a) reduced these dimensions to less than 325 ft (100 m) on each side of the mineralized zone, though drilling logs indicate the former figure of 500 ft is correct unless misclassification of drill cuttings has occurred. The sandstone is not present beneath the site of the disposal structure south of the mine, but drilling in that area has encountered the sandstone west, south, and east of the area.

On a regional scale, the sandstone is part of a more continuous basal-transgressive sequence covering more than two-thirds of the state (Devaul, 1975). It and other Paleozoic sediments dip to the west and south away from the uplifted Wisconsin arch. Though the unit is rather ill-defined and undifferentiated in the project area, Young and Hindall (1972) describe it as part of a thicker sequence which includes the Jordan, Franconia, Galesville, Eau Claire, St. Lawrence, and Mt. Simon sandstones to the distant south and west where the sequence is more areally persistent throughout southern and western Wisconsin and northern Illinois.

## CHAPTER III

### SURFICIAL GEOLOGY

#### Introduction

Unconsolidated surficial deposits related to four major glacial advances in the Pleistocene Epoch are thought to occur in Wisconsin. Deposits from the early advances, however, may be of limited extent as a result of nondeposition or obliteration by later glacial events. Most of the glacial drift now exposed at the surface is from the most recent ice advance occurring from 12,500 to 22,000 years ago during the Woodfordian substage of the Wisconsinan stage (Paull and Paull, 1980).

Unconsolidated deposits contain nearly all of the freely moving ground water within the Flambeau project area and their detailed characterization is essential to the numerical simulations discussed in later chapters. This chapter sets forth the physical properties and geometry of these deposits and their hydrogeologic characteristics are discussed in Chapter VI.

#### Mine Site

The Flambeau massive sulfide deposit and the Cambrian sandstone are completely mantled by a complex arrangement of Woodfordian glacial deposits. These unconsolidated materials range in thickness from less than 15 ft (5 m) at the extreme

west end and west-central parts of the proposed open pit to more than 65 ft (20 m) along its southeastern and southwestern margins, as illustrated on Plate 4. Thicknesses within the pit boundaries average 36 ft (11 m), though they vary considerably over short distances due to the irregularity of the sandstone and Precambrian surfaces beneath the surficial cover. On a broader scale, the glacial cover thickens rapidly southeastward and northwestward from the mineralization into possible ancestral valleys of the Flambeau River and its tributaries. The maximum thickness recorded in the pit vicinity exceeds 100 ft (30 m) west and north of the southernmost gravel pit. As shown on Plate 4, the thinnest deposits occur in a northeast-trending linear pattern over and near the mineralized zone due to its relatively higher elevation. Drift thicknesses within this zone typically range from less than 15 ft (5 m) to 25 ft (8 m). At present, data describing thicknesses of surficial deposits adjacent to the river and northeast of the ore body are sparse.

Plate 5 shows generalized longitudinal and tangential cross sections through the pit area. It is evident from Plate 5, Figure 2, and Figure 8 that areas enclosed by large meanders of the Flambeau River, including the western half of the pit location, are dominated by dense water-laid deposits of silt, sand, and gravel arranged in point-bar fashion. These deposits are typically stratified, better sorted, and more coarsely granular than other glacial materials because of their glaciofluvial origin (deposition by glacial melt-

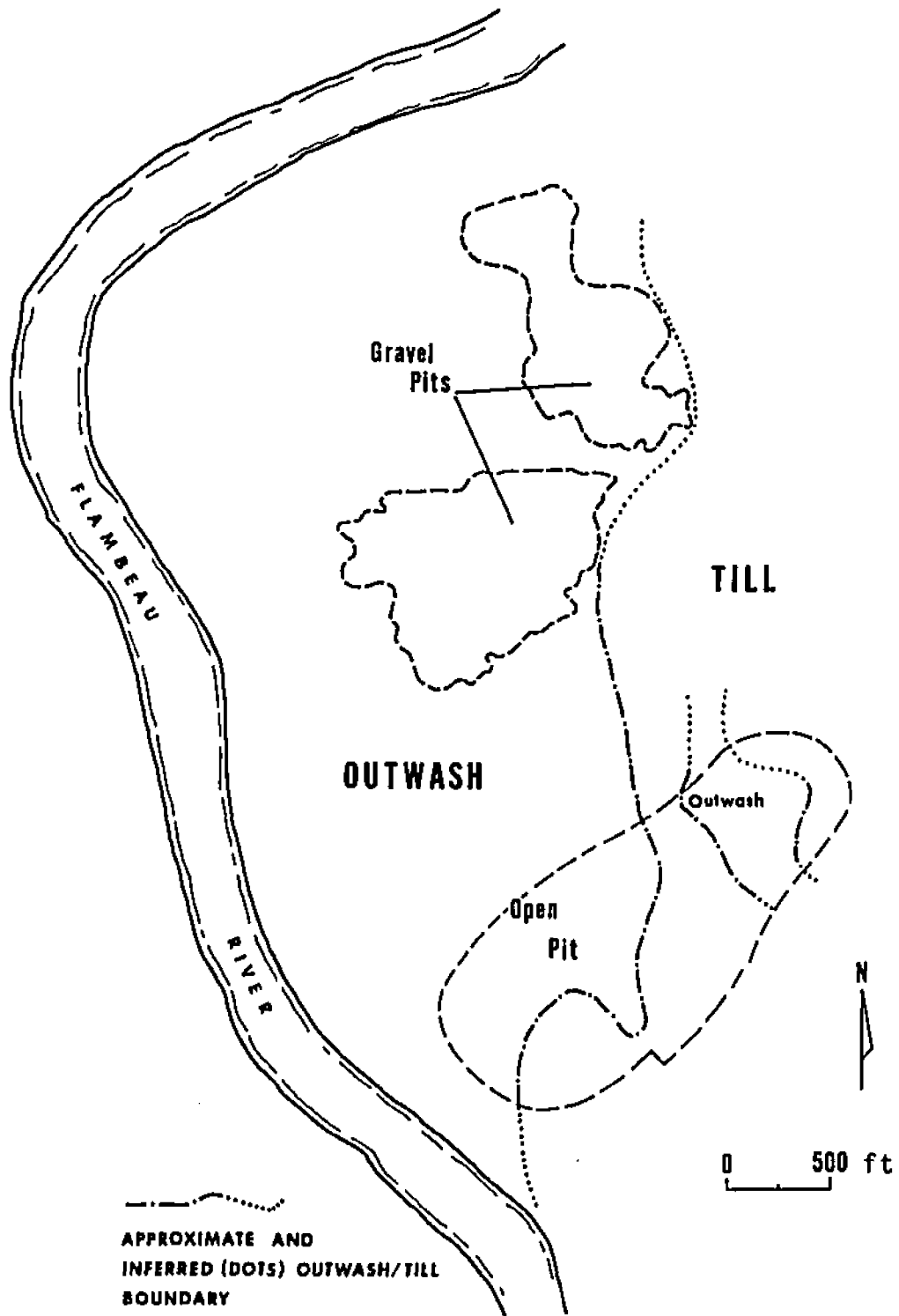


FIGURE 8. Areal distribution of granular outwash material and fine-grained glacial till in the vicinity of the proposed Flambeau mine pit.

water). Cahow (1973) and Hadley and Pelham (1976) broadly describe these deposits as pitted outwash and other ice-contact materials deposited as kames, eskers, and crevasse fillings comprised of poorly sorted and weakly stratified sand and gravel. Logs of soil borings in the area (Soil Testing Serv. of Wiscon., 1972a; 1972b; 1973; 1976a; 1976b; 1976c) describe the outwash as mixtures and discrete zones of poorly to moderately sorted, stratified, fine to coarse sand and gravel with varying amounts of silt matrix material. Small, discontinuous lenses of dense silty sand and sandy silt occur within the sand and gravel. Sieve data from outwash samples indicate that the silt and clay content, defined as the percentage weight of material passing the No. 200 Standard sieve (0.074 mm), ranges from 3 to 12 percent and averages about 8 percent.

The primary outwash area extends westward and northward from the western half of the pit site to the Flambeau River. At one time, sand and gravel were mined from the outwash at two locations north of the mineralization (Figure 8). The outwash ranges from less than 5 ft (1.5 m) to more than 35 ft (11 m) thick with the greatest documented thicknesses occurring in an area occupied by an apparent kame in the northwest part of the planned pit perimeter. Well logs suggest the outwash may approach thicknesses in excess of 70 ft (21 m) northwest of the pit adjacent to the Flambeau River.

At the east end of the pit location, the outwash occurs as a deeper zone overlain by till containing shallow, isolated granular lenses (see Plate 5). The deeper coarse-grained



sediments are associated with a channel feature incised through the Cambrian sandstone and into the Precambrian surface, suggesting that at least the lower portion of these deposits are preglacial alluvial sediments. The upper part of the channel deposits is contained within the till, indicating it is of glaciofluvial origin and may be continuous with the primary outwash body to the west. Lack of subsurface control, however, precludes the firm establishment of lateral continuity between these outwash areas.

The massive, silt-rich sandy till east and south of the outwash is ground moraine that was deposited beneath a mobile mass of glacial ice. Sandy tills are common in the Shield area because of the crystalline source rock. In the pit area, the till consists of a dense, heterogeneous mixture of clay, silt, sand, gravel, and boulders occurring as fine to coarse silty sands and sandy silts with varying amounts of gravel. Sieve data for this area indicate that only 17 to 30 percent of the till by weight (mean of 25 percent) consists of clay and silt. Intercalated with the till are lenses of fine to medium outwash sands and silts of probable limited lateral extent, though some lenses may be continuous with the main outwash area near the Flambeau River.

Soils borings conducted southeast of the open-pit site (Soil Testing Serv. of Wiscon., 1975, 1976b) in an area proposed for the ore-processing plant indicate the till is somewhat more clay-rich to the southeast, particularly between depths of 20 to 35 ft (6 to 11 m) within the surficial cover.

Clayey and silty sands extend to bedrock below this clay-rich zone. Sieve data from this locality show the till contains 25 to 57 percent (average of 35 percent) by weight of clay and silt. A continuous zone of outwash material 3 to 17 ft (1 to 5 m) thick also occurs in this area within a general elevation range of 1125 to 1145, thickening to the west and possibly extending into the area south of the pit. Drilling information between the ore-processing area and the main outwash body at the west end of the pit location is too limited to determine if the outwash is persistent from one locality to the other.

Clear evidence of a "transition zone" between the outwash and till, as described in the initial mining permit application (FMC, 1976; pages 15, 16, and 25), was not apparent during the review of the subsurface information. The presence of such a zone may be very weakly reflected by a local steepening of the hydraulic gradient in the areas of its reported existence (Figure 25). Presumably, the outwash interfingers with the till and becomes somewhat siltier along its eastern and southern margins, but explicit delineation of the area over which this occurs is difficult with available data. The topography of the pitted-outwash area is similar to that of the till to the east, making it difficult for an accurate morphological distinction between the two areas (Cahow, 1973). The till/outwash contact is most easily observed at the east edge of the gravel pits north of the mine site.

The ground moraine south of Ladysmith is mantled by a

layer of silt less than 1 ft (0.3 m) thick on some uplands to more than 10 ft (3 m) thick in some depressions (Cahow, 1973). The silt is generally interpreted as a loessial material derived from nearby outwash areas late in the glacial period and has had an important influence on soil development throughout the region. The silt is commonly stony, probably owing to the addition of pebbles from the underlying glacial materials through frost heaving. In some areas it is much thicker and less stony and appears to have been deposited in shallow depressions in the original ground-moraine surface. By virtue of a sandy layer commonly separating the silt from the underlying till, Cahow (1973) interpreted the silt in these depressions as deltaic or lacustrine sediments. He hypothesized that the silt was transported via surface drainage into late- or post-glacial ponds occupying closed depressions on the till surface.

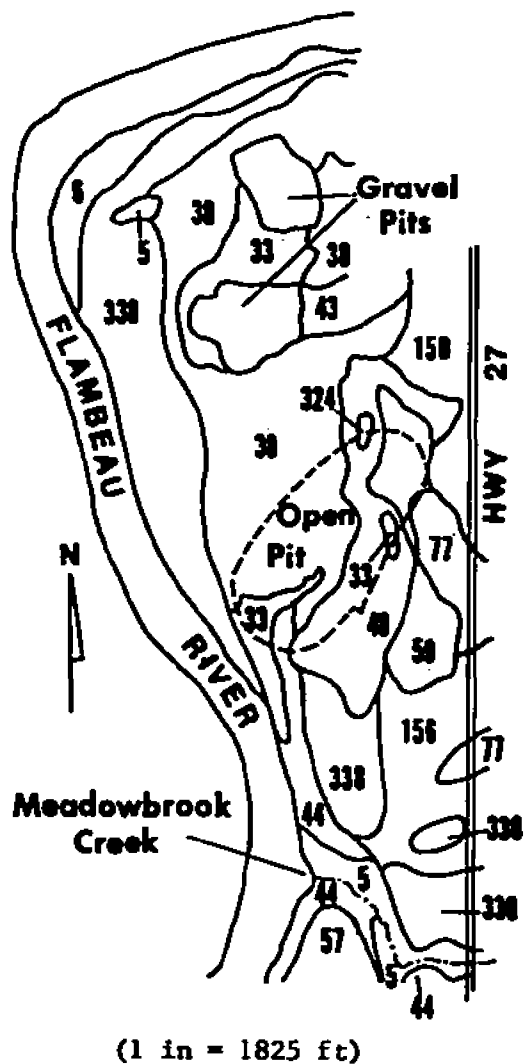
Soils at the surface in the pit area are predominantly silt loams derived from the wind-transported silt, the underlying outwash, and the pebbly sandy-loam till parent materials. Some soils derived from sand and gravel outwash have sandy loam surface textures (FMC, 1976). Paludal soils in wetland areas tend to occur along surface drainageways or in depressional areas and are most abundant east of Highway 27 and southeast of the mine site. These soils are characterized by a high content of organic matter and sometimes by an overlying mat of peat. The Soil Conservation Service has mapped soils in the mine area to a depth of about 5 ft (1.5 m) and

the six major types are described in Appendix I. The areal distribution of these and related soils is shown in Figure 9.

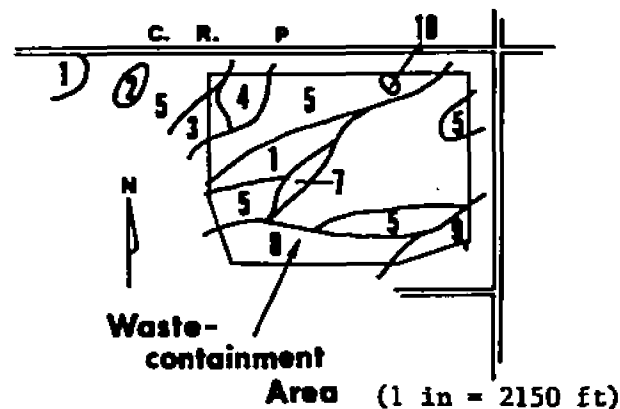
#### Waste-Containment Area

Like the mine area, the site of the proposed waste impoundment is entirely blanketed by Wisconsin glacial sediments. Thicknesses of the unconsolidated cover are generally greater than in the vicinity of the mineralization, ranging from about 50 ft (15 m) west and southwest of the structure site to more than 175 ft (53 m) to the south (Plate 3). A lack of subsurface data north and east of the waste area prevented an accurate delineation of the Precambrian surface and till thicknesses in those areas. The close correspondence between the till thickness and the configuration of the Precambrian surface in Plate 3 is evidence of the low topographic relief in the southern study area.

Figures 10 and 11 are generalized cross sections of the waste-containment area along lines A-A', B-B', and C-C' shown at the bottom of Figure 10. These sections are based on information from scattered deep drilling and numerous shallow soil borings. Approximately 3.5 to 11.5 ft (1.1 to 3.5 m) of surficial soils (described later) are underlain by fine to medium or fine to coarse sands with varying amounts of clay, silt, and gravel. The average silt and clay content of these sandy materials is 25 percent by weight. This deposit is a



- 5 ALLUVIAL LAND, WET
- 6 ALLUVIAL LAND
- 33 CHETEK LOAM
- 38 ONAMIA LOAM
- 43 ANTIGO SILT LOAM
- 44 TERRACE ESCARPMENT SANDY LOAM
- 48 BRILL SILT
- 57 SPENCER SILT
- 68 ALMENA SILT
- 77 AUBURDALE SILT
- 156 FREER SILT LOAM
- 324 POSKIN SILT
- 338 ALBAN LOAM
- 338 BEVENT SANDY LOAM



- 1 CLAYEY SILT OVER SILT
- 2 SILTY SAND
- 3 CLAYEY SILT OVER SILTY SAND OR SILT
- 4 SILT OVER CLAYEY SILT
- 5 SILT OVER SILTY SAND
- 6 SILTY CALY OVER SILT OR SILTY SAND
- 7 SILT OVER CLEAN SAND
- 8 SILT OVER SILT CLAY OR CLAYEY SAND
- 9 SILTY CLAY OVER CLAYEY SAND
- 10 ORGANIC CLAY

FIGURE 9. The areal distribution of surficial soils at the mine site and waste-containment area (pit area - U. S. Dept. of Agri., Soil Conservation Service, 1970; waste-containment area - unpubl. data, Flambeau Mining Co.).

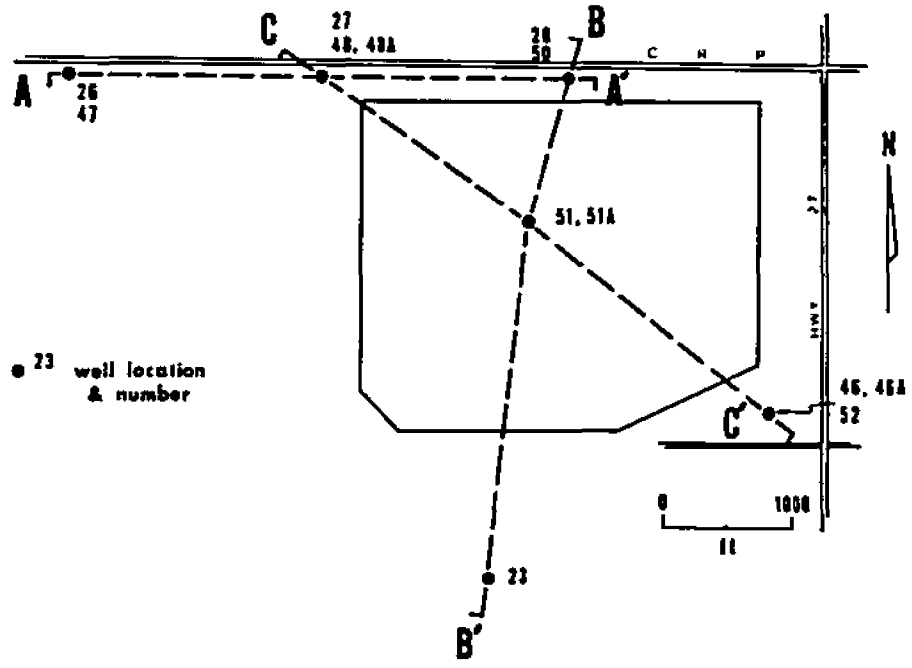
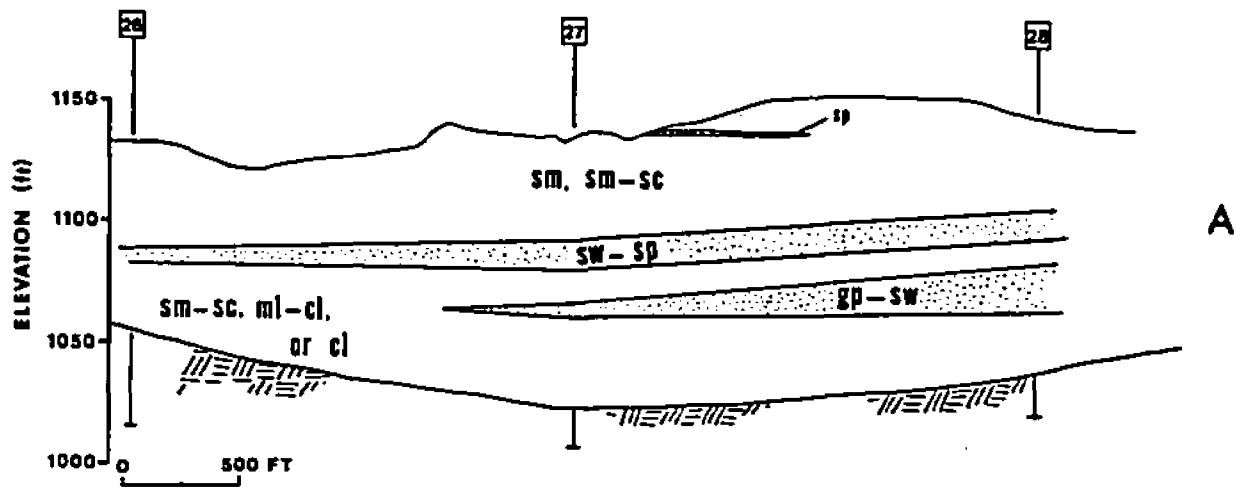


FIGURE 10. East-west cross section through the waste-containment area (see location map at left and Unified Soil Classification in Appendix I).

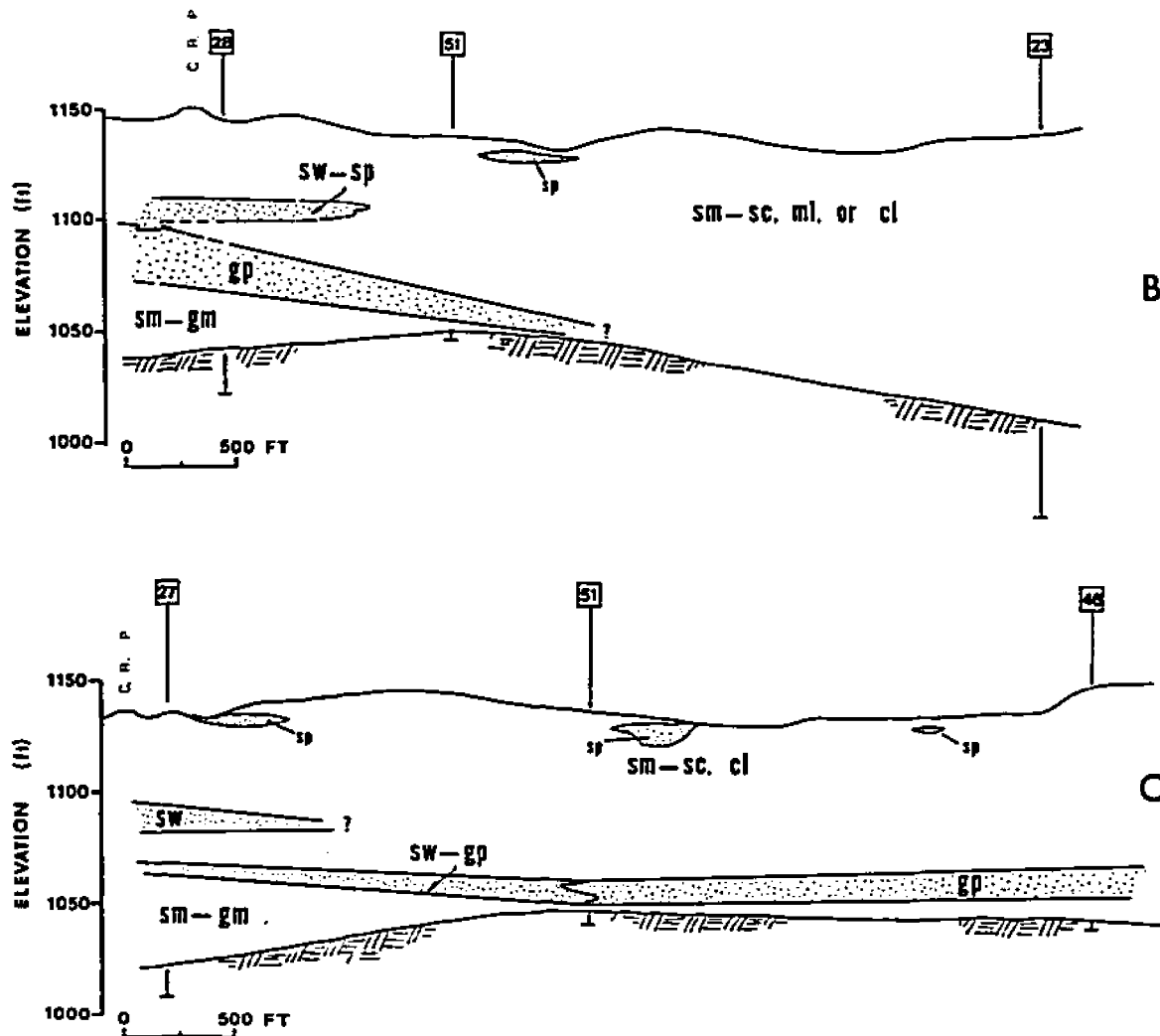


FIGURE 11. North-south (B) and northwest-southeast (C) cross sections through the waste-containment area (see location map in Fig. 10 and Unified Soil Classification in Appendix I).

dense, massive, and heterogeneous ground-moraine till (Hadley and Pelham, 1976) which is more aptly described as a dense silt, a silty and sandy clay, or a clayey or silty sand, depending on location (Soil Testing Serv. of Wiscon., 1972b).

Logs of wells and soil borings in the waste-containment area (Soil Testing Serv. of Wiscon., 1972b) indicate zones of relatively clean sand and gravel occurring at three elevation levels within the till, as illustrated in figures 10, 11, 12, and 13. Sands within the shallowest level occur as four linear bodies of predominantly fine to medium sand with variable fractions of coarse sand and gravel (Figure 12). These bodies generally occur within 5 to 15 ft (1.5 to 5 m) of the land surface with the greatest depths occurring at their western ends. According to sieve data, the silt and clay fraction of these sands is typically less than 10 percent by weight. The sands to the north and south thicken westward and southwestward in the direction of dip, while the middle body attains a maximum thickness of 10 ft (3 m) near its center. The small sand body near the west end of the middle zone occurs at a lower elevation than the linear bodies and may be an isolated lens. The three southernmost sand bodies approximately parallel the direction of Pleistocene ice advancement into the area; the one to the northeast is ill-defined and exhibits no apparent directional orientation. In addition, the three bodies to the west occur within similar elevation ranges, dip to the southwest at 4 to 9 percent grades, and have upper contacts at approximately 1125 ft msl at their western and southwest-



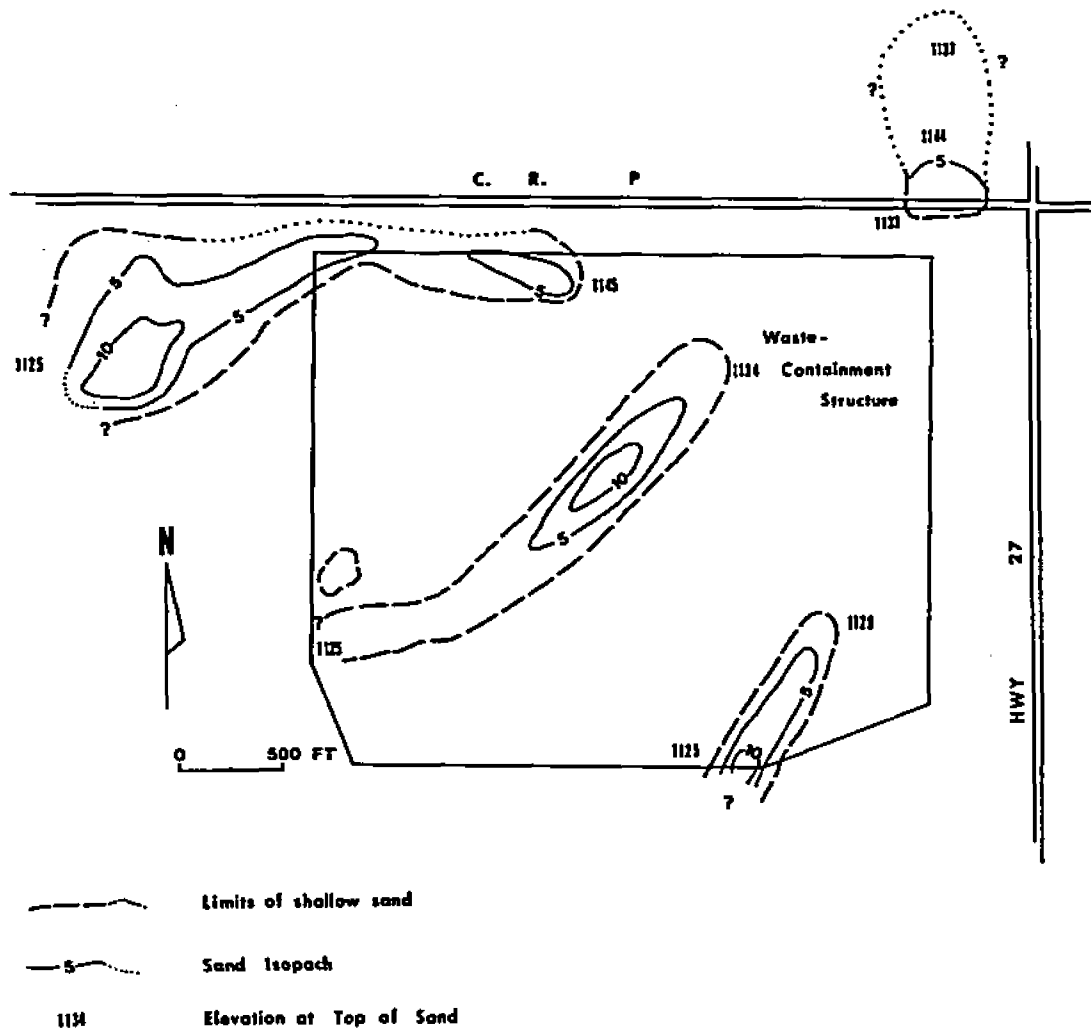


FIGURE 12. Sand zones near the surface of the disposal structure site as defined by shallow soil borings (data from Soil Testing Serv. of Wiscon., 1972b).

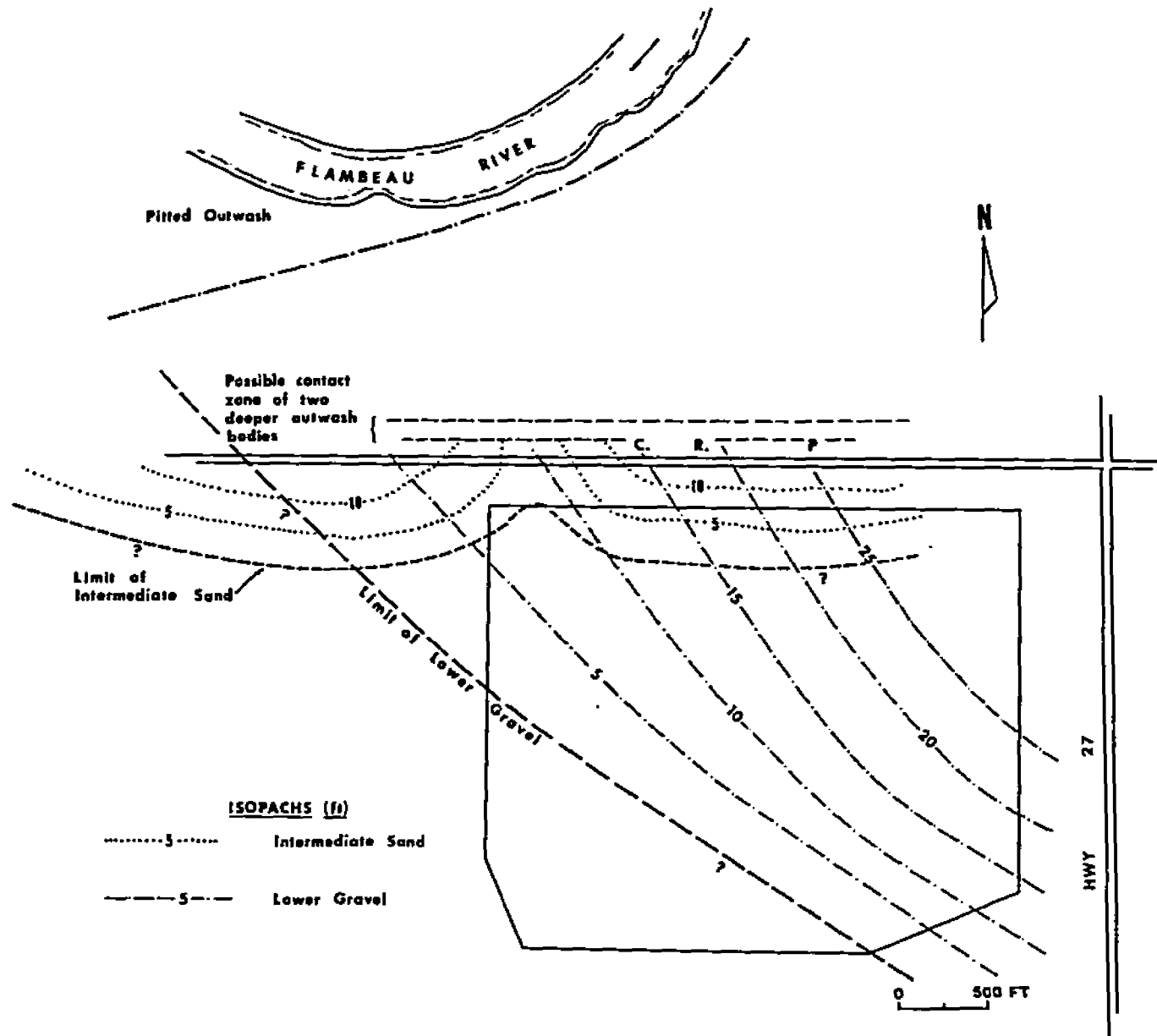


FIGURE 13. Extents and thicknesses of the intermediate and lower outwash zones at the disposal structure site (data from Soil Testing Serv. of Wiscon., 1972b; and Hadley and Pelham, 1976).

ern extremities. This information suggests contemporaneous deposition on a landscape of low relief or in channels of streams with concordant base levels. The three linear sand zones are interpreted as channel alluvium from glacial melt-water streams that drained to the west and southwest from the retreating ice mass. In support of this hypothesis is the common association between these linear zones and shallow surface swales (figures 10 and 11). This hypothesis is further supported by Hadley and Pelham (1976) who describe these deposits as stratified, well-sorted valley-train sands. An absence of drilling data prevented tracing the sand bodies further to the west, though Hadley and Pelham (1976) show them as continuous to the west and south where they coalesce into a single larger unit.

A second granular unit occurs at an intermediate elevation of 1085 to 1110. The southern boundary of this zone approximately parallels County Road P and occurs beneath the northern edge of the impoundment site (figures 10, 11, and 13). This zone consists of fine to coarse sand with some gravel and thickens northward to at least 10 ft (3 m). The top of the zone slopes westward at about 5 percent.

Beneath the intermediate outwash zone is a third layer comprised of fine to coarse gravel with some sand. The gravel occurs within an elevation range of 1052 to 1074 and is persistent beneath all but the southwest one-fifth of the disposal structure's location, as shown in figures 10, 11, and 13. The gravel thickens northeastward, attaining its greatest

known thickness of 21 ft (6 m) along the north-central margin of the disposal site. The northern part of the gravel layer near County Road P dips steeply southward, but beneath the eastern half of the site its dip is more gentle and to the west and southwest. Projecting its steep southerly dip northward suggests the lower gravel and the intermediate sand layer become a single unit 100 to 300 ft (30 to 90 m) north of the county road (figures 11 and 13). At present, there is no drilling information to indicate how far northward this outwash zone extends. Hadley and Pelham (1976) show a narrow band of pitted outwash along the Flambeau River north of the site which may be continuous with the buried deposits just described. The pitted outwash is more dominant northwest of the waste-containment area within a large meander of the River.

The areal distribution of soils within 6 ft (2 m) of the ground surface in the disposal area is illustrated in Figure 9. These soils consist chiefly of silt loams of the Almena-Auburndale association (see the description in Appendix I). Borings and test excavations (May, 1971; Soil Testing Serv. of Wiscon., 1972b) encountered 2 to 5 ft (0.6 to 1.5 m) of silt, clayey silt, silty clay, fine sandy silt, and silty sand beneath the silt loams. West and northwest of the containment area, soils are described as clayey silts and silty sands. The western half of the area that will be occupied by the disposal structure is characterized by silts except for a clayey silt in the west-central part of the site. As shown

in Figure 9, soils with higher clay contents (silty clays) are more prevalent in the eastern half of the site.

Much of the waste-containment area is mantled by a peat layer 0.3 to 1.5 ft (0.1 to 0.5 m) thick composed of decaying grasses, cattails, and fibrous woody materials (May, 1971). West and southwest of the structure location the peat thickens to 2 to 4 ft (0.6 to 1.2 m).

## CHAPTER IV

### SURFACE-WATER HYDROLOGY

#### Introduction

The study area is wholly contained within the drainage basin of the Flambeau River which flows diagonally southwestward from the northeast corner of Rusk County to a meandering segment near Ladysmith, across the west edge of the mine site, and over the west end of the ore deposit (Figure 14). It continues about 12 mi (19 km) southwest of the project area to its confluence with the Chippewa River, a major tributary of the Mississippi River. The Chippewa River basin encompasses approximately 9,435 mi<sup>2</sup> (24,426 km<sup>2</sup>) of northern Wisconsin (Young and Hindall, 1972), of which 1,993 mi<sup>2</sup> (5,160 km<sup>2</sup>) is drained by the Flambeau. About 875 mi<sup>2</sup> (2,265 km<sup>2</sup>) of Rusk County, or 95 percent of its surface area, is drained by the Chippewa-Flambeau system (Sather and others, 1971).

There are nine dams and impoundments on the Flambeau River, four in Rusk County alone. Those nearest the site are the Thornapple Dam (13-ft head) about 9 river miles (14.5 km) downstream and the Peavey Paper Mill Dam (17-ft head) located 3.8 mi (6.1 km) upstream. The project area includes an unimpeded 4.2-mile (6.8-km) segment of the river. In the vicinity of the project area the Flambeau is a broad, meandering, and entrenched system with little topographic evidence of a

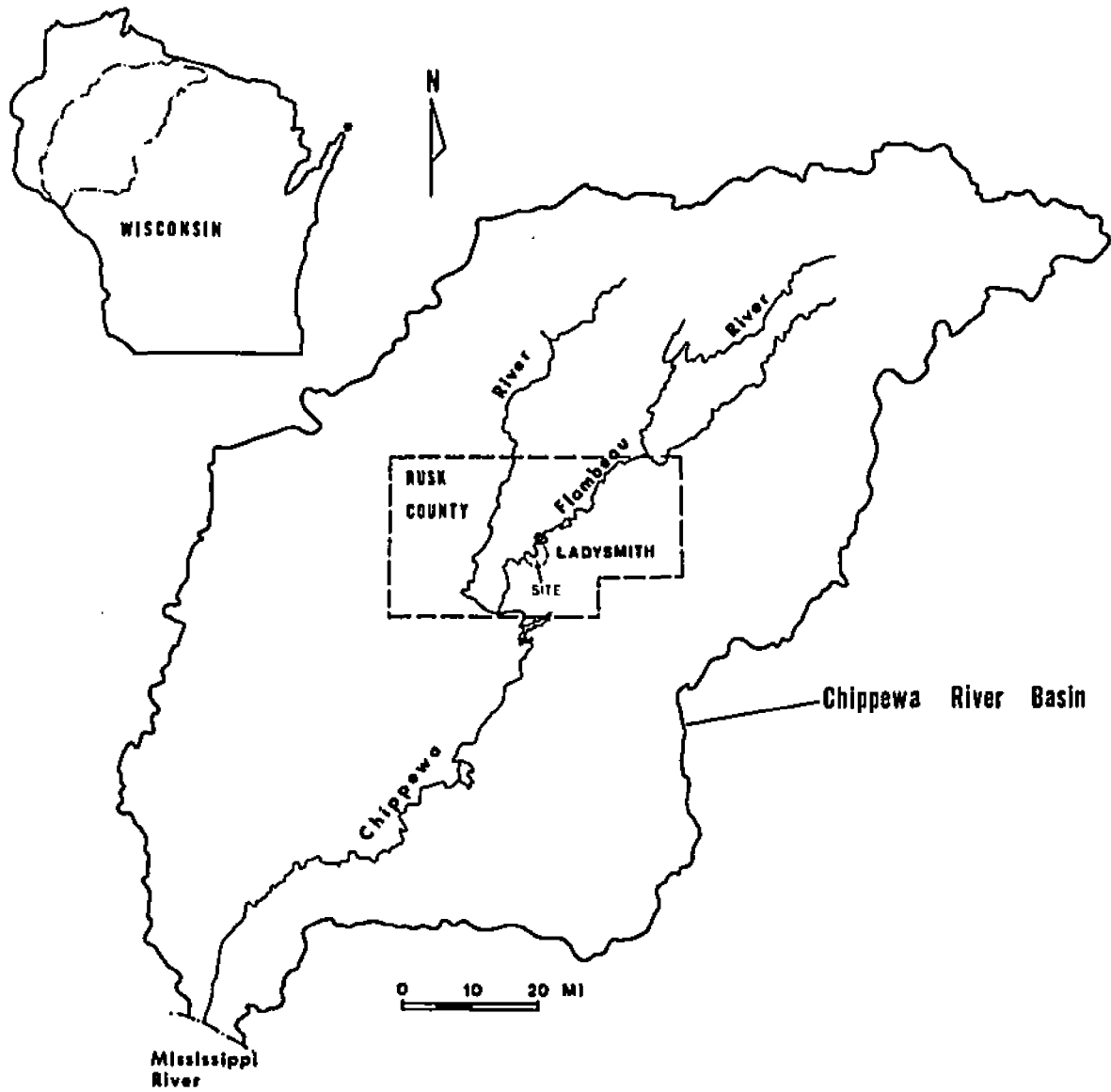


FIGURE 14. The Chippewa River drainage basin and its relation to the Flambeau River, Rusk County, and the project area.

flood plain. Its average fall throughout the basin is 3 ft/mi (0.6 m/km), though the gradient through the project area is about 2 ft/mi (0.4 m/km) (Cahow, 1973). The river's average depth and width in the project area is 3 ft and 350 ft (1 m and 107 m), respectively.

Total streamflow is largely dependent on the amount of precipitation falling within the basin, soil-moisture conditions, and the amount of base flow or ground-water contribution to streams. As shown in Figure 15, peak flows of the Flambeau River typically occur in April when runoff potential is greatest due to the snowmelt saturation of soils, spring rains, and low rates of evapotranspiration. Partially frozen ground early in the spring may also contribute to the large volume of overland flow at this time of the year. As spring becomes summer, precipitation increases but vegetation becomes active and temperatures rise so that evapotranspiration begins to exceed precipitation. This combination of conditions creates a soil-moisture deficiency which allows precipitation to infiltrate more readily into the soil, further decreasing the amount of surface runoff available for streamflow. Flow rates thus decrease as spring and summer progress. As fall progresses and vegetation becomes less active, the rate of evapotranspiration decreases. This increases the surface-runoff potential, but a contemporaneous decrease in precipitation and the fall soil-moisture deficiency may effectively buffer the amount of runoff that actually occurs. During this period, streamflow exhibits a decrease that continues throughout the



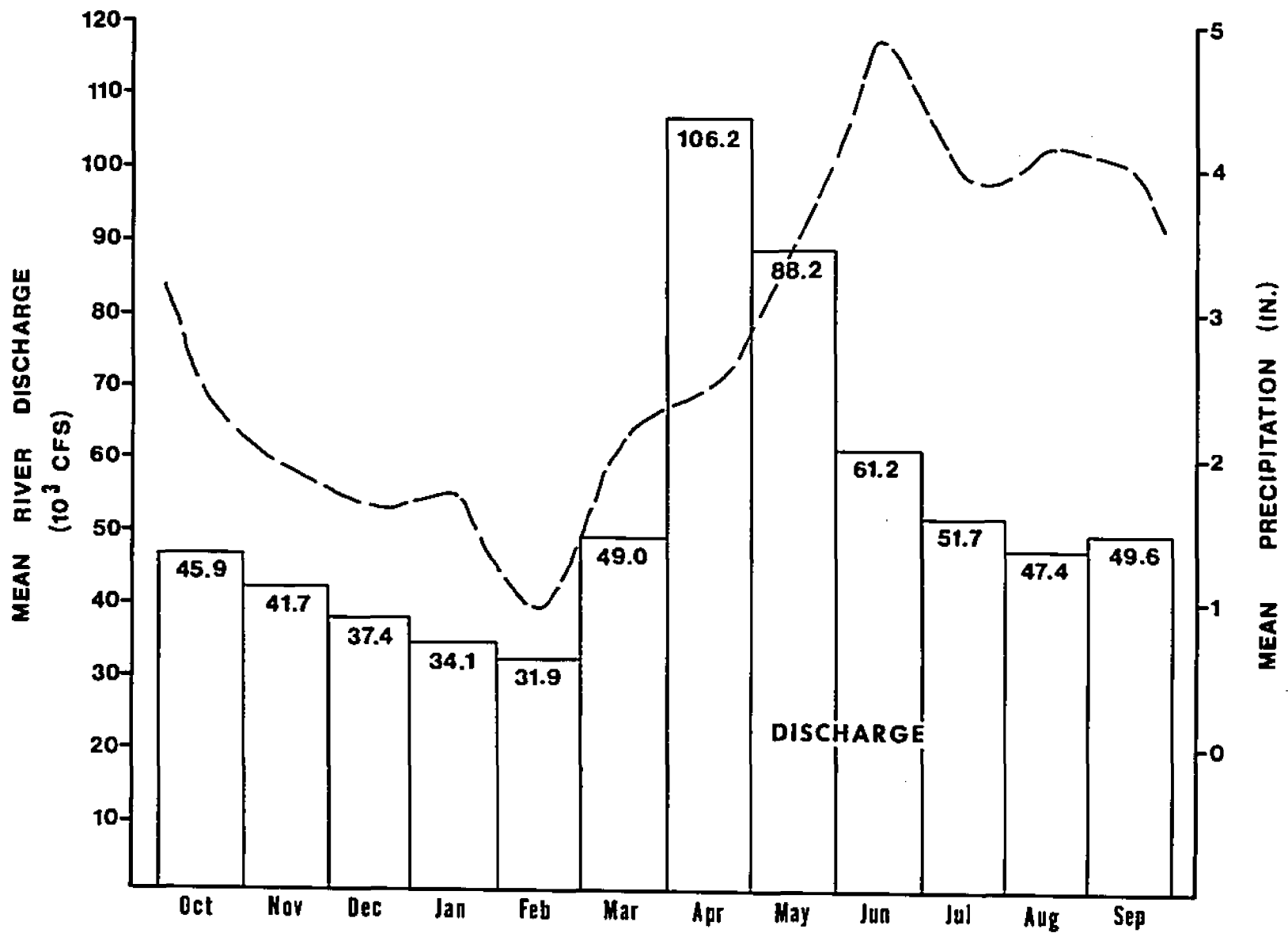


FIGURE 15. Comparison of average monthly precipitation and discharge of the Flambeau River (precip. data from NOAA, 1981; flow data from the USGS gaging station near Bruce).

winter until it begins to rise in March and peaks in April.

Flow data for the Flambeau River have been kept at a gaging station of the U. S. Geological Survey 2.5 mi (4.0 km) downstream of the Thornapple dam since 1951. It is apparent from these records that flow rates of the Flambeau vary considerably from year to year in response to variations in precipitation and soil-moisture conditions. The mean discharge at the station is 1,884 cubic feet per second (cfs) ( $53.3 \text{ m}^3/\text{s}$ ) and the median discharge rate is 1,500 cfs ( $43 \text{ m}^3/\text{s}$ ), placing the Flambeau among the 10 largest rivers in the state. At the point of measurement, 1,897  $\text{mi}^2$  ( $4,911 \text{ km}^2$ ) of the basin have been drained, yielding an average contribution of  $0.99 \text{ cfs}/\text{mi}^2$  ( $0.011 \text{ m}^3/\text{s}/\text{km}^2$ ). Recorded maximum and minimum discharges were 17,400 cfs ( $492 \text{ m}^3/\text{s}$ ) in May of 1954 and 100 cfs ( $3 \text{ m}^3/\text{s}$ ) in August, 1957 (Wiscon. Dept. of Natural Res., 1975). The discharge equalled or exceeded 95 percent of the time at Ladysmith has been established as 734 cfs ( $20.8 \text{ m}^3/\text{s}$ ).

Using the Manning equation and average flow conditions, a mean flow of approximately 1,600 cfs ( $45 \text{ m}^3/\text{s}$ ) was determined for the Flambeau River adjacent to both the pit and waste-containment areas. The Manning equation, when modified for discharge, has the form

$$\bar{Q} = \frac{1.486}{n} AR^{.66} S^{.5} \quad (1)$$

where  $\bar{Q}$  is the average discharge (cfs),  $n$  is a roughness coefficient describing the channel bed,  $A$  is the wetted cross-sectional area of the stream ( $\text{ft}^2$ ),  $R$  is the hydraulic radius, and  $S$  is the stream gradient. A roughness coefficient of 0.037 for the Flambeau River was obtained from Barnes (1967) by subjective comparison with streams having similar bed and stage characteristics. The hydraulic radius is defined as the wetted cross-sectional area divided by the wetted perimeter, where the wetted perimeter is approximated as the channel width for wide, shallow streams. The hydraulic radius may be approximated as the mean depth of a stream, or 3 ft (1 m) in the case of the Flambeau River.

In addition to natural phenomena such as snowmelt and base-flow runoff, flow rates in the Ladysmith area are influenced by the operations of several large power plants, especially the Dairyland REA Cooperative Dam (68-ft head) upstream of the city. Winter declines in streamflow may not correspond to declines in ground-water levels during January and February because water is released from the reservoirs to maintain uniform flow for hydroelectric power generation.

Measurements by the Wisconsin Department of Natural Resources since 1969 show an average water-level elevation of 1085 and a normal high-water elevation of 1086 for the Flambeau River west of the ore deposit (Wiscon. Dept. of Natural Res., 1975). The river is less subject to severe flooding than any other major water course in the Chippewa basin. According to Young and Hindall (1972), floods in the Chippewa

basin are of two general types: 1) Spring floods occurring in March through May due to rapid snowmelt and occasionally concurrent rains, and 2) summer floods in June through September caused by widespread, heavy rainfall of long duration. Most floods are of the spring type, but the largest are usually either summer floods or spring floods caused by a combination of snowmelt and heavy rains. Elevations and flows for the 100-year frequency flood have not been firmly established but have been estimated from data provided by the Big Falls gaging station 12 mi (19 km) northeast of the project area. A 100-year flow of 22,500 cfs ( $637 \text{ m}^3/\text{s}$ ) cresting at an elevation of 1098, or 13 ft (4 m) above the average water level, has been predicted from this information (FMC, 1976) using a flow velocity of 4.5 ft/s (1.4 m/s).

Primary nonwithdrawal uses of the Flambeau River in the area are power generation, disposal of treated sewage and paper-mill effluent, recreation, wildlife habitat, and livestock water. Of these, power generation is the most important. Daily water useage at the Dairyland REA dam in 1965 was estimated at 90.9 million  $\text{ft}^3$  ( $2.6 \times 10^6 \text{ m}^3/\text{d}$ ) (Young and Hindall, 1972). Most local withdrawal use is for industries in and around Ladysmith. The Flambeau is presently not used for domestic supply in Rusk County.

#### Pit-Area Hydrology

At its closest point, the proposed open pit will be about 280 ft (85 m) from the east bank of the Flambeau River.

The reach of the river near the pit varies in width from 280 to 350 ft (85 to 107 m).

Four small streams drain westward from the pit area into the Flambeau (Figure 16). Only one of these, Meadowbrook Creek, is characterized by perennial flow. The other three unnamed streams, called A, B, and C, intermittently drain small basins ranging in area from 101 to 168 acres (41 to 68 ha). This locality also contains two interbasin areas (diagonal pattern in Figure 16) drained by diffuse overland flow and channelized flow not discernible from available topographic data. All drainage basins in the vicinity of the pit location are partially bounded by elevated roadways and ditches which divert and impede surface runoff to varying degrees. Patterns of runoff cannot be accurately discerned from topographic information which does not include such cultural features.

The basin of Meadowbrook Creek covers an area of about 6.4 mi<sup>2</sup> (16.6 km<sup>2</sup>) and extends 6 mi (9.7 km) to the northeast beyond Highway 27 (Figure 16). The stream drains much of the area characterized by drumlinoid features and, as a result, its tributaries occupy linear depressions between the drumlins and are arrayed in a parallel pattern. The basin also contains numerous wetland areas distributed along intermittent streams tributary to Meadowbrook Creek. Though the discharge of the creek has not been measured, the 100-year frequency flood was estimated (FMC, 1976) at 1,800 cfs (50 m<sup>3</sup>/s).

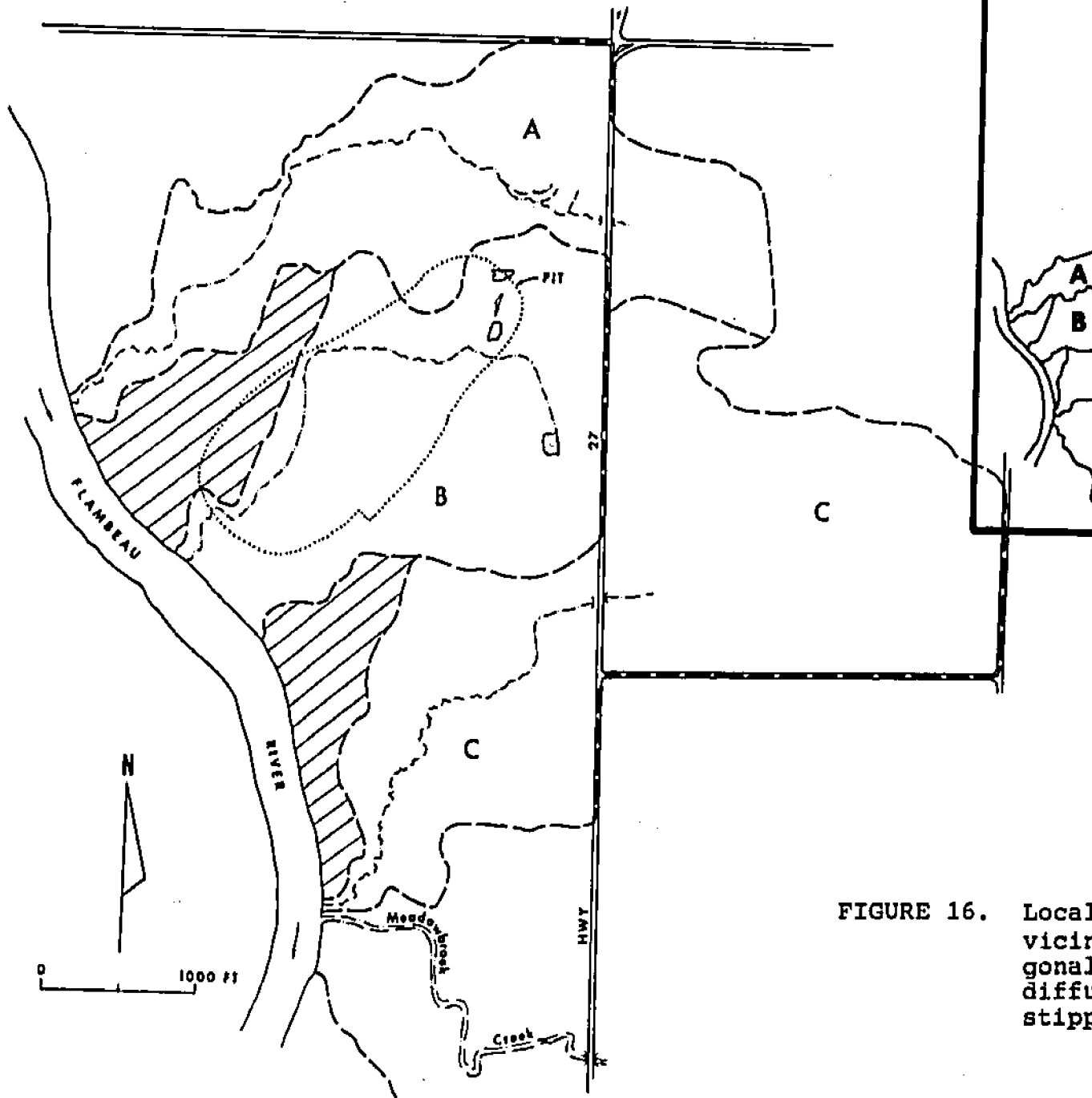


FIGURE 16. Local  
vicin  
gonal  
diffu  
stipp

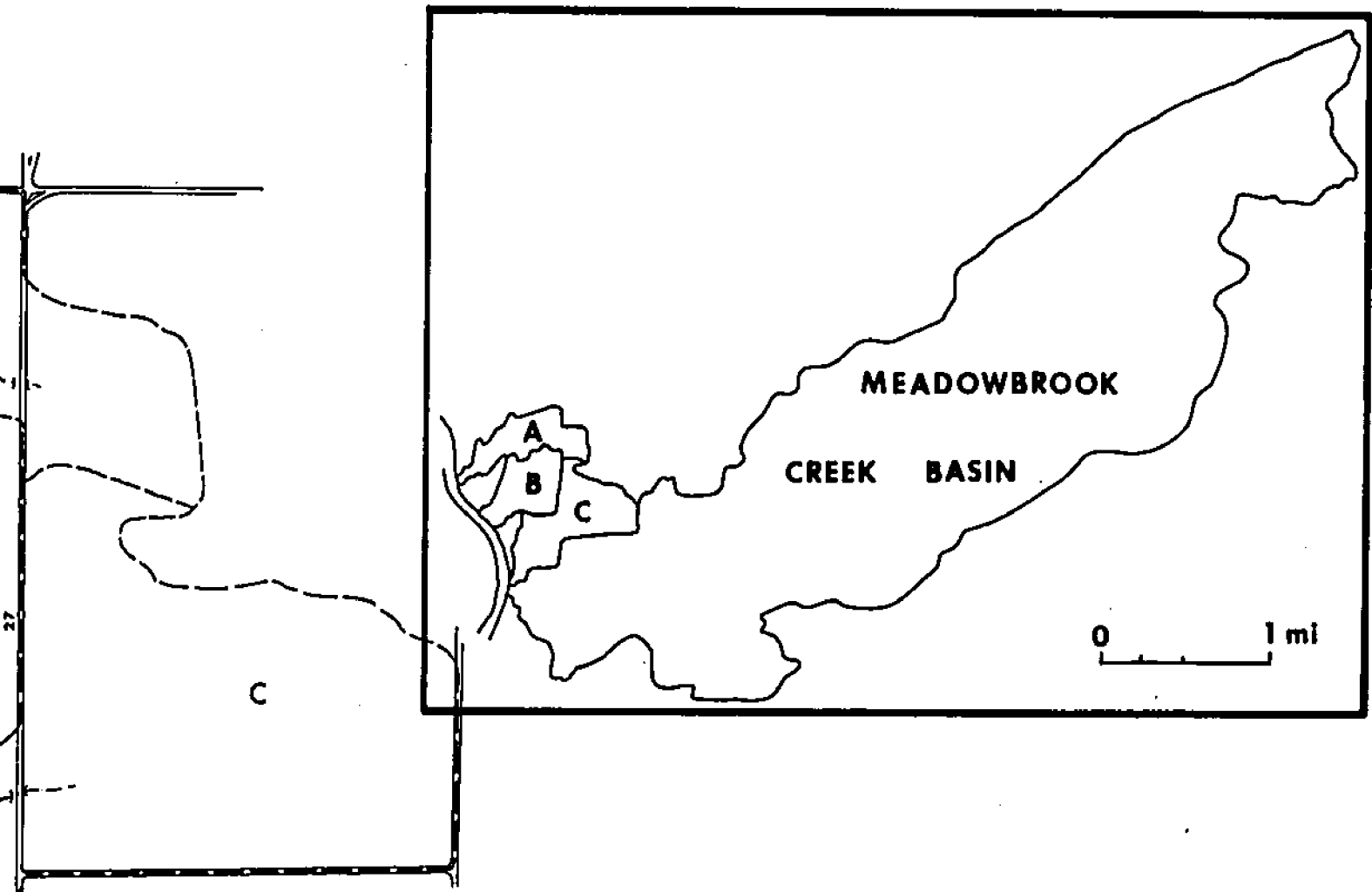


FIGURE 16. Local drainage basins (heavy dashes) in the vicinity of the proposed mine pit. The diagonal pattern indicates areas drained by diffuse overland flow and minor channels; stippled areas are ponds.

Personnel of the Flambeau Mining Corporation measured flows in streams A, B, and C in 1973 using weirs; the results of the measurements are provided in Table 3. It is apparent that flows are relatively minor and no-flow conditions were observed in July, August, and early September (Unpubl. data, FMC; 1973). The courses of streams A and B become less well-defined west of the outwash/till contact, probably due to the higher hydraulic conductivity of the sand and gravel. This evidence suggests that flows originating east of the outwash area may be partially or entirely absorbed by granular material close to the surface, resulting in an influent relationship between streams A and B and the outwash aquifer. Stream channels become better defined again near the Flambeau River. Plans call for the elimination of stream B as the pit reaches its maximum size since nearly all of its course and much of its watershed lie within the proposed excavation. The other streams will be undisturbed or will experience only minor disruptions in drainage area and flow.

There are four small man-made ponds located east and southeast of the initial pit (Figure 16). The ponds range in area from about 0.05 to 0.3 acres (0.02 to 0.12 ha) and are of little hydrologic significance. Three of them will be consumed by the advancing pit. Other very small ponds and wetland areas commonly occupy shallow depressions throughout the site. Wetland areas associated with both the pit and the waste-containment areas are discussed in a later section.



TABLE 3. Discharge data for small streams draining the area of the proposed open pit (modified from unpubl. data, FMC; 1973).

<u>Stream</u>	<u>Drainage Area</u>	<u>Mean Discharge</u> <sup>†</sup>	<u>Maximum Discharge</u> <sup>†</sup>
A	101 acres	0.13 cfs	1.0 cfs
B	101	0.16	1.5
C	168	0.59	6.7
Meadowbrook Creek	4,100	--	--

<sup>†</sup>For the 249-day period from March 20 to Nov. 23, 1973.

TABLE 4. Discharge data for streams draining the area of the proposed waste-disposal structure (from unpubl. data, FMC, 1973).

<u>Stream</u>	<u>Drainage Area</u>	<u>Mean Discharge</u> <sup>1</sup>	<u>Maximum Discharge</u> <sup>1</sup>
E	-- acres	-- cfs	3.1 <sup>2</sup> cfs
F	65	0.13	1.1
G	2,675 <sup>3</sup>	0.72	3.1

<sup>1</sup>For the 249-day period from March 20 to Nov. 23, 1973.

<sup>2</sup>Estimated from stream G data.

<sup>3</sup>Total area drained by streams E and G.

### Waste-Containment Area Hydrology

The proposed waste-disposal structure will be located about 1,600 ft (490 m) south of a large meander of the Flambeau, as shown in Figure 1. The river in this area ranges from 260 to 340 ft (79 to 104 m) in width.

Three unnamed and partially channelized streams, called E, F, and G for this study, drain to the northeast, west, and southwest into the Flambeau River, as shown in Figure 17. This figure also shows areas (diagonal pattern) drained by diffuse overland flow and by channelized flow not detectable from given topographic data. Discharges of the streams were measured with weirs in 1973 and the resulting data are given in Table 4. They generally exhibit sluggish flows and of the three, only stream G flows year-round. Streams E and F are intermittent and may be dry from July through early September (Unpubl. data, FMC; 1973).

The E-G drainage system, with a combined basin area of 4.2 mi<sup>2</sup> (10.9 km<sup>2</sup>), is the largest hydrologic entity near the disposal site, apart from the Flambeau River. Stream E terminates at the eastern edge of a large wetland area in sections 20 and 21 from which stream G originates and flows 2.6 mi (4.2 km) southwestward to the Flambeau. The E-G system will lose an estimated 156 acres (63 ha) from its watershed when the waste impoundment is built. Present plans call for re-routing stream E around the structure's southern side to an existing pond in that area (see Figure 4). Stream F, which

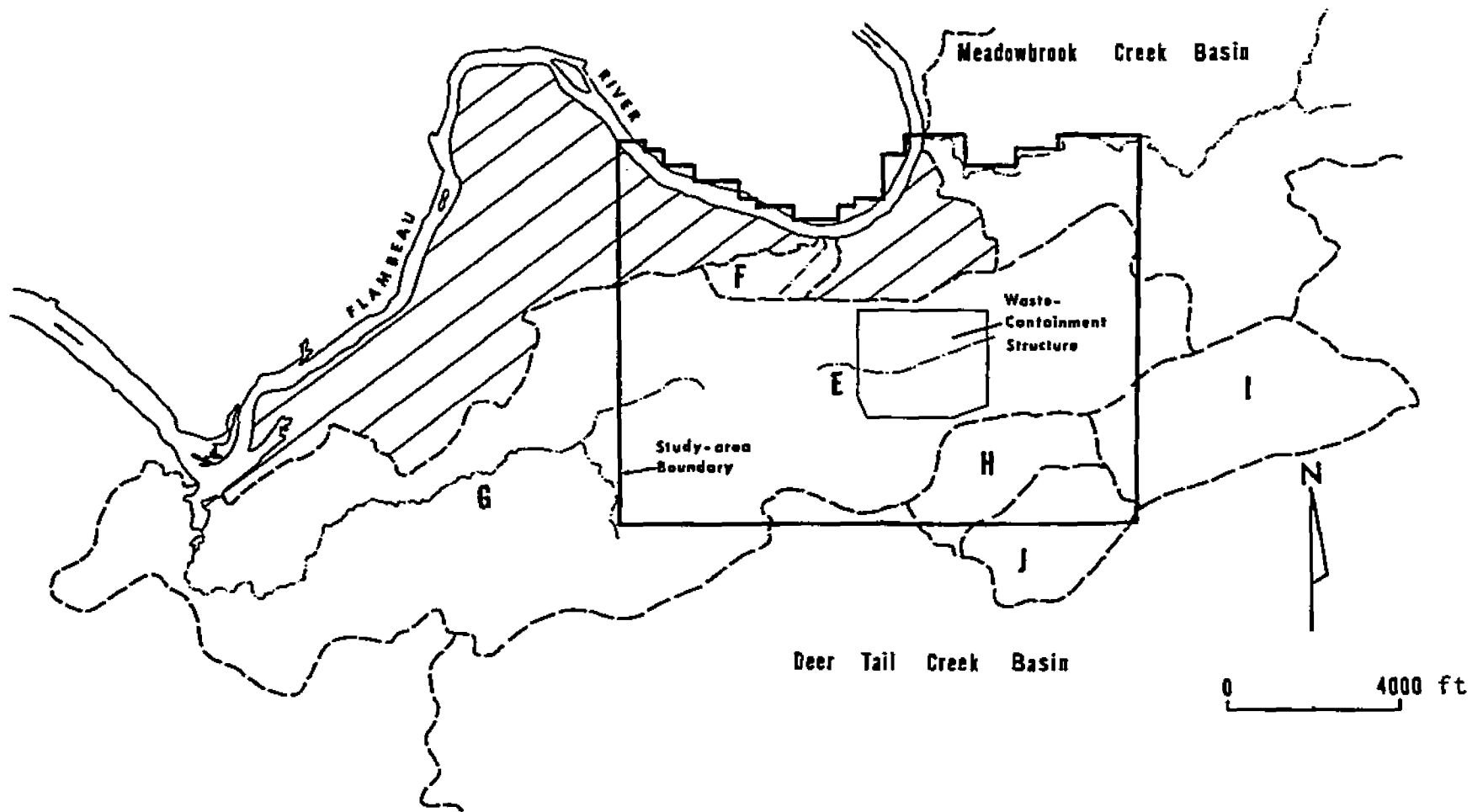


FIGURE 17. Surface-drainage features within the southern study area. The diagonal pattern indicates areas drained by diffuse overland flow and minor channels. Heavy dashes are basin boundaries.

drains an area of 65 acres (26 ha) northwest of the disposal site, will experience little or no modification from activities in the containment area.

Surface drainage in the southern study area, like that in the vicinity of the mine site, is disrupted by elevated roadbeds and ditches which divert and retard runoff. In addition, this area is characterized by an abundance of shallow, nearly closed depressions occupied by extensive wetlands such as basins H, I, and J of Figure 17. Many poorly drained areas of the E-G system and other local basins may contribute to surface flows only during periods of excessive rainfall or snowmelt when wetlands overflow into the encompassing drainage basins. Much of the area south and southeast of the disposal site lies within the basin of Deer Tail Creek which discharges directly into the Chippewa River to the south. This area is similar to the basin of streams E and G in that it is dominated by wetlands that may contribute to streamflow only during excessively wet periods.

#### Wetlands

Wetlands are broadly defined as areas which are periodically flooded by surface water or have ground water at or near the land surface for a major portion of the year (O'Brien and Motts, 1980). They are not a homogeneous group of phenomena and result from a wide array of geologic, hydrologic, and topographic conditions. The continuous conditions of exces-

sive soil moisture give rise to characteristic floral communities and soil associations which form the basis for many wetland classifications.

Wetlands play a prominent role in drainage-basin hydrology, particularly by modifying peak and low flows through the collection and slow release of surface and subsurface runoff, and by affecting water quality. In glaciated areas characterized by ground moraine over impermeable bedrock, Walton (1965) found that more than half of the apparent ground-water runoff in small drainage basins during years of near- or subnormal precipitation is water slowly released from storage within lakes and wetlands. He found that lakes and wetlands often act as natural reservoirs by sustaining and regulating flow within basins during rainless periods. Wetlands adjacent to drainageways often expand and contract during and following storms as a result of rising and receding water tables (Freeze and Cherry, 1979). Expanding wetlands yielding surface water to streams are termed variable source areas and are created by saturation from below, by direct precipitation on wetlands in areas of low relief and tight soils, or by a combination of these endmembers. In addition to these important roles, the recharge/discharge characteristics of the organic mat and the relation of the wetland to the underlying ground-water system are also significant modifiers of the hydrologic regime. The recharge and discharge characteristics of wetlands are discussed more fully in the section of Chapter V on ground-water recharge.

In Figure 20 (page 91), much of the eastern and central parts of Section 20 and the eastern and western portions of Section 21 near the proposed waste impoundment consist of wetlands in the forms of bogs, shrub swamps, sedge meadows, and wooded swamps (FMC, 1976). These wetland areas extend into the western half of Section 20 and beyond the project area, occupying a total area of approximately 1 mi<sup>2</sup> (2.6 km<sup>2</sup>) within the southern study area. Wetland areas also exist over much of the southern half of the area that will be occupied by the disposal structure in Section 21, as well as east and southeast of it in sections 22, 28, and 29. Other wetland areas on or near the project area occur southeast of the pit west of Highway 27, and east and northeast of the pit on the east side of the highway (Figure 19).

The large wetland west of the waste-containment area is drained by stream G which flows 2.6 mi (4.2 km) southwestward to the Flambeau River (Figure 17). Water commonly stands more than a foot (0.3 m) deep in this area, and it is underlain by a few inches to several feet of peat. Stream E is a constructed drainageway within the marshy area to be occupied by the impoundment and has no definite outlet. It terminates within the large shrub swamp west of the disposal site from which stream G originates.

The source of water, frequency and duration of flooding, and local hydrologic conditions are important factors in determining the type of wetland occurring in an area. Wetlands may be fed predominantly by surface water in the form of

direct precipitation, overland flow, or flood waters or by ground-water seepage of a more continuous nature. Wetlands are commonly the result of four groups of general physical characteristics, each producing its own type of wetland environment (Novitzki, 1979). The major endmember types can be grouped by water source and topographic setting. Figure 18A is a wetland occurring within a shallow depression which collects and retains surface runoff. If the bottom of the depression is above the water table, the depression receives only surface water. The water table may rise to the level of the water in the depression for a short time, but the ground-water contribution is minor compared to that of surface water. If the depression intercepts the water table, ground water will be the chief contributor to the wetland condition (Figure 18B).

Wetlands may also occur on slopes where water cannot be retained, as shown in figures 18C and 18D. In the first case, the wetland is perched above the water table and the primary source of water is a lake or river which periodically floods the shore or bank. If the water table intercepts the wetland, ground-water influx may exceed the temporary flood-water input. As in the case of Figure 18A, the water table may temporarily rise to the wetland level, though surface water is still the chief source of water. Water drains downslope as the lake or river stage recedes. Wetlands due to ground-water seepage may also occur on slopes above flood levels (Figure 18D). In this instance, excess ground-water inflow is discharged from the

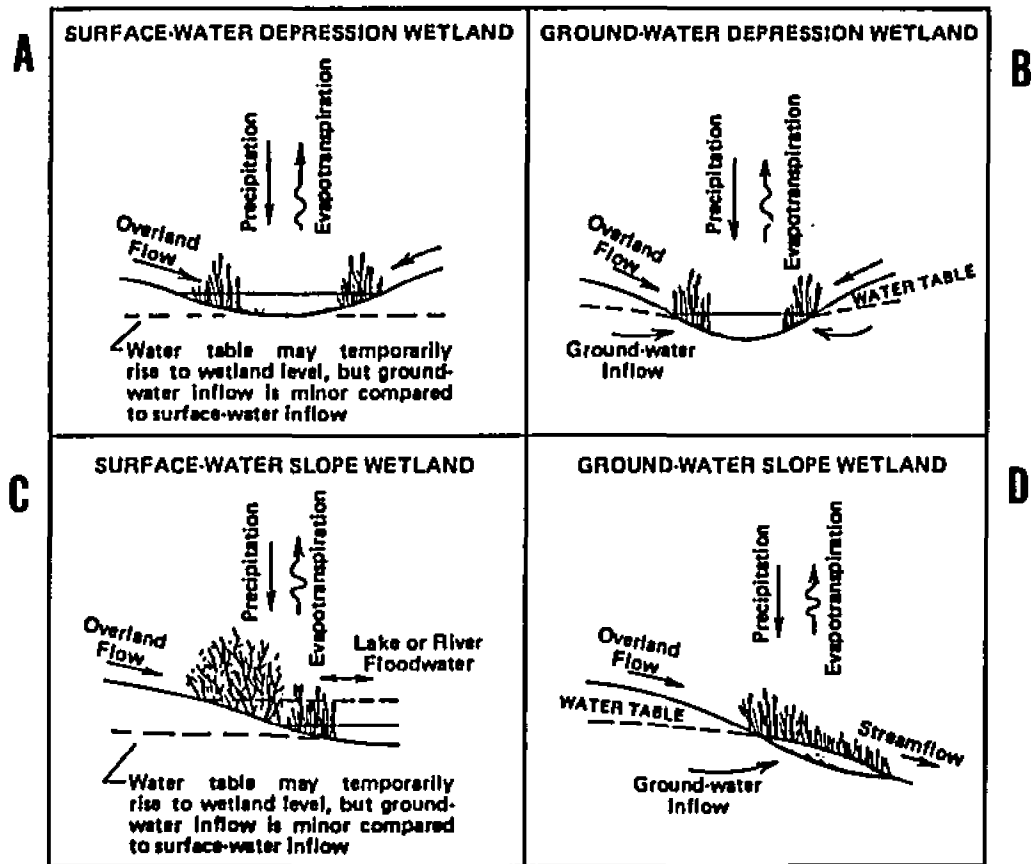


FIGURE 18. Basic hydrologic characteristics of wetlands; the above end members are defined by topographic position and water source (from Novitzki, 1979).



wetland as streamflow.

Wetlands within the project area have not been studied in detail and the hydrologic conditions responsible for their existence must be inferred from other information. In studying wetlands in the northeastern United States, Motts and Heeley (1973) found that those occurring in areas of glacial till commonly result from the perching of surface runoff or flood waters above the perennial water table by poorly permeable soils. Under these conditions, the wetlands are not in direct contact with ground water and are intermittently wet and dry in response to seasonal controls on surface runoff. Most wetlands in the project area, however, appear to be of the ground-water depression type (Figure 18B), though some may alternate between the endmembers in figures 18A and 18B as a result of seasonal variations in precipitation, runoff, recharge, and water-table elevation. In most cases, the wetlands are influenced by or closely related to the water table. In particular, the major wetland areas in sections 20 and 21, though situated in sandy till, appear to be of the permanent ground-water depression type. Supporting evidence for this premise is the perennial nature of stream G which drains the wetland, the propensity for water to stand in the area for much of the year, and water levels in nearby shallow wells that show the water table is nearly coincident with the land surface for most of the year. In addition, the persistent peat blanket in the wetlands near the disposal site indicates this area is perennially affected by ground-water

seepage, except possibly during months when the soil is frozen. Seasonal dry periods would retard peat accumulation by exposing the plant remains to decompositional agents.

## CHAPTER V

### HYDROLOGIC BUDGET

#### Introduction

The various components of the hydrologic cycle can be expressed as a hydrologic budget or water balance. The development of a hydrologic budget is an application of the continuity principle for mass conservation and is a quantitative statement of the balance between total gains and losses of water experienced by a basin during a prescribed time period. The budget includes all surface and subsurface water entering or leaving a basin and assumes the difference between total input and output is balanced by changes in water storage within the basin. For example, if inflows exceed outflows at any time, the total volume of water stored within a basin increases and water levels rise.

A general algebraic expression for the hydrologic budget is

$$P + GWF_i = ET + RO + GWF_o + \Delta GW + \Delta SW + \Delta SM + W \quad (2)$$

where  $P$  is precipitation,  $GWF_i$  is ground water entering a basin across divides (underflow),  $ET$  is evapotranspiration,  $RO$  is total runoff (including ground water discharged to surface drainage),  $GWF_o$  is ground water leaving a basin as underflow,  $\Delta GW$  is the change in ground-water storage,  $\Delta SW$  is the change in surface-water storage,  $\Delta SM$  is the change in soil-moisture storage, and  $W$  accounts for any artificial source or sink of

water. Precipitation is generally the only water source in a basin except for underflow across surface divides, which is usually negligible. Water leaving a basin is included in streamflow, evapotranspiration, underflow and possibly well abstraction. Differences between inputs and outputs are represented by the storage terms. Subsurface storage changes, which are reflected by changes in soil moisture and fluctuations of water levels in wells, are largely controlled by spatial and temporal patterns of precipitation, runoff, and evapotranspiration at the surface.

Some components of the hydrologic budget do not measurably affect the balance between gains and losses in a basin over long periods and may be eliminated from consideration to give a steady-state budget equation. Which components are dropped depends on available data, objectives of the study, the type and characteristics of the hydrologic system, the duration of the budget period, and the phase of the hydrologic regime (e.g., flood versus low-flow conditions). For the present study, each of the two study areas was treated as a basin after adopting the following simplifications to the budget equation:

1. Changes in ground-water storage ( $\Delta GW$ ) average near zero over long periods and can be dropped if precipitation during the data period has been relatively constant.
2. Changes in surface-water storage ( $\Delta SW$ ) are considered negligible since ponds are small and few in number in the project area.

3. The volume of underflow into the study areas (GWF) is regarded as small since surficial deposits up-gradient of each area have low hydraulic conductivities and water-table gradients are low; similarly, underflow from each area is considered small and was neglected in the budget computations.
4. Withdrawals from wells (W) are considered insignificant because the project area is sparsely populated and existing wells are for low-capacity domestic supply.

Given these modifications, the hydrologic budget for each area can be expressed as

$$P = RO + ET + \Delta SM \quad (3)$$

This simplified budget equation was used to define initial recharge and evapotranspiration rates for the digital flow models discussed in later chapters.

#### Major Budget Components and their Measurement

##### Precipitation

All forms of precipitation are measured as the daily accumulation of rainfall in a rain gage. This data is interpreted as the vertical depth of water that would accumulate on a level surface if the precipitation remained where it fell. In the case of snow or sleet, the frozen water is melted and recorded as an equivalent amount of liquid precipitation.

Rainfall data used in the Flambeau study are monthly averages from uninterrupted measurements by the National Oceanic and Atmospheric Administration station at Ladysmith for the 57-year period through 1980 (NOAA, 1981). Precipitation data have also been collected from the Ladysmith Ranger Station northwest of the mine site and by on-site instruments 600 ft (185 m) east of the pit location, though the periods of record are shorter and record-keeping has not been continuous. During the period of official record, the average annual precipitation at Ladysmith was 31.42 ins (798 mm). The reader is referred to the climatological section of Chapter I for an additional discussion of precipitation.

Precipitation is the ultimate source of all water in the study areas. Part of the rainfall runs off the land surface as overland flow and interflow into streams or is returned to the atmosphere via evaporation and vegetal transpiration. A fraction of the precipitation reaching the land surface percolates downward to the zone of saturation and recharges the ground-water system. As will be shown in ensuing pages, the amount of water reaching the water table can be determined by finding reasonable values for components of the simplified water-budget equation.

#### Evapotranspiration

Evapotranspiration, sometimes referred to as consumptive water use, is defined as the sum of water losses to the at-

mosphere by free-water evaporation, soil-moisture and ground-water evaporation, and plant transpiration through leaf stomata. It is typically the single largest outflow from the soil-water system except in very humid, cool climates (Fetter, 1980). Evapotranspiration is controlled primarily by atmospheric demand, soil-water availability, and other meteorological factors discussed in the following paragraphs.

Walton (1970) divided evapotranspiration into two components according to water source: 1) Surface and soil evapotranspiration derived from soil moisture and evaporation from water and vegetation surfaces, and 2) ground-water evapotranspiration derived directly from the water table. The second component is predominantly a function of season and ground-water stage and is sometimes considered a part of the ground-water runoff component of total runoff. In warm, humid climates the majority of the summer precipitation is removed from upper soil layers by evapotranspiration before it can infiltrate to the water table. In fact, evapotranspiration often exceeds summer precipitation in humid regimes, though it may be much less than precipitation during the fall, winter, and early spring. Thus, a large portion of the water discharged annually by evapotranspiration may not be derived from the ground-water reservoir. However, in areas where the water table is shallow enough to maintain capillary rise to the surface, large quantities of ground water may be discharged to the atmosphere by vegetation transpiration or by direct evaporation from the water table. This is especially

true in wetland areas and areas adjacent to gaining streams where water is available to streamside vegetation (Bloyd, 1975).

There are many methods for estimating evapotranspiration (Sokolov and Chapman, 1974), all varying widely in complexity, data requirements, and reliability. The methods are based on evapotranspiration aerodynamics, analysis of the balance between water and energy in a system (Tanner and Pelton, 1960), or are empirical techniques founded on regional relationships among meteorological, climatic, and physical conditions of a study area (Chow, 1964; Thornthwaite and Mather, 1955; 1957). Because of problems inherent in the absolute determination of evapotranspiration, it is often computed indirectly as the difference between precipitation and the sum of the other budget components. For example, rearranging Equation 3 gives

$$ET = P - (RO + \Delta SM), \quad (4)$$

If the term accounting for changes in soil-moisture storage is not included, Equation 4 cannot be used for daily, weekly, or monthly values of evapotranspiration. In January of most years, however, soil moisture in humid climates returns to near field capacity. Net annual changes in soil moisture are thus usually small and can be neglected in yearly estimates of evapotranspiration made with Equation 4.



## Runoff

Total runoff can be resolved into surface-water and ground-water components. Precipitation is subject to several paths within the hydrologic cycle - some is retained on vegetation surfaces (interception storage) from whence it may later evaporate or fall to the ground; water reaching the ground may infiltrate into the soil, collect in puddles as depression storage, or flow overland. Water in depression storage may also later evaporate and(or) infiltrate.

Overland flow may comprise a large part of the surface-water runoff component and occurs when the precipitation rate greatly exceeds the infiltration capacity of the soil and depression storage has been satisfied. Freeze and Cherry (1979) indicate that overland flow is actually a relatively rare phenomenon in time and space, particularly in densely vegetated basins in humid climatic regimes. They state that most overland flow may originate from 10 percent or less of the total basin area.

Water infiltrating into the unsaturated zone above the water table may also be deflected laterally by persistent soil horizons with relatively lower hydraulic conductivities. This horizontal flow above the water table is termed interflow, or storm seepage, and may contribute significantly to local streamflow. Its importance, however, varies widely. It is usually included in the surface-water portion of runoff with overland flow and direct channel precipitation. Surface runoff and interflow are jointly referred to as

direct runoff because of their relatively short residence times within a watershed and less circuitous paths to local drainageways.

Infiltrating water reaching the water table is stored within the ground-water reservoir as recharge to the system. In humid areas, it is eventually discharged to effluent streams and lakes as base flow, which continues to be discharged to surface-water systems long after surface runoff ceases. The ground-water contribution to streams and lakes, both from normal base flow and stream-bank storage, constitutes the ground-water runoff component of total runoff in the hydrologic budget. Base flow is usually not subject to the wide volumetric fluctuations exhibited by surface runoff because the ground-water system responds less rapidly to changes in precipitation and soil moisture. Net ground-water runoff depends in part on the position of the water table with respect to stream stage, which together define the hydraulic gradient and, hence, the rate of ground-water discharge to surface drainage. It is also a function of antecedent soil moisture, the annual distribution of precipitation, the conductivity and thickness of the streambed and underlying materials, water temperature, and the area of contact between the stream and its channel (Dove, 1961). Ground-water runoff to streams is generally at a maximum in spring and early summer due to heavy precipitation and low rates of evapotranspiration which increase recharge. It is effectively reduced by evapotranspiration during summer months

and is at a minimum in late summer.

Bloyd (1975) reported that where ground water sustains streamflow, the shallow water table near streams is a source of moisture for vegetation. As a result, plant growth is usually abundant along channels. Because vegetation near the streams is situated between upland recharge areas and the channels, the plants intercept ground water enroute to discharge. More ground water is thus diverted to vapor discharge during the summer than in winter, contributing to seasonal variations in base flow. In this case, evapotranspiration may be considered a component of ground-water runoff. Even though ground-water levels decline through the fall, ground-water runoff as base flow may increase because ground-water evapotranspiration decreases rapidly.

#### Ground-Water Recharge

Ground-water recharge from precipitation is irregularly distributed in time and space and involves the downward movement of water to the permanent water table under the influence of gravity, soil properties, and head differentials. Even in humid climates, only a small fraction of the annual precipitation usually reaches the water table.

The infiltration of water through the air/soil interface and its subsequent percolation to the water table is a function of such varied factors as topography, land use, vegetal cover, the hydraulic conductivity and thickness of soil above the water table, soil-moisture conditions, the interaction

between infiltrating water and the soil (e.g., swelling or shrinking and flocculation or deflocculation), the effects of raindrop impact on soil surfaces, the activities of soil fauna, and the accumulation of fines in surface depressions (Walton, 1970; Bouwer, 1978). Meteorological factors affecting infiltration and recharge, some of which are directly related to the rate of evapotranspiration, include the occurrence of precipitation as either rain or snow, air temperature, and the intensity, duration, and seasonal distribution of rainfall (Walton, 1970).

Vegetation is one of the most important of the above factors because it promotes infiltration by breaking up compacted soils during growth. The presence of vegetation also tends to retard the downslope movement of water, providing time for it to be absorbed into the soil. On the other hand, vegetation reduces recharge by transpiring much of the percolating water before it reaches the zone of saturation.

Land-use patterns also exert a profound influence on infiltration and recharge. Agricultural practices may either promote or retard infiltration by altering runoff and surface-detention regimes. The clearing of vegetation and plowing are particularly influential in this respect. Extensive areas of impermeable cover typical of urban settings affect recharge by preventing infiltration into the soil, increasing overland flow to surface drainage, and imposing artificial drainage controls.

In winter when temperatures are low, recharge is thought

to occur intermittently or not at all because upper soil layers are frozen, which reduces their hydraulic conductivity, and water is stored as ice and snow in the soil and on the land surface. In addition to this loss of potential recharge by freezing and the lowering of soil conductivities, the viscosity of water varies inversely with temperature so that colder seasons may experience lower recharge rates even if freezing does not occur. Generally, most recharge occurs in the spring when temperatures rise above freezing, evapotranspiration is at a minimum, and soil moisture is maintained at or above field capacity by snowmelt and frequent rains.

During the summer and early fall, evapotranspiration and soil-moisture requirements exceed precipitation so that little percolation to the water table occurs except during periods of excessive rainfall. When a soil-moisture deficit exists, some precipitation replenishes soil moisture rather than continuing downward to the ground-water system. Soil moisture is generally most deficient at the end of summer when evapotranspiration has exceeded precipitation for a prolonged period. It is replenished in the fall and early winter, after which recharge to the ground-water reservoir may resume intermittently until late spring or early summer.

The quantity of water recharging the ground-water system is most reliably determined by measuring the amount of ground-water runoff leaving a basin via streams. This is typically accomplished by using streamflow measurements to devise a rating curve that describes stage/discharge relationships at

any time. From the rating curve, discharge hydrographs are constructed and the base-flow component is isolated through standard graphical separation techniques such as those described by Corbett and others (1945), Chow (1964), and Gray (1970). This basin approach was not satisfactory for the Flambeau project area, however, because the study areas encompass only small portions of Flambeau subbasins, many of which have intermittent surface drainage. The waste-disposal area, in particular, is dominated by wetlands characterized by internal drainage and ill-defined basin divides. In addition, no streamflow records exist for local perennial streams and those for the Flambeau River are available only for the U. S. Geological Survey gaging station 9 river miles (14 km) downstream from the site. These records are unreliable for basin runoff determinations since peak flows are artificially modified by dams upstream of the station.

Assuming that soil water escaping evapotranspiration and soil-moisture replenishment moves below the root zone and eventually joins the ground-water reservoir, the rate of recharge can be determined indirectly as the difference between precipitation and the sum of evapotranspiration, surface runoff ( $RO_s$ ), and changes in soil moisture according to

$$\text{Recharge} = P - (ET + \Delta SM + RO_s) \quad (5)$$

This approach was employed to estimate the annual rate of ground-water recharge at the site and is a combination of

largely empirical procedures outlined by Thornthwaite and Mather (1957) and Fenn and others (1975). Assuming that all ground water recharged locally is eventually discharged to surface drainage, the recharge term in Equation 5 is equivalent to the ground-water runoff component of total runoff.

The method of estimating ground-water recharge first involved the computation of surface runoff ( $RO_g$ ) occurring monthly. The approach employed in this study is based on the rational method for runoff determination and makes use of empirical runoff coefficients (Chow, 1964) dependent on soil texture, slope, vegetation cover, and soil conditions (e.g., frozen, cultivated, impermeable cover, etc.). Runoff coefficients are essentially multipliers for the 100-percent runoff case. Choosing the coefficients requires a considerable amount of judgment so that this method is less reliable than those based on basin hydrograph theory. It was, however, the only approach possible with the data available for the project area. Applying the coefficients to mean monthly values of precipitation gives estimates of the mean monthly surface runoff.

The second part of the estimation procedure consisted of computing the potential evapotranspiration (PET). PET is the water loss occurring if no limit exists to the amount of soil moisture available for plant use. It is dependent on the evaporative capacity of the atmosphere and is determined from meteorological data. The method used for this work (Thornthwaite and Mather, 1957) is based on an exponential rela-

tionship between mean monthly air temperature and PET with adjustments made for the duration of sunlight by including a factor for month and latitude. The effects of soil-moisture availability, changes in soil-moisture storage, and rooting depths of major vegetation types are incorporated into subsequent calculations to arrive at a monthly rate of actual evapotranspiration, neglecting growth stages of vegetation. Equation 5 is then used to arrive at an annual rate for deep percolation by summing the monthly rates. The rates of PET for the pit and waste-containment areas were considered to be equivalent since differences in climatic factors between the two areas are nil.

The PET-determination technique outlined in Thornthwaite and Mather (1957) is embodied by the Thornthwaite Equation (Thornthwaite and others, 1944; Chow, 1964):

$$U = 1.62 \left( \frac{10 t}{TE} \right)^\alpha \quad (6)$$

where

U = monthly PET (cm)

t = mean monthly temperature ( $^{\circ}$ C)

TE = temperature-efficiency index  
(sum of monthly heat indices,

$$\sum_{i=1}^{12} (t_i/5)^{1.514})$$

$$\alpha = 6.75 \times 10^{-7} (TE)^3 - 7.71 \times 10^{-5} (TE)^2 + .01792 (TE) + .49239$$



Monthly PET values computed with Equation 6 must be adjusted for month and latitude to account the for duration of solar insolation (see Table III.2 of Gray, 1970). Further adjustments are needed for vegetation characteristics to obtain values for true evapotranspiration.

A distributed parameter approach accounting for areal variations in budget components was adopted by dividing the pit and waste-containment areas into four major physical categories on the basis of vegetation and general soil type: 1) Wooded loams and silt loams, 2) loams and silt loams with pasture vegetation, 3) wooded fine sandy loams, and 4) fine sandy loams with pasture conditions. These areas are shown in figures 19 and 20 along with other factors affecting ground-water recharge. The pasture types include all fields and residential areas; the wooded areas are characterized by deciduous or mixed deciduous-coniferous vegetation. These groupings were used to arrive at estimates of annual ground-water recharge through a determination of actual evapotranspiration rates and surface runoff (Appendix II). The results of the calculations are summarized in Table 5.

Given a mean annual precipitation rate of 31.42 ins (798 mm), the values in Table 5 indicate that 70 to 73 percent of rainfall is consumed annually through evapotranspiration. From 10 to 12 percent of the precipitation in areas of sandy soils runs off via overland flow compared to 24 to 27 percent in areas dominated by heavier soils. Approximately 16 percent of the precipitation on sandy soils becomes deep percolation

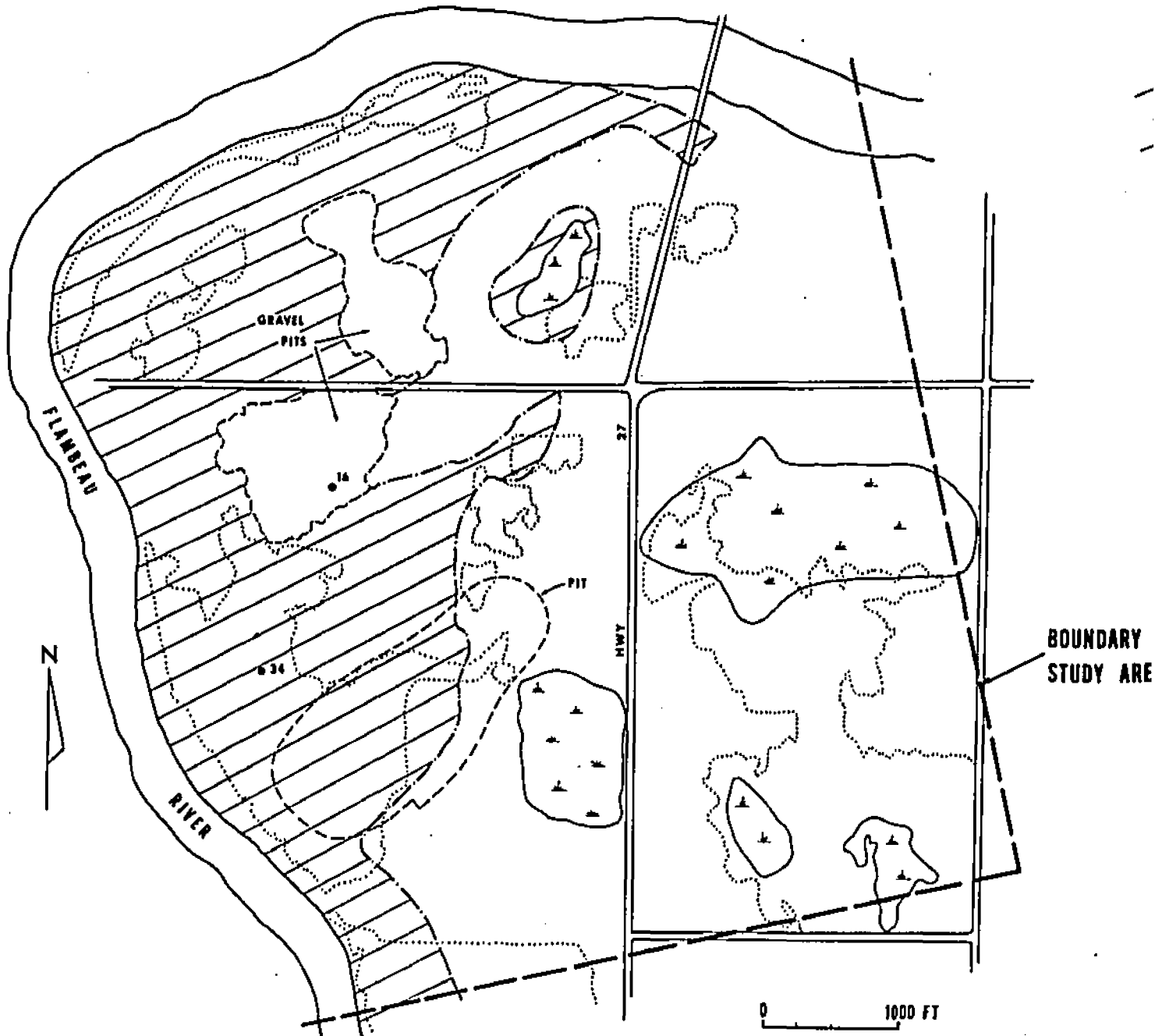
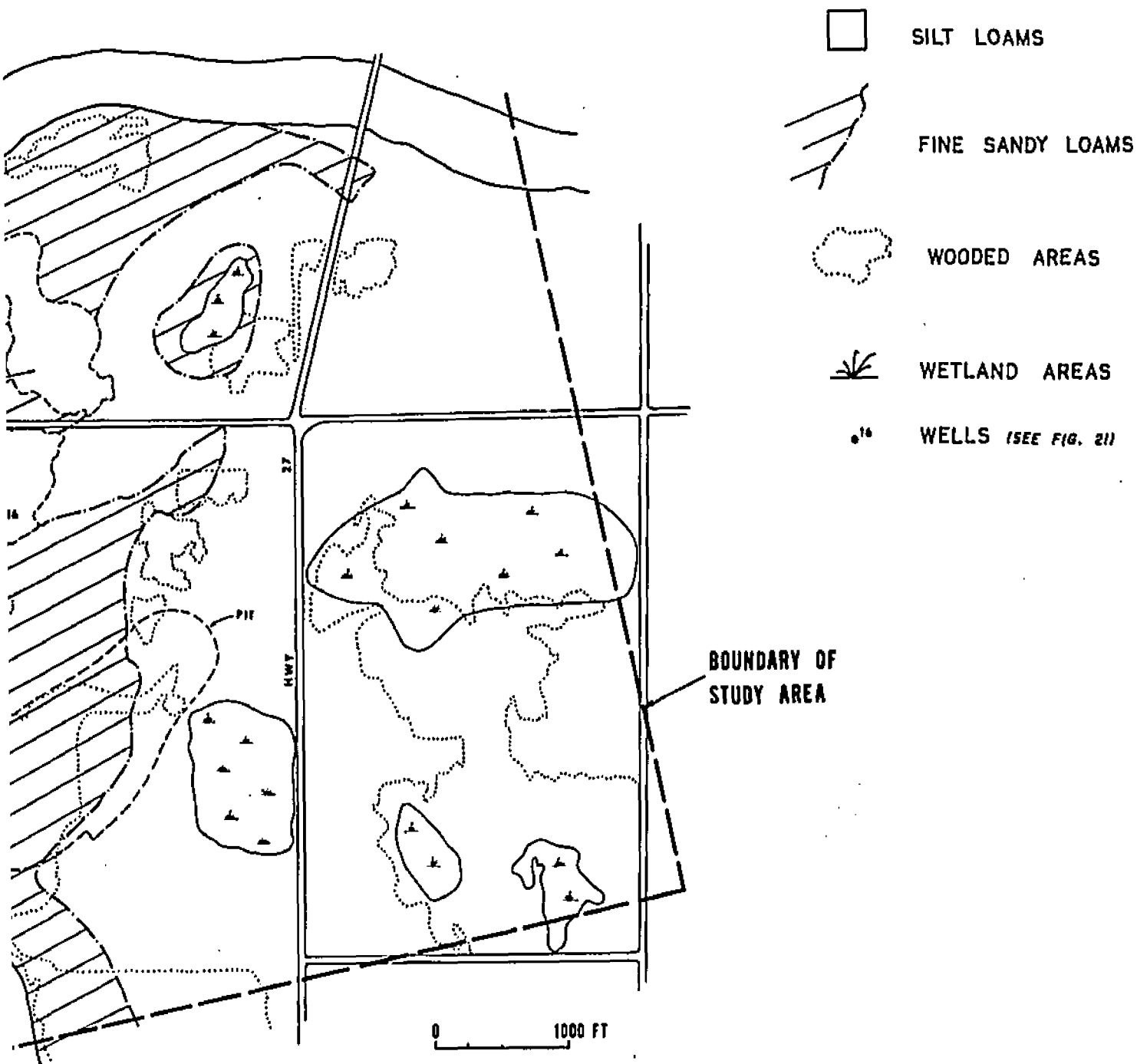


FIGURE 19. Distribution of features affecting ground-water recharge location. Nonwooded areas are assumed to be characterized by conditions (grassy or shrub vegetation).



distribution of features affecting ground-water recharge near the open-pit cation. Nonwooded areas are assumed to be characterized by pasture conditions (grassy or shrub vegetation).

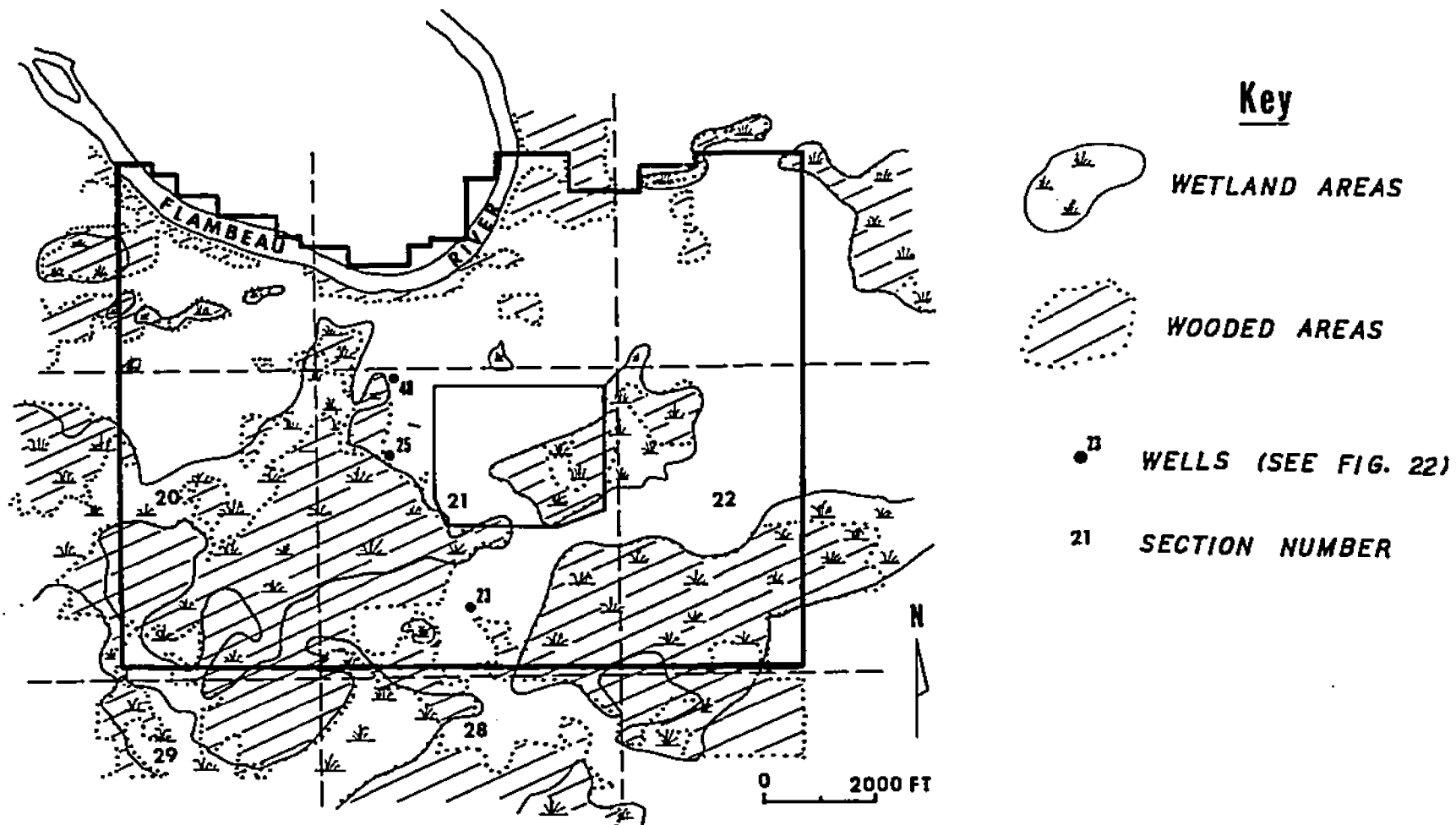


FIGURE 20. Distribution of features affecting ground-water recharge in the waste-containment area. Nonwooded areas are assumed to be characterized by pasture conditions (grassy or shrub vegetation). Only loams and silt loams are known to occur in this area.

TABLE 5. Annual rates of evapotranspiration, runoff, and recharge for each of the four area categories identified in the Flambeau project area (see Appendix II for calculations).

<u>Area Type</u>	<u>Evapotranspiration</u>	<u>Surface Runoff</u>	<u>Recharge</u>
Sandy Loam:			
pasture	22.6 ins	3.9 ins	4.9 ins
wooded	22.8	3.2	5.4
Silt Loam:			
pasture	22.0	8.4	0.8
wooded	22.5	7.6	1.3

(ground-water recharge) while only 4 percent or less becomes deep percolation in areas with silty soils. The calculations in Appendix II show that most recharge occurs in December through April with March having the greatest monthly volume. Evapotranspiration occurs from April through October with 60 percent of all vapor discharge taking place in June, July, and August.

It is important to note that estimates of deep percolation made with this indirect method accumulate errors from estimates of all the other components. Since recharge is often small compared to the other budget components from which it is derived, large percentage errors in the recharge rate may result. Rushton and Ward (1979) note that classical empirical methods for periods greater than one day may significantly underestimate recharge because short periods of recharge may be masked by the averaging of weekly or monthly

data. They determined that the use of monthly data could lead to underestimates of about 3 percent for recharge. Due to uncertainties in other inputs as well, overall recharge calculations of the type employed for the project area may be in error by as much as 15 percent. Further, the empirical approaches do not usually permit recharge during any period in which a soil-moisture deficiency exists, as shown in Appendix II. Kitching and others (1977), however, reported recharge during nearly every month in a lysimeter study on the Bunter Sandstone of North Nottinghamshire, England, in spite of a regional soil-moisture deficiency. An examination of potential recharge routes provides an explanation for this discrepancy. In nearly every case, empirical methods for estimating ground-water recharge do not account for deep percolation through vertical fractures in the unsaturated zones of soils and rock through which water may reach the water table with little or no effect on general soil-moisture conditions. Also, most of these methods do not account for water running overland and collecting in influent ditches, depressions, and stream channels, as may occur with intermittent streams A and B near the mine site.

Annual water-level changes in wells at the site suggest that recharge does occur more uniformly throughout the year than the computations indicate. Figures 21 and 22 compare monthly ground-water levels in five observation wells in the project area with the computed monthly recharge rates in Appendix II. Two wells (Figure 21) are located in the area of the proposed mine pit: Well 16 in sandy soil with pasture

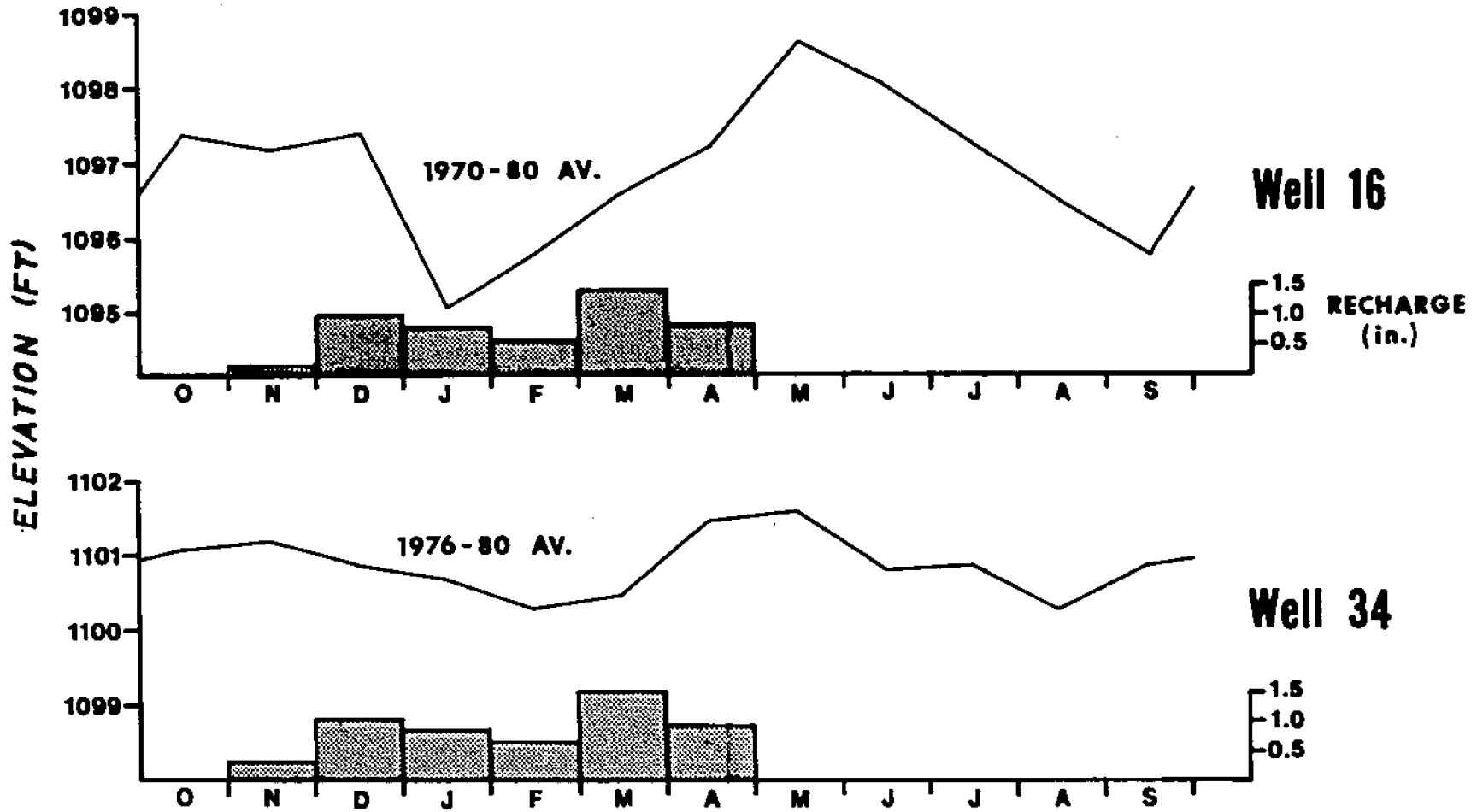


FIGURE 21. Comparison of average monthly fluctuations in ground-water levels and estimated recharge in the pit area (water levels from unpubl. data, FMC; recharge rates from Appendix II).

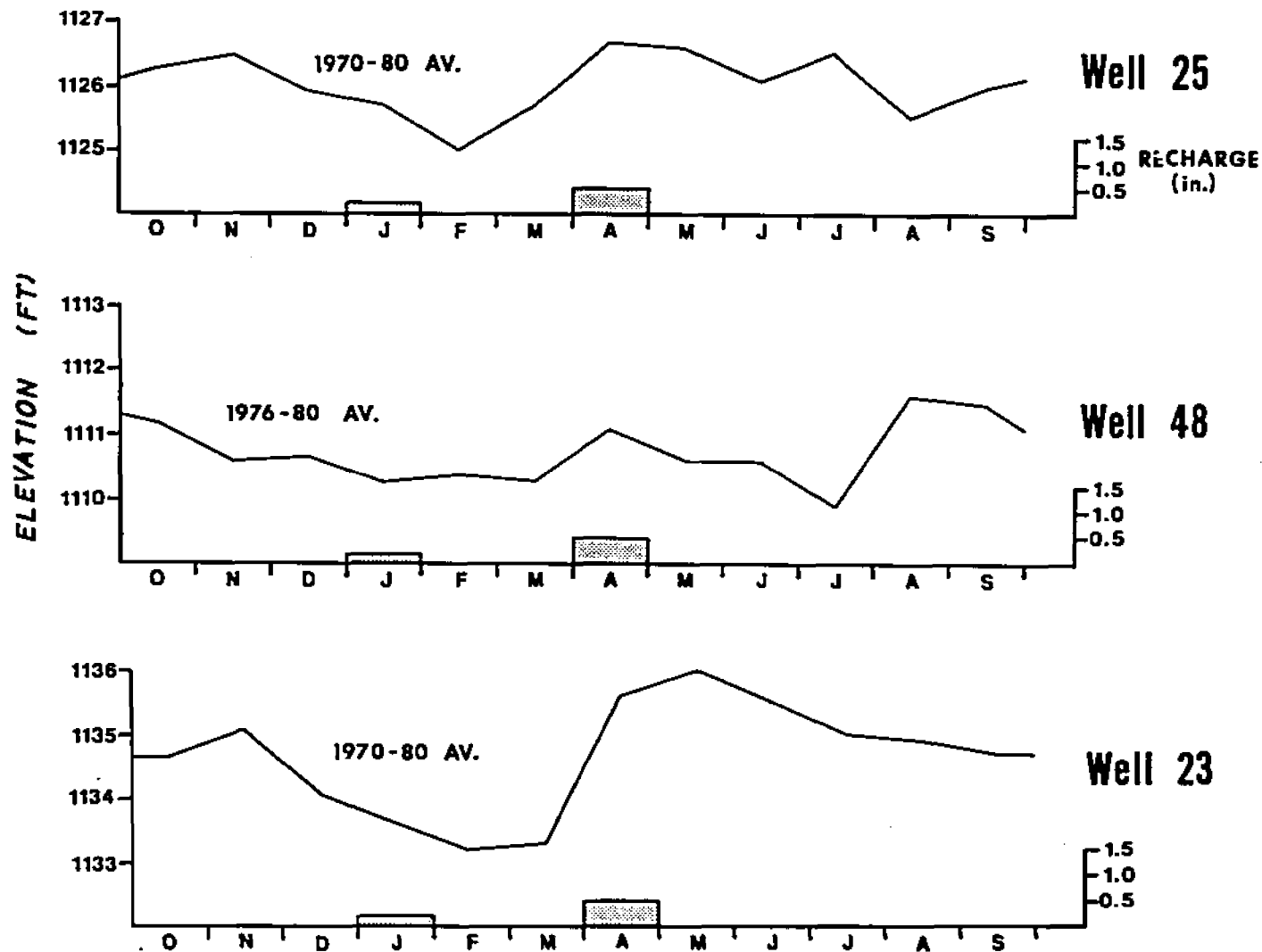


FIGURE 22. Comparison of average monthly fluctuations in ground-water levels and estimated recharge in the waste-containment area (water levels from unpubl. data, FMC; recharge rates from Appendix II).



conditions (in a gravel pit) and well 34 in wooded sandy soil. Similarly, Figure 22 shows fluctuations in three wells in the waste-containment area: Well 25 in till near a wetland area, well 48 which is finished in a deep outwash zone overlain by 46 ft (14 m) of till, and well 23 in a non-wetland till area. The areas around these three wells have silt-loam soils at the surface. The locations of all five wells are shown in figures 19 and 20.

Once melting begins in February and March ice, snow, rainfall, and low rates of evapotranspiration contribute to deep percolation. Figures 21 and 22 demonstrate a direct relationship between spring recharge and water-level increases on the sites. Water levels begin to rise as early as January in well 16 which is finished in outwash near the mine pit. In all cases except that of well 48, maximum water levels are attained in April or May in response to the input from earlier melting and spring rainfall. After the April/May peak, water levels generally decline as recharge effectively ceases due to increasing evapotranspiration, even though precipitation peaks and then slowly decreases in June through August. Only well 23 in the non-wetland till setting exhibits a more or less continuous water-level regression from the April/May peak to the February low. Wells 34 and 25 show gradual increases in water levels from August to a secondary peak in November, possibly illustrating recharge in late summer as evapotranspiration declines while precipitation is maintained at high rates through mid-October. Wells 23 and 16 show a

similar pattern with secondary highs in November and from October through December, respectively. Late-summer/early-fall recharge is not indicated by the empirical methods used in the study, pointing to possible limitations in the technique, as noted by Rushton and Ward (1979). In the absence of more definitive information, however, the computed recharge values in Table 5 were used in numerical simulations described later with the acknowledgement of possible limitations and with modifications reflecting local conditions.

An interesting characteristic of Figure 22 is the subdued response of well 48 to spring recharge. This well is finished in a deep outwash zone and is insulated from the immediate effects of snowmelt, precipitation, and soil-moisture changes by the overlying till layer. Not only do water levels remain more constant with time compared to the other wells, but the water level begins rising in July and peaks in August, probably reflecting the delay required for the large pulse of spring recharge to reach the outwash through the till layer. On the other hand, the pronounced seasonal water-level fluctuations in well 16 (Figure 21) may indicate direct recharge to the shallow outwash in pasture areas near the ore deposit. The rapidity of recharge in areas dominated by highly conductive materials probably translates into less water loss from surface runoff and evapotranspiration during infiltration, allowing a greater fraction of total precipitation to recharge the system. The large pulse of spring recharge therefore results in fluctuations of larger amplitude than in areas

characterized by heavier soils. Stored water is also easily lost from the outwash as base flow to the nearby Flambeau River so that rapid rises are typically followed by rapid recessions. Well 34 might be expected to behave in a manner similar to that of well 16, but its static water level fluctuates much less. The difference may be attributed to the placement of well 16 within an internally drained gravel pit where finer surface soils have been removed, exposing coarse materials which are less densely vegetated and more efficient at capturing precipitation than undisturbed sandy loams. The large amplitudes of fluctuations in well 23, in spite of its location within an area of heavier soils, may be due to its position in a relatively flat area at the base of slopes to the south. Runoff from the slopes is directed onto the flat area where conditions are more conducive to infiltration and recharge.

Williams (1968) concluded that many wetlands occupying small closed depressions in glacial till in Illinois commonly alternate as recharge and discharge areas in response to the seasonal availability of water. Evapotranspiration from wetland surfaces during dry seasons causes many of them to become ground-water sinks. During periods of heavy rainfall, however, surface runoff into the lowlying wetlands results in the creation of underlying ground-water mounds with the subsequent reversal of local gradients and recharge to the ground-water reservoir. There is presently no information to quantitatively document this phenomenon at the Flambeau

site, but for purposes of the study it was assumed that wetlands are always discharge areas or that seasonal recharge is approximately balanced by discharge in areas where alternating conditions occur. In either case, net recharge is near zero for long time periods.

#### Validation of Budget Values

To check the validity of the computed values in Table 5, comparisons were made with published estimates for this geographic area and other physically similar areas. Young and Hindall (1972) cite average annual conditions for the Chippewa River basin based on measurements at 30 gaging stations of the U. S. Geological Survey during the period from 1931 to 1960. These data show an average of 10.7 ins (272 mm) of total runoff. Sather and others (1971) estimate that total runoff for all of western Wisconsin averages 11.6 ins (295 mm). For comparison, total runoff for the pit and waste-containment areas may be approximated as the sum of surface runoff and recharge (or precipitation minus actual evapotranspiration), assuming all recharged water eventually becomes base flow. This is a valid assumption if long-term changes in ground-water storage are negligible. The values in Table 5 yield total runoff rates from 8.6 to 9.2 in/yr (218 to 234 mm/yr), or 27 to 29 percent of the average annual precipitation. These values compare reasonably well with the published basin-wide and regional averages.

Bloyd (1975) reported an estimated annual rate of slightly less than 24 ins (610 mm) for potential evapotranspiration in north-central Wisconsin. The empirical Thornthwaite method yielded a PET rate of 23.0 in/yr (584 mm/yr) which agrees closely. The rate of actual evapotranspiration for the Chippewa basin cited by Young and Hindall (1972) is 20.5 in/yr (521 mm/yr) while the average rate computed from the site-specific rates is 22.5 in/yr (572 mm/yr). The computed rate is 10 percent greater, however, the two study areas together include only about 0.05 percent of the total basin area, so deviation from basin norms are expected for some budget components due to site-specific conditions.

Harder and Drescher (1954) determined an average annual recharge rate of 5.4 ins (137 mm) for an area of sandy outwash in Langlade County about 100 mi (160 km) east-southeast of Ladysmith. Precipitation in that area averages 30.5 in/yr (775 mm/yr) which is nearly identical with that of the project area. Their recharge value agrees very well with those computed for sandy soils on the Flambeau site which average 5.1 in/yr (130 mm/yr).

Young and Hindall (1972) reported a generalized low-flow runoff (base flow) rate of 0.0 to 0.19 cfs/mi<sup>2</sup> (0.0 to 0.002 m<sup>3</sup>/s/km<sup>2</sup>) for the Chippewa River basin. Bloyd (1975) derived a rate of 0.26 cfs/mi<sup>2</sup> (0.003 m<sup>3</sup>/s/km<sup>2</sup>) for much of the same region using 60-percent flow duration data to approximate base flow at times when evapotranspiration is at a minimum, such as during the winter. His value is thus a maximum.

With the exception of a small area south of the proposed pit location, all recharge occurring within the northern study area (delineated by the boundaries in Figure 25) becomes base flow to the Flambeau River. By summing the total volume of annual recharge in each of the four area categories in Table 5, an annual average of 0.234 cfs ( $0.007 \text{ m}^3/\text{s}$ ) was computed for the area around the mine site (Table 6). The northern study area encompasses  $1.6 \text{ mi}^2$  ( $4.1 \text{ km}^2$ ), but only  $1.1 \text{ mi}^2$  ( $2.8 \text{ km}^2$ ) of this area contributes to base flow once the areas of the river, wetlands, and areas not contributing directly to the Flambeau are excluded. Normalizing the total recharge rate gives a value of  $0.15 \text{ cfs}/\text{mi}^2$  ( $0.002 \text{ m}^3/\text{s}/\text{km}^2$ ) which agrees well with the range given by Young and Hindall (1972), though it does not include underflow into the study area contributing to base flow.

Similar calculations were made for the waste-containment area which is almost entirely mantled by silts and silt loams. These calculations were made using unpublished maps of wetland and wooded areas more detailed than Figure 20 so that areas could be determined more accurately. Only those parts of the southern study area north of a ground-water divide roughly paralleling County Road P (see Figure 26) contribute base flow directly to the Flambeau River. The computed volumetric rate of recharge to the entire study area of  $3.8 \text{ mi}^2$  ( $9.8 \text{ km}^2$ ) is 0.147 cfs ( $0.004 \text{ m}^3/\text{s}$ ), of which about 0.05 cfs ( $0.001 \text{ m}^3/\text{s}$ ) accounts for base flow from the area north of the disposal site. This latter rate represents

TABLE 6. Recharge data for the mine and waste-containment areas based on the water-budget rates in Table 5.

---

OPEN-PIT AREA:

<u>Area Type</u>	<u>Estimated Area</u>	<u>Recharge Rate</u>	<u>Annual Recharge Volume</u>
Sandy Loam:			
Wooded	6,038,000 ft <sup>2</sup>	0.450 ft/yr	2,717,100 ft <sup>3</sup> /yr
Pasture	8,195,000	0.408	3,343,560
Silt Loam:			
Wooded	3,510,000	0.108	379,080
Pasture	13,843,000	0.067	927,480
Totals:	31,586,000 <sup>1</sup>		7,367,220
	(1.13 sq. mi.)		(0.234 cfs)
WASTE-CONTAINMENT AREA:			
Silt Loam:			
Wooded	8,963,000	0.108	968,000
Pasture	54,848,000	0.067	3,674,820
Totals:	63,811,000 <sup>2</sup>		4,642,820
	(2.29 mi. sq.)		(0.147 cfs)

---

<sup>1</sup> Total area is the portion of the pit area contributing base flow directly to the Flambeau River, exclusive of wetlands and other non-contributing areas.

<sup>2</sup> Total area is that portion of the waste-containment area receiving recharge, i.e., total area minus discharge areas.

a contributing area of 1.3 mi<sup>2</sup> (3.4 km<sup>2</sup>). The lower base-flow seepage rate in the waste-containment area may be related to a lack of shallow granular soils in the contributing areas adjacent to the Flambeau River. The slowly permeable till impedes ground-water recharge and underflow, resulting in lower discharges to streams.

It should be noted that much of the wooded acreage in the waste-containment area corresponds to wetlands. These areas were not suited for cultivation and so were not cleared. The net recharge in these areas is considered to be near zero and they were not included in the recharge calculations for wooded portions of the site.



## CHAPTER VI

### HYDROGEOLOGY

#### Occurrence of Ground Water

Ground water is contained primarily within the saturated voids of the unconsolidated glacial materials and the Cambrian sandstone that overlie the Precambrian surface. For this reason, the hydrologic study was limited to the Paleozoic and Pleistocene sediments within the project area.

The intercrystalline voids in unweathered crystalline rocks are very small and are usually not interconnected. The primary hydraulic conductivity of the fresher Precambrian rocks is thus sufficiently small for them to be considered impermeable. To some extent, however, ground water may exist in fractures within several hundreds of feet of the weathered Precambrian surface, although the dense, fine-grained saprolite probably inhibits free water movement between the basement rocks and the overlying younger materials. The secondary hydraulic conductivity of the shallow crystalline rocks, while perhaps important, is poorly documented at present. Its existence is known from drilling data. For example, oxidized copper minerals were noted in drill cores from as deep as 100 ft (30 m) (May, 1973b), suggesting water movement along fractures. In addition, an artesian flow of water was reported from a drill hole north of the pit location. The flow rate was less than 5 gpm (gallons per minute) (19 l/min) and the source was an apparent fault zone 300 ft (90 m) below

the surface.

The occurrence and areal geometry of the glacial deposits and sandstone at both study areas were discussed in Chapter III. The saturated thickness of the surficial cover and Cambrian sandstone in the pit area, as defined by drilling and water-level measurements in wells, is illustrated in Plate 6. The thickness of the zone of saturation was examined in detail only in the vicinity of the open pit where a well-defined lower boundary of low hydraulic conductivity (the Precambrian surface) could be established with confidence. Data from the area of the proposed disposal impoundment did not permit clear definition of the Precambrian surface and water table over much of the southern study area, so no attempt was made to map the saturated thickness there. It may be approximated near the structure site as the thickness of the glacial deposits in Plate 3.

The saturated thickness in the vicinity of the mine pit ranges from less than 5 ft (1.5 m) at the west end of the proposed pit perimeter to more than 75 ft (23 m) to the northwest (Plate 6). In general, areas of lesser saturated thickness are associated with surface drainageways near the Flambeau River and bedrock highs where unconsolidated materials are thinner due to nondeposition or removal by erosion. Areas where saturated thicknesses are 25 ft (7.6 m) or less extend eastward from the pit's west end and occur both north and south of the pit perimeter. The greatest saturated thicknesses occur beneath topographic highs composed of unconsol-

dated deposits and in areas where preglacial drainage features incised into the bedrock have been filled with sediments. Examples of such areas occur northwest, northeast, and southeast of the pit perimeter. The saturated thickness increases to the northwest and southeast into probable preglacial drainage courses and also to the east as the land elevation increases away from the Flambeau River valley. Within the planned pit perimeter, the saturated thickness increases uniformly eastward from less than 5 ft (1.5 m) at the west end to 60 ft (18 m) or more in several places at the eastern margin. The saturated zone may approach 45 ft (14 m) in thickness at the southwest edge of the pit.

#### Availability of Ground Water

The Precambrian bedrock here and throughout most of the Superior Upland is a poor aquifer with well yields ranging from zero to 10 gpm (38 l/min) from fracture porosity (Borman, 1971b). Summers (1972) cited the low specific capacity of Precambrian rocks in the Rothschild area of Marathon County 82 mi (132 km) southeast of Ladysmith and proposed special techniques for locating wells in areas of greater fracture density to improve yields. The poor productivity of most crystalline materials attests to their very low conductivity which is directly related to their low porosities. Weathered granitic material near the Precambrian surface may possess porosities of up to 10 percent, but the porosities of unweathered granites and schists seldom exceed 1 percent (U. S.

Geological Survey, 1977). These figures indicate that, in addition to their inability to transmit large quantities of water, crystalline rocks have little capacity to store water and so cannot offer sustained yields to wells.

The till is generally not a source of water supply because of its fine-grained character. It is quite sandy and transmits and stores water in sufficient volumes to be important in terms of the total hydrologic system. Its hydraulic conductivity, however, is such that well completion is normally not feasible, though in places sand and gravel lenses within it are sufficiently productive to satisfy domestic water needs. The quantity of water available from outwash zones within the till depends on their extent, their hydraulic conductivity, and sources of recharge. Within the Chippewa River basin, yields of 5 to 15 gpm (19 to 57 l/min) may be obtained from buried outwash lenses which are typically less than 5 ft (1.5 m) thick (Young and Hindall, 1972).

The aquifers in the area with the greatest productive potential are the buried sand and gravel deposits within the ancestral Flambeau River valley (Figure 2). These deposits are evident in drilling data from the mine site, but their local extent has not been firmly established beyond the immediate project area. Devaul (1975) indicates they extend northward just beyond Ladysmith and southward to County Road P near the waste-disposal site, though his boundaries appear to reflect limitations in data rather than actual deposit limits. Potential yields of more than 500 gpm (1,900 l/min)

have been reported from this thick sequence of granular material (Borman, 1971a; Devaul, 1975). The City of Ladysmith draws its water from four wells completed in these sediments on the far side of the river northeast of the mine area. Yields from these wells range from 260 to 590 gpm (984 to 2,233 l/min) (Unpubl. data, City of Ladysmith).

The Cambrian sandstone, while capable of storing and yielding modest quantities of water, is thin and areally sporadic, especially north and east of the project area where existing information indicates it is completely absent. It probably constitutes only a minor source of ground water for users in the region.

#### Aquifer Characteristics

To examine the physical properties of the ground-water flow system within the project area, 28 observation wells were installed in 1970, eight wells in 1971, five in 1972, and two in 1975. Eleven other wells, for which no drilling dates are available, were installed prior to 1976. To augment this network, water levels in eight residential wells in the project area, one diamond drill hole, and seven cased soil borings have also been monitored. Some observation stations have been abandoned over the years because of silting and access problems. Presently, 60 monitoring stations (figures 23 and 24) are included in the hydrologic surveillance network.

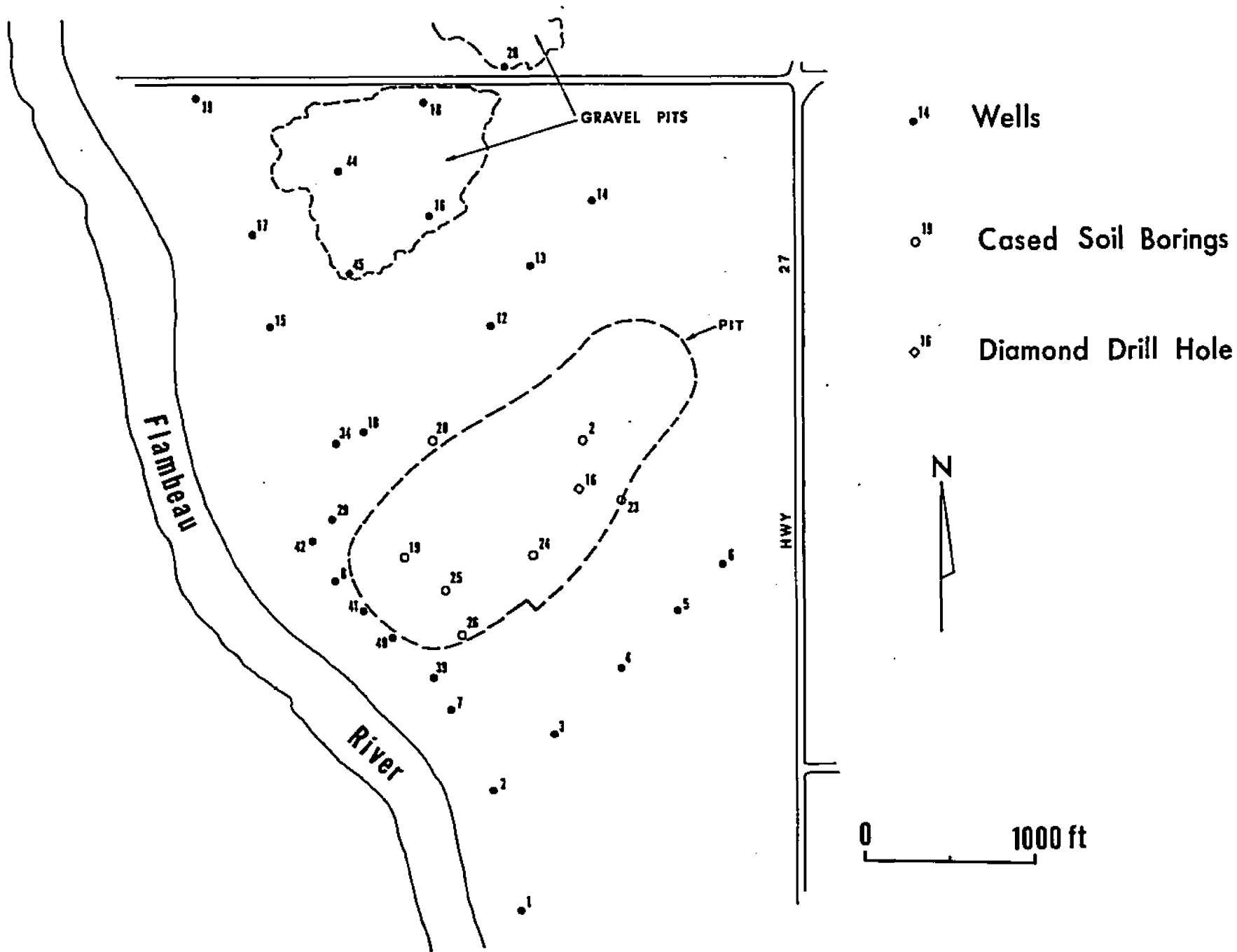


FIGURE 23. Network of water-level observation stations at the mine site.

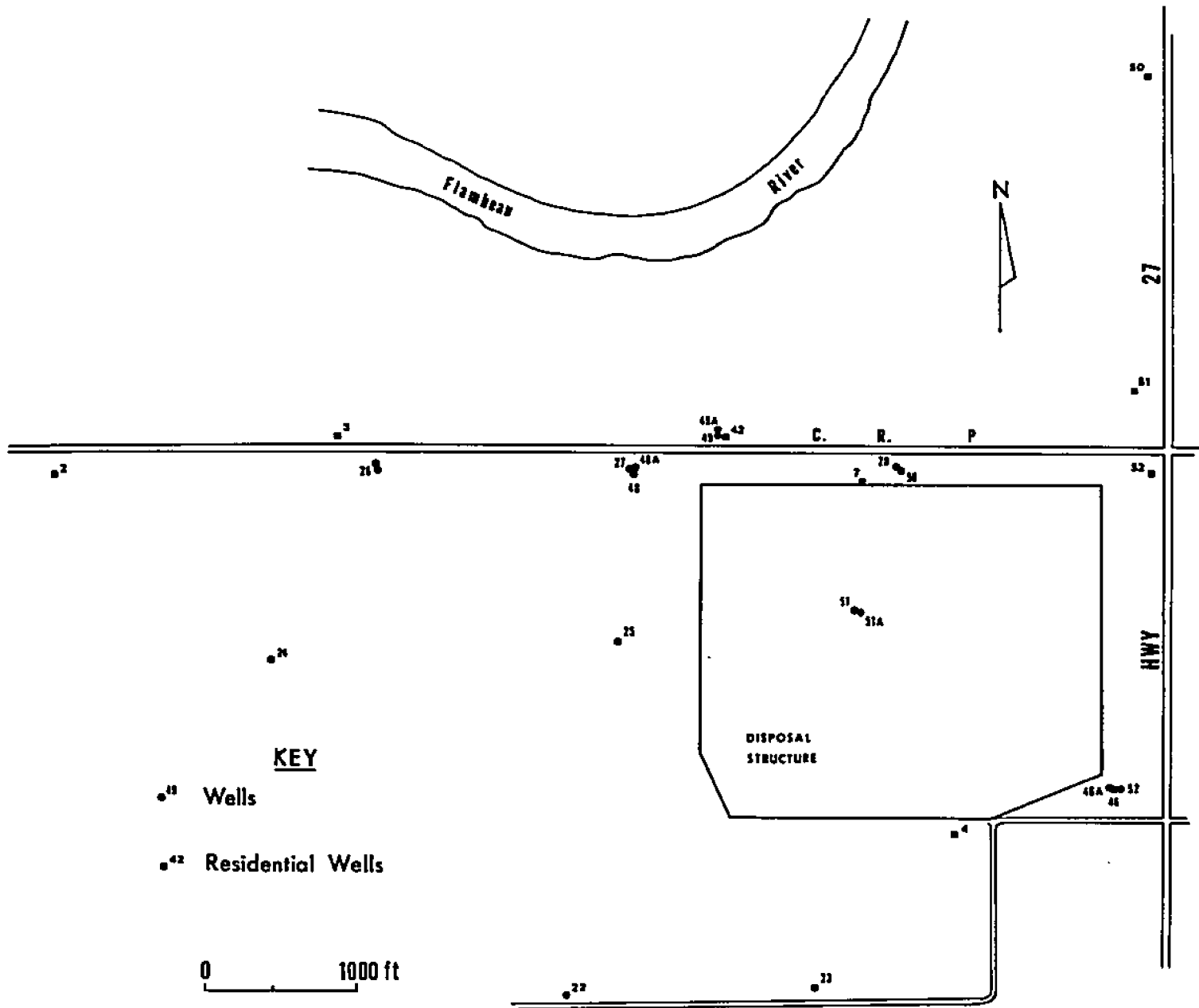


FIGURE 24. Network of water-level observation stations in the waste-containment area.

Hydraulic conductivity and storativity are the hydraulic parameters most influential in controlling the response of a flow system to stresses. Both parameters are most reliably measured by field methods such as pumping tests, though hydraulic conductivity is subject to laboratory determination. Hydraulic conductivity, denoted by  $K$ , is broadly defined as the ease with which water passes through a porous medium and is expressed in units of  $Lt^{-1}$  or in field units as gallons per day per square foot of aquifer ( $gpd/ft^2$ ). It is a function of the size, shape, and degree of interconnection of the voids in a porous medium and the properties of the transmitted fluid. Sands and gravels typically have high conductivities because their large pores offer low resistance to water movement. Clays and silts, on the other hand, do not readily transmit water because the adhesive, cohesive, and viscous properties of water inhibit its passage through the small pores in these fine-grained materials. As a result, clays and silts commonly act as flow barriers and confining layers.

A common trait of glacially derived sediments is their wide variability in hydraulic conductivity resulting from deposition in diverse environments by several transporting media. The saturated conductivities of the deposits are partially a function of their medium of transport and mode of deposition which directly affect the degree of sorting by grain size. Till deposited directly from ice, for example, has experienced little sorting and initially consists of a wide range of particle sizes. The silt and clay fractions



of the till become matrix material which fills voids between larger grains and imparts a low conductivity to the deposit. Sediments eroded from the till and subsequently transported by air and water, such as outwash deposits and loessial silts, are texturally more mature and are typified by more uniform physical properties. Outwash sands and gravels, in particular, are characterized by relatively high conductivities due to their predominantly coarse grain size and the absence of most matrix material.

Glacial tills commonly have vertical fractures with separations of several inches to many feet (Freeze and Cherry, 1979). Shallow fractures close to the land surface are caused by stresses accompanying wetting and drying cycles and seasonal freezing and thawing. Hendry (1982) and Prudic (1982) note that fractures in tills are often most prevalent and extensive in their upper oxidized portions. The origin of till fractures occurring at great depths is more problematic but may be related to the unloading of glacial ice, crustal rebound, and volumetric changes due to geochemical processes. From laboratory evidence, Prudic (1982) observed that hydraulic conductivities in till generally decrease with depth, probably owing to increased confining pressures which retard fracture development and(or) partially close extant fractures. With regard to water movement, Williams and Farvolden (1967) showed that fractured tills have higher infiltration rates in their unsaturated zones and higher conductivities in their zones of saturation, resulting in elevated

recharge rates compared to unjointed tills.

Transmissivity, commonly denoted by  $T$ , is a function of hydraulic conductivity and the saturated thickness ( $b$ ) of the medium according to the relation  $T = Kb$ . In broad terms, it may be defined as the ease with which a porous medium transmits water through its entire saturated thickness. Transmissivity is expressed in units of  $L^2t^{-1}$  or in field units as gallons per day per foot of aquifer (gpd/ft).

Storativity, indicated by  $S$ , is also referred to as the coefficient of storage of confined aquifers and as the specific yield for unconfined systems. It is a dimensionless quantity describing the volume of water released from or taken into storage per unit of horizontal surface area of the aquifer per unit change in the component of hydraulic head normal to that surface. Storativity is generally of lesser significance in affecting aquifer response than hydraulic conductivity or transmissivity.

Several methods of measuring the saturated hydraulic conductivity of surficial deposits and Paleozoic rocks on the mine property were used in initial studies. These were 1) a modified packer and other field methods, 2) laboratory measurements, and 3) low-capacity pumping tests. In the course of the present study, supplemental estimates of hydraulic conductivity and transmissivity were made from the logs of wells and soil borings on the site. Attempts have been made to determine storativities from pumping-test data, though this study is concerned with the steady-state case

in which long-term changes in storage are considered small and are therefore neglected. The methods for determining saturated conductivities provided the necessary initial data for the digital models of the flow systems at the pit and waste-containment areas.

#### Modified Packer and Other Field Methods

The packer method is a constant-head technique which was employed by Soil Testing Services of Wisconsin at 16 locations near the pit in 1973. The test procedure consisted of advancing a borehole to some depth, usually to the saprolite, flushing the hole of mud and cuttings, and then backfilling with quarter-inch pea gravel while retracting the casing to a point 1 ft (0.3 m) below the top of the test zone. Either a 1.56- or 3.0-inch (3.96 or 7.62-cm) internal diameter PVC pipe was inserted into the casing until it rested on the gravel backfill. Pea gravel was then continuously placed in the annulus between the casing and the PVC pipe, usually to the top of a more impervious zone, while retracting the casing another 2 ft (0.6 m). At this level, 3 ft (0.9 m) of bentonite pellets were added to the inside annulus and the casing was pulled back another foot to form a seal which prevented water movement along the outside of the casing and PVC pipe. Approximately 6 ft (2 m) of fine-grained cuttings were then placed above the bentonite seal to hold it in place during swelling (Soil Testing Serv. of Wisc., 1973). This procedure produced a bentonite packer sealing off the hole above the test zone.

In conducting the field tests, water was injected down the small PVC pipe with a centrifugal pump equipped with valves to regulate the injection rate. Discharge was measured with a water meter accurate to the nearest 0.1 gpm (0.4 l/min). At holes where the flow rate was low, water was added by gravity flow from a calibrated 55-gallon drum. In some cases, it was necessary to determine the injection rate from the time required for water to flow from a one-gallon container. At wells where the flow was extremely low, the injection rate was determined from the drop in the water level inside the PVC pipe, which is essentially a falling-head technique. Hydraulic conductivities of materials encompassing the test zones were then determined from the equation

$$K = \frac{C_p Q}{H} \quad (7)$$

where

$$K = \text{hydraulic conductivity (ft/yr)}$$

$$C_p = \frac{25,700 \log_{10} (12L/r)}{L}$$

$$L = \text{thickness of the test zone (ft)}$$

$$r = \text{radius of the inner pipe (ft)}$$

$$Q = \text{injection rate (gpm)}$$

$$H = \text{head differential between the water level maintained in the inner pipe and the surrounding water table (ft)}$$

In addition to the packer tests, field conductivities were measured at eight boreholes in the waste-containment

area in 1972 and at two wells in the gravel pit north of the mine site in 1975. Falling- and rising-head techniques were employed in these test series.

The results of the field tests, averaged per material type, are provided in Table 7. Average field conductivities of the till at the mine and disposal areas are comparable, ranging from 0.7 to 1.0 ft/d (0.2 to 0.3 m/d). For comparison, Summers (1972) estimated that the bulk hydraulic conductivity of sandy till in Marathon County, Wisconsin, ranges from 1.3 to 13 ft/d (0.4 to 4 m/d). Field values of outwash in the two areas cannot be confidently compared because only one measurement is available for the waste area. The conductivity range of the sandstone is similar to that of the outwash tested in this manner, though it averages somewhat lower. Hydraulic conductivities of sandstones in general vary considerably due to differing degrees of fracturing and cementation.

The field conductivities of the surficial soils reported in Table 7 are probably lower than the true values because the packer method measures primarily lateral conductivities influenced by soil texture and laterally continuous vertical fracturing. Vertical components of conductivity due to more discrete properties occurring near the land surface, such as root penetration, are not as readily determined with this method and field measurements may be biased toward horizontally oriented properties. The abundance of plant growth in the fine-grained surficial soils in the waste-containment

TABLE 7. Summary of field hydraulic conductivities by general material type for the open-pit and waste-containment areas.

<u>Material</u>	<u>Location</u>	<u>K range (ft/d)</u>	<u>Mean K (ft/d)</u>
Till - silty fine to coarse sand	Pit area <sup>1</sup>	$7.1 \times 10^{-3}$ to 3.1	$1.0 \times 10^{-1}$
Till - silty fine to coarse sand	Waste area <sup>2</sup>	$2.2 \times 10^{-1}$ to 2.1	$7.1 \times 10^{-1}$
Outwash - fine to coarse sand	Pit area <sup>1,3</sup>	1.3 to 11	8.2
Outwash - fine to medium sand	Waste area <sup>2</sup>	---	1.7 <sup>4</sup>
Surficial soil (0 to 5 ft) - silts, fine sandy silts	Waste area <sup>2</sup>	$1.6 \times 10^{-4}$ to $7.1 \times 10^{-3}$	$2.0 \times 10^{-3}$
Cambrian sandstone	Pit area <sup>1</sup>	1.9 to 8.5	4.8

<sup>1</sup> Soil Testing Serv. of Wisc., 1973.

<sup>2</sup> Soil Testing Serv. of Wisc., 1972b.

<sup>3</sup> Soil Testing Serv. of Wisc., 1976.

<sup>4</sup> Single measurement

area suggests that vertical conductivities are higher than those reported in Table 7. In support of this statement, Young and Hindall (1972) cite average conductivities of 0.4 to 1.6 ft/d ( $1.4 \times 10^{-4}$  to  $5.6 \times 10^{-4}$  cm/s) for soils over the entire project area.

The stress applied to the aquifer with the field methods is limited by the small volume of injected water and may not be transmitted beyond the immediate area of the borehole. The resulting values of hydraulic conductivity may accordingly represent only a small part of the medium and may not be widely applicable. These values, however, are still probably more reliable than those derived through laboratory methods and were used as initial information in the simulative studies.

#### Laboratory Determination of K

Saturated hydraulic conductivities were measured in the laboratory on relatively undisturbed soil samples collected by hydraulically forcing thin-walled sample tubes through unconsolidated materials without rotation (Soil Testing Serv. of Wisc., 1972a). The samples were left in the tubes and their conductivities determined with either falling- or constant-head methods using the sample tubes as permeameters. Since most samples consisted of fine-grained material, the constant-head method was used most often with applied heads ranging from 1.5 to 84.5 ft (0.5 to 25.8 m).

For falling-head permeameters, the volumetric flow rate

through the sample is expressed in terms of the head loss within the tube and the conductivity is determined using the equation

$$K = \frac{Lr^2}{tR^2} \ln \frac{H_1}{H_2} \quad (8)$$

where  $H_1$  and  $H_2$  are head values at the beginning and end of time interval  $t$ ,  $L$  is the sample length,  $r$  is the radius of the manometer tube in which the head loss is measured (the sample tube in this case), and  $R$  is the radius of the sample (Bouwer, 1978). Details of the test procedures were not provided in the consultant's report (Soil Testing Serv. of Wisc., 1972a), though methods are generally standard and most falling-head equations are equivalent to Equation 8.

With constant-head permeameters, stable heads are maintained at both the inflow and outflow ends of the device rather than just at the outflow end as in the falling-head method. If the flow rate through the sample can be determined, applying Darcy's law and solving for  $K$  yields

$$K = \frac{LQ}{H\pi R^2} \quad (9)$$

where  $H$  is the constant head loss across the sample and  $Q$  is the volumetric flow rate (Bouwer, 1978).

Hendry (1982) found that field and laboratory tests for hydraulic conductivity are sensitive to the length of the



tested interval and the sample size, respectively. He concluded that the sensitivity is due to differences in fracture spacing and that small samples collected for laboratory analysis are less likely to intersect a representative number of fractures. The problem is further compounded by the observation that tills, like consolidated materials, often have multiple fracture sets, each of which is likely to have a different fracture spacing. Because field tests are normally conducted over larger, more representative sections of a formation, they usually yield hydraulic conductivities 1 to 3 orders of magnitude greater than laboratory tests of the same material. The disparity is mostly due to the fact that laboratory methods measure mostly the intergranular conductivity of a material. In addition, the small samples required for laboratory tests are less likely to encompass other types of physical discontinuities affecting water movement such as small layers of coarsely granular material. As a result, laboratory methods may underestimate the conductivity and there is often doubt as to whether their results are representative and widely applicable. For this reason, laboratory values for hydraulic conductivity were not used in site analyses except as broad indicators of conditions in areas where other data are lacking.

The results of the laboratory measurements are given in Table 8. Comparison of these figures with the values in Table 7 illustrates the tendency for laboratory conductivities to be lower. More than an order of magnitude difference in aver-

TABLE 8. Summary of laboratory hydraulic conductivities of samples from the waste-containment area (from Soil Testing Serv. of Wisc., 1972b)

<u>Material</u>	<u>K range (ft/d)</u>	<u>Mean K (ft/d)</u>
Till - silt and sand, silty fine to coarse sand	$1.8 \times 10^{-3}$ to $3.1 \times 10^{-1}$	$5.2 \times 10^{-2}$
Surficial soil (0 to 5 ft) - silts, fine sandy silts	$6.2 \times 10^{-5}$ to $6.4 \times 10^{-3}$	$1.6 \times 10^{-3}$

age conductivities of the till is evident; conductivities of surficial soils are more comparable.

Both the field and laboratory conductivities indicate that the 2- to 7-ft (0.6- to 2.1-m) layer of surficial silt and fine sand (probably loess) in the waste-disposal area is less permeable than the underlying till, though the difference is probably not as great as the measurements suggest, as stated earlier. The lower conductivities of the surficial soil probably reflect its finer-grained character compared to the heterogeneous till which contains a larger fraction of coarsely granular material.

#### Pumping Tests

Pumping or aquifer tests allow the in situ determination of the average transmissivity and storativity within the aquifer volume stressed by a test well. Parameters found through properly designed pumping tests are more representative of the ground-water system than point or local values found by laboratory and some field techniques. Once the formation constants have been defined, the average hydraulic conductivity within the area of influence may be found from the relation  $T = Kb$ , where  $b$  is the average saturated thickness.

In 1971, low-capacity pumping tests of short duration were conducted on wells 5, 6, 8, 9, 10, 16, 18, 29, and 34 installed in the pit area in 1970; the well locations are shown in Figure 23. Discharges during these tests ranged from 0.5 to 52 gpm (1.9 to 197 l/min). Most of the test

wells are located in the outwash areas north and northwest of the planned pit; no tests were performed in the vicinity of the proposed disposal structure. The hydraulic parameters summarized in Table 9 were determined mostly from recovery data collected from the test wells after pumping was stopped. The precise method used to arrive at these values was not specified in the consultant's report (Harshbarger, 1971), but preliminary efforts by Flambeau Mining Corporation staff to interpret the data (Passavant, 1971) made use of the straight-line method devised by Cooper and Jacob (1946).

The test results are questionable for several reasons stated by Passavant (1971). First, the surface-mounted centrifugal pump used for the tests was limited to about 28 ft of lift; if the drawdown in a well approached this limit, the pumping phase of the test was terminated and recovery commenced. Many wells at the site are characterized by low specific capacities and the rapid drawdowns resulted in very short test periods. Pumping periods ranged from 6 to 479 minutes and were often less than an hour in length. The short test periods raise the question of whether or not enough of the aquifer was affected for the computed formation constants to be applicable beyond the immediate vicinity of the wells. Furthermore, casing storage often causes large errors in data from low-discharge tests of short duration where drawdown is measured in the pumping well. Another factor affecting the reliability of properties computed from the drawdown measurements is the design of the wells, which

TABLE 9. Summary of hydraulic properties determined from low-discharge pumping tests conducted near the open-pit location in 1971 and 1972.

1971<sup>1</sup> :

<u>Well</u>	<u>Transmissivity (ft<sup>2</sup>/d)</u>	<u>Hydraulic Con- ductivity (ft/d)</u> <sup>2</sup>	<u>Storativity</u>	<u>Remarks</u>
5	1 to 7	0.1	---	
6	1 to 13	0.1	---	
8	267	11.4	---	
9	1,337	33.4	---	
10	---	---	---	
16	267	5.3	---	Gravel pit
18	6,684	93.6	---	Gravel pit
29				
30	267	6.7	---	Average T for well 29 and obs. wells 30, 31, and 32
31				
32				
34				
35	53	1.1	---	Average T for well 34 and obs. wells 35 and 36
36				

(Continued on next page)

TABLE 9 Continued.

1972<sup>3</sup>:

Well	Transmissivity (ft <sup>2</sup> /d)		Hydraulic Con-	Storativity	Remarks
	Drawdown	Recovery	ductivity (ft/d) <sup>2</sup>		
8	1,208	714	32	.0028 to .00066	Obs. well for test at well 42
8	1,238	---	---	.0021	Obs. well for test at well 41
9	123	68	.8	---	
9	2,708	---	---	.0026	Obs. well for test at well 43
29	698	299	10.2	.00027	Obs. well for test at well 42
31	393	338	---	.0018	Obs. well for test at well 42
33	---	227	---	.00051	Obs. well for test at well 42
39	---	9	.4	---	
40	45	33	1.9	---	
41	61	19	1.1	---	
42	24	44	1.2	---	
43	3,912	2,934	44	---	
43	2,156	---	---	.0015	Obs. well for test at well 9

125

<sup>1</sup> Harshbarger (1971)

<sup>2</sup> From recovery data only

<sup>3</sup> Unpubl. data, FMC.

is not suited for efficient pumping. The wells were constructed with slotted pipe instead of screens and most of them are slotted over one large or several smaller intervals which commonly do not correspond to zones of transmissive material. It is thus impossible to discount the effects of well losses in drawdown measurements, particularly since drawdown was measured in the pumping wells in most instances.

Though records are unclear, it appears additional pumping tests were conducted in September of 1972 on wells 9, 39, 40, 41, 42, and 43 with discharges ranging from 1.5 to 40 gpm (5.7 to 150 l/min). All of these wells except 9 and 43 are shown in Figure 23; wells 9 and 43 are approximately 250 and 500 ft (76 and 152 m) northwest of well 42, respectively. The results of this test series are also given in Table 9. These tests were subject to the same limitations cited with regard to the 1971 series and, consequently, the results are similarly suspect. Test periods for this series ranged from 60 to 270 minutes. Storativity values computed from these tests are also included in Table 9; the tests yielded storativities of  $2.7 \times 10^{-4}$  to  $2.8 \times 10^{-3}$ , normally indicative of semi-confined to confined aquifer conditions. The test periods, however, were of insufficient length to produce reliable values. If transient conditions within the flow systems are considered at a later time, it will be necessary to obtain storativity values from either pumping tests or less-reliable estimation techniques such as that of Lohman (1972). The storage values cited above also raise the possibility that leakage through

fine-grained materials overlying outwash may have to be considered for best results.

Of particular note in Table 9 are the large disagreements between 1971 and 1972 values for transmissivity at the same wells, especially for wells 8, 9, and 29. In addition, large differences within the 1972 results are apparent for wells 9 and 43. Wells 5, 6, and 39 are located within the till area southeast of the pit location (Figure 23) and consequently exhibit the lowest transmissivities. The other wells in Table 9 are within or near the outwash area which has greater transmissivities.

Though obvious shortcomings in test conditions and methods make the 1971 and 1972 results questionable, these values did constitute an important source of comparative information. In this respect, they show that the ground-water system varies widely in character over relatively short distances. The data were cautiously employed as initial information in the simulative studies.

#### Estimation of Hydraulic

#### Parameters from Drilling Logs

For boreholes described by detailed drilling logs, supplemental estimates of the mean hydraulic conductivity of the vertical section penetrated by the drilling were made with a modified form of the technique described in Lohman (1972) using measured data for individual material types. The method



consists of making reasonable estimates of the hydraulic conductivity of individual material layers below the water table using the log descriptions, multiplying each conductivity by its corresponding saturated thickness to obtain the transmissivity of each layer, summing the transmissivities of all layers to obtain a total transmissivity for each hole, and then dividing this value by the total saturated thickness to obtain a mean K. The procedure is given by

$$\bar{K} = \frac{1}{b_t} \sum_{m=1}^n K_m b_m = \frac{1}{b_t} (K_1 b_1 + K_2 b_2 + \dots + K_n b_n) \quad (10)$$

where  $\bar{K}$  is the mean conductivity of the saturated vertical section at the well bore ( $Lt^{-1}$ ), the  $b$ 's are the individual layer thicknesses (L),  $b_t$  is the total saturated thickness (L), and  $n$  is the number of saturated material layers. Use of this approach often requires subjective judgment, but the technique was useful for determining the hydraulic conductivities and transmissivities in some areas where no field or laboratory measurements had been made. Hydraulic parameters found with this method are tabulated in Appendix III.

#### Hydrostratigraphic Units

For purposes of the present site study, the entire surficial cover and sandstone in the pit area were considered a single unconfined and heterogeneous hydrostratigraphic unit.

This simplification is considered a reasonable approximation since contrasts in hydraulic conductivity between adjacent outwash, sandstone, and till materials are rarely greater than two orders of magnitude. This grouping was also partly a function of the difficulty in choosing precise boundaries between subsurface materials with contacts that are gradational or otherwise ill-defined. This problem was greatest in areas near the pit where discontinuous outwash deposits are distributed randomly throughout the till unit. Similarities in hydraulic conductivity precluded the need for defining each unit individually and enabled them to be grouped into a single hydrostratigraphic unit.

System geometry in the waste-containment area, while complex, is more uniform and predictable than in the mine area. The outwash zones generally occur as thin, well-defined bodies exhibiting considerable lateral persistence. These characteristics allow the outwash and the intervening till layers to be treated three-dimensionally as separate hydrostratigraphic units even though conductivities vary by about two orders of magnitude. As shown in Table 7, however, only a single measured conductivity value is available for the outwash deposits in the disposal area. It would thus be necessary to augment this information with largely unverified estimates from drilling logs using Equation 10 if separate aquifers were considered. An acute lack of hydraulic-head data for individual aquifers also prevented the division of the surficial deposits in the southern study area into separate

hydrostratigraphic units. Instead, as in the case of the mine site, a lumped approach treating the entire surficial cover as a single hydraulic unit was used.

#### Ground-Water Movement

To further define the hydrogeology of the project area, existing directions and rates of ground-water movement were delineated by mapping the water-table surface. In any subsurface flow system, ground water is continually moving from areas of high to low fluid potential as a consequence of differences in pressure and elevation. The rate of movement is proportional to the hydraulic conductivity of the saturated medium and the hydraulic gradient in accordance with Darcy's law. The hydraulic gradient in isotropic media is the slope of the water table or potentiometric surface expressed as the change in hydraulic head per unit of length or distance.

The direction of ground-water flow is a function of 1) the potential field of the flow system and 2) the degree of anisotropy and orientation of the axes of the hydraulic conductivity tensor (Fetter, 1981). Under isotropic conditions, flow is simply parallel to the gradient of hydraulic head, that is, in the direction of maximum head loss in the potential field. In anisotropic systems, however, the true flow direction is determined by the components of the hydraulic conductivity tensor and may be at some angle to the hydraulic gradient indicated by a potential surface.

### Mine Area

The water table approximates the top of the zone of saturation in the subsurface and is generally defined by the level to which water rises in shallow standpipes. This level represents the depth at which the fluid pressure within the porous medium equals atmospheric pressure. Most wells near the mine site were slotted over several intervals or over a single large interval so that water levels in the wells more closely approximate the top of the saturated zone rather than hydraulic potentials at depth within the system. Though the system is treated as unconfined in numerical simulations described later, parts of it may actually be semi-confined or confined, especially near the till/outwash contact in Figure 8 where zones of sand and gravel are capped by less permeable soils.

Figure 25 shows the average configuration of the water table in the vicinity of the proposed mine pit. The map was constructed from mean water levels in over 40 wells, cased soil borings, and exploration holes for the period from 1970 through 1980 (Unpubl. data, FMC). Water levels at completion in some uncased soil borings were used to augment more reliable, long-term data where it was scanty. Springs, wetlands, and water levels in ponds were used for additional elevation control. Reliable control was completely lacking in parts of the study area north of the gravel pits and east of Highway 27; water-table contours were extended into those areas using wetlands and topography as guides.

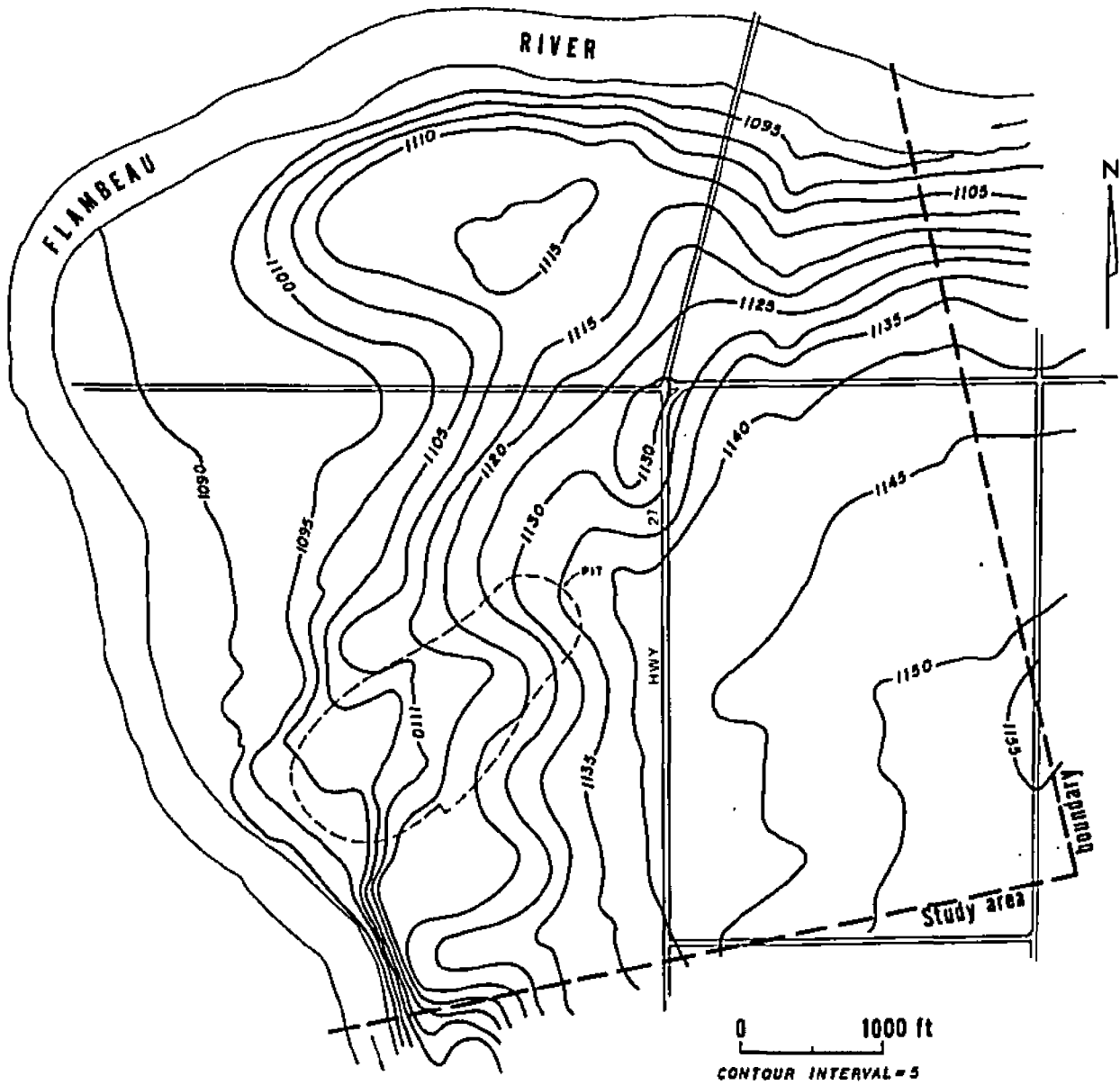


FIGURE 25. Average configuration of the water table in the area of the mine pit based on water levels from 1970-1980, topography, and wetlands.

Since little ground-water development has taken place in the project area, the average position of the water table in the pit area (Figure 25) is essentially a steady-state pre-development surface. It is evident that the water table bears some relation to the topography at the site and that ground-water runoff patterns are similar to those for surface runoff. Flow generally radiates westward, northwestward, and northward from the water-table high to the southeast. Throughout much of the area, both the water table and land surface slope north and west at gradients of 0.5 percent or less in flat areas southeast of the mine and at 2 to 3 percent beneath valley slopes adjacent to the Flambeau River. Numerous local variations in gradient and flow direction are associated with local drainage and other topographic features. An obvious flattening of the hydraulic gradient to less than 1 percent occurs north of the west end of the pit location, even though ground slopes in that area range from 2 to 6 percent. This is readily explained by the presence of the coarse outwash and alluvial sediments in that part of the project area which offer less resistance to flow than the finer-grained till to the east. A similar but less extensive flattening of the water table occurs at the west end of the pit perimeter where outwash materials are thicker and coarser in relation to surrounding areas. No major ground-water divides are apparent within the northern study area, though small local divides are common. From earlier descriptions of the site geology, it is probable that the Precambrian surface exerts substantial con-

trol over the rate and direction of ground-water flow through the Paleozoic and Pleistocene deposits in the pit area as a consequence of its high relief and impermeable nature and the thinness of the younger sediments.

To facilitate later numerical simulations, ground-water flow in the area of the mine was considered horizontal and parallel to the slope of the water table at any point. This simplification neglects the effects of anisotropy and flow may locally deviate from directions indicated by the contours in Figure 25. The assumption of isotropy was invoked as an acceptable approximation at the scale of this problem and also because of a lack of data defining directional variations in hydraulic conductivity within the till and outwash. The two-dimensional treatment also assumes that vertical flow gradients within the system are small.

Rough estimates of the average linear velocity of ground water  $\bar{V}$  (also called the seepage or porewater velocity) through the site may be made with the relation

$$\bar{V} = \frac{K}{n} \frac{dh}{dl} \quad (11)$$

where  $\bar{V}$  is in  $Lt^{-1}$ ,  $K$  is the hydraulic conductivity ( $Lt^{-1}$ ),  $dh/dl$  is the hydraulic gradient, and  $n$  is the effective porosity of the medium expressed as a fraction of unity. For example, in till areas within the eastern half of the pit site hydraulic conductivities are typically less than 1 ft/d (0.3 m/d) and the gradient is about 2 percent (0.02). Using

Equation 11 and an estimated effective porosity of 25 percent, an average linear velocity of 0.08 ft/d (2.4 cm/d) is determined. Similarly, some outwash materials northwest of the pit have conductivities ranging from 20 to 30 ft/d (6 to 9 m/d). Using a representative K of 25 ft/d (7.6 m/d), an effective porosity of 20 percent, and a hydraulic gradient of 0.004 from Figure 25, an average linear velocity of 0.50 ft/d (15.2 cm/d) results. More meaningful velocities may be obtained by applying Equation 11 on a more local scale with specific values for conductivity, gradient, and porosity. In general terms, it is reasonable to state that average linear ground-water velocities throughout the northern study area are less than 1 ft/d (0.3 m/d) and that in areas composed of till, velocities are probably less than 0.1 ft/d (3 cm/d).

Average yearly fluctuations of the water table were examined at wells 1 through 8, 10, and 12 through 20 near the mine site (Figure 23) using unpublished data spanning the 1970-71 to the 1979-80 water years, inclusive. Average fluctuations during this period ranged from 3.3 to 14.8 ft (1.0 to 4.5 m). The amplitudes of the fluctuations are somewhat more variable from well to well in till areas versus areas characterized by outwash deposits. Average fluctuations in the till wells ranged from 3.3 to 8.3 ft (1.0 to 2.5 m), while fluctuations in wells in outwash were confined to a comparatively narrower range of 3.9 to 6.4 ft (1.2 to 2.0 m).



Waste-Containment Area

Figure 26 illustrates the water-table surface in the upper till layer at the waste-containment area as delineated by shallow wells and piezometers, surface-water bodies, topography, and some wetland areas. As in the case of Figure 25, precise water-level control was absent in many areas, especially north of County Road P, east of Highway 27, and west and south of the disposal structure site. Water-table contours in those areas were inferred from topography and wetland locations.

It is apparent that the water table is related to the topography and that gradients correspond closely to surface slopes. A ground-water divide approximately paralleling County Road P separates dominant flow directions into 1) flow to the north toward the Flambeau River, Meadowbrook Creek, and stream F and 2) the generally westward flow through streams E and G (refer to Figure 17 for E, F, and G). Hydraulic gradients north of the divide are moderate to steep, ranging from less than 1 to nearly 5 percent. The gradient steepens significantly and abruptly near the channel of the Flambeau River. Gradients south of the divide are associated with extensive wetland areas and are quite flat, commonly on the order of 0.5 percent or less, especially west of the disposal site. The steepest gradients south of the divide occur southeast of the impoundment site where they locally range up to 1 percent. The Precambrian surface in this part of the project area is generally deeper than at the mine site, ranging

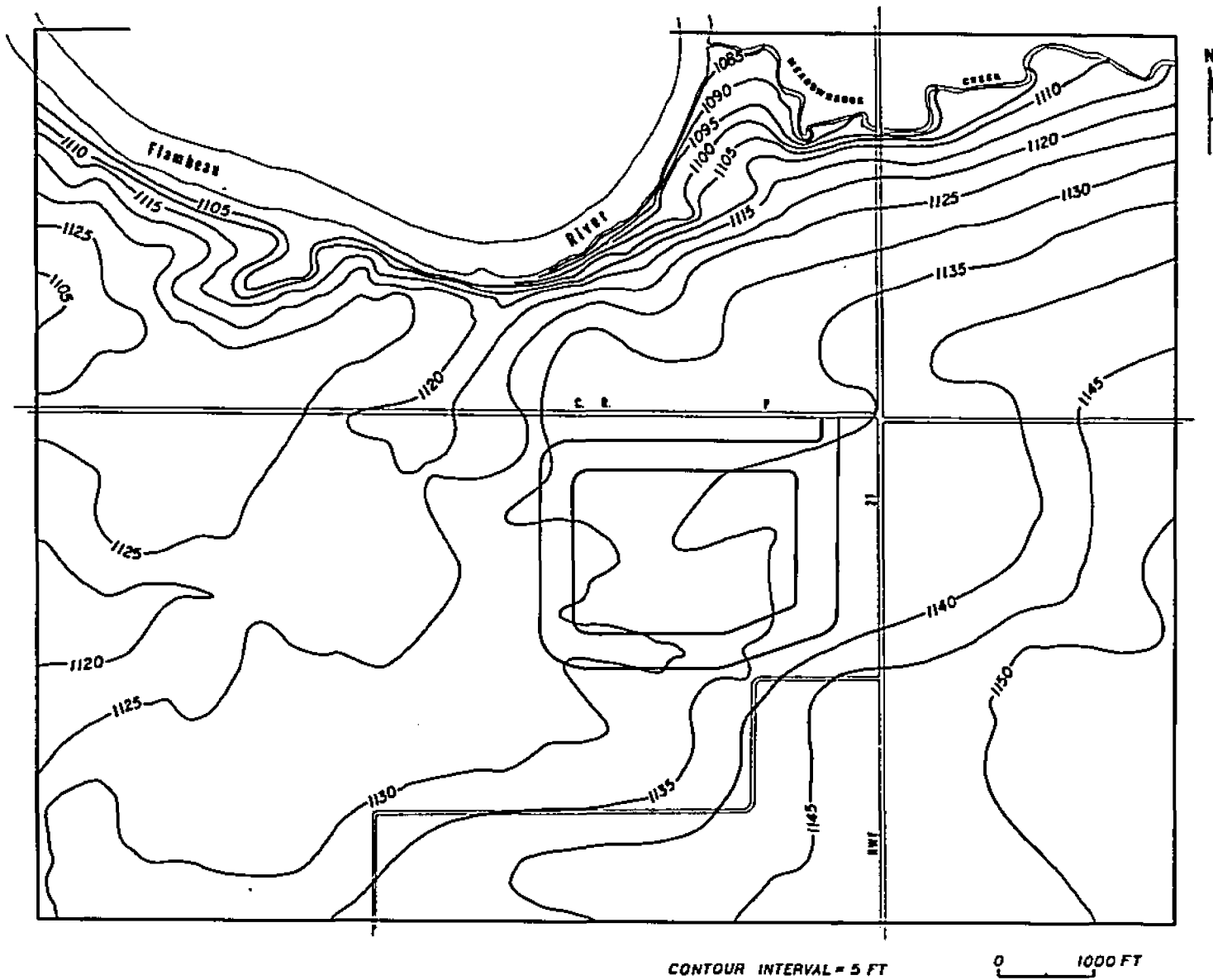


FIGURE 26. Average configuration of the water table in the waste-containment area based on shallow wells, piezometers, topography, and wetlands.

from 50 to 175 ft (15 to 53 m) in depth. It is accordingly less important in terms of influencing shallow ground-water movement. If anisotropy is neglected, ground-water flow is assumed to be horizontal and parallel to the slope of the water-table surface, or perpendicular to the contours defining the surface at any point in Figure 26.

The approximate rate of horizontal water movement through the area of the waste-containment structure may be determined with Equation 11 using a representative porosity of 25 percent for the till, an average hydraulic conductivity of 1 ft/d (0.3 m/d), and a hydraulic gradient of 0.6 percent (0.006). The resulting average linear velocity is about 0.02 ft/d (0.6 cm/d). More precise velocities may be obtained from locally specific values of conductivity, gradient, and effective porosity.

Average yearly fluctuations of water levels were computed for wells 22 through 28 (see Figure 24) in the disposal area from unpublished records for the water years from 1970-71 through 1979-80. Mean fluctuations during this period ranged from 2.3 to 5.9 ft (0.7 to 1.8 m). Wells 24 and 25, which are in or near wetland areas, tended to have fluctuations of 2 to 3 ft (0.6 to 0.9 m), particularly well 24. The rest of the wells in areas remote from the wetlands showed fluctuations on the order of 5 to 6 ft (1.5 to 1.8 m).

The potential for water-quality impacts in the vicinity of the disposal structure accentuates the need for more definitive hydrologic data, especially hydraulic heads and conductivities. The collection of accurate head information for

determining horizontal and vertical flow gradients would require the installation of a piezometer network; hydraulic conductivity and transmissivity values would require pumping tests in the outwash zones. Other information needed in this area is additional drilling to better define the extent of deep outwash zones to the west, north, and east. This information would enable the total flow system in the southern study area to be separated into a water-table system within the till layer at the surface and deeper confined flow systems with separate potentiometric surfaces (the two buried outwash zones of figures 10 and 11). Flow patterns within and hydraulic interaction between individual members of the flow system could then be defined more completely.

## CHAPTER VII

### SIMULATION OF GROUND-WATER SYSTEMS

#### Introduction

In its most basic sense, a model is any concept or device which represents a simplified version of some real entity and(or) duplicates the observed behavior of that entity. The modeling and simulation of a ground-water system, in particular, refers to the construction and operation of a model whose behavior assumes the appearance of the real flow system (Mercer and Faust, 1981). For a flow model to be a valid representation of a real system, it must reflect the complexity of the system as much as is practically possible. If an acceptable level of correspondence can be achieved between the model and system behavior, the model may be useful in predicting the response of the real system to various stresses and management schemes.

It is emphasized that hydrologic modeling in any form does not eliminate the need for collecting reliable data, for hydrologic experience, and common-sense judgment. It is only one of several techniques used to enhance understanding of ground-water systems and must always be used in conjunction with more conventional hydrologic methods. Though models are often the only means of analyzing a large quantity of hydrologic data in a coherent fashion, their use must be tempered by an awareness of the simplifying assumptions upon

which they are based and of their limitations in applicability to a given problem.

In spite of the cautions, modeling is a powerful tool which 1) guides data collection and provides a framework for organizing hydrologic information, 2) assists in acquiring a qualitative understanding of the system, 3) quantifies the properties and behavior of the system, and 4) allows quantitative predictions of system responses to external stresses (Faust and others, 1981). This predictive capability is an important attribute of most modeling methods and it often allows costly experimentation with the real system to be avoided.

#### Types of Ground-Water Flow Models

Most models used to simulate ground-water flow are some variation of two major types, analog and mathematical models. The two most common analogs are physical and electrical. A physical analog is a scaled-down version of a real aquifer constructed of materials having properties similar to those of the natural system it represents. Examples are the sand tank, in which a granular material and colored fluid are used to represent the aquifer, and Hele-Shaw models (also called viscous-flow or parallel-plate models) which employ viscous liquids between closely spaced parallel plates to simulate laminar flow under varying conditions. Physical models are commonly subject to scaling factors which make their applica-

bility to field situations tenuous in some cases. They have, however, offered valuable insight into the behavior of simple ground-water systems. Physical models are only occasionally used at present owing to the advent of high-speed digital computers and numerical modeling. They are often problem-specific, expensive to construct, and not readily adaptable to different boundary conditions. Physical models may still have utility in ground-water quality and contamination research, particularly in the study of dispersion, diffusion, and saline-water/fresh-water boundaries.

Electrical analogs enjoyed immense popularity in the 1950's and 1960's and are based on the similarities between equations governing fluid flow through porous media and those for the flow of electricity through conductors. There are several varieties but most typically consist of a network of resistors and capacitors, the former representing the transmissivity of the aquifer and the latter components simulating storage (Fetter, 1980). Current flow is analogous to fluid movement, electrical potential represents hydraulic potential, and coulombs of electricity correspond to water volume. An important trait of electrical analogs is the ease with which multilayer systems can be modeled. As in the case of physical models, however, electrical analogs are usually problem-specific and expensive to build. Other disadvantages are their inability to adequately simulate mass transport, dispersion, diffusion, and flow in unconfined systems where transmissivity varies with hydraulic head.

While analog models are based on mathematical principles, mathematical models actually solve the equations of flow and continuity (Thomas, 1973). A mathematical model consists of a set of equations describing the physical processes operative within an aquifer, subject to certain conditions. In developing a deterministic mathematical model (one defining a cause-effect relationship), a conceptual model of system behavior is translated into mathematical terms using appropriate simplifying assumptions. The mathematical terms are usually expressed as the governing differential equations with their initial and boundary conditions using variables that are continuous over the area of interest (Remson and others, 1971). The terms also include various phenomenological statements describing rate processes such as Darcy's law.

Once the mathematical model has been formulated, its solution may be obtained in one of two general ways, analytically or numerically. A subset of the general ground-water flow equation can be obtained by invoking additional simplifying assumptions such as radial flow, homogeneity, isotropy, an infinitely extensive aquifer, and confined conditions. This simpler relationship may then be amenable to solving using an analytical model such as the nonequilibrium method of Theis (1935). Unfortunately, many ground-water systems are so complex that the approximating assumptions necessary to achieve an analytical solution may depart considerably from the detailed reality of the system. The analytical assumptions are usually dependent on simple system geometry



and constant aquifer coefficients which limit their accurate application to many problems. Also, the governing equations are often nonlinear and an exact analytical solution may be difficult or impossible to obtain (Remson and others, 1971).

For cases where analytical techniques are not applicable, the governing partial differential equations may be approximated numerically. Numerical methods were introduced into ground-water methodology by Stallman (1956) for problems involving the analysis of regional potentiometric surfaces to determine the hydraulic conductivity of aquifers. The use of large numerical models has since been inextricably linked to advances in computer capabilities. Since the 1960's, when access to high-speed digital computers improved, numerical models have been the most popular tool for studying complex ground-water systems.

Numerical methods are not burdened with many of the restrictive assumptions of the analytical methods and, consequently, they are extremely useful for solving realistic mathematical models of complex hydrologic systems. Numerical methods are particularly appropriate for problems involving irregular boundaries, heterogeneities, and highly variable recharge and discharge rates. They are based on discretization of the continuums comprising both the flow field and time. Through discretization, variables defining properties and processes that are continuous in time and space are replaced with discrete variables defined at specific points. In terms of ground-water flow, this means the single contin-

uous differential equation defining hydraulic head everywhere is replaced by a set or system of algebraic equations defining head at discrete points within the flow field. The unknowns for which this algebraic system is solved are the heads at the points. To discretize the flow field, the study area is divided into a finite number of blocks, each with its own uniform hydrologic properties and each containing a nodal point at which hydraulic head is defined for the entire block (Freeze and Cherry, 1979). In transient-flow problems, the time dimension is similarly divided into discrete steps.

Numerical flow models employ either finite-difference or finite-element methods to approximate the flow equations. Finite-difference methods use a differential approach based on truncated Taylor series and the finite-element approach uses an integration scheme requiring more mathematical sophistication. Another important difference between the two methods is the manner in which the flow field is discretized. The finite-difference method employs rectangular grid blocks formed by either regularly or irregularly spaced orthogonal lines; nodes are defined either at the center of each block or at the line intersections (block- and mesh-centered grids, respectively). The nodes in the finite-element method are at the corners of triangular or quadrilateral elements which comprise an irregular grid. This type of grid often permits better representation of irregular boundaries and may require fewer nodes than a finite-difference model of the same system. For many problems, the finite-element method is also better

able to deal with aquifer heterogeneities and anisotropy and with coupled problems such as solute transport and moving boundaries.

In practice, numerical methods require an inordinate number of arithmetic calculations, even for simple problems. This fact alone explains the kinship between the popularity of numerical models and improvements in computer technology, but there are other advantages to using computers. Computers facilitate the rapid modification of stresses and boundary conditions which increase the flexibility of computer models versus the less-adaptable physical and electrical analogs. The same computer program can be used for a large number of different models but, in contrast, separate analog models are necessary for different aquifers. Other important advantages of computer models are their widespread availability in the literature and their usefulness in solute-transport problems.

#### Model Selection

Each type of model has inherent advantages and disadvantages and no single method should be touted as superior to others for all types of problems (Mercer and Faust, 1981). The choice of a particular model must be based on the specific problem to be addressed and the preference and experience of the investigator. A numerical model may not be an appropriate choice for many types of problems. For example, the effects of a single pumping well in an extensive, relatively isotropic aquifer may be more conveniently simulated with an

analytical model based on assumptions approximating conditions within the real system. In addition, a lack of data may not justify using a sophisticated model of any kind. The overall hydrogeologic complexity of the Flambeau project area and the variety of potential stresses dictated that a numerical model was the proper choice for simulating the flow systems at the mine site and waste-containment area. Having decided that the problem called for a numerical model, the next step was to choose the most appropriate one.

Bair (1980) lists several factors to be considered when selecting a suitable existing numerical model: 1) The model should be tested and validated for the types of problems it is designed to address, 2) the model code should be thoroughly documented and readily available, 3) the code should lend itself to modification so it can be tailored to individual problems, and 4) model output should be in a useable form or easily reduced to a useable form. With these criteria in mind, the two-dimensional finite-difference model of the U. S. Geological Survey (Trescott and others, 1976) was selected to simulate the two study areas. This model is described in a later section after a review of finite-difference mathematics.

Finite-Difference Mathematics  
and Numerical Considerations

Finite-Difference Analogs

The fundamental process of using finite-difference analogs is to replace continuous derivatives by ratios of changes in appropriate variables over small but finite intervals about discrete points (Remson and others, 1971). The basic operation in finite-difference mathematics is differencing, denoted by  $\Delta$ , which is the difference in the values of a function at two adjacent points so that

$$\Delta f(x) = f(x + \Delta x) - f(x) \quad (12)$$

Then, from the definition of the derivative,

$$\frac{df}{dx} = \lim_{\Delta x \rightarrow 0} \frac{\Delta f}{\Delta x} \approx \frac{\Delta f}{\Delta x} \quad (13)$$

where  $\Delta x$  is small relative to the problem domain. This type of approximation can be made at each node of a discretized potential field where spatial changes in the dependent variable are approximately linear between nodes. It further reduces the continuous boundary-value problem to a set of algebraic equations efficiently treated with a digital computer. Inaccuracies resulting from the use of these approximations are generally outweighed by errors in hydrologic parameters used in models.

Finite-difference approximations of derivatives can be constructed from Taylor series, allowing the error associated with the approximations to be determined. A continuous and infinitely differentiable function  $f(x)$  may be expanded about any value of  $x$  into a Taylor series in the positive direction as

$$f(x + \Delta x) = f(x) + f'(x)\Delta x + \frac{f''(x)(\Delta x)^2}{2!} + \frac{f'''(x)(\Delta x)^3}{3!} + \dots \quad (14)$$

where  $f'$  is the first derivative,  $f''$  is the second derivative, and so on. Solving Equation 14 for  $f'$  gives

$$f'(x) = \frac{f(x + \Delta x) - f(x)}{\Delta x} - O(\Delta x) \quad (15)$$

where  $O(\Delta x)$  represents the remaining terms in the infinite series. The forward-difference approximation of the first derivative can be obtained from Equation 15 by dropping the  $O(\Delta x)$  terms to give

$$f'(x) = \frac{f(x + \Delta x) - f(x)}{\Delta x} \quad (16)$$

The error introduced by discarding the  $O(\Delta x)$  terms is called the local truncation error. The order of the first term truncated in the series determines the order of the truncation error; the forward-difference analog is thus first-order correct.

Similarly,  $f(x)$  may be expanded in the negative direction about any  $x$  to give the Taylor series

$$f(x - \Delta x) = f(x) - f'(x)\Delta x + f''(x)\frac{(\Delta x)^2}{2!} - f'''(x)\frac{(\Delta x)^3}{3!} + \dots \quad (17)$$

Solving for  $f'$  and dropping the  $O(\Delta x)$  terms as before gives the backward-difference approximation for the first derivative:

$$f'(x) = \frac{f(x) - f(x - \Delta x)}{\Delta x} \quad (18)$$

which is also first-order correct.

A third type of finite-difference analog may be obtained by subtracting Equation 17 from Equation 14 to give

$$f(x + \Delta x) - f(x - \Delta x) = f'(x)(2\Delta x) + f'''(x)\frac{2(\Delta x)^3}{3!} + \dots \quad (19)$$

The central-difference approximation for the derivative at  $x$  obtained from Equation 19 is then given by

$$f'(x) = \frac{f(x + \Delta x) - f(x - \Delta x)}{2\Delta x} \quad (20)$$

after solving for  $f'$  and discarding all terms of  $(\Delta x)^2$  or higher degree. This type of approximation is second-order correct and results in less truncation error than either

the forward- or backward-difference types.

It is perhaps more intuitive to examine the geometrical interpretation of these methods. Figure 27 illustrates how the slope of  $f(x)$  at B is approximated using the three difference techniques just described. The chord slopes of lines a and b are the finite-difference analogs of the first derivative at  $x$  given by the forward- and backward-difference methods, respectively, while the slope of line c is the central-difference approximation of the first derivative. It is clear that differences between the methods decrease as  $\Delta x$  (or the distance between adjacent nodes) is reduced and that the central-difference analog c is often a better approximation of the slope of the tangent at B than either a or b.

To obtain an approximation of the second derivative of  $f(x)$ , the two Taylor-series expansions, equations 14 and 17, are added to give

$$f(x + \Delta x) + f(x - \Delta x) = 2f(x) + \frac{2f''(x)(\Delta x)^2}{2!} + O(\Delta x)^4 \quad (21)$$

Solving for  $f''(x)$  and truncating the  $O(\Delta x)^2$  terms yields

$$f''(x) = \frac{f(x + \Delta x) + f(x - \Delta x) - 2f(x)}{(\Delta x)^2} \quad (22)$$

Equation 22 is second-order correct and is sometimes called the second central-difference approximation. Approximations of higher derivatives are obtained in a similar manner. The



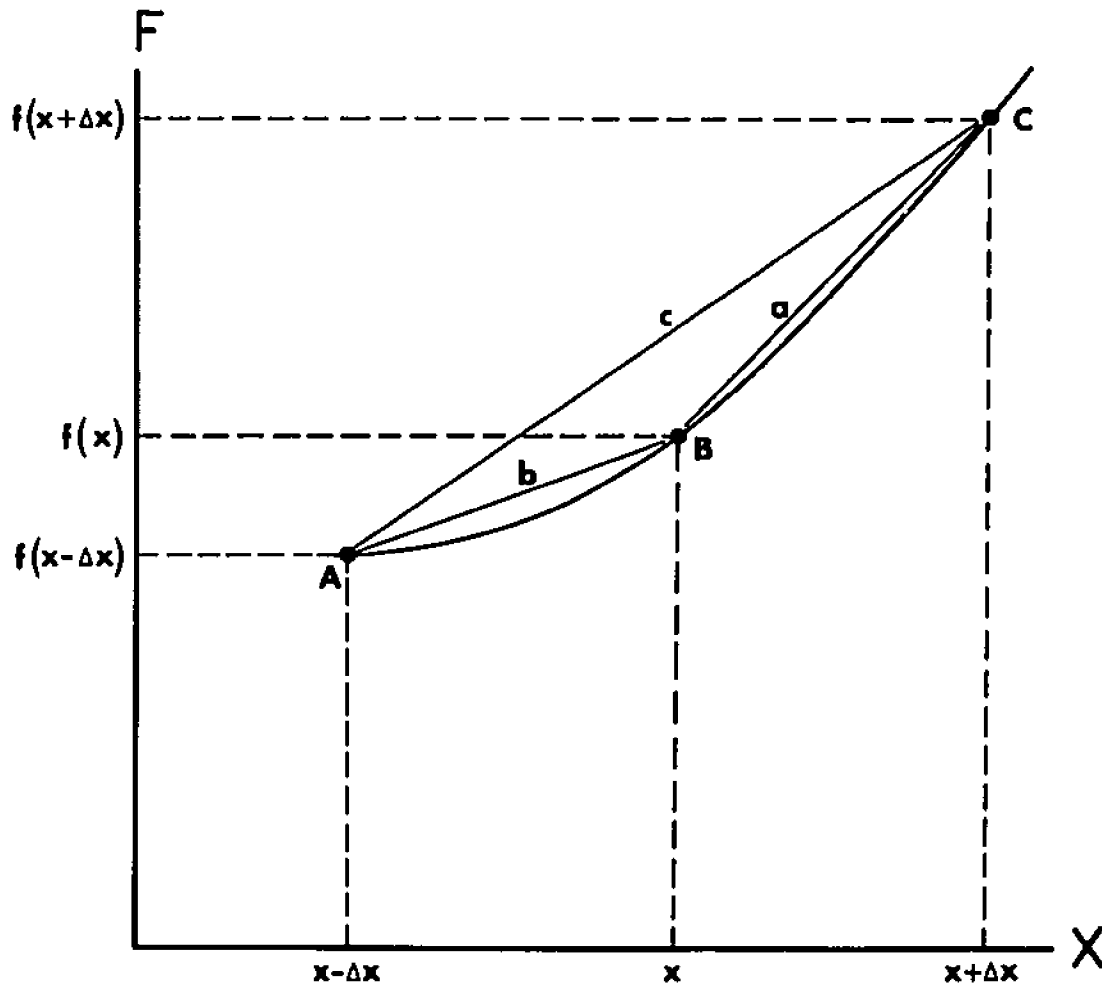


FIGURE 27. Geometrical interpretation of the forward (a), backward (b), and central (c) finite-difference analogs (after Remson and others, 1971).

continuous derivatives in the flow equations are replaced by the difference analogs to yield an algebraic equation which can be solved for the dependent variable at specific points in space and time.

In hydrologic applications, a more intuitive method for determining the finite-difference equations uses the continuity equation and mass balance, although the resulting approximating equations are identical to those derived above. Prickeet and Lonnuquist (1971) and McWhorter and Sunada (1977) develop the finite-difference equations for mesh-centered and block-centered grids, respectively, using the mass-balance approach. Freeze and Cherry (1979) describe both the series-expansion and mass-balance methods for block-centered grids. The mass-balance technique is used later to derive difference analogs for transient flow.

To illustrate the application of finite-difference approximations, we will use the Laplace equation describing steady-state, saturated flow in two dimensions through a homogeneous and isotropic medium with hydraulic head as the dependent variable (h):

$$\frac{\partial^2 h}{\partial x^2} + \frac{\partial^2 h}{\partial y^2} = 0 \quad (23)$$

Substituting the appropriate approximation (Equation 22) for the partial derivatives gives

$$\frac{h(x + \Delta x) + h(x - \Delta x) - 2h(x)}{(\Delta x)^2} + \frac{h(y + \Delta y) + h(y - \Delta y) - 2h(y)}{(\Delta y)^2} = 0 \quad (24)$$

Assuming a regular grid ( $\Delta x = \Delta y$ ) and referring to the computational cell of Figure 28, Equation 24 may be rewritten using  $(i, j)$  coordinate notation as

$$h_{ij+1} + h_{ij-1} + h_{i+1j} + h_{i-1j} - 4h_{ij} = 0 \quad (25)$$

Rearranging and solving for  $h_{ij}$  produces

$$h_{ij} = \frac{1}{4}(h_{ij+1} + h_{ij-1} + h_{i+1j} + h_{i-1j}) \quad (26)$$

which simply states that for steady flow in a homogeneous, isotropic medium, the hydraulic head at any internal node (one not on a boundary) may be approximated as the average head at the four surrounding nodes. Similar equations may be derived for nodes at impermeable corners (two adjacent nodes) and along impermeable linear boundaries (three adjacent nodes). The unknown head value  $h_{ij}$  at each node in a discretized flow field, then, may be expressed as a separate algebraic equation similar to Equation 26.

When solving a finite-difference equation for transient conditions, two broad approaches are possible. One of these is the explicit method whereby the unknown head at a node is

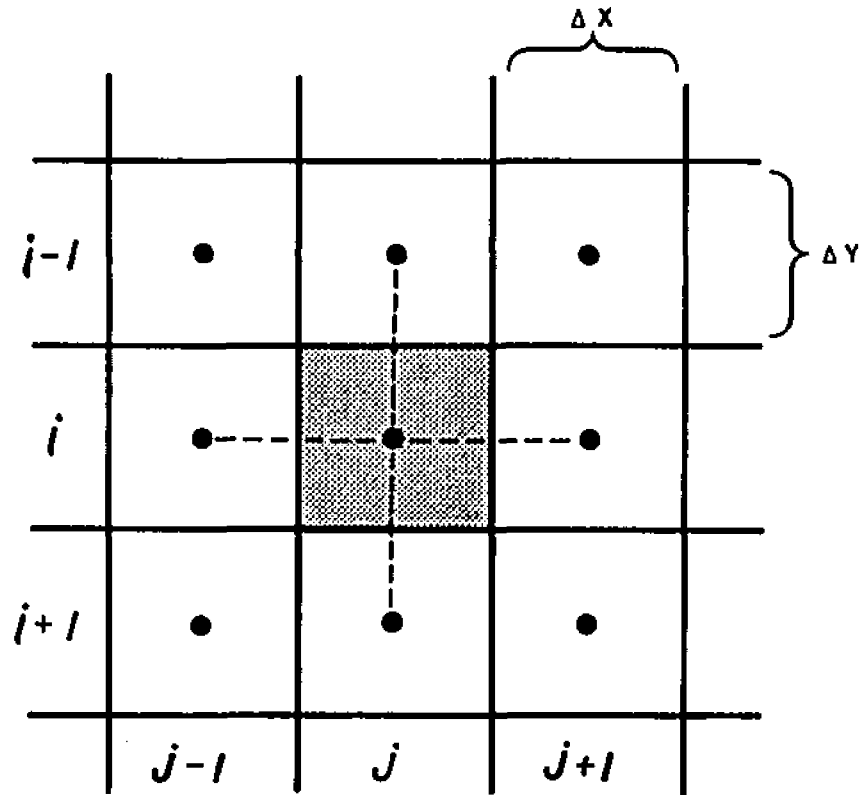


FIGURE 28. Finite-difference computational cell for a regular grid ( $\Delta X = \Delta Y$ ) showing the common 5-point star used in deriving derivative analogs.

computed from the known head values at neighboring nodes determined during the previous time step. The explicit approach makes use of the forward-difference analog for the time derivative in the flow equation and is demonstrated in the following derivation adapted from McWhorter and Sunada (1977).

Using a mass balance to represent the flow rate  $Q$  in one dimension from node  $(i, j-1)$  to node  $(i, j)$  and omitting the  $(i)$  index of Figure 28 for clarity, Darcy's law may be written

$$Q_{j-1 \rightarrow j} = \frac{K}{\Delta x} (h_{j-1}^n - h_j^n) \Delta y b \quad (27)$$

where  $K$  is the hydraulic conductivity between the nodes,  $b$  is the saturated thickness of the aquifer, and  $n$  is the time-step index. Here,  $(n + 1)$  denotes the current time step. Assuming an irregular grid ( $\Delta x \neq \Delta y$ ), letting  $\Delta y = 1$  to consider a unit width of aquifer, and recognizing that transmissivity ( $T$ ) is the product of  $K$  and  $b$ , Equation 27 can be written

$$Q_{j-1 \rightarrow j} = \frac{T}{\Delta x} (h_{j-1}^n - h_j^n) \quad (28)$$

Likewise, flow from node  $(i, j+1)$  to  $(i, j)$  is given by

$$Q_{j+1 \rightarrow j} = \frac{T}{\Delta x} (h_{j+1}^n - h_j^n) \quad (29)$$

The rate of change in storage within a unit width of node  $(i, j)$  for the time interval  $(n)$  to  $(n + 1)$  is

$$\frac{V_j}{\Delta t} = \frac{S\Delta x}{\Delta t} (h_j^{n+1} - h_j^n) \quad (30)$$

where  $S$  is the aquifer storativity and  $V$  is the change in the volume of water in storage at node  $(i, j)$  during  $\Delta t$ . The quantity in parantheses is the forward-difference approximation of the time derivative, including the step length  $\Delta t$ . The principle of continuity requires that

$$Q_{j-1+j} + Q_{j+1+j} = \frac{V_j}{\Delta t} \quad (31)$$

which, upon substitution of equations 28, 29, and 30, results in

$$\frac{T}{\Delta x} (h_{j-1}^n - h_j^n) + \frac{T}{\Delta x} (h_{j+1}^n - h_j^n) = \frac{S\Delta x}{\Delta t} (h_j^{n+1} - h_j^n) \quad (32)$$

which may be simplified to

$$h_{j-1}^n + h_{j+1}^n - 2h_j^n = \frac{S(\Delta x)^2}{T\Delta t} (h_j^{n+1} - h_j^n) \quad (33)$$

Equation 33 is first-order correct in time and second-order correct in space. The forward-difference equation is obtained by further rearranging Equation 33 to obtain

$$h_j^{n+1} = \frac{T\Delta t}{S(\Delta x)^2} (h_{j+1}^n + h_{j-1}^n) + h_j^n \left[ 1 - \frac{2T\Delta t}{S(\Delta x)^2} \right] \quad (34)$$

The space derivatives are evaluated at the earlier (known) time step (n) and  $h_j^{n+1}$ , the head at the current time step, is the only unknown. Since  $h_j^{n+1}$  depends only on known head values from the previous time level, Equation 34 is an explicit expression. It represents a system of equations, one for each of N nodes, and it can be solved explicitly by substituting known heads computed for nodes (i,j), (i,j-1), and (i,j+1) during the previous time step (n) for the head at the new time level (n + 1). The heads at all nodes are changing between the time levels (n) and (n + 1) so that using heads at (n) to approximate the space derivatives is valid only for small time increments.

The explicit approach is straight-forward but requires the imposition of severe restrictions on the space and time increments selected. Inappropriate choices of  $\Delta x$  and  $\Delta t$  may cause errors that are amplified from one time level to the next, resulting in inaccurate or even unstable solutions. The time step cannot be selected independently of the space increment and is related to  $\Delta x$  in the one-dimensional case by

$$\frac{T\Delta t}{S(\Delta x)^2} < 0.5 \quad (35)$$

as noted in Remson and others (1971). For the two-dimensional case, the left side of Equation 35 must be less than 0.25 to insure a stable solution (Rushton and Redshaw, 1979). Since  $\Delta x$  must remain small to minimize truncation error, Equation 35 or its two-dimensional equivalent can usually be satisfied

only by placing an upper bound on the value of  $\Delta t$ . This restriction often results in the need for many time steps and, hence, in excessive computer time to achieve a solution to transient problems encompassing long time periods. Given this limitation, explicit methods are not commonly used for ground-water modeling.

The second broad approach for transient-flow problems includes the implicit methods which are both more sophisticated and more versatile than explicit schemes. With the fully implicit approach, the backward-difference equation is obtained for the time derivative by evaluating the space derivatives at the  $(n + 1)$  (unknown) time level. Equation 33 then becomes

$$h_{j-1}^{n+1} + h_{j+1}^{n+1} - 2h_j^{n+1} = \frac{S(\Delta x)^2}{T\Delta t}(h_j^{n+1} - h_j^n) \quad (36)$$

which is also first-order correct in time and second-order correct in space. By using this method, one assumes the space derivatives are best approximated at the unknown time level. Rearranging Equation 36 so that the unknown head value at node  $(i, j)$  at the current time step is on the right side of the equation, we obtain

$$h_j^n + \frac{T\Delta t}{S(\Delta x)^2}(h_{j+1}^{n+1} + h_{j-1}^{n+1}) = \left[1 + \frac{2T\Delta t}{S(\Delta x)^2}\right] h_j^{n+1} \quad (37)$$

In this case, the unknown head at node  $(i, j)$  at time  $(n + 1)$ , the present time step, depends on the head at  $(i, j)$  evaluated at the previous time  $(n)$  and the unknown heads at nodes  $(i, j+1)$  and  $(i, j-1)$ . Equation 37 is an implicit expression because



$h_j^{n+1}$  is not expressed in terms of known heads.

Stability is generally not a concern with the fully implicit, backward-difference method and the space and time increments can be chosen independently to reduce truncation error (McWhorter and Sunada, 1977). The lack of restrictions on the size of the time increment permits the use of larger  $\Delta t$  to reduce computer execution time. Because of their unconditional stability and convergence, some type of implicit procedure is normally used to solve the approximated groundwater flow equations.

The finite-difference equations used in the digital model of Trescott and others (1976) are derived from equations for confined and unconfined flow in a manner similar to that outlined earlier. The reader is directed to that paper, to Pinder and Bredehoeft (1968), and to Freeze and Cherry (1979) for more detailed equation development. A brief description of their derivation is provided in a later section on model theory.

#### Matrix Solution Methods

From the foregoing discussion, it follows that there are  $N$  algebraic equations in  $N$  unknowns at each time step for a flow field discretized into  $N$  nodes. In a transient scheme, this set of equations is solved simultaneously at each time step. As a general rule of thumb, if  $N$  is less than about 1,000 the matrix of algebraic equations may be solved most efficiently with direct methods such as matrix inversion,

Cramer's rule (determinants), or some form of Gaussian elimination (Mercer and Faust, 1981). With direct methods, a sequence of operations is done only once, yielding a solution to the algebraic system that is exact except for round-off error. In addition, no initial conditions or closure tolerance is needed.

For  $N$  greater than 1,000 nodes, iterative matrix techniques or iterative methods in combination with direct techniques may have greater computational efficiency (Mercer and Faust, 1981). Iterative methods attempt solution through successive approximation and avoid the storage of large matrices, making them attractive for problems with large numbers of nodes. They require an initial guess at the solution and then improve this guess by some iterative process until convergence is achieved. In sweeping through the matrix, the head values most recently determined with the algebraic equation are used to arrive at improved estimates of the head at each node. Consequently, the computed heads more closely approximate their final values after each iteration. Since these methods begin with an initial estimate of the solution, their efficiency (measured as the number of iterations required to reach a solution) is dependent on the closeness of the initial values to the final values. The difference between two successive approximations of head at a node is called the residual, which decreases with each iteration through a matrix having a stable solution. The iterative process is terminated when the maximum residual for

any iteration falls below a prescribed error tolerance or closure criterion.

There are several types of iterative schemes, though all entail successive sweeps or iterations through a matrix composed of initial and boundary values. Commonly used solution techniques are the alternating-direction implicit method (ADI), line-successive over-relaxation (LSOR), and the strongly implicit procedure (SIP). Remson and others (1971) and Trescott and others (1976) provide a systematic treatment of these methods and their hydrologic applications; only brief descriptions of each are given here.

In the two-dimensional case, the ADI method is a perturbation of the Crank-Nicolson method where each time step is subdivided into two equal substeps in order to obtain tridiagonal coefficient matrices. In the first substep, heads are approximated column by column at the  $(n + 1)$  time level using heads at adjacent nodes known at the start of the step. Consequently, the heads are obtained implicitly within each column and explicitly between columns (that is, along rows) for the first substep, resulting in a tridiagonal coefficient matrix for each interior column which is solved directly. For the second substep, a second set of algebraic equations is solved row by row at the  $(n + 1)$  time level using known heads at surrounding nodes from the first substep. The heads are thus obtained implicitly in each row and explicitly along columns. As before, a tridiagonal coefficient matrix for each interior row is generated and solved directly.

The ADI method available in the model of Trescott and others (1976) is an improved version called the iterative ADI procedure in which the normal ADI scheme outlined above is repeated several times per time step until convergence is achieved. In this case, a complete iterative cycle consists of two iteration levels, one oriented along columns, the other along rows. A set of algebraic equations is generated and solved column by column in the first iteration level of the cycle. In the second part, a second algebraic system is generated and solved for each row of nodes. These two steps are repeated until convergence is achieved, as determined by a specified error tolerance. Thus, to advance a single time step in the iterative ADI process requires the solution of many small sets of linear equations rather than a single large set by repeatedly alternating solutions in the x and y directions (Wang and Anderson, 1982). As do many iterative methods, the iterative ADI scheme in the U. S. Geological Survey model uses acceleration parameters to improve the rate of convergence. The ADI process is very fast since the algorithm for directly solving tridiagonal matrices is efficient and the matrices are generally small. However, it may be difficult to obtain solutions for some problems with the ADI method, particularly for steady-state simulations with highly variable coefficients.

Line-successive over-relaxation (LSOR) is similar to the ADI method except every sweep through the matrix occurs in only one direction. The solution is obtained in either column-by-column or row-by-row fashion, resolving the two-dimensional

problem into a series of temporary one-dimensional problems that are efficiently solved with some direct method imbedded within the iterative scheme. Assuming a column-by-column method, the general process consists of 1) sweeping through the matrix one column at a time, updating head values after each column solution for use in the next solution, and 2) checking for convergence by comparing computed heads at the new iteration level with those from the previous iteration for compliance with some closure tolerance. These steps constitute one iteration. An acceleration (over-relaxation) parameter is used to improve the convergence rate.

The strongly implicit procedure (SIP) is one of the most sophisticated matrix techniques available for solving numerical problems. It was developed by Stone (1968) and is characterized by a higher rate of convergence and lower sensitivity to iteration parameters than other types of iterative methods, especially for problems involving heterogeneous or anisotropic media. Moreover, its effectiveness is not a function of the complexity of the problem as is sometimes the case with the ADI method. The SIP is more implicit than the ADI or LSOR techniques because it is more closely related to direct methods for solving matrix equations. It involves solving a system of simultaneous linear equations by an elimination process working on a modified form of the original matrix. Instead of solving the matrix equation  $(A)\{h\} = \{f\}$  where  $A$  is the coefficient matrix,  $f$  is the vector of known information, and  $h$  is the unknown head vector, one solves  $(A + B)\{h\} = \{f\} + Bh$

where  $(A + B)$  is a modified matrix which is in some sense close to  $(A)$ . The matrix  $(A + B)$  is constructed so that it can be decomposed into sparse upper and lower triangular matrices which allow the set of equations generated by the equation  $(A + B)\{h\} = \{f\} + Bh$  to be solved with a simple direct scheme similar to the Thomas algorithm. The theory of the SIP method is rather complex and the reader is directed to Stone (1968), Remson and others (1971), Trescott and others (1976), Larson and Trescott (1977), and Trescott and Larson (1977) for an indepth treatment.

#### Sources of Error in Numerical Modeling

It is important that possible sources of error in numerical modeling are recognized so that the misuse of models and invalid interpretations of their results can be avoided. All numerical models are founded on simplifying assumptions which limit their applicability to some types of problems (Mercer and Faust, 1981). It is thus necessary to understand the underlying assumptions and the behavior of the real aquifer system to prevent misapplication of a model.

Dettinger and Wilson (1981) divide the uncertainty associated with ground-water systems into two classes, intrinsic uncertainty and information uncertainty. Intrinsic uncertainty is related to the variability in natural system parameters and processes, while information uncertainty is associated with one's knowledge of that variability. System parameters in-

clude aquifer properties, boundary values, source/sink strengths, and initial conditions. From this description, it is apparent that intrinsic uncertainty is an inherent, irreducible factor of the system. It exists because spatial and temporal variations in parameters (such as recharge rates) and the spatial variability of properties (such as hydraulic conductivity) are very complex and can never be completely described.

The second class of uncertainty is related to data errors which, in turn, may cause misconceptualization of the aquifer system. It represents a qualitative and(or) quantitative lack of valid system information but, unlike intrinsic uncertainty, it may be reduced by further and more accurate data collection and analysis. Estimates of parameters and properties of a ground-water system will generally contain many inaccuracies arising from such sources as measurement error or incomplete information. Unfortunately, errors in data describing an aquifer are particularly difficult to evaluate because the true aquifer description is never fully known due to the intrinsic uncertainties. The final parameters characterizing a system are usually found by obtaining the best agreement between simulated and real system behavior during some period for which a historical record of behavior exists. The process of obtaining a match between real and simulated heads is called model calibration and is discussed in chapters VIII and IX.

There is another type of error which was mentioned in

the previous paragraph. A model is an abstract representation of a real system synthesized from available information. It is thus a conceptual model that has been translated into a mathematically or intuitively manageable analog of the real system. The underlying conceptual model, however, may itself be faulty resulting in conceptual or model errors. Such errors often result from information uncertainties.

There are several sources of error inherent in the numerical methods and digital equipment used in obtaining solutions to numerical models (Singh, 1977). If  $h_p$  is the exact solution to the partial differential equation governing groundwater flow and  $h_d$  is the exact solution to the corresponding finite-difference equation, their difference ( $h_p - h_d$ ) is the discretization or truncation error. If the solution is convergent, this error will decrease as  $\Delta x$  and  $\Delta t$  approach zero. Discretization error is the dominant type in schemes having stable and convergent solutions and is always present regardless of the precision of the calculations.

Another source of error in computed results is round-off or stability error. Numerical computations are carried out to a finite number of significant places by the computer so that round-off error is introduced each time a calculation is made. The computer solution  $h_c$  thus differs from the exact solution of the algebraic difference equations. If the difference ( $h_d - h_c$ ) is restricted with increasing  $\Delta x$  or  $\Delta t$ , the solution is stable. There are thus two types of errors affecting convergence and stability and the total computational



error E is given by their sum:

$$E = (h_p - h_d)(h_d - h_c) \quad (38)$$

Evaluating the level of computation error can be a difficult task, depending on the nature of the numerical problem. The degree of truncation error may be estimated by successive applications of the approximating equations using smaller space and(or) time increments. Significant sensitivity of the computed results to these changes indicates a substantial level of truncation error and the need for smaller  $\Delta x$  and  $\Delta t$ . Round-off error is generally negligible compared to other sources of error (Mercer and Faust, 1981).

### Description of Two-Dimensional Model

#### General Model Features

The finite-difference model of Trescott and others (1976) was chosen to simulate the flow systems in the Flambeau project area. Of the many digital flow models currently available, this code is probably the most widely used. It is well documented, completely debugged, and has been verified by field studies. The model can simulate a wide array of hydrologic conditions including transient and steady-state flow in confined and unconfined aquifers, systems with both confined and unconfined parts, and confined systems which undergo conversion to unconfined aquifers. The model can

also accounts for such complicating factors as heterogeneity, anisotropy, and irregular boundaries. Where warranted, the program permits transient or steady leakage from confining beds or streambeds, constant areal recharge, evapotranspiration, and discharge and recharge by wells. For added flexibility, the user may choose from several equation-solving schemes and various input/output options. A theoretical description follows.

### Theoretical Development

If the Cartesian coordinate axes imposed on the modeled area are colinear with the principal components of the transmissivity tensor (i.e., the directions of anisotropy coincide with the coordinate axes), the linear partial differential equation governing confined ground-water flow in two-dimensions is

$$\frac{\partial}{\partial x} \left( T_{xx} \frac{\partial h}{\partial x} \right) + \frac{\partial}{\partial y} \left( T_{yy} \frac{\partial h}{\partial y} \right) = S \frac{\partial h}{\partial t} + W(x, y, t) \quad (39)$$

where  $T_{xx}$  and  $T_{yy}$  are the principal components of the transmissivity tensor ( $L^2 t^{-1}$ ),  $h$  is hydraulic head (L),  $S$  is storativity (dimensionless), and  $W$  is the volumetric flux of recharge or discharge per unit of aquifer surface area ( $Lt^{-1}$ ). This is a diffusion-type equation derived from mass-conservation (water-balance) and momentum-conservation (Darcy's law) equations. The first two terms represent the difference in

flow rates into or out of a control volume of porous medium and the term  $S\partial h/\partial t$  is the change in the amount of water stored in the control volume expressed as a rate. Pinder and Bredehoeft (1968) give a more complete development and discussion of Equation 39.

In unconfined aquifers, transmissivity is a function of hydraulic head. Assuming colinearity between the coordinate axes and the principal components of the hydraulic-conductivity tensor, Equation 39 can be modified to allow the transmissivity to change with time as the saturated thickness changes. The equation for unconfined horizontal flow through an anisotropic medium is then given by

$$\frac{\partial}{\partial x} \left( K_{xx} b \frac{\partial h}{\partial x} \right) + \frac{\partial}{\partial y} \left( K_{yy} b \frac{\partial h}{\partial y} \right) = S_y \frac{\partial h}{\partial t} + W(x, y, t) \quad (40)$$

where  $K_{xx}$  and  $K_{yy}$  are the principal components of the conductivity tensor ( $L^{t-1}$ ),  $S_y$  is the specific yield (dimensionless), and  $b$  is the saturated thickness ( $L$ ). Equation 40 is nonlinear because transmissivity is a function of hydraulic head which, in turn, depends on  $b$ . In general, a differential equation is nonlinear if it includes products of the dependent variable and its derivatives or products of the derivatives. In effect, each term on the left side of Equation 40 is a product of a function of the dependent variable  $h$  and the derivative of  $h$ . Bredehoeft and Pinder (1970) provide a brief discussion of Equation 40.

With reference to a block-centered grid with variable

spacing, Equation 39 is approximated with finite-difference analogs as

$$\frac{1}{\Delta x_j} \left[ \left( T_{xx \frac{\partial h}{\partial x}} \right)_{i, j+\frac{1}{2}}^n - \left( T_{xx \frac{\partial h}{\partial x}} \right)_{i, j-\frac{1}{2}}^n \right] + \quad (41)$$

$$\frac{1}{\Delta y_i} \left[ \left( T_{yy \frac{\partial h}{\partial y}} \right)_{i+\frac{1}{2}, j}^n - \left( T_{yy \frac{\partial h}{\partial y}} \right)_{i-\frac{1}{2}, j}^n \right] = \frac{S_{i,j}}{\Delta t} (h_{i,j}^n - h_{i,j}^{n-1}) + W$$

where  $\Delta x$  and  $\Delta y$  are the space increments,  $\Delta t$  is the time increment, and  $(n)$  is the time-level index. Equation 41 may be further approximated as

$$\frac{1}{\Delta x_j} \left[ T_{xx_{i, j+\frac{1}{2}}} \left( \frac{h_{i, j+1}^n - h_{i, j}^n}{\Delta x_{j+\frac{1}{2}}} \right) - T_{xx_{i, j-\frac{1}{2}}} \left( \frac{h_{i, j}^n - h_{i, j-1}^n}{\Delta x_{j-\frac{1}{2}}} \right) \right] +$$

$$\frac{1}{\Delta y_i} \left[ T_{yy_{i+\frac{1}{2}, j}} \left( \frac{h_{i+1, j}^n - h_{i, j}^n}{\Delta y_{i+\frac{1}{2}}} \right) - T_{yy_{i-\frac{1}{2}, j}} \left( \frac{h_{i, j}^n - h_{i-1, j}^n}{\Delta y_{i-\frac{1}{2}}} \right) \right]$$

$$= \frac{S_{i,j}}{\Delta t} (h_{i,j}^n - h_{i,j}^{n-1}) + W \quad (42)$$

where  $T_{xx_{i, j+\frac{1}{2}}}$  is the interblock transmissivity between nodes  $(i, j)$  and  $(i, j+1)$ , and  $\Delta x_{j+\frac{1}{2}}$  is the distance to the common block boundary between these nodes (these conventions apply throughout the equation). This is an implicit equation with the time derivative approximated by the backward-difference analog; head values on the left side are at the new time level  $(n)$  and are thus unknown. Equation 42 is also used in

the model to approximate Equation 40 for unconfined flow by replacing storativity with specific yield and defining transmissivity as a function of head from the previous iteration according to the relation

$$T^k = K^k b^{k-1} \quad (43)$$

in which  $k$  is the iteration index. The saturated thickness  $b$  is computed by subtracting the bottom elevation of the aquifer at each node from the head computed at the previous iteration.

Equation 42 can be multiplied by  $\Delta x \Delta y$  to make the final coefficient matrix symmetric and, following notation introduced by Stone (1968), may be written

$$B_{i,j} h_{i-1,j}^n + D_{i,j} h_{i,j-1}^n + E_{i,j} h_{i,j}^n + F_{i,j} h_{i,j+1}^n + H_{i,j} h_{i+1,j}^n = Q_{i,j} \quad (44)$$

where  $B$ ,  $D$ ,  $E$ ,  $F$ , and  $H$  are coefficients occurring within the resulting pentadiagonal matrix. The coefficients are defined by

$$B_{i,j} = \Delta x_j \frac{T_{YY_{i-\frac{1}{2},j}}}{\Delta y_{i-\frac{1}{2}}} \quad D_{i,j} = \Delta y_i \frac{T_{XX_{i,j-\frac{1}{2}}}}{\Delta x_{j-\frac{1}{2}}}$$

$$F_{i,j} = \Delta y_i \frac{T_{XX_{i,j+\frac{1}{2}}}}{\Delta x_{j+\frac{1}{2}}} \quad H_{i,j} = \Delta x_j \frac{T_{YY_{i+\frac{1}{2},j}}}{\Delta y_{i+\frac{1}{2}}}$$

$$E_{i,j} = - \left( B_{i,j} + D_{i,j} + F_{i,j} + H_{i,j} + \Delta x_j \Delta y_i \frac{S_{i,j}}{\Delta t} \right)$$

$$Q_{i,j} = - \Delta x_j \Delta y_i \left( \frac{S_{i,j}^{n-1}}{\Delta t} h_{i,j} + W \right) \quad (45)$$

The coefficients B, D, F, and H are the weighted harmonic-mean evaluations of the interblock transmissivities between adjacent nodes. Use of the harmonic mean insures continuity across block boundaries at steady state for variable grids and makes the appropriate coefficients zero at impermeable boundaries (Trescott and others, 1976). Appel (1976) indicates that using the harmonic mean to compute interblock transmissivities may result in values that are higher or lower than the true values depending on the relative sizes and transmissivity contrasts of adjacent nodes. The harmonic mean is the best method where adjacent nodes have large contrasts in transmissivity.

The source term  $W(x,y,t)$  in equations 39 and 40 can include well discharge and recharge, transient or steady leakage from a confining layer or streambed, recharge from precipitation, and evapotranspiration. These quantities are represented in the model by

$$W_{i,j} = \frac{Q_w}{\Delta x \Delta y} - q_{re} - q' + q_{et} \quad (46)$$

where  $Q_w$  is the well discharge or recharge distributed over the nodal area ( $L^3 t^{-1}$ ),  $q_{re}$  is the areal-recharge flux per

unit area ( $Lt^{-1}$ ),  $q'$  is the leakage flux per unit area from a confining bed ( $Lt^{-1}$ ), and  $q_{et}$  is the evapotranspiration flux per unit area ( $Lt^{-1}$ ). The leakage term is

$$q'_{i,j} = T_L (h_{i,j}^o - h_{i,j}^n) + \frac{K'_{i,j}}{m_{i,j}} (\bar{h}_{i,j} - h_{i,j}^o) \quad (47)$$

and consists of two parts. The first term on the right side describes transient leakage in which storage is considered;  $T_L$  is a complex coefficient modified from Bredehoeft and Pinder (1970). The notation  $h_{i,j}^o$  is the head at node  $(i,j)$  at the start of pumping. The second term on the right describes steady leakage due to the initial gradient across the confining layer where  $K'_{i,j}$  is the hydraulic conductivity of the confining bed ( $Lt^{-1}$ ),  $m_{i,j}$  is its thickness ( $L$ ), and  $\bar{h}_{i,j}$  is the head on the other side of it ( $L$ ) (Trescott and others, 1976).

Evapotranspiration is computed in the model as a linear function of depth below the land surface according to the following relationships:

$$q_{et} = \begin{cases} Q_{et} & , h_{i,j}^n \geq G_{i,j} \\ 0 & , ET_z \leq (G_{i,j} - h_{i,j}^n) \\ Q_{et} - \frac{Q_{et}}{ET_z} (G_{i,j} - h_{i,j}^n) & , ET_z > (G_{i,j} - h_{i,j}^n) \end{cases} \quad (48)$$

in which  $Q_{et}$  is the maximum rate of evapotranspiration ( $Lt^{-1}$ ),

$ET_z$  is the depth at which evapotranspiration ceases,  $G_{i,j}$  is the elevation of the land surface at node  $(i,j)$ .

### Boundary and Initial Conditions

To obtain a unique solution to a partial differential equation describing a physical process, additional information about physical constraints on the process is required. These constraints are described by boundary and initial conditions.

Boundary conditions, in general, describe the geometry of the region for which the system of differential equations is to be solved. They generally consist of values of the dependent variable defined on the boundary or its derivative normal to the boundary (Mercer and Faust, 1981). In groundwater applications, there are three main types of boundaries: 1) Specified-value boundaries (also known as constant-head or Dirichlet boundaries), 2) specified-flux or constant-flux boundaries (also called the Neumann condition if the derivative of the dependent variable normal to the boundary is specified), and 3) value-dependent flux boundaries, where the flow rate across the boundary is related to both the normal derivative of head and the value of head. The model selected for the Flambeau study can accommodate the first two types.

For constant-head boundaries, known hydraulic heads are specified along the boundary and remain unchanged throughout



the simulation. This type of boundary is used in areas where flow is perpendicular to the boundary and the boundary is an equipotential line parallel to adjacent lines. Constant-head boundaries are often used to simulate surface-water bodies such as lakes and rivers which may have water levels that are largely independent of ground-water inflow or are relatively stable for the time period encompassed by the simulation. They are also useful in simulating underflow into and out of modeled areas.

For specified-flux boundaries, flow rates are specified along the boundary and equated to the derivative of head normal to the boundary. The model allows the use of recharge or discharge wells to simulate fluxes through permeable or semi-permeable boundaries and underflow into or out of the modeled area. A constant-flux rate may be zero in the case of an impermeable boundary. The no-flow case is treated in the model by assigning a transmissivity or hydraulic conductivity of zero to nodes outside the boundary.

The model of Trescott and others (1976) requires a no-flow boundary around the entire grid perimeter; all other boundaries must be placed within this continuous boundary. This feature may affect heads at interior nodes and its influence is minimized by expanding the modeled area so that the artificial boundary has little impact on nodes within the area of interest.

The initial conditions for numerical models are values of the dependent variable (usually hydraulic head) specified

everywhere within the boundaries of the model. Initial conditions are not required for the steady-state case since the model can generate a steady-state head distribution from the given boundary conditions and hydraulic properties. For transient simulations, a steady-state head configuration is commonly employed as the initial conditions so that transient flow is not already occurring at the start of simulation. This assures that head changes during the simulation result only from stresses applied to the system.

The hydraulic properties first assigned to nodes within a discretized region may also be considered initial conditions since many of these values are modified during the calibration process. Almost without exception, this initial information is obtained through conventional hydrologic methods such as water-level measurements, hydrologic budgets, pumping tests, and laboratory measurements.

#### Model Input/Output

Input for the model is dependent on the type of system being simulated and which simulation options are selected by the user. All data inputs consist of some or most of the following information:

1. The type of system (confined, unconfined, leaky, or a combination of these);
2. Specification of an equation-solving scheme, closure criteria, acceleration or iteration parameters, and grid dimensions;

3. Aquifer anisotropy;
4. Initial heads (optional for steady-state simulations);
5. Storage coefficients and(or) specific yields;
6. Transmissivities and(or) hydraulic conductivities;
7. Data for determining aquifer thickness (aquifer bottom and(or) top);
8. Rates of areal recharge and evapotranspiration;
9. Grid spacings;
10. Number and lengths of pumping periods;
11. Number of time steps, length of initial step, and an incremental time-step multiplier; and
12. The location, type, and magnitude of stresses (wells).

Several of these input categories (e.g., storativity, areal recharge, and evapotranspiration) may be zero for some problems.

Model output, too, depends largely on the various options invoked, though all input data are listed in the output to provide for easy error detection regardless of option selection. Output options include printing matrices and maps of the final head and drawdown values, and the results of mass-balance computations. In addition, there are options to save computed heads and mass-balance results on disk or tape, for punched output, and to compute drawdowns at real well radii.

## CHAPTER VIII

### SIMULATION OF THE PROPOSED OPEN-PIT MINE

#### Model Development Objectives

The chief objective in developing a ground-water flow model for the Flambeau mine site is to produce a management tool capable of forecasting the effects of mining activities on the local hydrologic regime. Such effects could include a decline in water levels in some areas due to ground-water abstraction and increased or decreased water levels in other areas as a result of altered recharge/discharge patterns or the obstruction of subsurface flow. Foreknowledge of the location and extent of these changes will allow them to be monitored more effectively and, if necessary, to be reduced or eliminated through engineering modifications and various management schemes.

Besides determining potential influences on the surrounding flow system, simulation capabilities may assist in routine mine-management activities such as collecting ground-water seepage into the pit and the subsequent discharge of collected seepage during each phase of mine development. An accurate prediction of flow rates into the excavation will assist in determining the need for and capacity of water-treatment facilities. In addition, sites for water-supply wells which are optimal in terms of productivity and pumping effects may be located in advance and with greater precision

with a model than by using more conventional siting techniques.

#### Modifications to the Two-Dimensional Model

The two-dimensional model chosen to simulate the flow systems at the mine site (Trescott and others, 1976) is capable of treating a wide variety of hydrologic phenomena. Several changes in the model code, however, were made to improve its flexibility for the problem at hand.

#### Modifications to Print Flow Rates at Constant-Head Nodes

The subroutine CHECKI was modified after Bair (1980) to allow flow rates to and from individual constant-head nodes to be printed. For transient simulations, this modification prints only the flux rates prevailing during the final time step. The modifications allow seepage rates into the pit to be estimated using the fluxes at constant-head nodes within the pit perimeter. This information can facilitate the development of plans for dealing with water entering the excavation. The modification also allows base flow to the Flambeau River and underflow into and out of the study area to be quantified.

Modifications to Print  
Evapotranspiration Rates

The CHECKI subroutine was further modified to allow the rates of evapotranspiration occurring at individual nodes during the final time step to be printed in the output. This change was prompted by the recognition that the evapotranspiration of ground water is an important hydrologic process in some parts of the project area and enables rates in specific areas to be quantified.

Miscellaneous Modifications

Other minor changes were made to the model code to enhance its useability. For example, the size of the primary matrix in the main program which allocates total computer core storage was reduced from the published figure of 70,000 words to 28,000 words to increase execution priority and improve turnaround time. Also, format statements in the subroutine DATAI were changed to allow very small pumping rates to be printed.

Steady-State Simulation  
of the Existing System

General Discussion

After reviewing field and laboratory data, it was determined that the information was insufficient to warrant a

transient simulation of the flow system at the mine site. The simulations presented later are thus based on steady-flow characteristics. Important factors considered in arriving at this conclusion are the lack of reliable storativity values, the absence of any transient phenomena with which to calibrate and verify a nonsteady flow model, and the decision to simulate the system as a single-layer water-table aquifer. This last factor is discussed in Chapter VI and is related to problems in monitoring-well construction which precluded the separation of water levels into the potentiometric surface associated with confined outwash zones and the water table in the overlying till. In view of the treatment of the system as unconfined, the remainder of this discussion is directed at water-table situations. In any case, most modeling studies, including transient simulations, begin with a steady-state simulation in order to verify the mathematical representation of the natural, unstressed system, to facilitate model calibration, and to provide initial conditions for transient simulations.

Steady flow exists when the magnitudes and directions of velocity vectors within the flow field are constant with time. Under unstressed conditions and over long periods of time a flow system is in a state of dynamic equilibrium in which the volume of water entering the system is balanced by the volume leaving it through natural discharge mechanisms. Under these conditions, the water table will exhibit only seasonal fluctuations around a relatively constant mean

elevation. The volume of water stored in the system is similarly constrained. If the water-table fluctuations are small with respect to the saturated thickness of the system and the configuration of the water-table remains approximately the same during the cycle of fluctuations, the fluctuating system can be represented by a steady system with the water table fixed at its mean position. The depression-focused recharge of surface-water runoff to the ground-water system, which is usually seasonal or otherwise occurs as discrete events, introduces temporary transient elements to the behavior of the system. If, however, recharge is considered constantly distributed in time or if a complete annual cycle of recharge is encompassed, the flow system may still be viewed as being in steady-state equilibrium.

Given conditions of relatively constant storage and water-table geometry, the primary factors determining the volume of water transmitted from recharge to discharge areas are the hydraulic conductivity of the aquifer and the water-table gradient. Since time is not an independent variable, steady flow in two dimensions through a saturated, anisotropic, and unconfined porous medium is described by

$$\frac{\partial}{\partial x} \left( K_{xx} b \frac{\partial h}{\partial x} \right) + \frac{\partial}{\partial y} \left( K_{yy} b \frac{\partial h}{\partial y} \right) = W(x, y, t) \quad (49)$$

where variables are defined as they were for Equation 40 on page 170. If  $K_{xx}$  and  $K_{yy}$  are equal (isotropic conditions), the medium is homogeneous (constant conductivity), and the

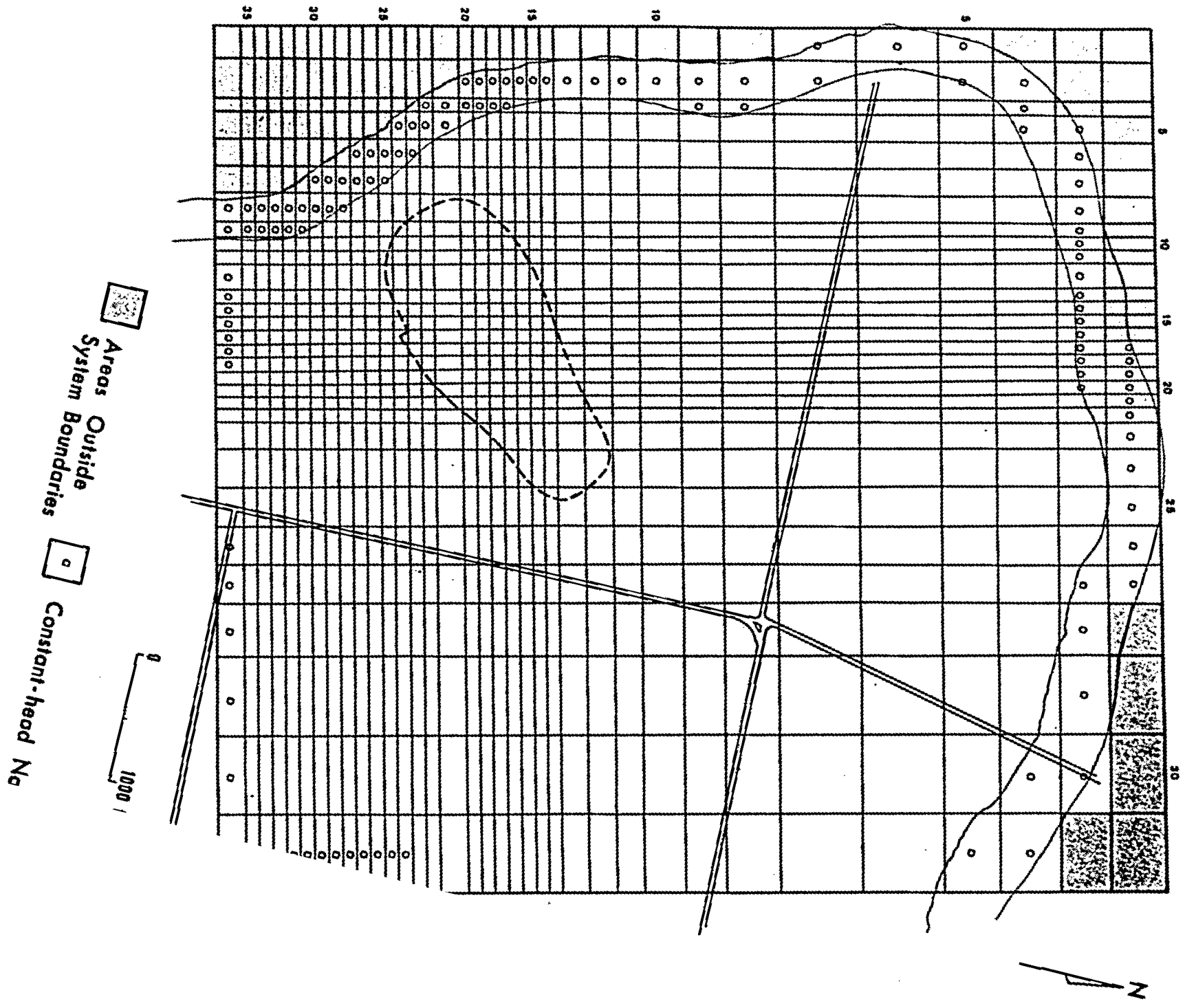


saturated thickness  $b$  is uniform, Equation 49 reduces to the Laplace equation (Equation 23). The solution to Equation 49 is a function  $h(x,y)$  describing the dependent variable  $h$  in relation to the  $xy$ -plane.

The steady-state case minimizes differences in storage characteristics between confined and unconfined aquifers. Future transient simulations accounting for changes in storage will require accurate storativity values for the flow system since some of the outwash zones may be best represented as confined aquifers. Because of the large differences in storativities between confined and unconfined aquifers, assuming that the system is totally unconfined may result in large errors in computed heads during transient simulations, especially if head changes caused by stresses are significant.

#### Steady-State Input Data

The modeling of a ground-water system is conducted in three stages: 1) Specification of system characteristics from field, laboratory, and published information, 2) model calibration and verification, and 3) prediction of the system's response to various stress schemes. The first of these stages was initiated by discretizing the mine area into a block-centered 35 X 30 variable grid encompassing the large meander of the Flambeau River and an area of approximately  $1.6 \text{ mi}^2$  ( $4.1 \text{ km}^2$ ), as shown in Figure 29. The grid is oriented to facilitate the representation of the arcuate course



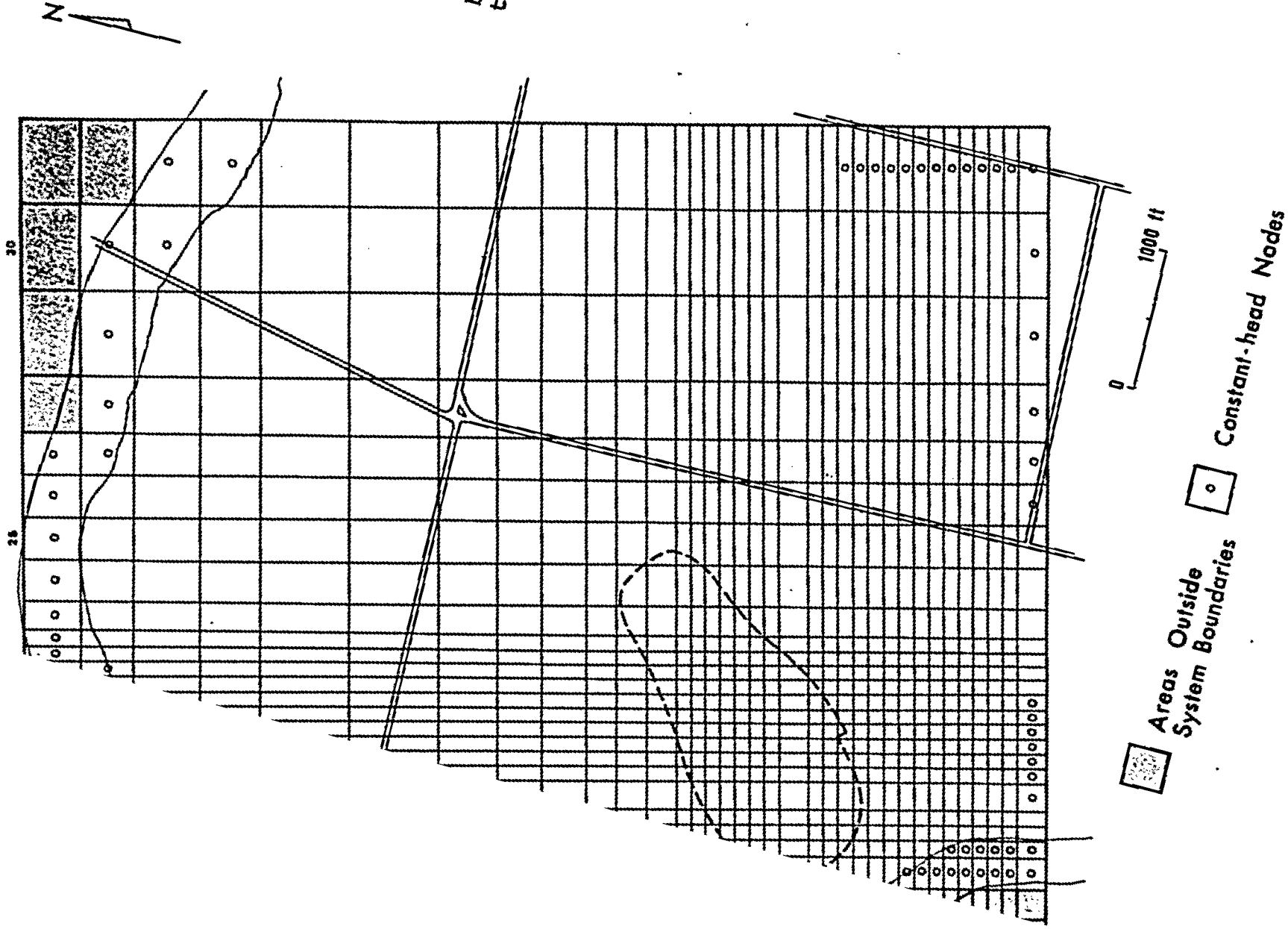


FIGURE 29. Finite-difference grid of the mine site showing the distribution of hydrologic boundaries used in the simulations.

of the Flambeau River. The boundaries to the south and east are arbitrary and were established as a compromise between the areal coverage of available data and the need to minimize artificial boundary influences in the area of the open pit. Of the 1,050 nodes in the grid, 941 occur within the boundaries of the modeled area. Grid blocks range in area from 0.23 to 8.26 acres (0.09 to 3.34 ha) with the smallest being 100 X 100 ft (30.5 X 30.5 m) and the largest 600 ft (183 m) per side. The variable grid permitted the irregular course of the river and areas with steep hydraulic gradients to be characterized more accurately. It also facilitated the use of larger grid blocks in areas where a lack of data did not warrant more detail.

The flow system at the mine site was considered unconfined and isotropic. The latter property was assumed because of a lack of information defining anisotropies within the surficial materials. In terms of the model inputs, the assumption of isotropy required that multipliers for hydraulic conductivity in the x and y directions be set equal to unity. Initial head values were taken from Figure 25 showing the average head distribution in the vicinity of the proposed pit. This map was constructed from averages of on-site water-level measurements made monthly between 1970 and 1980 and so represents an approximate steady-state configuration of the water table.

Initial hydraulic conductivities were obtained from the data collected through the methods described in Chapter VI.

The values are summarized in tables 7, 8, and 9. Since the model boundaries extend well beyond the area for which measured conductivity values are available, reasonable estimates of conductivity were used for distant parts of the modeled area. This procedure of parameter estimation also applies to other parameters in areas near the model periphery, including hydraulic head. For this reason and because much of the conductivity data collected on the site are suspect for various reasons (see Chapter VI), it was anticipated that final values resulting from model calibration might differ significantly from the initial conductivities. Specific remarks regarding the final hydraulic-conductivity distribution are withheld until a later section describing the calibration of the model.

Since the system is considered unconfined, transmissivity is a function of the hydraulic conductivity and the saturated thickness within each grid block. The conductivity remains constant during pumping, but the decline in head results in a corresponding decrease in transmissivity. The saturated thickness at each node is computed for each iteration by subtracting the aquifer base elevation from the head computed at the previous iteration, allowing transmissivity to vary with head according to Equation 43. The Precambrian surface is considered the aquifer bottom and elevations from Plate 2 were assigned to each node for use in the transmissivity computations.

The water budget used to determine areal recharge rates

was outlined in Chapter V; calculated values are given in Table 5 and their areal distribution as used in the pit model is shown in Figure 19. Values assigned to each node were further adjusted to reflect local conditions affecting the rate of recharge such as ground slopes and the presence of wetlands and drainage features. The gravel pits north of the mine site (Figure 8) were assigned the maximum recharge rate in Table 5 of 5.4 in/yr (137 mm/yr).

Early trial simulations using a crude version of the pit model indicated that certain types of water-control facilities might increase heads in some parts of the study area (to be discussed later). Because of this possibility and the occurrence of prominent wetlands in the eastern part of the study area, the model was devised to include the evapotranspiration of ground water. The evapotranspiration rate used, 22 in/yr (560 mm/yr), was obtained from the water budget. This option requires the specification of the land-surface elevation at each node and a maximum depth below which the effects of evapotranspiration are negligible. A depth of 3.5 ft (1.1 m) was determined by trial and adjustment during the calibration process and produced heads which agreed most favorably with measured values.

Simulations with the model require several additional input specifications. The user must select an equation-solving algorithm from among line-successive over-relaxation, the iterative alternating-direction implicit method, and the strongly implicit procedure. The last scheme (SIP) was used

for the pit model because of its rapid convergence, suitability for problems with strong heterogeneities, and independence from problem complexity. Use of the SIP requires the specification of an iteration parameter  $B'$  to further improve the rate of convergence. Initially specified as 1.0, trial-and-error runs during calibration indicated 0.6 to be an optimal  $B'$  value for the unstressed system in terms of decreasing the number of iterations required to achieve a solution. The user must also select a closure criterion which dictates when convergence has occurred. A criterion of 0.001 was used most often in the model. Larger values may lead to inaccurate results by terminating the iterative process too soon, and smaller criteria may significantly increase the number of iterations required for convergence without proportionately improving the accuracy of the solution. Occasionally, larger criteria were necessary to obtain convergence in some simulations, as noted later. Since the simulations were for steady-state conditions, the specific yield of the aquifer was set at zero and the model run for a single time step of arbitrary length. Also specified was the option to include the results of mass-balance calculations in the output to assist in model calibration.

### Boundary Conditions

Figure 29 shows the distribution of hydrologic boundaries within the modeled area near the pit. Constant-head boundaries

were assigned to peripheral parts of the study area where ground water enters or leaves it as underflow, largely to the southeast and due south of the pit location. The constant-head nodes regulate flow into or out of the area based on the local hydraulic gradient and aquifer properties. The constant-head boundaries accurately account for underflow in this manner if the effects of stresses do not extend to them.

The Flambeau River was also represented as a constant-head boundary. Water-surface elevations from detailed topographic information were assigned to river nodes so that the average stream gradient of 2 ft/mi (0.38 m/km) was preserved. This approach assumes an average river stage and may not be suitable for short-term simulations in which the river stage affects the results. The use of the constant-head condition in this situation also assumes a fully penetrating river. Consequently, base flow computed as the flux to constant-head river nodes may be greater than the actual rate because streambed properties and river/aquifer head relationships are ignored. A more precise method is to treat the streambed as a semi-permeable confining layer which regulates base flow (leakage) according to its hydraulic conductivity and thickness and the head loss across it (the head differential between the river stage and the potentiometric surface of the aquifer beneath the bed). This method, however, is often difficult to implement since the conductivity of the streambed must usually be determined indirectly and the bed's thickness is rarely known. Modelers of the U. S. Geological Survey



often assume a streambed thickness of 1 ft (0.3 m) and then determine a streambed conductivity through calibration (Person. commun., R. Shedlock; 1981). In many instances, too, the relation between the river stage and head in the underlying aquifer is poorly known.

The model algorithm requires the study area to be artificially bounded on all sides by nodes with zero hydraulic conductivity or transmissivity. Other boundaries must be placed within this no-flow barrier. If ground-water flow near a model border was parallel to this outer no-flow zone, no other boundary conditions were assigned there since the no-flow boundary acts appropriately as a flow line across which no flow occurs.

### Model Calibration

Before the effects of future stresses on a flow system can be simulated, a model must be capable of reproducing the present state of the system. Water levels measured in the field and those generated by a model from the initial hydraulic information will almost always differ, sometimes significantly. The calibration of a digital flow model, also called the inverse or identification problem, is a process in which the initial input parameters (usually transmissivity, hydraulic conductivity, and storativity) are adjusted to achieve an acceptable match between the real and computed heads.

Calibration is generally a two-phase process. One usually

attempts to first reproduce or recreate the steady-state head distribution in a flow system. The next phase is reproducing the effects of a known stress and is called history matching or model verification. The general rule of calibration is to decrease flow to and increase flow from nodes at which the computed water levels are too high. This is accomplished by decreasing the hydraulic conductivity (or transmissivity) at up-gradient nodes and increasing it down-gradient. The reverse procedure is applied to nodes at which computed heads are too high. The model is rerun after each series of adjustments and further changes are made as needed to obtain an acceptable match. Numerous model runs are usually required to complete the calibration process.

The technique of trial-and-error parameter adjustment is not unreasonable since the aquifer parameters are always imprecisely known. Usually, parameters having the most uncertainty associated with them are adjusted and the range of adjustments is guided by field values of the parameters. Since the parameters can be arbitrarily adjusted in infinitely many ways to obtain a match, the final solution is not unique or may have large errors. This underscores the need for applying reliable data and good judgment. The inverse process is also subject to pronounced errors in areas where computed heads are relatively insensitive to perturbations in transmissivity, hydraulic conductivity, or storativity (McElwee, 1982). The best calibration results are achieved in areas where small changes in these parameters produce large changes

in computed heads, allowing the modeler to bracket in on reliable parameter values with a higher degree of precision. In general, sensitivity to transmissivity or hydraulic conductivity is greatest where these parameters have low values and is least in areas of high T or K such as near the Flambeau River.

The verification of a flow model is the demonstration that it can simulate a real transient event such as a pumping test or seasonal fluctuations in water levels. It is usually considered the second part of calibration and additional refinement of the aquifer parameters in the model normally takes place during this process. After calibration and a demonstration of a model's ability to reproduce historical hydrologic events, it may be used in a predictive mode. Confidence in predictive results, however, must be seasoned with an awareness of the underlying model assumptions, the numerical accuracy of the solution, the accuracy of the history match, and the reliability of the data used for calibration.

In recent years, considerable effort has been devoted to developing automated methods for estimating aquifer parameters during calibration. In broad terms, these methods usually employ statistical or interpolating routines which systematically check and adjust parameters until a best fit is obtained between measured and generated heads. These techniques greatly accelerate the calibration process while removing much of the subjectivity associated with trial-and-error procedures. For

examples of automated calibration methods, see Lovell and others (1972), Neuman (1973), and Cooley (1977, 1979).

Since the project area is essentially undisturbed and a large body of water-level data exists, calibration of the pit-area model was carried out by attempting to reproduce the steady-state head distribution of Figure 25. Hydraulic conductivity values and the maximum depth of evapotranspiration were repeatedly adjusted and the model rerun until a reasonable correspondence was obtained between the model output and Figure 25. Recharge values used in the model were considered reliable and were not adjusted. Figure 30 is the head distribution in the northern study area generated by the model after calibration. Comparing it with Figure 25 shows excellent agreement, though some detail is inevitably lost during discretization when averaging heads within each grid block for input data. Figure 30 implies that water-table gradients in the northern half of the study area may be less steep than shown in Figure 25. This difference was not unexpected since the water-table configuration in remote areas north and east of the pit location was estimated largely from topographic information.

Figure 30 also shows areas in which the simulated evapotranspiration of ground water occurs within 3.5 ft (1.1 m) of the land surface. Except for isolated areas adjacent to the Flambeau River, most ground-water evapotranspiration occurs at or near the wetland areas shown in Figure 19. The fact that areas of vapor discharge in Figure 30 do not precisely

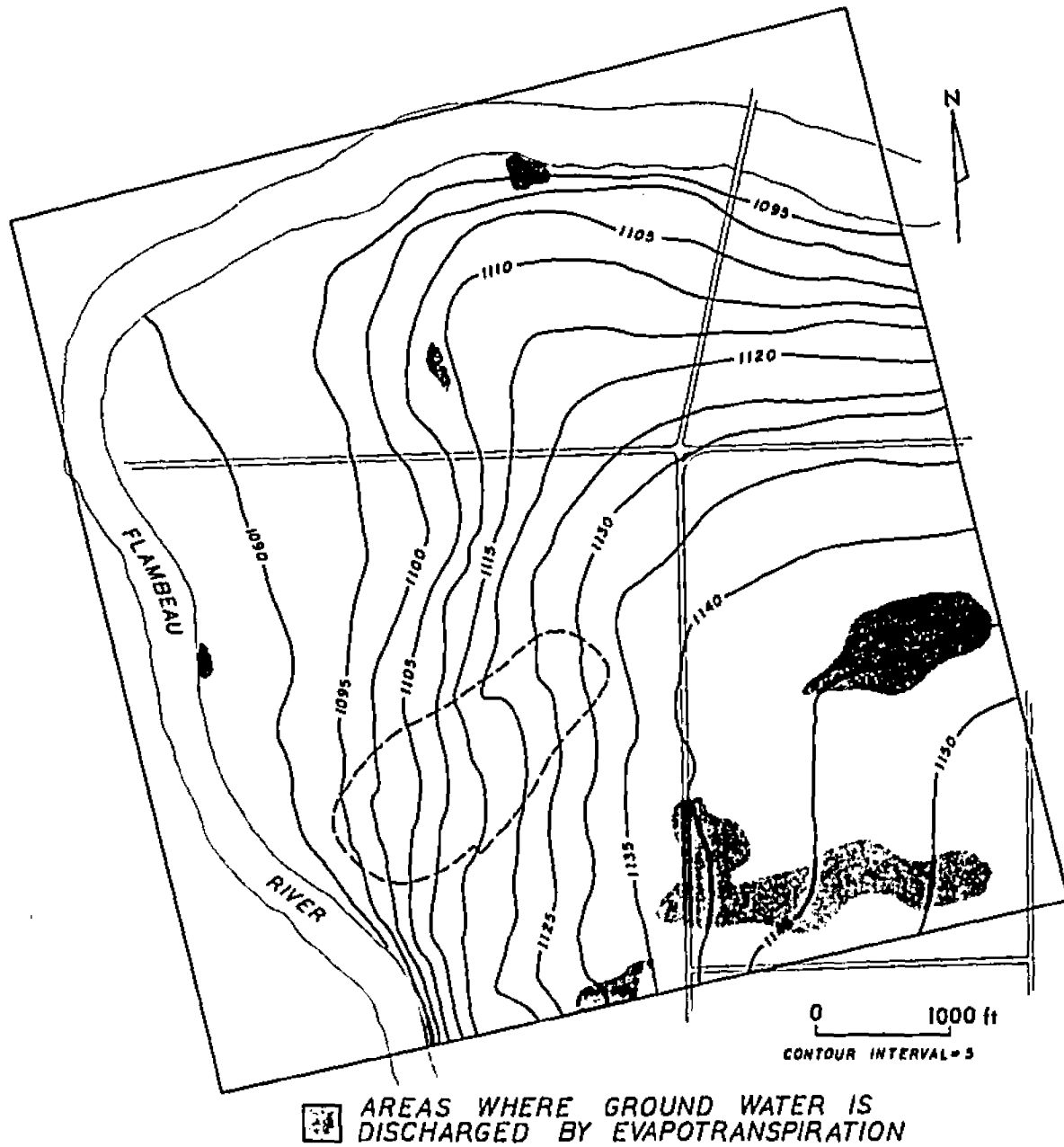


FIGURE 30. Steady-state head distribution in the mine area generated by the model after calibration.

correspond to the wetlands in Figure 19 suggests the large wetlands northeast and southeast of the pit location may owe their existence to 1) ground water discharged from surface seeps in adjacent areas where the water table intersects the the land surface and(or) 2) to ponded surface water (see figures 18A and 18D). The vapor-discharge areas in Figure 30 probably represent the average condition since fluctuations in water-table elevations throughout the year would cause these areas to differ in extent and shape.

Figure 31 illustrates the distribution of hydraulic conductivity values resulting from calibrating the model. The water table in upland till areas in the eastern portion of the study area is reproduced best with conductivities ranging from 0.2 to 0.9 ft/d (0.1 to 0.3 m/d). This range compares very well with the field conductivities at the mine cited in Table 7. There are several areas where till conductivities are somewhat higher but still within the range of the values in Table 7. The most notable of these areas occurs just south of the planned pit perimeter and corresponds to a topographic high. Calibrated hydraulic conductivities there range from 1.2 to 4.2 ft/d (0.4 to 1.3 m/d) indicating, perhaps, a greater abundance of coarsely granular material in the till at that locality. The small area of slightly greater conductivity occurring along the southern margin of the study area corresponds to a prominent drainage swale which discharges into the Flambeau River near the mouth of Meadowbrook Creek. The higher conductivities there may be



FIGURE 31. Areal distribution of hydraulic conductivity resulting from the calibration of the mine-pit model.

related to the presence of partially sorted alluvial sediments associated with the swale.

Figure 31 displays an increase in hydraulic conductivities westward toward the Flambeau River through the area dominated by the outwash materials. Values range from 1.4 ft/d (0.4 m/d) just west of the till area to nearly 60 ft/d (18 m/d) along the river west of the proposed pit. The upper range of outwash conductivities departs considerably from those in Table 7, but few field tests were conducted in unconsolidated materials close to the river. An area of moderate conductivity within the pit perimeter extends farther eastward than might be expected from the location of the till/outwash contact in Figure 8. One reason for this is the occurrence of outwash sediments east of the primary till/outwash boundary. Moreover, the Cambrian sandstone over the ore deposit has hydraulic conductivities similar to those of outwash in the study area, resulting in a high average conductivity within the pit boundaries where the sandstone is thick in relation to the till.

Table 10 lists the results of a steady-state groundwater budget computed by the model from all sources and discharges at every node. It is evident that total sources and discharges are well balanced in the study area. The areal recharge rate computed by the model agrees very well with the rate determined in Chapter V from the empirical results (Table 6, 0.234 cfs), indicating that recharge has been well represented in the model. This value was also used in Chap-



TABLE 10. Steady-state ground-water budget for the natural pit area determined from mass-balance computations by the model.

---

	Rates (cfs)
SOURCES:	
Areal recharge	0.2292
Constant-head	0.0397
Total	0.2689
DISCHARGES:	
Evapotranspiration	0.0303
Constant-head	0.2386
Total	0.2689

---

ter V to approximate base flow to the river. The constant-head source represents underflow into the study area which amounts to about 15 percent of the total sources; recharge accounts for the remainder. Approximately 97 percent of the constant-head discharge (0.2313 cfs or  $0.0065 \text{ m}^3/\text{s}$ ), or 86 percent of all ground-water discharges, represents the base-flow contribution to the Flambeau River. This rate is within 2 percent of the estimate (exclusive of underflow) made in Chapter V by summing the recharge rates in Table 5 over the corresponding areas of the site. The remaining 3 percent of the constant-head discharge is underflow out of the model boundaries near the large swale south of the pit location.

Evapotranspiration accounts for about 11 percent of all

ground-water discharges in the unstressed state. The rates in Table 10 represent average conditions and similar determinations based on specific seasonal data may depart from the values reported here.

### Steady-State Stress Simulations

#### General Discussion

The simulations of the mine pit were carried out for two major cases: 1) The large, 55-acre open pit portrayed in previous figures and 2) a smaller direct-ship open pit shown later. Each of these case studies included simulations of several subcases such as the pit with and without an enclosing slurry wall. In the direct-ship case, the use of dewatering wells was also examined.

All of the simulations are for steady flow conditions. In most cases, steady state will be attained only if a given set of hydrologic conditions persists long enough for the flow system to achieve equilibrium. In this sense, the simulative results for the pit area may be looked upon as upper limits on the range of possible hydrologic effects caused by each set of conditions.

#### Large Open Pit - Interior Drainage System

Any excavation below the water table will result in the seepage of ground water into the hole. Rates of inflow depend on the size and depth of the excavation and on the water-

transmitting properties of soils surrounding it. Generally, soils with low hydraulic conductivities restrict seepage into open excavations while those with high transmissive properties facilitate seepage.

To establish a basis for comparison with later simulations, the mine pit was first simulated with no external water-control facilities such as wells and flow barriers. In real terms, this represents the collection of ground-water seepage with a system of sumps, ditches, and pumps inside the pit. Given this particular geologic setting and the limitations of the numerical model, this phase of the study was quite problematic. Since the Precambrian surface is a relatively impermeable boundary, excavation to or below it will result in the establishment of a seepage face on the side-walls of the pit above this surface. This seepage face is critical in defining hydraulic gradients near the pit perimeter and its characterization posed several modeling problems.

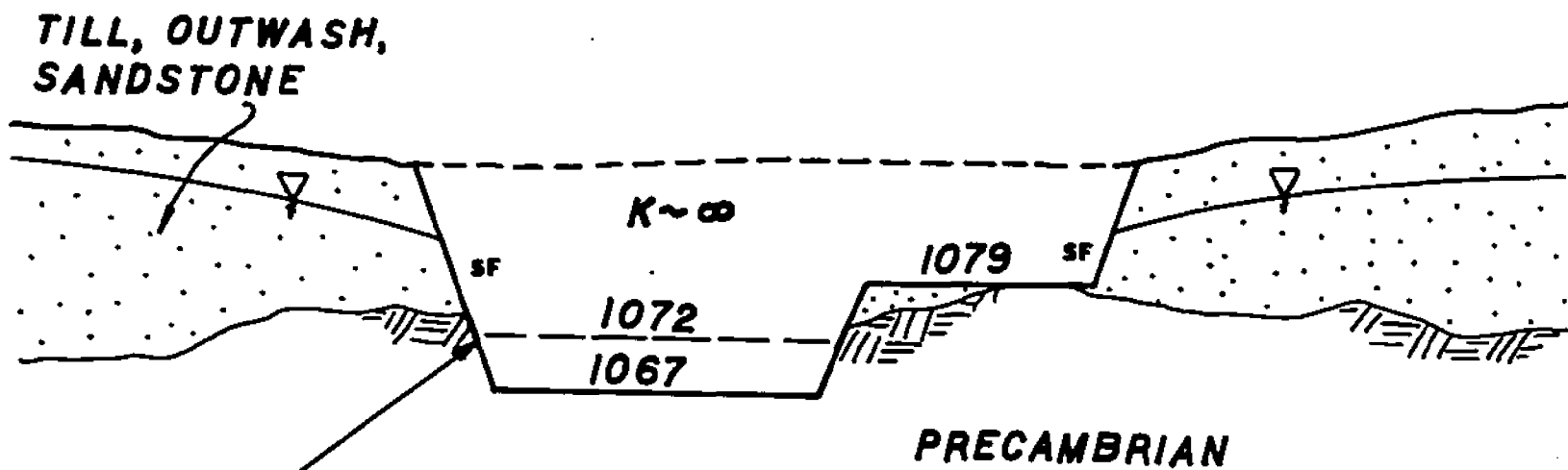
An attempt was made to define the top of the seepage face using the analogy of the pit wall to an earthen dam for which free-water surface approximations exist (see, for example, DeWiest, 1965; pp. 223-226). These methods, however, rely on homogeneous conditions and a constant value of hydraulic head on the up-gradient side of the dam, causing the pit/dam analogy to break down. In addition, had this method been successful, it would have required the manual calculation of a separate seepage-face elevation for each node adjoining the pit perimeter.

Searching further for an adequate approach, several trial runs were made by choosing arbitrary seepage-face heights. Nodes just inside the pit boundary were assigned constant-head values equal to the elevation of the Precambrian surface at each point plus the arbitrary face height. Nodes within this peripheral constant-head boundary were then assigned zero heads and hydraulic conductivities so that only fluxes toward the constant-head nodes from outside the pit were evaluated. Though this technique produced numerical results which established the mine pit as a ground-water sink, it had several shortcomings which compromised its plausibility. First, there was no physical justification for the selected face heights and, since the top of the face was fixed, it could not adjust itself to a more reasonable value based on system properties. Secondly, the method assumed that the top of the seepage face was the same height above the Precambrian surface at each node, causing the upper face boundary to parallel the Precambrian contact. It is more likely that the top of an actual seepage face would occur at a more or less uniform elevation around the circumference of the pit with some undulation resulting from differences in soil conductivities, the topography of the Precambrian surface, and the influence of the Flambeau River. It was possible to choose an upper face elevation which was constant around the pit perimeter, but the validity of the selected height would have remained in doubt.

It was finally decided that the most supportable and

realistic approach would be to allow the model to generate an approximation of the seepage-face height based on the properties of water-bearing materials and prevailing hydraulic gradients along the pit perimeter. This was accomplished by first giving nodes within the pit boundary a very high conductivity to represent the infinite conductivity of the excavated void, as shown in Figure 32. The format in the model code for the conductivity matrix and the matrix multiplier established during data preparation permitted a maximum hydraulic conductivity of 23,328 ft/d (7,110 m/d) which is beyond the highest values for natural materials by about an order of magnitude. Additionally, recharge to all nodes within the pit was eliminated.

The next step in the procedure was the assignment of a uniform pit-floor elevation which placed the bottom of the pit at least 5 ft (1.5 m) below the aquifer/Precambrian contact. For example, the floor within most of the 3-year mine pit was set at an elevation of 1067 by modifying the matrix of Precambrian surface elevations (Figure 32). In the eastern part of the 3-year pit, the Precambrian surface was lowered to the true pit-floor elevation of about 1079 at nodes where the Precambrian elevation is greater than 1079 (see cross section in Figure 3). To provide a sink for ground water entering the pit, a single node with a constant head set at 4 to 5 ft (1.2 to 1.5 m) above the pit floor (but below the aquifer/Precambrian contact) was designated at the center of the excavation. The 4- to 5-ft range was chosen in



Elevation to which the pit is dewatered by the central constant-head sink.

FIGURE 32. Schematic representation of the method used to approximate the seepage face (SF) and its effects on surrounding flow gradients. Elevations shown are those used in simulating the 3-year mine pit.

order to provide a high transmissivity at the sink (a 5-ft saturated thickness yields a sink transmissivity of 116,640  $\text{ft}^2/\text{d}$ , or 10,836  $\text{m}^2/\text{d}$ ). This representation of the pit allows the simulated excavation to dewater to the constant-head sink elevation below the aquifer/Precambrian contact at nearly every point along the pit perimeter, as illustrated diagrammatically in Figure 32. The lower hydraulic conductivities of materials along the pit walls then maintain higher groundwater levels which approximate the height of the seepage face. As an added benefit, the steady-state rate of groundwater seepage into the pit is computed as the flux to the central sink.

The results of the above procedure are encouraging except for oscillations of the solution. Using the 3-year pit as an example, convergence could not be achieved within 600 iterations using an error tolerance of 0.001 and relaxation-parameter values ( $B'$ ) less than 0.5. Decreasing  $B'$  tended to dampen large oscillations early in the iterative process but did not reduce residuals below the error tolerance. The tolerance was subsequently increased to 0.002 and the solution converged within 100 iterations using an optimal  $B'$  of 0.4 (for comparison, the unstressed model requires only 15 iterations to converge using an error tolerance of 0.001 and a  $B'$  of 0.6). The oscillatory behavior may be due in part to the large contrasts (3 to 5 orders of magnitude) in hydraulic conductivities at the pit boundaries stemming from the high conductivities used to represent the interior of the excava-

tion. Another contributing factor may be the large differences in hydraulic head between the constant-head sink in the pit and heads outside the pit perimeter. These pronounced disparities may be accentuating the nonlinearities of the water-table problem at some nodes to produce the oscillations. Lowering B' causes additional under-relaxation of the solution and dampens oscillatory behavior.

Figure 33 shows the hydraulic-head distribution resulting from the 3-year mine pit, as outlined in Figure 3, with no water-control facilities other than the removal of water within the pit through the sink. It is evident that the pit, even at early stages of its construction, could exert a substantial influence on the southern half of the study area. The effects extend to the constant-head boundaries along the southern and eastern margins of the modeled area, indicating that drawdowns may actually be more pronounced and extensive than suggested by Figure 33. Particularly interesting is the induced ground-water flow from the Flambeau River at the pit's west end, and the areas to the southwest and east where water-bearing materials along the pit perimeter are completely dewatered. The dewatered areas generally correspond to places where thin soils and sandstone overlies highs on the Precambrian surface. The flux into the pit computed at the central constant-head sink, exclusive of evaporation and incident precipitation, is approximately 0.1 cfs ( $0.0028 \text{ m}^3/\text{s}$ ), or about 45 gpm. Approximately 26 percent of this flow is derived from the Flambeau River. Though this seepage rate ap-



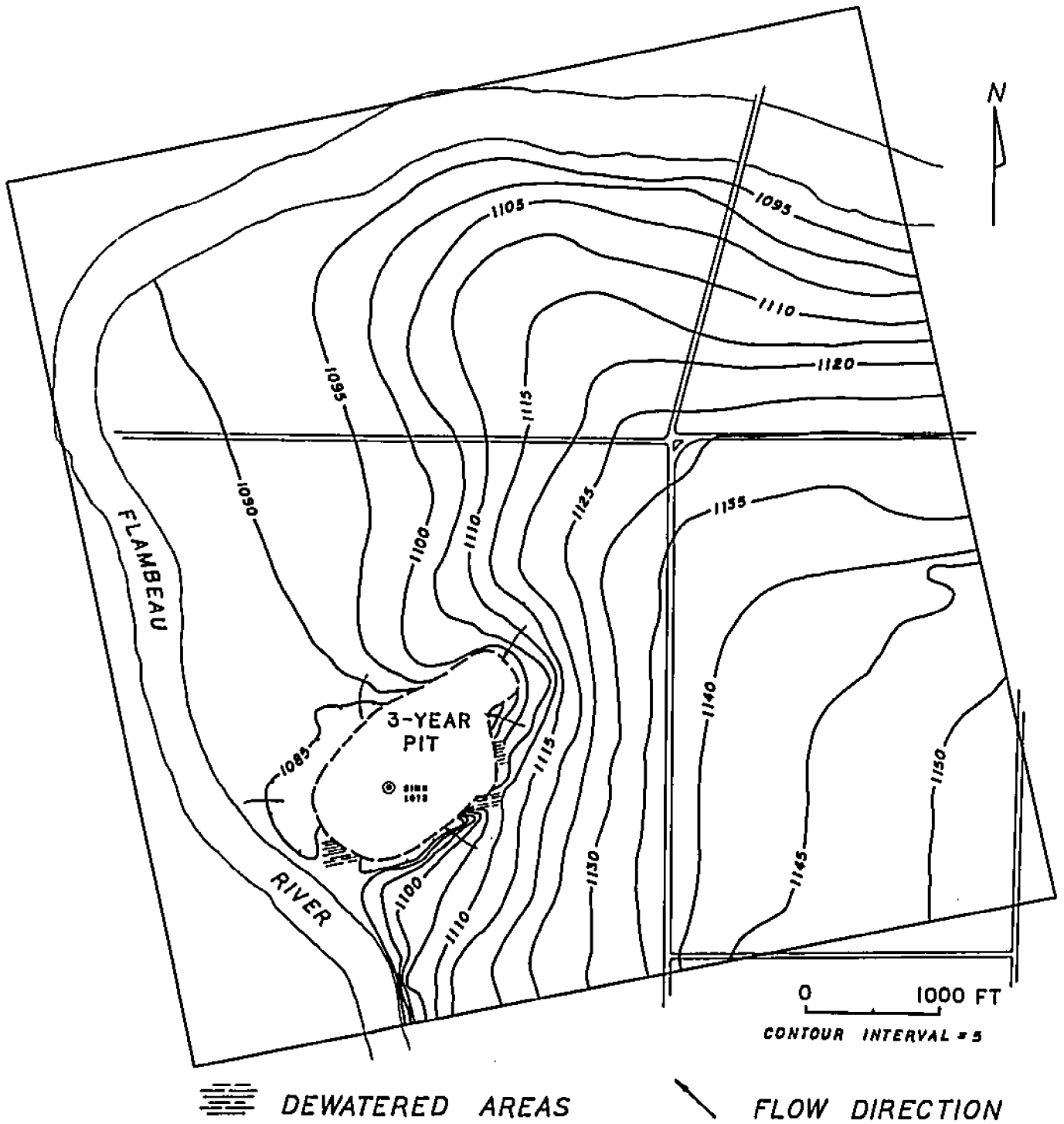


FIGURE 33. Simulated steady-state distribution of hydraulic head due to the 3-year mine pit with internal drainage facilities.

pear to be quite low, it is important to note that it is strictly valid only for steady-state conditions; it is probably lower than initial seepage rates.

Simulating the 4-year open pit required extending the pit to the northeast in the model (Figure 3). The pit floor in the extension area was maintained at an elevation of 1079 and the floor in the western part of the pit was kept at 1067 as in the case of the 3-year pit. The additional area was then assigned the maximum hydraulic conductivity of 23,328 ft/d (7,110 m/d) cited earlier and an areal recharge of zero. Due to convergence problems, the simulation could be accomplished only by increasing the error tolerance to 0.003 and decreasing  $B'$  to 0.3. In addition, the elevation of the central constant-head sink was decreased to 4 ft (1.2 m) above the pit floor (1071 ft msl) to lower its transmissivity, increase flow gradients, and accelerate discharge from the pit. This was done in an attempt to minimize large mass-balance errors which showed that water sources exceeded discharges by nearly 10 percent when a saturated thickness greater or less than 4 ft was used. Increasing the elevation of the sink above 4 ft, while raising its transmissivity, also reduced flow gradients toward the sink so that discharges declined and the mass-balance error became larger. When saturated thicknesses less than 4 ft were used, the accompanying increases in hydraulic gradients toward the sink were apparently insufficient to overcome the additional resistance caused by the lower transmissivity, also increasing

the error in the mass balance. Even at the optimal 4-ft thickness, sources exceeded discharges by more than 8 percent. In spite of these modifications, convergence was still very slow and was achieved only after 561 iterations.

The simulated steady-state head distribution resulting from seepage into the 4-year mine pit is illustrated in Figure 34. The effects in the southern half of the study area are similar to those exerted by the 3-year pit only exaggerated to some degree. Similarly, the drawdowns in Figure 34 are probably less than the true drawdowns would be because of dampening by the constant-head boundaries to the south and east. Drawdowns west of the pit have increased in response to the greater up-gradient interception of flow by the enlarged pit, and induced flow from the Flambeau River has increased accordingly. The dewatering of soil and sandstone to the southeast is slightly more extensive in relation to the 3-year pit and additional desaturation is evident along the northern margin of the pit. The steady-state seepage flux at the central constant-head sink is about 0.07 cfs ( $0.002 \text{ m}^3/\text{s}$ ), or approximately 31 gpm. Induced seepage from the Flambeau River is approximately 0.028 cfs ( $0.0008 \text{ m}^3/\text{s}$ ), or about 13 gpm. As explained earlier with regard to the 3-year pit, these seepage rates are meaningful only for steady-state conditions.

The internally drained mine pit was next simulated using the pit dimensions expected to be attained after 11 to 12 years of operation (Figure 3). Data modifications accounting

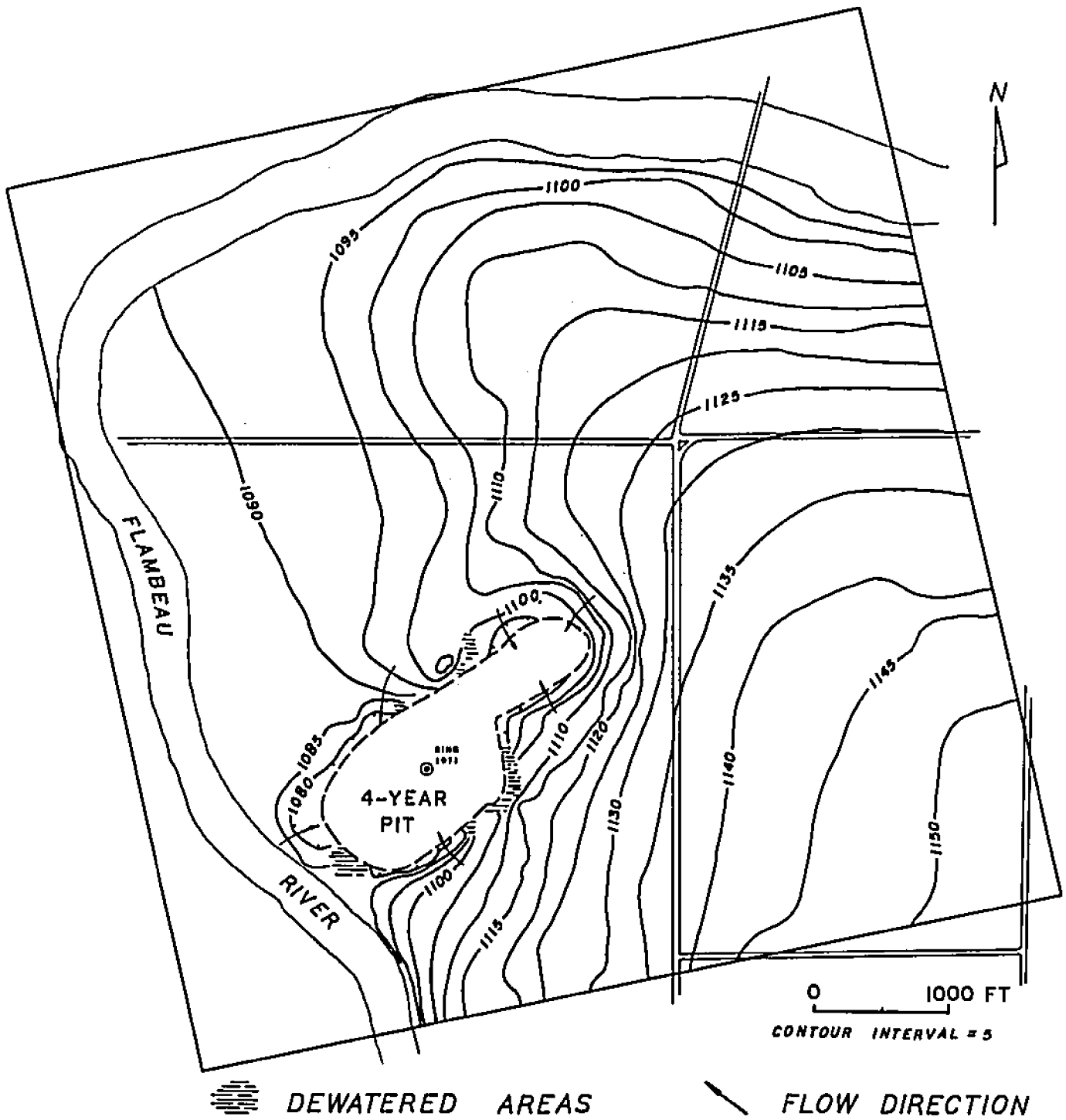


FIGURE 34. Simulated steady-state distribution of hydraulic head due to the 4-year mine pit with internal drainage facilities.

for the enlargement of the pit were the inclusion of nodes along the pit's southeastern margin, the assignment of the maximum hydraulic conductivity and zero areal recharge to these nodes, and lowering the pit bottom to a uniform elevation of 1060.

Lowering the pit floor to 1060 ft msl placed it approximately 5 ft (1.5 m) below the aquifer/Precambrian contact. The elevation of the central constant-head sink was then set 5 ft above the pit floor. The assumption that the entire interior of the pit occurs at 1060 is, of course, a simplification and requires the simulated excavation to have vertical sidewalls at its boundaries. In reality, the pit walls will consist of a series of benches with an overall slope angle of  $35^{\circ}$  to the bottom (see Figure 3). The scale of the problem prevented the representation of the benches in the model. In any case, the assumption of vertical walls at the pit perimeter is a limiting supposition; simulated hydraulic gradients at the pit boundaries and associated water-level changes near the excavation are probably larger than would occur under real conditions with sloping sidewalls owing to the high conductivity of the pit interior in the model.

The final-pit simulation had no convergence problems and produced the best overall results. Successive runs allowed an optimal error tolerance of 0.001 and a B' of 0.5 to be determined. Convergence occurred after 74 iterations with these values and mass-balance errors were generally less than 0.05 percent. Simulated seepage into the final pit

produced the steady-state head distribution shown in Figure 35. The most significant drawdowns occur within 500 ft (150 m) of the perimeter and are most pronounced at the east end where simulated gradients approach 12 percent. That area is characterized by low-conductivity soils capable of supporting steep gradients and simulated head losses there approach 40 ft (12 m). Flow patterns in the remainder of the study area are little changed from Figure 34. Extensive areas of dewatered soils and sandstone occur along the northern, western, and southern sides of the excavation. Desaturation is most widespread where thin water-bearing materials occur over Precambrian features of positive relief. The steady-state seepage rate into the pit computed by the model is approximately 0.08 cfs ( $0.0023 \text{ m}^3/\text{s}$ ), or about 36 gpm. About 15 gpm ( $0.0009 \text{ m}^3/\text{s}$ ) of this total is induced infiltration from the Flambeau River. In spite of more seepage-face area, the total flux is lower for the final pit than for the 3-year configuration; this is the result of dewatering adjacent to the pit and the eastward expansion of the pit into less-transmissive materials.

Table 11 is the steady-state ground-water budget computed by the model for the final-pit conditions using all sources and discharges of water. Comparison with rates for the undisturbed case in Table 10 shows some significant changes. Considering areal recharge, the effect of the final pit is a 12 percent reduction brought about by the loss of recharge formerly occurring through the excavated soils. Increased

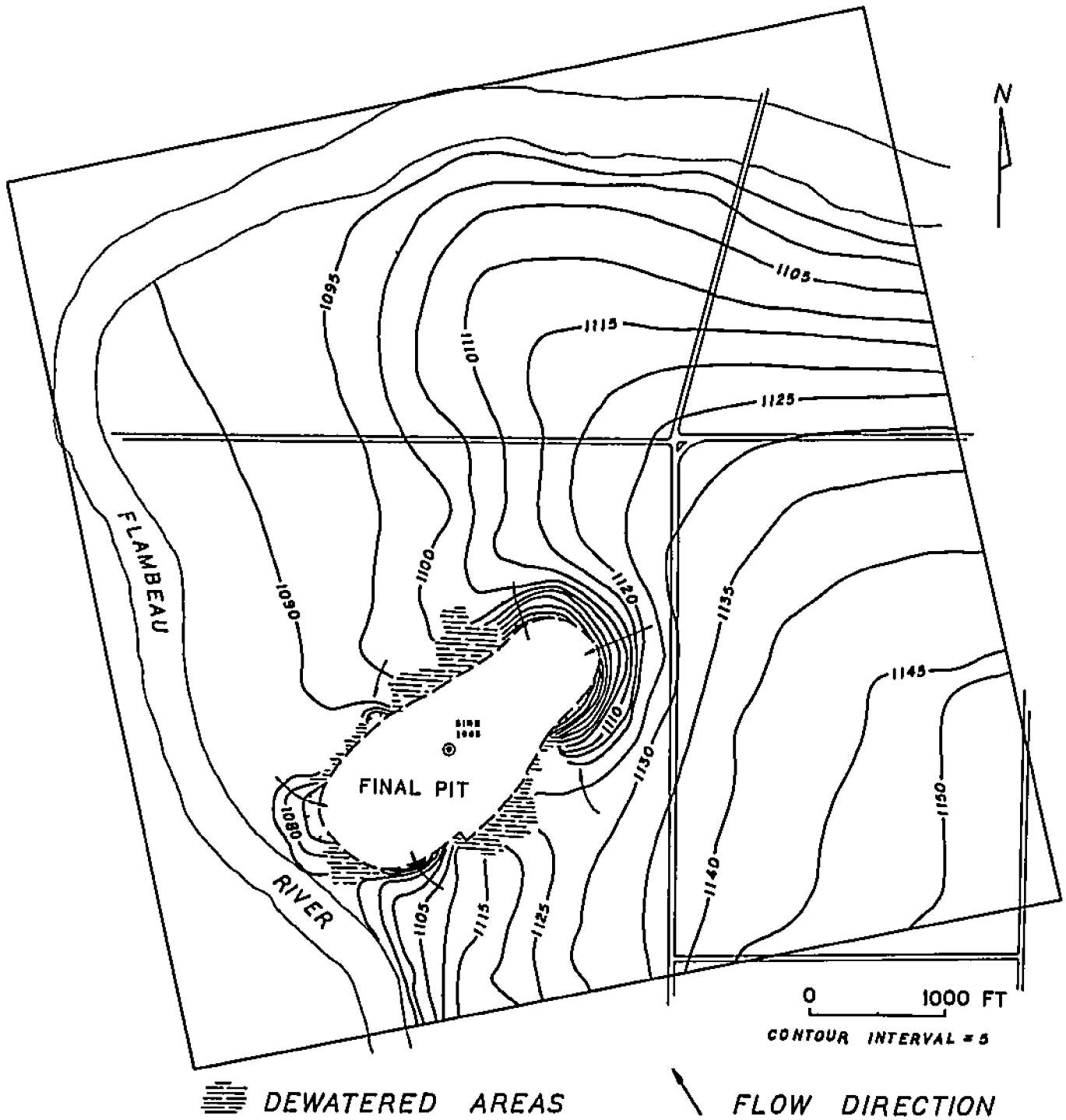


FIGURE 35. Simulated steady-state distribution of hydraulic head due to the final mine pit with internal drainage facilities.

TABLE 11. Steady-state ground-water budget for the pit area resulting from the final pit with an internal seepage-collection system.

---

	Rates (cfs)
<b>SOURCES:</b>	
Areal recharge	0.2021
Constant-head	0.0708
Total	0.2729
<b>DISCHARGES:</b>	
Evapotranspiration	0.0187
Constant-head	0.2541
Total	0.2728

---

underflow into the study area and induced flow from the Flambeau River combine to increase constant-head sources by nearly 180 percent.

Discharges are also significantly affected. Evapotranspiration is reduced by about 38 percent owing to water-level declines near the pit which drop the water table below the effective depth of vapor discharge. Though not shown in Figure 35, the total area through which the evapotranspiration of ground water occurs is also greatly diminished. The constant-head discharge rate in Table 11 is approximately 6 percent larger than the corresponding rate in Table 10 in spite of the reduction in base flow to the Flambeau River. The difference is the discharge of seepage at the central constant-head sink.



### Large Open Pit - Perimeter Slurry Wall

Another possible water-control strategy is to enclose the mine pit with a slurry wall 2 to 3 ft (0.6 to 0.9 m) thick. Slurry walls, or slurry-trench walls, are constructed in unconsolidated materials by first excavating a narrow vertical trench. As the soil is removed, a bentonite slurry with a specific gravity of 1.2 to 1.8 g/cm<sup>3</sup> is pumped into the trench to support the walls of the excavation. The trench is then backfilled with excavated soil or selected imported materials. The backfilling displaces most of the slurry, but much of the bentonite fills voids within and between the backfill particles to create a relatively homogeneous and continuous mass of low hydraulic conductivity. Excavations by this process have been carried out through several hundred feet of unconsolidated material (Person. commun., B. D. Trexler; 1983).

A slurry wall around the mine pit would penetrate the full saturated thickness of the Paleozoic and Pleistocene sediments and would be keyed into the low-conductivity saprolite covering the Precambrian surface. Its purpose would be to minimize the need for collecting and treating large volumes of water by significantly retarding the rate of ground-water flow into the pit. The expected range of *in situ* hydraulic conductivities for the wall material is  $2.83 \times 10^{-3}$  to  $5.67 \times 10^{-3}$  ft/d ( $1 \times 10^{-6}$  to  $2 \times 10^{-6}$  cm/s) (Xanthakos, 1979). This range places the conductivity of the wall material 5 to 7 orders of magnitude lower than the till at the site and indicates near impermeability. The wall was therefore simulated

by treating the area within the final pit perimeter as in impermeable island within the flow system. This area is represented in the model by 153 nodes and was defined by assuming that the wall would be approximately coincident with the pit perimeter.

The simulated effects of the wall on the surrounding flow system are shown in figures 36 and 37. The most apparent results are the mounding of ground water on the eastern and southern (up-gradient) sides of the pit and a relatively smaller decline in water levels to the west and northwest. The largest water-level changes occur close to the wall and diminish rapidly with distance away from it. These changes are the direct result of ground-water flow obstruction and recharge loss.

The wall acts as a barrier to subsurface flow, impounding water on its up-gradient side. Increases in heads of 0.2 ft (6 cm) or more extend up to 2,900 ft (880 m) to the northeast, 1,600 ft (490 m) to the east, and at least 1,275 ft (390 m) to the south. The extent of effects beyond the southern boundary of the modeled cannot be defined absolutely, though it is unlikely they reach beyond Meadowbrook Creek 2,400 ft (730 m) from the pit. Simulated head increases of up to 14 ft (4.3 m) occur along the south-central margin of the pit perimeter. The mounding of ground water is reflected in Figure 36 by a westerly displacement of water-table contours east and south of the pit. Since the wall acts as a flow line, the water-table contours along the northern and southern sides of the

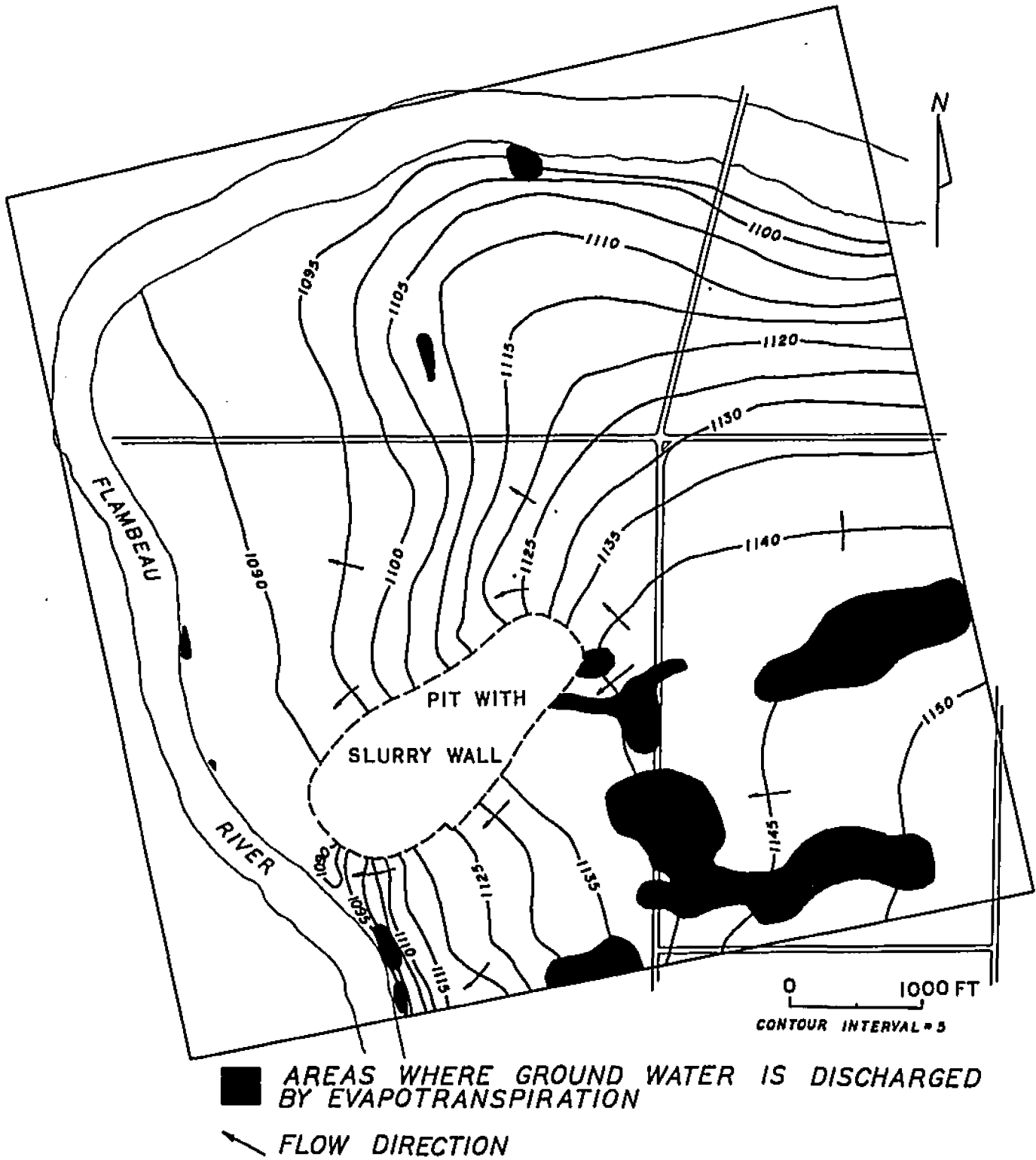


FIGURE 36. Simulated steady-state distribution of hydraulic head due to a low-conductivity slurry wall around the large open pit.



—±5— INCREASES/DECREASES IN WATER LEVELS (FT)

FIGURE 37. Changes in hydraulic head caused by encircling the large pit with a slurry wall.

pit reflect the diversion of ground water to the southwest parallel to the wall. If the effects of the small amount of seepage through the wall are considered, the areal extent and magnitude of the water-level increases would be slightly less.

The up-gradient damming of water and the loss of recharge through the pit deprive down-gradient areas of water, causing the head losses to the west and northwest. Declines in water levels are less pronounced and extensive than the up-gradient changes because of the moderating influence of the Flambeau River and the inability of the highly conductive outwash deposits to maintain steep flow gradients. The area of simulated declines does not extend more than 1,400 ft (425 m) northwestward from the pit and the most prominent head losses are limited to areas adjacent to the slurry wall where they do not exceed 8.3 ft (2.5 m).

Table 12 summarizes the changes in the steady-state ground-water budget due to the slurry wall. Several important differences are noted with respect to Table 10. The rate of recharge is decreased notably by the loss of recharge formerly occurring through the area occupied by the mine pit. This condition contributes in part to the fall in water levels down-gradient of the pit. Underflow into the modeled area, represented as a constant-head source, decreases slightly as the hydraulic gradient southeast of the pit is decreased by the mounding.

A significant change in the budget is an increase in the area affected by ground-water evapotranspiration. As ground

TABLE 12. Steady-state ground-water budget for the pit area resulting from the installation of a low-conductivity slurry wall around the mine pit.

	Rates (cfs)
<b>SOURCES:</b>	
Areal recharge	0.2067
Constant-head	0.0391
Total	0.2458
<b>DISCHARGES:</b>	
Evapotranspiration	0.0380
Constant-head	0.2078
Total	0.2458

water is dammed on the eastern and southeastern sides of the slurry wall, the accompanying mounding raises the water table close enough to the land surface in some areas for ground water to be discharged by vegetation and evaporation. Figure 36 illustrates the proportion of the study area affected by ground-water evapotranspiration with the slurry wall in place. The vapor-discharge areas have been enlarged by more than 25 percent to about 67 acres (27 ha) compared to natural conditions. Evapotranspiration also comprises more than 15 percent of the total discharges versus 11 percent in the undisturbed state.

The largest budget change is the decline in the rate of constant-head discharge which accounts mainly for base flow to the Flambeau River. The mounding east of the slurry wall

and the loss of recharge through the pit location reduce flow gradients west and northwest of the pit, proportionately reducing the rate of flux toward the river. The flow rate to the Flambeau diminishes from 0.2313 cfs ( $0.0065 \text{ m}^3/\text{s}$ ) in Table 10 to 0.2011 cfs ( $0.0057 \text{ m}^3/\text{s}$ ), a decrease of 13 percent. The area of depressed water levels in Figure 37 is obviously smaller than the area of increased heads to the east; it appears the reduction in base flow partially compensates for the decrease in underflow and the loss of recharge from the east and southeast sides of the pit.

#### Direct-Ship Pit - Interior Drainage System

An alternative to the large open pit featured previously is the direct-ship or direct-smelt method. This approach involves the construction of a smaller pit to extract only ore rich enough to be economically transported directly to a smelting facility without on-site processing. A pit of this type would be constructed at the southwest end of the ore deposit and, as presently envisioned, would have a life of 5 to 6 years. Its estimated maximum dimensions are a length of 975 ft (300 m) along strike and a width of about 700 ft (215 m), encompassing an area of 11 acres (4.5 ha). The direct-ship pit was simulated for the cases of an interior drainage system, dewatering wells, and an enclosing slurry wall.

The direct-ship pit was initially studied for the case

in which only an internal seepage-collection system is employed to control flow into the pit. Such an interior system normally consists of a series of sumps, ditches, and pumps. As for the larger pit, this physical situation will result in the genesis of a seepage face above the Precambrian contact on the sidewalls of the excavation. This similarity dictated that the direct-ship pit be simulated in the same manner for these conditions.

The problem first required that all interior nodes be assigned zero areal recharge rates and the maximum hydraulic conductivity of 23,328 ft/d (7,110 m/d). The Precambrian surface inside the pit boundaries was set at a uniform elevation of 1074 so that it was everywhere at least 5 ft (1.5 m) below the contact of the aquifer and the saprolite. A central constant-head node was designated 5 ft above the pit floor to provide a sink for inflowing water. This method allows the interior of the pit to desaturate to the level of the sink below the aquifer/Precambrian contact during simulation. The soils of lower conductivity outside the pit perimeter then maintain water levels approximating the seepage face and hydraulic gradients in the vicinity of pit are accurately represented. The central sink has the additional advantage of permitting the steady-state rate of seepage into the pit to be computed.

The above method is successful in simulating the internally drained direct-ship pit, though it may tend to overestimate local head losses because of the assumption that the



entire pit interior occurs at the floor elevation. When an error criterion of 0.001 and a  $B'$  of 0.4 are used, convergence occurs after 63 iterations. The mass-balance computations, however, indicate that simulated discharges exceed sources of water by over 4 percent. Decreasing the saturated thickness at the sink prevents convergence and increasing the sink elevation 1 ft (0.3 m) to 1080 only slightly improves the mass balance.

The hypothetical direct-ship pit with no external water-control facilities generates the head distribution displayed in Figure 38; actual decreases in simulated heads are illustrated in Figure 39. The areal influence of the pit is limited compared to the simulated stresses induced by the large mine pit. Comparison with the unstressed case (Figure 30) shows that the most obvious effect is a local distortion of the water-table contours reflecting flow toward the excavation. A small amount of flow is also diverted from the area between the pit and the Flambeau River, although the result is a reduction in base flow to the river rather than induced infiltration from it. Figure 38 also shows the relatively minor areas to the southwest and northeast where water-bearing materials are dewatered by seepage into the pit. Drawdowns in excess of 2 ft (0.6 m) in Figure 39 are limited to within 1,200 ft (370 m) of the excavation perimeter; declines of 0.2 ft (6 cm) or more extend up to 3,100 ft (950 m) to the northeast. The steady-state flux to the central sink from the surrounding soils and sandstone is approximately 0.055 cfs

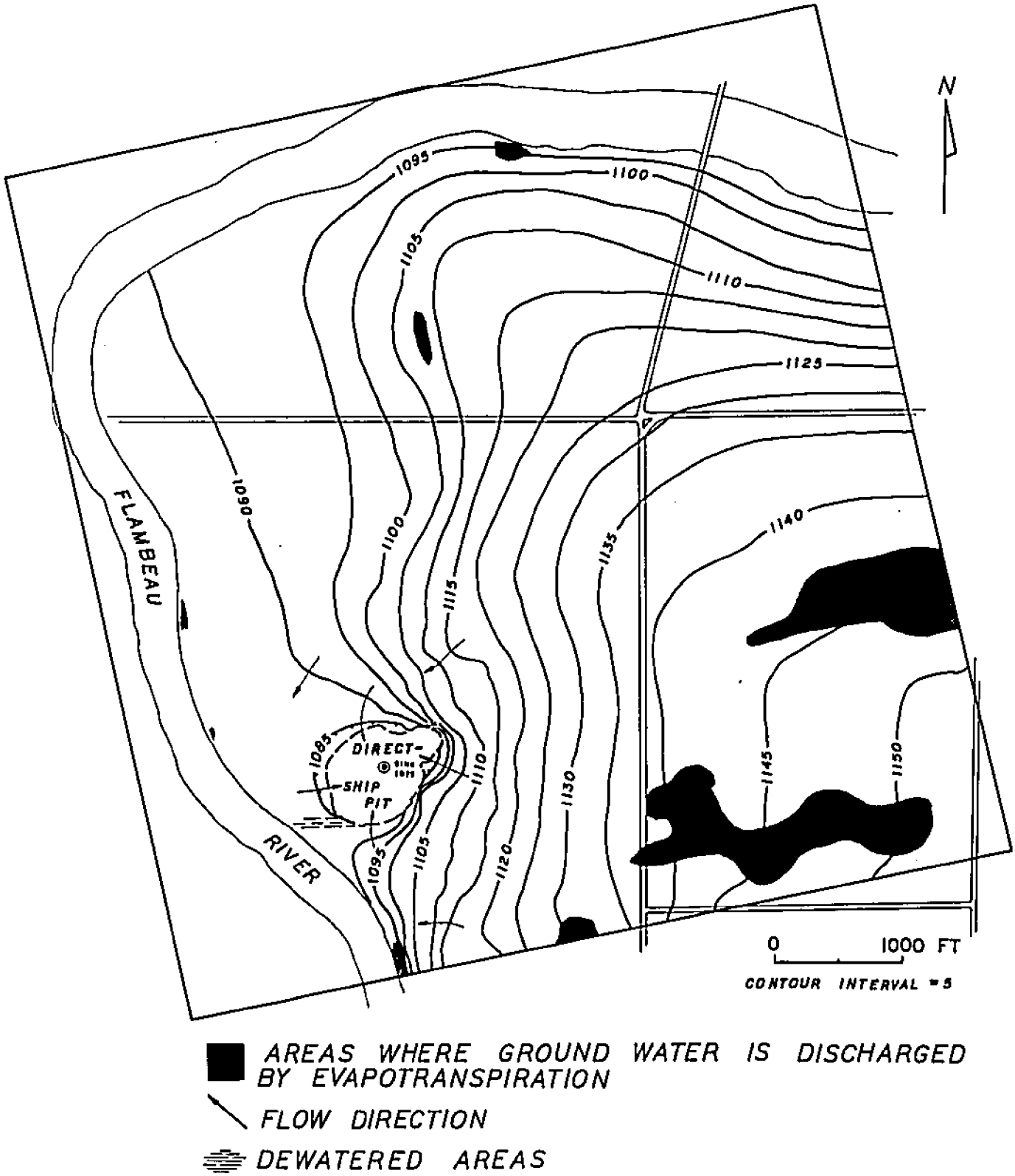


FIGURE 38. Simulated steady-state head distribution due to an internally drained direct-ship pit.



-5- DECREASES IN WATER LEVELS (FT)

FIGURE 39. Changes in hydraulic head due to an internally drained direct-ship pit.

(0.0016 m<sup>3</sup>/s) which is equivalent to about 25 gpm.

The steady-state ground-water budget for this simulation is presented in Table 13. Only small changes are noted with respect to the budget for the undisturbed case given in Table 10. Areal recharge decreases by a small amount owing to the loss of input through the excavated pit, and the rate of underflow (constant-head source) increases slightly as gradients steepen somewhat in response to water collection by the mine. For the discharges, evapotranspiration is lessened by the head losses in the vicinity of the pit; figures 30 and 38 show the accompanying shrinkage in the area affected by vapor discharge. The constant-head discharge increases in spite of diminished base flow to the Flambeau River as a result of the discharge through the central sink in the pit.

#### Direct-Ship Pit - Dewatering with Wells

The direct-ship pit was next simulated using a series of wells around the pit to dewater the sediments within its perimeter. External dewatering is used when expected seepage rates are so high that internal collection might be unmanageable. It is accomplished by using closely spaced, mutually interfering wells to create a composite cone of depression over the work area. This technique is often used in advance of pit construction to promote slope stability, so that excavation and mine working can take place in relatively dry conditions below the natural elevation of the water table, and to protect water

TABLE 13. Steady-state ground-water budget of the mine area for the direct-ship pit with an internal seepage-collection system.

---

	Rates (cfs)
<b>SOURCES:</b>	
Areal recharge	0.2218
Constant-head	0.0404
Total	0.2622
<b>DISCHARGES:</b>	
Evapotranspiration	0.0284
Constant-head	0.2453
Total	0.2737

---

quality. At sites where saturated materials occur beneath the excavation, dewatering is used to prevent heaving or boiling in the bottom or, for underlying confined aquifers, to reduce uplift pressures and prevent blowouts as overburden is removed.

When contemplating the use of wells for a dewatering system, numerous potential problems must be considered to fully assess the physical and economic feasibility of the method. For example, use of a well system must usually be preceded by expensive and time-consuming aquifer tests. Knowledge of the aquifer parameters from pumping tests lends a degree of predictability to the aquifer behavior and allows the dewatering system to be designed to efficiently achieve

the desired results. An efficient dewatering system must be designed to maximize the amount of drawdown in the table or potentiometric surface with minimum pumping. Thus, the volume of water that must be pumped to reach a dewatering objective must be physically and economically reasonable. Other considerations are the high initial costs of installing wells, pumps, power facilities, and discharge-handling equipment; the availability and costs of power, maintenance, and record keeping; the length of time dewatering must occur before excavation is possible (often on the order of months); the usually continuous nature of advanced dewatering; and the cost of pumping during work stoppages.

Various well placements and pumping rates were tested with the pit model to find an optimal scheme for dewatering the direct-ship pit. Wells 6 inches (15.2 cm) in diameter were used at all pumping sites (Figure 40). The model algorithm assumes wells are fully penetrating, which accurately represents a real dewatering effort in this particular geologic setting. For excavations underlain by a relatively impermeable layer which limits drawdown (such as the saprolite), available drawdown is often increased by setting the well screens in holes that partially penetrate the surface of the barrier (U. S. Bureau of Reclamation, 1977). Inputs to the model to simulate the well system were the total number of wells, the column-row location of each well within the finite-difference grid, pumping rates, and well radii. Since the drawdown computed for a well node is an average

for the entire nodal area, the option to compute actual drawdowns at the wells was invoked to provide a more complete picture of the dewatering effects. Convergence problems were minimal and reducing B' from 0.6 to 0.5 decreased the number of iterations required for a solution from more than 75 to 25.

Trial-and-adjustment runs of the simulator resulted in a program consisting of nine peripheral wells and a central interior well, as illustrated in figures 40 and 41. The wells were located at nodes with relatively high average hydraulic conductivities to permit larger pumping rates and drawdowns. The simulated discharge rates, drawdowns, and heads at individual wells are given in Table 14. The pumping rates are maximums above which the wells go dry in the simulations. The 10 wells have a maximum combined discharge rate of 0.03767 cfs ( $0.00107 \text{ m}^3/\text{s}$ ), or 16.9 gpm. In reality, however, locally higher pumping rates may be possible since the averaging of hydraulic conductivities over the entire saturated thickness at each node masks the effects that small zones of high transmissivity have on pumping capacity.

Figure 40 depicts the simulated steady-state water table resulting from the pumping. Average computed water levels at all nodes were plotted to construct Figure 40, so cones of depression at each well are only weakly apparent using a 5-ft contour interval. At this stage, the pumping is not sufficient to reverse gradients and induce flow from the Flambeau River west of the pit but, instead, it reduces base

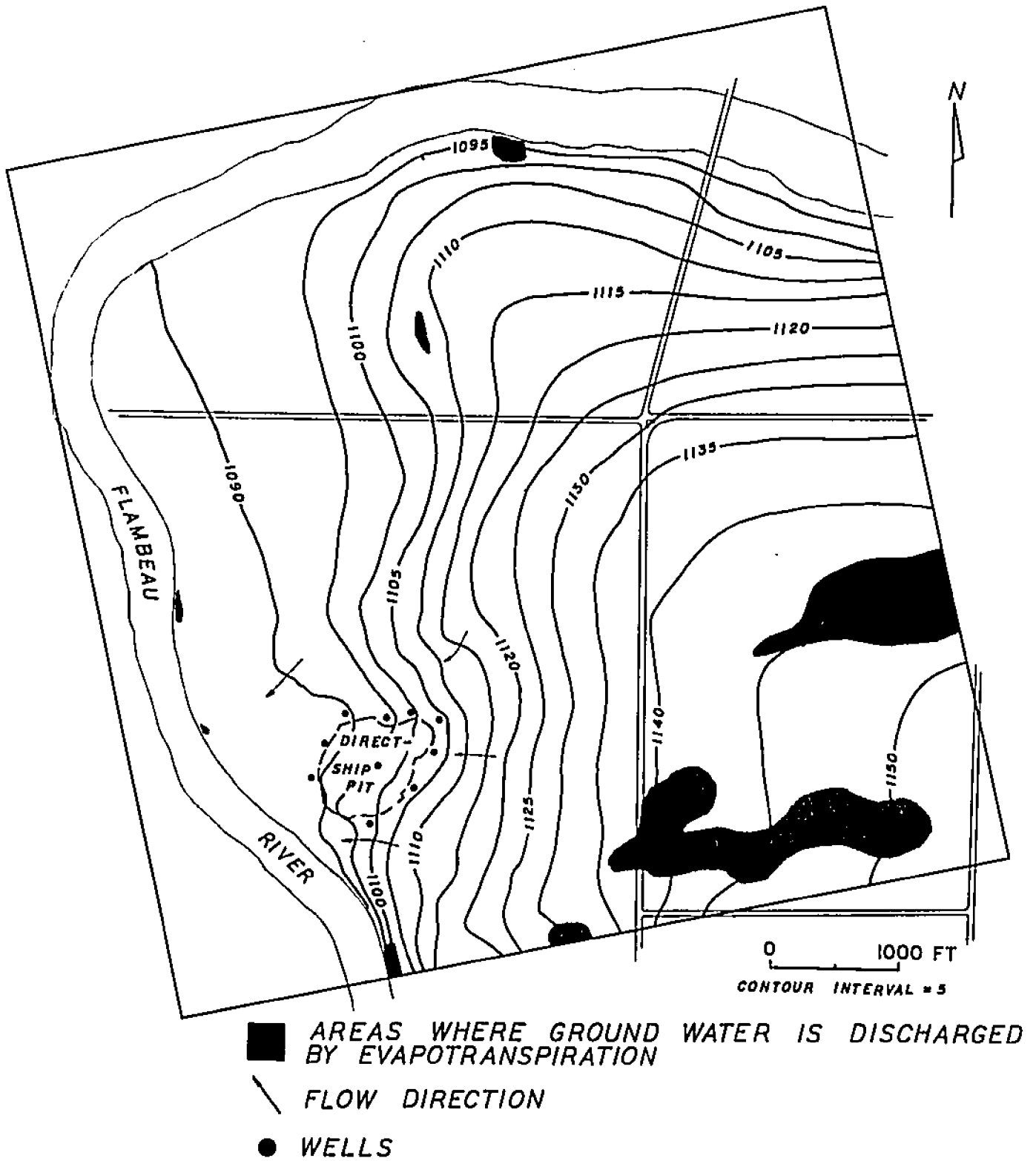


FIGURE 40. Simulated steady-state head distribution due to partially dewatering the area of the direct-ship pit with 10 wells discharging at a combined rate of 16.9 gpm.



TABLE 14. Discharges, drawdowns, and steady-state heads at individual dewatering wells near the direct-ship pit (see Figure 41 for well locations). Well radii = 0.25 ft.

WELL	PUMPING RATE (cfs)	DRAWDOWN (ft)	HEAD (ft msl)
A	0.0125	23.8	1078.7
B	0.0047	20.0	1083.8
C	0.00108	18.2	1090.9
D	0.0054	17.2	1096.9
E	0.0037	18.2	1083.0
F	0.00415	23.2	1090.3
G	0.00073	12.3	1093.0
H	0.00106	14.0	1084.4
I	0.00193	25.0	1088.8
J	0.00242	20.7	1079.3

1 cfs = 448.83 gpm

flow slightly by intercepting ground water en route to the river. In general, however, the effects of the wells are restricted to the immediate vicinity of the mine.

The average thicknesses of saturated till, outwash, and some sandstone at steady state are shown in Figure 41. It is seen on this map that the thin water-bearing materials on the bedrock high trending northeast along the strike of the ore deposit are easily dewatered to saturated thicknesses of less than 5 ft (1.5 m). Finer-grained materials to the southeast, however, are not as readily dewatered and maintain saturated thicknesses of up to 25 ft (7.6 m). The mean saturated thickness for nodes within the pit perimeter is approximately 9 ft (3 m).

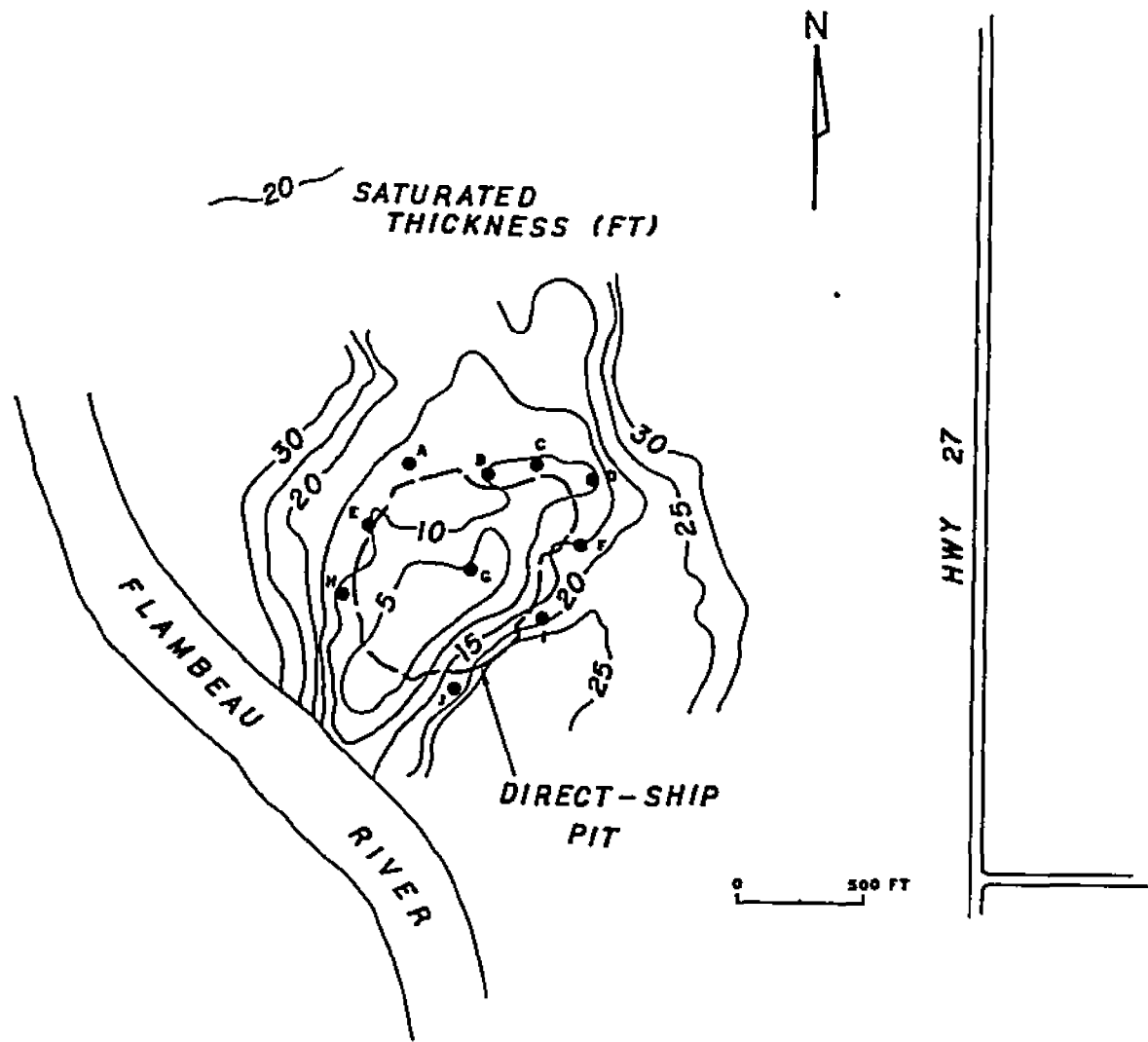


FIGURE 41. Average saturated thickness of water-bearing materials at steady state due to dewatering in the area of the direct-ship pit. Contour interval = 5 ft.

Table 15 is the steady-state ground-water budget computed for the direct-ship simulation with dewatering wells. A review of the budget rates for the existing natural system (Table 10) shows that the pumping scheme has practically an inconsequential effect on recharge and discharge in the study area. The wells cause the largest budget changes in the discharge rates: Evapotranspiration decreases slightly as the wells draw down the water table, and constant-head discharge is lowered by 15 percent, reflecting a moderate reduction in the rate of base flow to the Flambeau River. The minor effect on vapor discharge is evident by noting that differences in areas through which ground water is evapotranspired shown on figures 30 and 40 are negligible.

The low combined pumping rate of the wells listed in Table 14 raises questions regarding the applicability of cased wells for water control at the Flambeau site. The low rates of individual wells, ranging from 0.00073 to 0.0125 cfs (0.33 to 5.6 gpm), casts further doubt on their practical use. Reflecting on geologic generalities, the site may not be suited to this type of dewatering for several reasons. Foremost factors are 1) the physical properties of the aquifer are highly variable and uniform dewatering cannot be assured, 2) fine-grained sediments, especially those to the east, cannot be adequately dewatered with moderate- to large-diameter wells, and 3) the level to which the water table can be lowered is limited by the Precambrian surface. As a consequence of the last item, any type of external dewatering

TABLE 15. Steady-state ground-water budget of the mine area for the direct-ship pit with dewatering wells.

---

	Rates (cfs)
<b>SOURCES:</b>	
Areal recharge	0.2290
Constant-head	0.0402
Total	0.2692
<b>DISCHARGES:</b>	
Pumping	0.0377
Evapotranspiration	0.0287
Constant-head	0.2029
Total	0.2693

---

with wells will still result in the creation of a permanent seepage face above the aquifer/saprolite contact which will require seepage collection with an internal drainage system.

If advanced dewatering is used, perhaps the most attractive option for conditions at the site is the use of well points to which a vacuum is applied. A well-point system typically consists of closely spaced wells 1.5 to 3.5 ins (3.8 to 8.9 cm) in diameter and with screens 18 to 40 ins (46 to 102 cm) in length. All are connected by risers to a common header pipe through which 15 to 22 ft (4.6 to 6.7 m) of effective suction lift is developed with centrifugal pumps (U. S. Bureau of Reclamation, 1977). This method is partic-

ularly suitable for fine- to medium-grained soils that cannot be readily drained by gravity of high-capacity wells alone because of the soil's high specific retention (the ratio of the volume of water retained against gravity to the total soil volume). The application of a vacuum to the well points creates negative pore pressures in the soil and induces flow toward the screens. In this manner, the soils can be at least partially drained and stabilized. Assuming a desired drawdown of 20 ft (6 m), a nomographic method in Cedergran (1967) indicates that well points in a soil composed of fine sand would have to be installed on 2.5- to 3-ft (0.8- to 0.9-m) centers.

The well-point method lends itself well to saturated thicknesses occurring over much of the area that a direct-ship pit would encompass. Where saturated thicknesses are greater, such as east and northeast of the pit location, lift limitations may be overcome by excavating close to the water table before installing the well points or by using a second stage of points on an outer bench within the open pit. Since the Flambeau River is a potentially limitless source of water, combining a well-point system with a slurry wall around the west end of the pit is yet another drainage-control option.

#### Direct-Ship Pit - Perimeter Slurry Wall

Another water-control possibility for the direct-ship pit is a low-conductivity slurry wall to inhibit the lateral seepage of ground water into the excavation. A brief description of slurry-wall construction and properties was given in

an earlier section outlining this approach for the large open pit. The wall encompassing the direct-ship pit would penetrate the full saturated thickness of the Paleozoic and Pleistocene deposits and would be keyed into the fine-grained saprolite.

It was stated in the earlier section on the slurry-wall method that the hydraulic conductivity of the wall material could be as much as 5 to 7 orders of magnitude lower than the till at the site. The pit and surrounding impervious barrier were therefore represented in the model as an impermeable island within the flow system. This area consisted of 33 nodes and was defined by assuming the wall will approximately correspond to the pit perimeter.

The simulated effects of the direct-ship mine pit on the flow system are illustrated in figures 42 and 43. The wall produces a slight mounding of ground water to the east and south and minor head losses to the west. As cited earlier with regard to the large pit, these effects are due to the obstruction of ground-water flow by the wall and the loss of recharge formerly occurring through the interior of the pit. The most notable changes occur in close proximity to the wall and diminish rapidly with distance away from it. Increases in head of 0.2 ft (6 cm) or more extend up to 3,400 ft (1,035 m) to the northeast, 2,500 ft (760 m) to the east, and at least 1,300 ft (400 m) southward. The extension of effects beyond the southern boundary of the model cannot be quantified, but it is doubtful that head changes reach beyond

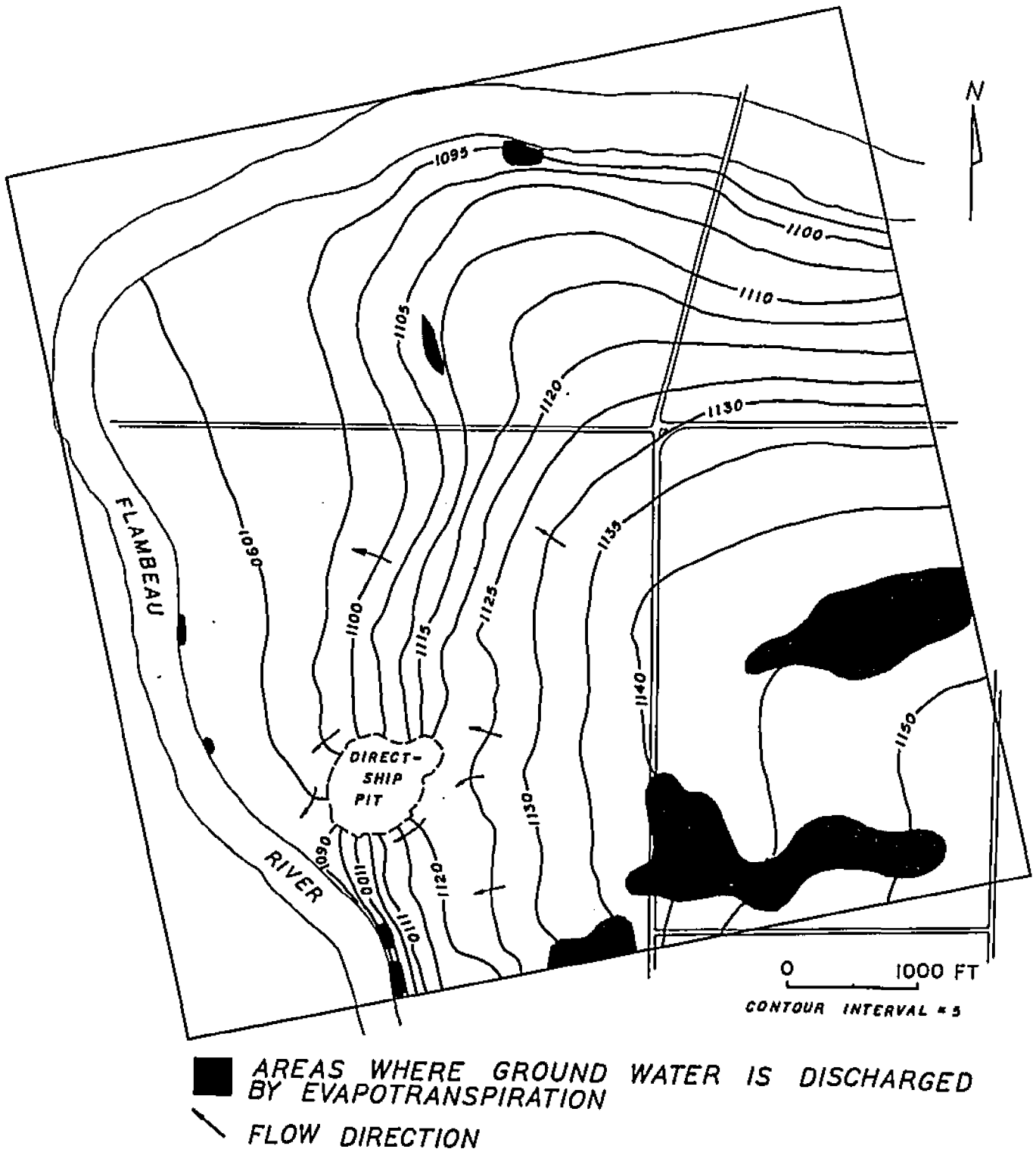
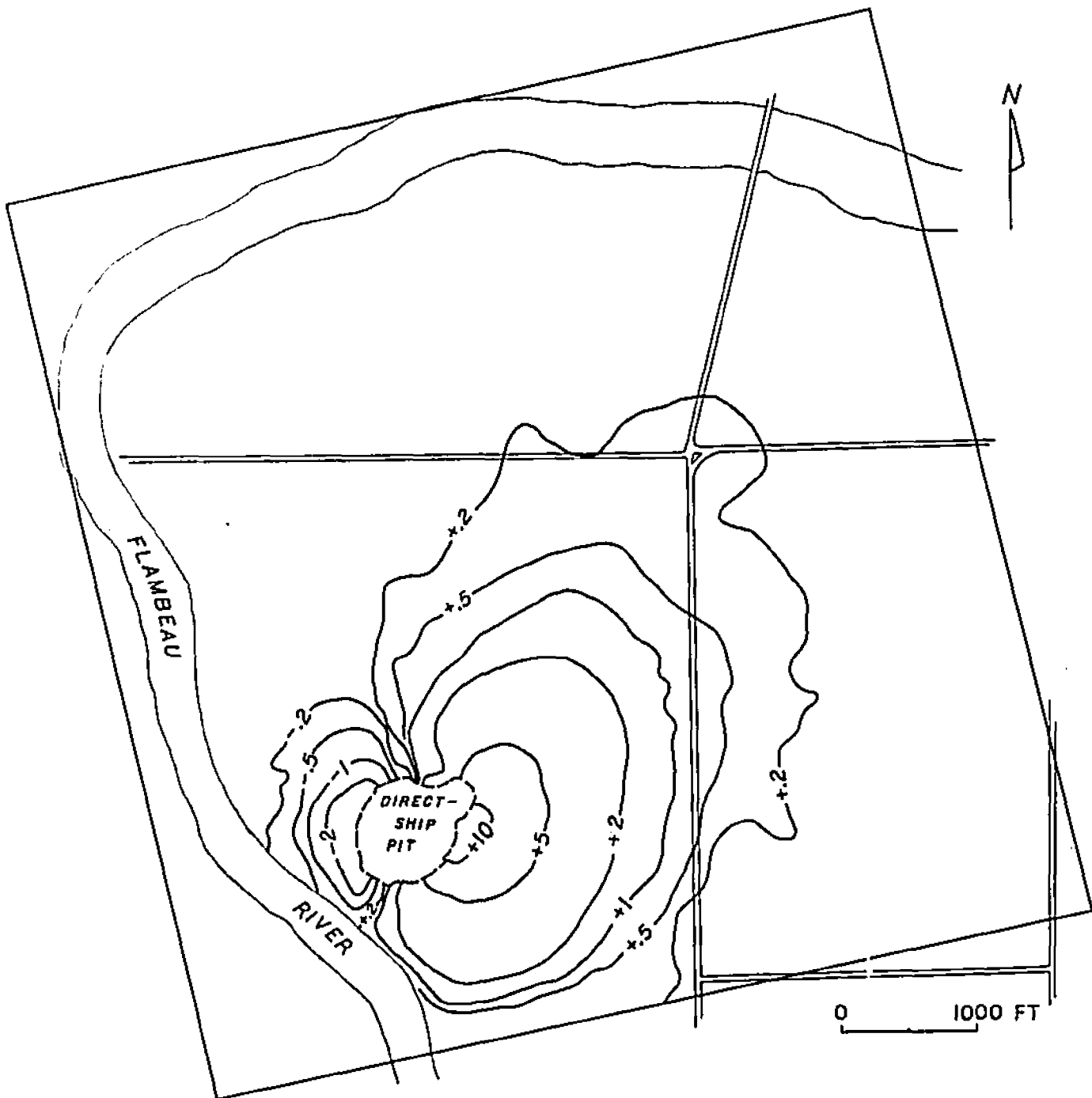


FIGURE 42. Simulated steady-state head distribution due to a low-conductivity slurry wall around the direct-ship mine pit.



$\pm 5$  INCREASES/DECREASES IN WATER LEVELS (FT)

FIGURE 43. Changes in hydraulic head caused by encircling the direct-ship pit with a slurry wall.



Meadowbrook Creek about 2,425 ft (740 m) south of the pit. The mounding is reflected in Figure 42 by a slight westward displacement of the water-table contours east and south of the pit. Head increases of up to 11.5 ft (3.5 m) occur along the southeast margin of the slurry wall. Since the wall is a flow line, the contours also show the diversion of ground water around and parallel to the wall. If the small amount of seepage through the wall is considered, the ground-water mounding would be slightly reduced in extent and magnitude.

Decreases in water levels west and northwest of the pit are less pronounced and extensive than the increases due to the inability of the transmissive outwash sediments to maintain large hydraulic gradients and the moderating influence of the Flambeau River (Figure 43). Water-table declines do not reach more than 750 ft (230 m) northwestward from the pit and are largest adjacent to the slurry wall. Maximum simulated head losses near the wall are on the order of 4.5 ft (1.4 m).

Alterations of the steady-state ground-water budget resulting from the emplacement of a slurry wall around the pit are shown in Table 16. Only minor changes are evident in comparison to the undisturbed conditions of Table 10. Overall, the total budget is affected by only about 3 percent. Areal recharge is decreased by approximately 5 percent due to the loss of recharge through the materials excavated to create the pit. Underflow, as the constant-head source, is decreased by only about 1 percent by the slight flattening of hydraulic

TABLE 16. Steady-state ground-water budget of the mine area for the direct-ship pit enclosed by a slurry wall.

	Rates (cfs)
<b>SOURCES:</b>	
Areal recharge	0.2215
Constant-head	0.0393
Total	0.2608
<b>DISCHARGES:</b>	
Evapotranspiration	0.0327
Constant-head	0.2281
Total	0.2608

gradients east and southeast of the pit by the ground-water mounding.

Comparing discharge rates, the evapotranspiration of ground water increases by 7 percent because the mounding elevates the water table close to the land surface and within range of the vapor-discharge mechanisms in some areas. Ground-water evapotranspiration increases from 11 to 13 percent of total discharges. In contrast to the effects of the larger mine pit and slurry wall (Figure 36), the wall surrounding the direct-ship pit has virtually no effect on the areas in which vapor discharge occurs, as illustrated in Figure 42. The areas shown for the natural, undisturbed case in Figure 30 are nearly identical to those for the direct-ship case with the slurry wall. Base flow to the Flambeau River, represented

by most of the constant-head discharge, is reduced by about 4 percent to 0.2216 cfs (0.0063 m<sup>3</sup>/s) as flow gradients west and northwest of the pit are lessened by the up-gradient mounding and loss of pit recharge. Base flow decreases from 86 to 85 percent of all discharges.

## CHAPTER IX

### SIMULATION OF THE PROPOSED WASTE-CONTAINMENT AREA

#### Model Development Objectives

The reasons for constructing a digital ground-water flow model of the area surrounding the proposed waste-containment structure echo those stated at the beginning of Chapter VIII concerning the mine site. The intent is to provide a means of predicting the effects of the structure's presence on the surrounding flow system. The physical consequences one might expect are an increase in water levels due to seepage through the bottom of the structure and an increase in discharge area by the creation or enlargement of wetlands. The purpose of the digital model is to determine if water levels will be affected and, if so, to learn where and to what extent. Water-level changes could produce accompanying changes in patterns of contaminant migration and the capability to determine beforehand the locations and magnitudes of adverse effects will allow the existing ground-water monitoring systems to be improved. Simulation of the system may also point to needed design modifications aimed at minimizing the impact of the disposal structure on the local flow regime.

The development of the waste-containment area model paralleled that of the mine-site model. Consequently, much of the rationale for specific assumptions and hydrologic characterizations presented here occurs in Chapter VIII. Fre-

quent reference to the previous chapter is made as a result.

### Steady-State Simulation of the Existing System

#### General Discussion

As in the case of the mine area, available information did not permit transient simulations of the flow system at the waste-containment site. This conclusion was based on 1) the lack of hydraulic-head, hydraulic-conductivity, and storativity data for the deeper outwash layers which would have enabled them to be considered as discrete aquifers in a three-dimensional system, 2) problems with observation-well construction cited in the previous chapter which also occur at most wells in the waste-containment area, and 3) a lack of pumping tests at the southern study area to provide transient data for verifying a nonsteady flow model. Given these constraints on information, the waste area was simulated as a single-layer unconfined aquifer using a steady-state configuration. A discussion of model assumptions and steady-state flow systems is presented in Chapter VIII. The reader is also directed to the discussion on page 184 regarding system storativities and transient simulations.

#### Steady-State Input Data

The waste-containment area and surrounding vicinity were discretized into a block-centered 18 X 24 finite-difference

grid with a variable spacing and covering a gross area of 3.8 mi<sup>2</sup> (9.8 km<sup>2</sup>). The grid is illustrated in Figure 44. Of the 432 nodes in the grid, 365 are within the boundaries of the actual study area. Grid blocks range in area from 1.43 to 14.63 acres (0.58 to 5.92 ha) and in dimension from 250 X 250 ft (76 X 76 m) to 850 X 750 ft (259 X 229 m). The variable grid allowed the arcuate course of the Flambeau River and the sinuous pattern of Meadowbrook Creek to be better represented in the model. It also permitted greater grid spacings in areas remote from the disposal structure where less resolution was desired and in areas where insufficient data did not warrant greater nodal control.

The flow system in the waste area was considered unconfined and isotropic. The latter assumption was invoked because no data exist with which to define anisotropic trends within the zone of saturation. The transmissivity multipliers for the x and y space dimensions in the model were thus set at 1. Initial hydraulic heads were obtained from the average distribution shown in Figure 26 which was constructed from monthly water-level measurements made between 1970 and 1980. Initial hydraulic conductivities were taken from data collected with the methods described in Chapter VI and summarized in tables 7 and 8. The model boundaries were extended outside the area for which measured values of system properties are available so that reasonable estimates of conductivity and hydraulic head had to be made for remote parts of the modeled area. Specific comments regarding the final conduc-

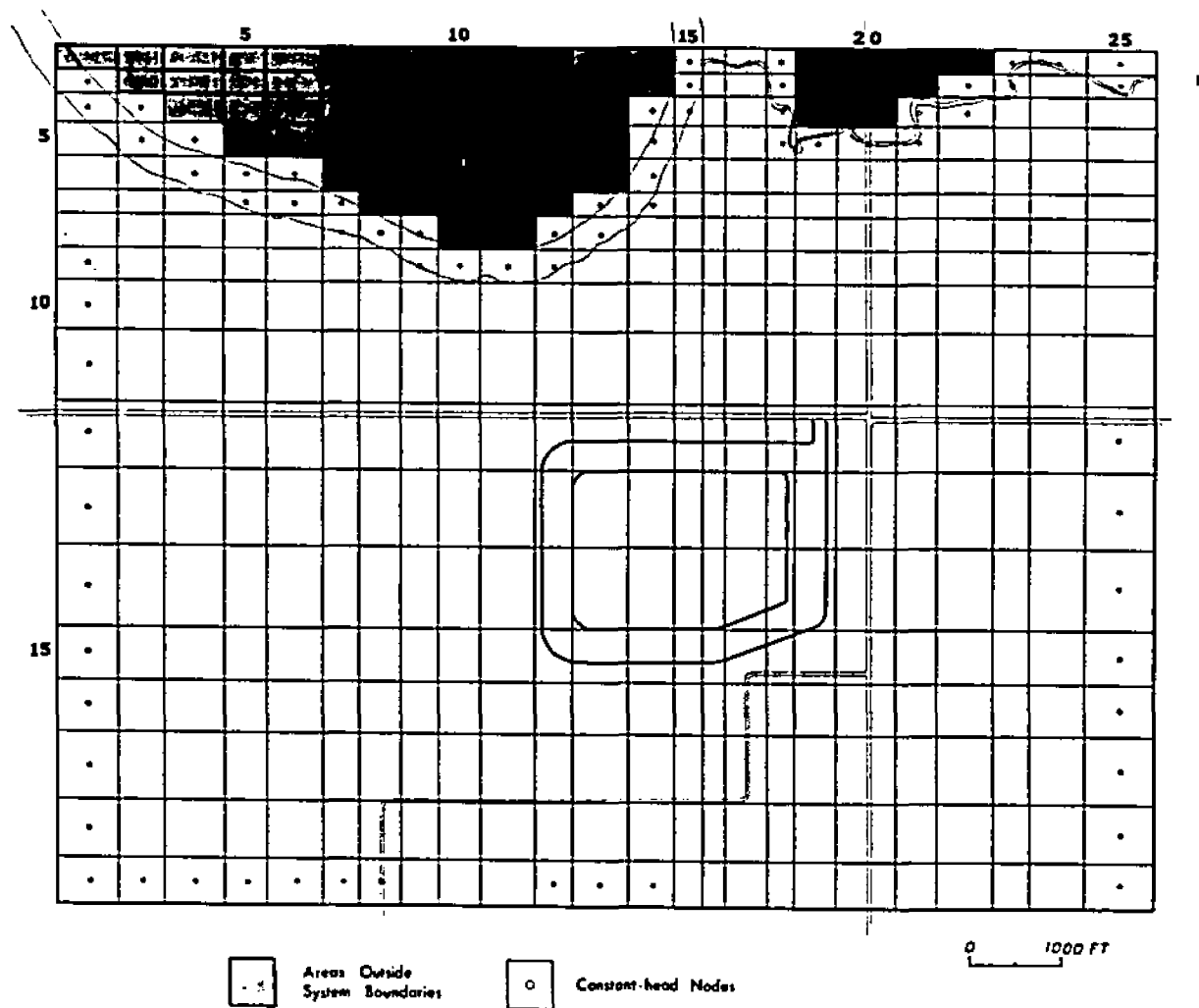


FIGURE 44. Finite-difference grid of the waste-containment area showing the distribution of hydrologic boundaries used in the simulations.

tivity distribution are given in the section on model calibration.

As explained in the preceding chapter, the transmissivity of a water-table aquifer at any point in space and time is a function of the hydraulic conductivity and saturated thickness at that point. The transmissivity of unconfined systems is computed in the model by multiplying the constant conductivity at a node by the saturated thickness there. The saturated thickness is found by subtracting the aquifer-bottom elevation from the head at each node computed during the previous iteration. The transmissivity is then able to vary in time and space according to Equation 43 on page 172. The pit model used the Precambrian surface as the bottom of the aquifer because it acts as a flow barrier and is well-defined over the immediate area of the proposed open pit. The Precambrian surface in the waste-containment area, however, is less well-defined (see Plate 3) and probably exerts less influence on shallow ground-water flow in many areas because of its greater depth in comparison to the mine site. An effective aquifer bottom for the disposal area was thus defined through a sensitivity analysis described in the section on calibration.

The water-budget technique of Chapter V yielded the areal recharge rates used in the disposal-area model. Sandy-loam soils have not been documented in this area and only recharge rates for silt loams from Table 5 were used. The distribution of other major factors affecting recharge is



shown in Figure 20. Recharge values assigned to each node were modified to account for local factors, particularly in wetland areas where recharge is reduced. As is shown later, evapotranspiration values from Table 5 were also used in the model.

Several additional input specifications are required by the model, apart from the basic hydrologic data. The closure criterion for determining convergence was usually chosen to be 0.001. For steady-state simulations, storativity or specific yield is set at zero and the model run for a single time step of arbitrary length. The option to have the model compute a mass balance was selected to assist in calibration.

The user must also designate an equation-solving scheme and, for reasons cited in the previous chapter, the strongly implicit procedure (SIP) was selected. The iteration parameter  $B'$  required for the SIP was initially chosen as 1.0 but was revised during calibration to an optimal value of 0.8. This value allowed convergence to be achieved in the fewest number of iterations for the simulation of the natural, undisturbed disposal area. It was found that a solution could not be obtained for  $B' \geq 1.0$  due to oscillations which eliminated nodes from the solution and prevented convergence. The oscillations probably result in part from the nonlinearities of the water-table problem and the need to calculate transmissivity at the present iteration level (Trescott and others, 1976). A value for  $B' < 1.0$  causes under-relaxation and dampens oscillations from one iteration to the next (see Larson and Trescott, 1977).

### Boundary Conditions

The distribution of hydrologic boundaries within the study area is shown in Figure 44. Constant-head boundaries were assigned to model boundaries wherever ground water enters or leaves the study area. Ground water enters the area as underflow along its eastern margin and near its southwest corner and leaves at the west and south-central margins.

The Flambeau River was also approximated as a constant-head boundary using water-surface elevations at river nodes which preserved the average stream gradient of approximately 2 ft/mi (0.38 m/km). Meadowbrook Creek, the only other perennial stream in the area, was also characterized in this fashion. This method, as explained in conjunction with the mine-pit model, assumes an average river stage and does not adequately represent short-term seasonal phenomena such as increases in stream stage and concomitant bank storage. It also tends to overestimate base flow because the constant-head nodes assume a fully penetrating boundary feature. A more accurate approach for modeling streams is described in Chapter VIII, though data required for that method, namely the hydraulic conductivity and thickness of the streambed and the head differential across the bed, are often lacking and difficult to obtain.

No boundary conditions were assigned to the borders of the study area where ground-water flow is approximately parallel to the artificial boundary required by the model algo-

rithm. At these locations, the no-flow boundary merely serves as a flow line.

### Model Calibration

A detailed description of the calibration process is given in Chapter VIII. In general terms, it is a direct, deterministic method which entails the adjustment of hydrologic input parameters in the model until a match between measured and computed hydraulic heads is obtained to the desired range of accuracy. In this respect, hydraulic head and pumping rates are considered known values while hydraulic conductivity (or transmissivity) and storativity (or specific yield) are unknowns subject to adjustment.

Calibration of the waste-containment area model under steady-state conditions first involved the determination of an effective aquifer bottom since subsurface control defining the Precambrian surface is inadequate. This was accomplished using a technique called sensitivity analysis. In the simulation of real systems, there is always uncertainty regarding the exact values of physical parameters and properties such as hydraulic conductivity, storativity, and boundary conditions. It is often possible to establish a range within which a given parameter may vary without appreciably affecting the numerical solution. A sensitivity analysis may establish this range by determining to what degree perturbations in the parameter affect the solution. The analysis thus indicates which parameters and value ranges the model is most sensitive

to and, therefore, implies their relative importance in characterizing the system. This knowledge can be used to guide the collection of more reliable data. A simulated flow system will usually be more sensitive to changes in some parameters than in others. In fact, different parts of a discretized area may exhibit differing degrees of sensitivity, may be sensitive to different parameters, or may have sensitivities that vary with time. McElwee (1982) indicates that low-sensitivity areas are generally associated with low values of transmissivity or hydraulic conductivity and with small values of  $\partial h/\partial x$ ,  $\partial h/\partial y$ , and  $\partial h/\partial t$ .

To determine an effective aquifer bottom, a range of physically plausible elevations was found from Plate 3. The range tested in the model was from 1035 to 1060 ft msl. Repeated runs using various elevations within this range indicated that an elevation of 1050 affected the solution most favorably and best reproduced the steady-state head distribution of Figure 26. Elevations greater than 1050 caused excessive water levels at most nodes in the northeast corner of the modeled area, although the rest of the study area was only slightly affected. At elevations less than 1050, simulated heads in much of the eastern part of the site began to decrease significantly. The effective aquifer bottom was thus placed at 1050. This elevation is not untenable; the information on Plate 3 and figures 10 and 11 indicate that most of the hydrologically influential features in the immediate area of the disposal site occur at elevations greater than

1050. This bottom elevation only slightly affected most of the heads in the study area, but the model exhibited only moderate sensitivity to any elevations within the test range. Sensitivity was greatest, however, to elevations greater than 1050.

After defining the bottom elevation, model calibration continued by the adjustment of hydraulic conductivities at and around nodes where computed heads departed from those in Figure 26. Recharge values from Table 5 were not adjusted. During this phase, it was discovered that simulated water levels in the southern third of the study area remained excessively high in spite of calibration efforts. This anomalous occurrence hinted at the existence of a ground-water discharge mechanism not included in the initial model. A comparison of the simulated head distribution and topographic data showed that areas of consistently high heads corresponded closely to wetlands. Since the water table is close to the surface in those areas, this correlation pointed to the evapotranspiration of ground water as a probable discharge mechanism. The recharge values in Table 5 implicitly include evapotranspiration according to Equation 5 on page 86. Nodes in wetland areas, however, were assigned recharge values at or near zero, making it acceptable to consider evapotranspiration separately in those areas. The model was consequently revised to include vapor discharge at an annual rate of 22.0 ins (559 mm) from Table 5. The model algorithm decreases the effects of evapotranspiration linearly with depth (see Equation 48,

page 174), requiring the user to specify the land-surface elevation at each node and the maximum depth at which vapor discharge is negligible. Much of the area is dominated by pasture conditions and grassy vegetation with rooting depths on the order of 1.5 to 4 ft (0.5 to 1.2 m) (Thorntwaite and Mather, 1957). Available data not allow the initial analysis to be more precise and the assumption was made that the vapor discharge of ground water effectively ceases at depths greater than about 4 ft (1.2 m).

Subsequent simulations which included evapotranspiration exhibited much better agreement with observed heads. It was found, however, that the initial maximum depth of evapotranspiration effects cited above resulted in water levels that were too low in the wetland areas. Through trial-and-adjustment, an optimal vapor-discharge depth of 2.5 ft (0.8 m) was found to give the best correspondence between real and simulated heads in the wetlands and also the lowest mass-balance error in the model computations.

Figure 45 is the distribution of hydraulic head in the waste-containment area generated by the model after calibration. The results are in excellent agreement with Figure 26, though some detail has been lost in areas with irregular water-table configurations and steep gradients as a result of the discretization process. The most pronounced differences occur in the northwest corner adjacent to the Flambeau River where the model suggests a shallower hydraulic gradient. This area, however, is prone to large averaging errors due

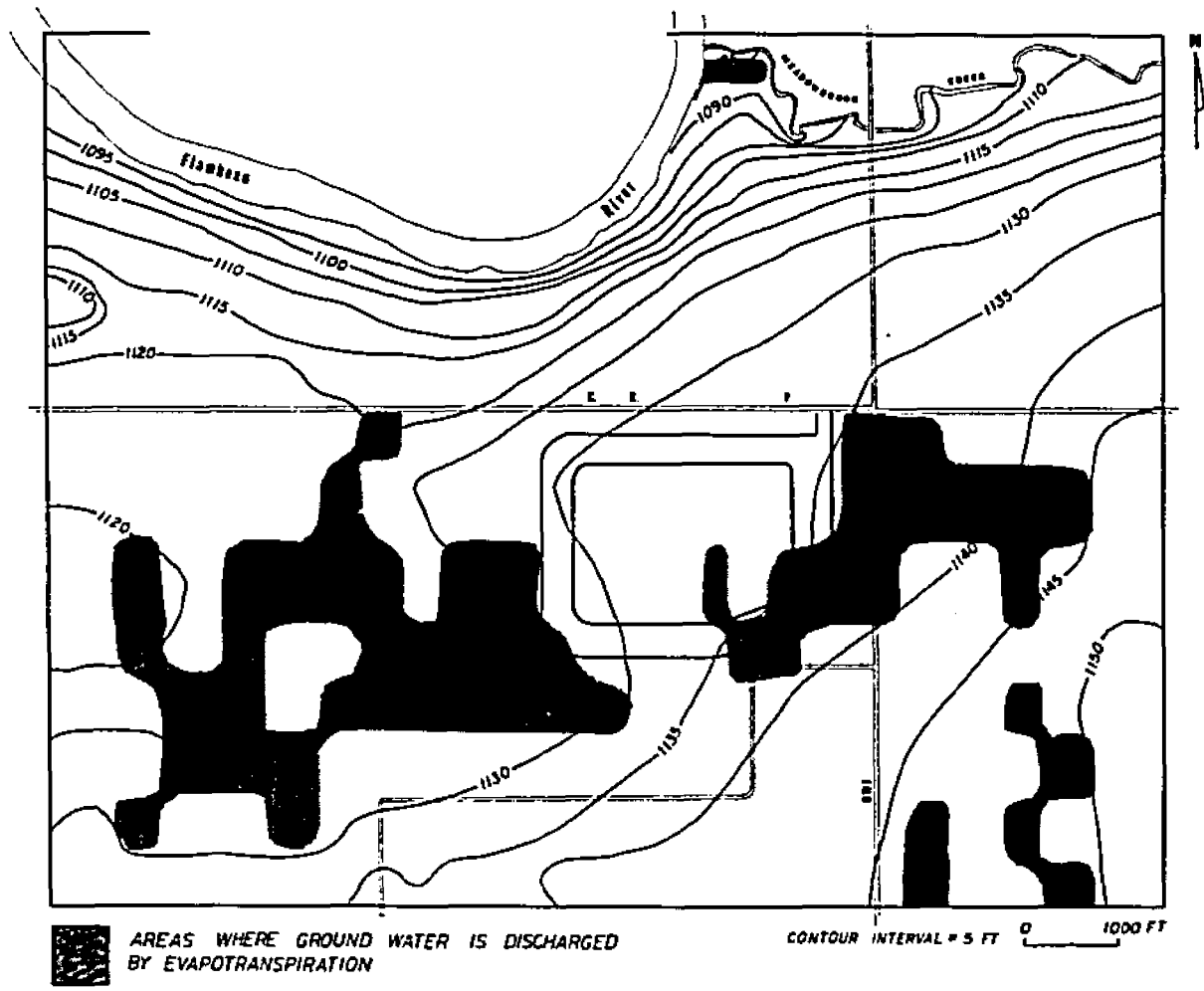


FIGURE 45. Steady-state head distribution in the waste-containment area generated by the model after calibration.

to the steep and irregular gradients shown in Figure 26. Moreover, initial water-table elevations along the Flambeau River generally had poor control and were inferred from topographic data, a method subject to error.

Areas in which the evapotranspiration of ground water is significant within 2.5 ft (0.8 m) of the land surface are also shown in Figure 45. Comparison with Figure 20 depicts the correlation between these areas and wetlands in the study area. The shaded areas are interpreted to represent average conditions because water-table fluctuations throughout the year probably cause them to differ somewhat in shape and extent. The vapor-discharge areas determined with the model closely correspond to actual wetland locations, indicating that wetlands on the site may be the ground-water depression type illustrated in Figure 18B.

The calibrated hydraulic conductivities occur within the relatively narrow range of 0.2 to 2 ft/d (0.06 to 0.6 m/d) which is nearly identical to the range of field values given in Table 7. Conductivities at the lower end of the range occur primarily along the Flambeau River and the western reach of Meadowbrook Creek, extending southward through the site of the disposal structure to the southern boundary of the study area. Conductivities from the middle to the high end of the calibration range generally occur northeast of the impoundment site and in areas to the southeast and west dominated by wetlands.

Table 17 is a steady-state ground-water budget for the



TABLE 17. Steady-state ground-water budget for the unstressed waste-containment area determined from mass-balance computations in the model.

---



---

	Rates (cfs)
<b>SOURCES:</b>	
Areal recharge	0.1198
Constant-head	0.0525
Total	0.1723
<b>DISCHARGES:</b>	
Evapotranspiration	0.0952
Constant-head	0.0770
Total	0.1722

---

natural, undisturbed waste area determined by the model from inflows and outflows at all nodes. The results show an excellent mass balance within the study area. The areal recharge rate compares reasonably well with the figure of 0.147 cfs determined empirically in Chapter V and listed in Table 6. The value found by the model is lower by about 19 percent. The constant-head source represents underflow into the study area, mainly from its eastern border and the southwest margin. The relatively flat hydraulic gradients and low hydraulic conductivities result in a flux rate which accounts for about 30 percent of the total sources; the remainder is comprised of areal recharge by infiltration. Approximately 95 percent of the constant-head discharge is base flow to the Flambeau

River and Meadowbrook Creek. Of this total, 60 percent or  $4.4 \times 10^{-2}$  cfs ( $1.2 \times 10^{-3}$  m<sup>3</sup>/s) is gained by the river and 40 percent or  $2.9 \times 10^{-2}$  cfs ( $8.3 \times 10^{-4}$  m<sup>3</sup>/s) flows to the creek. The rest of the constant-head discharge is underflow out of the modeled area across its western edge. The underflow discharge amounts to about 5 percent of the total constant-head discharge and only about 2 percent of the total discharge. Evapotranspiration is the principal discharge mechanism, accounting for approximately 55 percent of all ground water lost from the area. The large amount of wetland area accounts for the prominent role of vapor discharge. Table 17 represents average conditions and similar determinations made from short-term seasonal data may differ from the values provided here, especially with regard to evapotranspiration which is greatly dependent on fluctuations of the water table.

### Steady-State Stress Simulations

#### General Discussion

It was necessary to modify the original model data and to make several simplifying assumptions to simulate the waste-disposal structure. Where reliable information is lacking, conservative assumptions thought to represent extreme or worst-case conditions were used in order to facilitate planning. As a result, many of the simulative findings are perhaps less favorable than may actually occur under real site conditions.

Present design plans call for placing a cutoff wall of compacted saprolite 13 to 18 ft (4 to 5.5 m) below the original grade around the western and most of the northern edge of the impoundment (FMC, 1976). The wall will be installed beneath the core of the perimeter dike and is intended to reduce lateral seepage through the shallow sands shown in Figure 12. Judging from the soil-boring data, a wall may also be needed at the southeast corner of the structure where a sand zone extends southwestward beyond the dike. The cutoff wall cannot be represented in the two-dimensional framework of the model and its possible effects on the flow system and seepage regime are therefore unknown. The wall should divert seepage to somewhat greater depths and through less permeable soils. Likewise, the perimeter dike could not be explicitly represented in the model and its influence on flow patterns near the disposal structure could not be evaluated.

Some wetlands will be destroyed when the disposal structure is built and evapotranspiration at affected nodes in the model must be set at zero to reflect this. The model code, however, does not permit the adjustment of evapotranspiration rates at individual nodes. This limitation was circumvented by assigning ground elevations well above the water table at the affected nodes so that simulated heads were never within the 2.5-ft (0.8-m) depth range of vapor discharge determined by calibration. This change allows evapotranspiration at other nodes to be simulated normally and does not affect

other parts of the solution process (the ground-elevation matrix is used only in the evapotranspiration computations). Natural recharge rates at nodes corresponding to the dike were also lowered in proportion to the area of each grid block the dike occupies to reflect infiltration losses in those areas.

Since tailings will be discharged into the impoundment as a slurry, it was assumed that the chief hydrologic effect of the structure will be the loss of water through its bottom. In all simulations, this additional seepage was represented by increases in the rate of areal recharge at nodes within the containment dike. According to Darcy's law, the rate of seepage is directly dependent on the unsaturated and saturated hydraulic conductivities of materials through which flow occurs and on the loss of hydraulic head through the materials. Of particular importance are the contrasts in hydraulic conductivities among the various soils and waste materials. The conductivity and degree of saturation of the soil upon which wastes are deposited will decide whether the soil base or the waste will control the rate of water loss from the disposal site, at least initially. Field conductivities of surficial soils at the disposal site were measured at  $1.6 \times 10^{-4}$  to  $7.1 \times 10^{-3}$  ft/d ( $5.6 \times 10^{-8}$  to  $2.5 \times 10^{-6}$  cm/s) and average  $2.3 \times 10^{-3}$  ft/d ( $8.1 \times 10^{-7}$  cm/s), according to Table 7. These conductivities, however, are unusually low for soils of this type, suggesting the field values are not representative (see the discussion in Chapter VI). The

lower end of the conductivity range cited by Young and Hindall (1972), 0.4 ft/d ( $1.4 \times 10^{-4}$  cm/s), is more plausible and is used in subsequent analyses as a conservative assumption. This value is about half the average field conductivity of the underlying till, which is 0.71 ft/d ( $2.5 \times 10^{-4}$  cm/s).

Mine tailings are difficult to characterize because of their heterogeneity. In general, tailings deposits consist of a wide range of particle sizes and hydraulic conductivities. Grains in a given deposit may range in size from coarse sand to silt and clay, but the silt/clay fraction is usually dominant and may comprise from 45 to 95 percent of the total volume (W. A. Wahler and Assocs., 1974). The Flambeau mine is expected to produce 840 to 860 tons (762 to 780 metric tons) of tailings per day consisting of 50 to 70 percent quartz, mica, and clay particles and from 30 to 50 percent iron sulfides as pyrite (FMC, 1976). A water-balance study (INTERA, Inc.; 1983) of tailings ponds at Kennecott's Chino mine near Hurley, New Mexico, yielded an estimated bulk hydraulic conductivity of 8 ft/yr ( $7.7 \times 10^{-6}$  cm/s) for the tailings. In a similar investigation (IECO, Inc.; 1960) of tailings ponds near Hayden, Arizona, laboratory measurements of vertical conductivities were found to be on the order of 8.8 ft/yr ( $8.5 \times 10^{-6}$  cm/s). A conductivity of 8 ft/yr was assumed for the tailings in later analyses, though the large amount of waste rock within the waste pile may give it a higher bulk value.

Unlike the mine pit, the shape of the waste-containment

structure will remain static and only the level to which it is filled with tailings and waste rock will change with time. Simulations of the structure, then, need only account for changes in head within the impoundment as the volume of waste changes. Two cases were explored: 1) The effects of depositing wastes on a floor of natural, undisturbed soil and 2) the results of placing the wastes on a liner of compacted saprolitic material similar to that comprising the dike core. This second case represents an effort to better seal the bottom against leakage.

A complete analysis of the water-loss regime associated with the waste impoundment would require the consideration of unsaturated flow in the soil zone above the water table and below the base of the structure. Unfortunately, information needed to carry out this type of analysis, such as volumetric water contents, porosities, and displacement (air-entry) pressure heads, is completely lacking. Several assumptions, however, make it possible to treat the seepage problem in the first case using saturated-flow theory.

#### Containment Structure - Undisturbed Soil Bottom

The first case examined with the model was the deposition of waste directly on the natural, undisturbed soil within the containment dike. If the soil zone above the water table is only partially saturated, the rate of vertical seepage through it is independent of the depth to the

water table. If the transmission zone becomes saturated, however, this characterization no longer suffices and flow rates increase significantly. Deficiencies in information allow only the saturated case to be considered.

Assuming the bottom soils have relatively low hydraulic conductivities on the order of 0.4 ft/d ( $1.4 \times 10^{-4}$  cm/s), the additional seepage from the waste will probably cause the water table beneath the disposal structure to rise rapidly until it is in direct hydraulic contact with the waste materials. This is likely to happen over most of the site since the water table is only 2 to 10 ft (0.6 to 3.0 m) below the land surface in that area and may be at the surface near the southern and southeastern parts of the structure location. Contact between the water table and wastes would create a continuous saturated flow system treatable with existing data. The rate of rise of the water table is dependent on the seepage rate, the fraction of porosity in the transmitting zone available for water storage, and the resistance to lateral flow of ground water as the phreatic surface rises (McWhorter and Nelson, 1979).

Actually, only the capillary fringe above the water table need make contact with the waste (Bouwer, 1982). The capillary fringe in fine sands and silts ranges from 1 to 5 ft (0.3 to 1.5 m) (Fetter, 1980) which places the bottom of the tailings pile either below or no more than 5 ft (1.5 m) above the top of the capillary fringe at the start of operations. Once the capillary fringe is in contact with the wastes, the trans-

mission zone is at or near saturation. Saturated conditions increase the hydraulic conductivities and will temporarily accelerate the rate of water loss until the resistance to lateral spreading of the ground-water mound offered by the receiving soil elevates fluid pressure at the base of the wastes. This will reduce vertical gradients within the wastes which, in turn, will reduce the seepage rate to an equilibrium level. These concepts are developed more fully below.

Once the soils beneath the structure are saturated, the waste-soil system can be considered analogous to an aquifer that is partially confined by an overlying leaky aquitard composed of the tailings. If the hydraulic conductivity ( $K'$ ) and saturated thickness ( $m'$ ) of the aquitard and the head loss across it are known, the steady-state rate of seepage through it can be computed with the form of Darcy's law

$$v = \frac{K'}{m'}(h_2 - h_1) \quad (50)$$

where  $K'/m'$  is the leakance ( $t^{-1}$ ),  $h_2$  is the head in the source bed or aquitard, and  $h_1$  is the head at the base of the aquitard (the potentiometric surface of the aquifer). Due to the continuous discharge of the tailings slurry,  $h_2$  is considered constant in our analogy, even though the water level within the waste will increase slowly as the structure fills. Equation 50 clearly shows that a rise in the potentiometric surface ( $h_1$ ) above the base of the tailings would reduce the seepage rate.



The anticipated rise in pressure beneath the impoundment cannot be simulated explicitly given the available data and the capabilities of the numerical model. Instead, an approximate steady-state seepage rate was determined by computing an initial rate based on the system properties and then refining this estimate by trial-and-error. The initial head beneath the impoundment was conservatively approximated as the average elevation of the area occupied by the disposal structure, 1138 ft. This elevation corresponds to the average base of the tailings and is equivalent to  $h_1 = 0$  if the average ground elevation is used as a datum. Considering only the saturated portion of the wastes,  $m'$  then equals  $h_2$  and a unit vertical gradient across the tailings pile results. The average conductivity of the tailings may be from 15 to 20 times lower than that of the bottom soils, indicating the tailings will initially control the rate of seepage from the structure (that is, the underlying soils cannot transmit a volume of water greater than the volume supplied by the tailings). According to Equation 50, a unit gradient results in vertical seepage through a unit cross-sectional area of the porous medium at a rate approximated by the average hydraulic conductivity of the medium. Accordingly, an initial water-loss rate of 0.022 ft/d ( $7.8 \times 10^{-6}$  cm/s) was employed in the simulations for this set of conditions. This initial rate is the bulk conductivity of tailings at the Chino mine estimated from a water-balance study (INTERA, Inc.; 1983). The initial rate in this analysis corresponds to the flux

when the rising water table first intersects the wastes and the gage pressure beneath the structure is zero. It is independent of the hydraulic properties of the underlying soils and is truly valid if the wastes restrict the seepage to a rate less than the hydraulic conductivity of the foundation soils. Even if this condition is not rigorously satisfied, this rate still provides a good starting point for the simulations.

If the thickness of the saturated waste is small in relation to the width of the disposal structure, most seepage will occur through the structure's bottom (Bouwer, 1982). Averaging the north-south and east-west widths of the bottom and dividing by the final fill depth of 50 ft (15 m) indicates the waste pile will be approximately 40 times wider than it is deep, validating the application of Equation 50 to the bottom area. The total bottom area of the impoundment will be approximately 84 acres according to Exhibit F in the original permit submittal (FMC, 1976); applying Equation 50 to this area using the initial flux rate yields an initial volumetric seepage-loss rate of 0.93 cfs ( $0.026 \text{ m}^3/\text{s}$ ), or 417 gpm.

It is probable that a build-up of artesian pressure beneath the impoundment will elevate the potentiometric surface ( $h_1$ ) above the original land surface. These head levels are not known a priori and cannot be determined explicitly by simulation. The increased heads, however, are the direct consequence of the resistance to flow offered by the receiving soils beneath the structure and the initial flux rate deter-

mined above will ultimately decline to a steady-state rate as the pressure increases toward an equilibrium level. An upper bound on the steady-state rate of seepage can therefore be obtained by assuming that the resistance to lateral flow through the bottom soils wholly governs the steady flow rate (McWhorter and Nelson, 1979).

The waste-containment area was simulated with virtually no mass-balance error using the earlier assumptions and the initial seepage rate. Convergence was impossible within 600 iterations using the original iteration parameter ( $B'$ ) of 0.8; reducing  $B'$  to 0.6 caused convergence in only 16 iterations.

For an average saturated waste thickness of 25 ft (7.6 m), the associated constant head elevation within the impoundment is 1163, assuming an average bottom elevation of 1138. The high initial seepage rate produced heads within the structure as much as 110 ft (34 m) above the phreatic line within the waste. The seepage rate prevailing at equilibrium when the water loss is balanced by flow away from the site was found by successively decreasing the seepage rate until computed heads inside the structure approximated the 1163-ft elevation. Convergence to a numerical solution became more difficult as the recharge rates were lowered but occurred within 25 iterations using a  $B'$  of 0.4. Larger values of  $B'$  prevented convergence within 600 iterations.

The recharge-adjustment process resulted in the hydraulic-head distribution shown in Figure 46 for a 25-ft (7.6-m) thickness of saturated tailings and waste rock. The total seepage

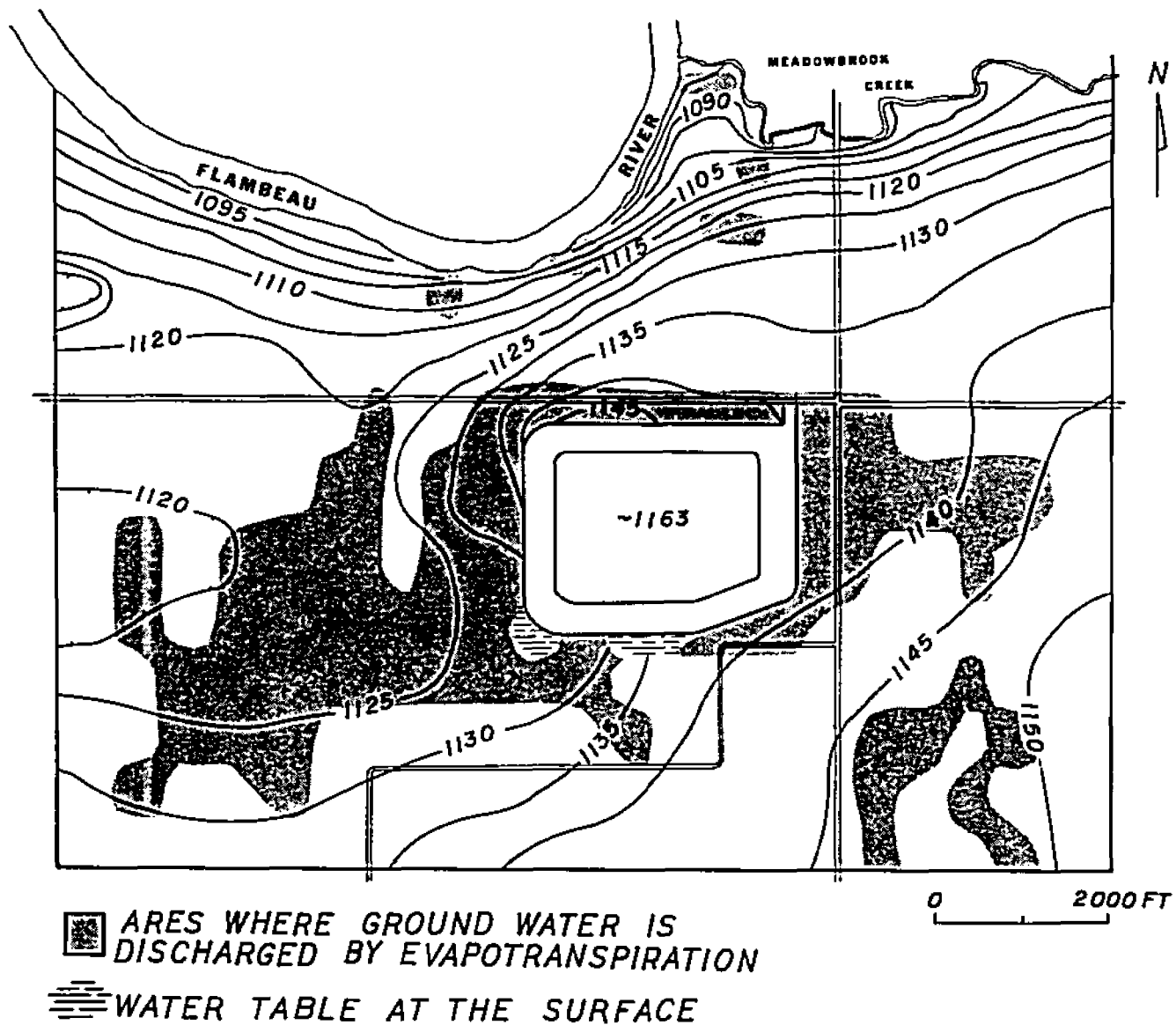


FIGURE 46. Simulated steady-state head distribution in the waste-containment area for a natural-soil bottom and 25 ft of saturated waste.

flux required to maintain a water-table elevation of 1163 within the impoundment is 0.16 cfs ( $0.0045 \text{ m}^3/\text{s}$ ), or about 72 gpm. This rate is 2 to 3 times greater than the 19 gpm ( $0.0012 \text{ m}^3/\text{s}$ ) cited in the original permit application submittal (FMC, 1976), exclusive of minor seepage losses through the perimeter dike. These earlier calculations assumed a surficial-soil conductivity of 0.0028 ft/d ( $1.0 \times 10^{-6} \text{ cm/s}$ ) and that only the expected 30 percent of the waste surface occupied by the tailings pond would contribute to vertical seepage. It is possible, however, that a large portion of the tailings pile will remain at or near saturation throughout the life of the operation because of the continuous influx of mill slurry from the peripheral distribution system. The saturated thickness is approximately equal to the waste thickness under these conditions.

Using the results of the simulation, the steady-state elevation of the potentiometric surface due to pressures beneath the structure is found by solving Equation 50 for  $h_1$ .  $K'$  is 0.022 ft/d ( $7.8 \times 10^{-6} \text{ cm/s}$ ),  $m'$  is 25 ft (7.6 m), and  $h_2$  is the constant height of the phreatic surface within the wastes, 63 ft (19 m). The specific discharge  $v$  through the bottom is found by dividing the steady-state seepage rate of 0.16 cfs ( $0.0045 \text{ m}^3/\text{s}$ ) by the bottom area, giving  $4.37 \times 10^{-8} \text{ ft/s}$  ( $1.33 \times 10^{-6} \text{ cm/s}$ ). Substituting into Equation 50 yields a potentiometric-surface elevation of about 1159 for the 25-ft (7.6-m) waste accumulation. A higher value for  $K'$  would result in a proportionately lower elevation.

By comparison with Figure 45, effects visible in Figure 46 are the steepening of hydraulic gradients north of the structure and some distortion of water-table contours to the west, south, and east. Large increases in simulated water levels, though, are restricted to the northern side of the disposal site. The shallow water table is raised to the ground surface along the southern edge of the dike where design plans call for maintaining a small existing pond (see Figure 4). In addition, the area affected by the evapotranspiration of ground water has expanded to the north and south from the impoundment as water levels rise closer to the land surface.

The possibility of surface seepage emanating from the disposal structure, as suggested by the simulation, is in contrast to the interpretation offered by Soil Testing Services of Wisconsin (1972a, p. 24) but is wholly consistent with the wetland's function as an area of ground-water discharge to the local surface drainage system. Since the seepage areas are sites of ground-water discharge, their representation in the model was improved by eliminating areal recharge at affected nodes.

Tables 17 and 18 show the alterations to the steady-state ground-water budget caused by the increased seepage from the disposal structure. A significant change, of course, is the more than two-fold increase in the rate of areal recharge representing water losses from the impoundment. The recharge rate in Table 18 also includes about 0.12 cfs ( $0.0034 \text{ m}^3/\text{s}$ )

TABLE 18. Steady-state ground-water budget for the waste-containment area with a natural-soil bottom and 25 ft of saturated waste within the disposal structure.

	Rates (cfs)	
<b>SOURCES:</b>		
Areal recharge		
- Impoundment	0.1600	
- Other areas	0.1216	
	<u>0.2816</u>	0.2816
Constant-head		0.0517
	<b>Total</b>	<b>0.3333</b>
<b>DISCHARGES:</b>		
Evapotranspiration		0.2516
Constant-head		0.0817
	<b>Total</b>	<b>0.3333</b>

of natural recharge through areas distant from the structure. Underflow into the study area across the eastern and southern borders of the model is reduced by approximately 2 percent as the added recharge slightly lessens local flow gradients. The most dramatic response of the system is the 260-percent increase in the rate of ground-water evapotranspiration caused by the elevated water table. Vapor discharge accounts for over 75 percent of all ground-water discharges, an increase from 55 percent under natural conditions. Constant-head discharges from the area, mostly as base flow to Meadowbrook Creek and the Flambeau River, increase by about

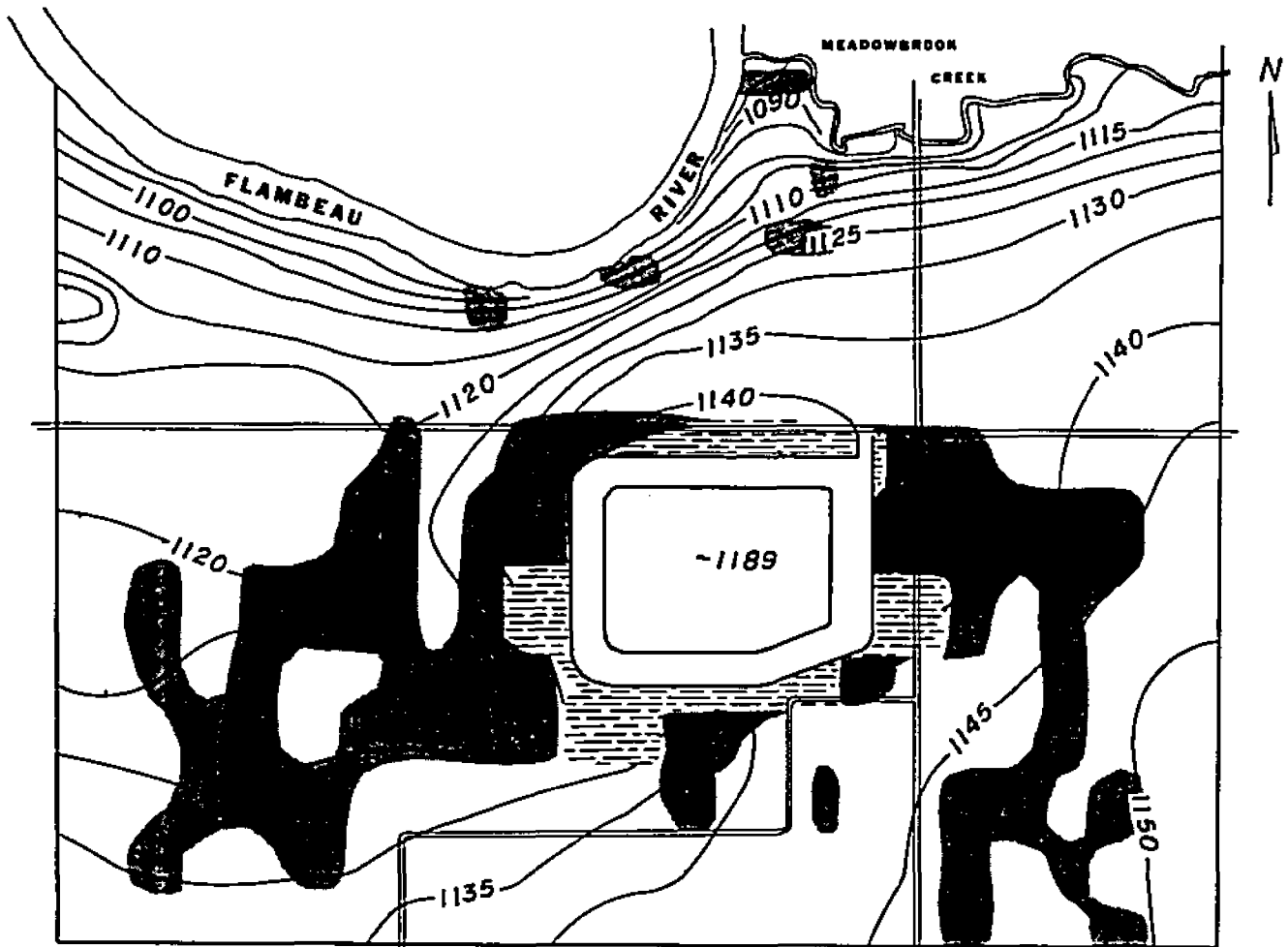
6 percent as gradients north of the disposal site steepen in response to the ground-water mounding around the facility. The base-flow rate to Meadowbrook Creek increases only slightly to 0.03 cfs ( $0.00085 \text{ m}^3/\text{s}$ ) and discharge to the Flambeau increases from 0.044 to 0.047 cfs (0.0012 to  $0.0013 \text{ m}^3/\text{s}$ ).

The simulation was repeated for a saturated thickness of 50 ft (15 m) which is the proposed average maximum fill depth. Starting at the initial rate, seepage rates at nodes within the dike were lowered until heads were maintained at an elevation of about 1189. The adjustment process resulted in the head distribution shown in Figure 47. The total rate of flow necessary to maintain the phreatic-surface elevation at 1189 inside the impoundment is 0.312 cfs ( $0.0088 \text{ m}^3/\text{s}$ ). This rate is approximately double the seepage flux associated with the 25-ft (7.6-m) waste thickness and is equivalent to about 140 gpm. Some convergence problems were experienced during this simulation and it was found that B' values greater than 0.3 prevented convergence. A B' of 0.3 caused the solution to converge within 31 iterations.


The steady-state elevation of the potentiometric surface was computed by solving Equation 50 for  $h_1$  using known information and the seepage rate for the 50-ft (15-m) tailings pile determined through simulation. The associated specific discharge was calculated as  $8.53 \times 10^{-8} \text{ ft/s}$  ( $2.60 \times 10^{-6} \text{ cm/s}$ ) and yielded a potentiometric elevation of 1172.

Comparing figures 46 and 47, little change is evident





 AREAS WHERE GROUND WATER IS DISCHARGED BY EVAPOTRANSPIRATION

 WATER TABLE AT THE SURFACE

0 2000 FT

FIGURE 47. Simulated steady-state head distribution in the waste-containment area for a natural-soil bottom and 50 ft of saturated waste.

in the configuration of the water table. The most obvious changes occur along the south side of the impoundment. Seepage at the surface south of the site occurs over a greater area and also extends northward along the east and west sides of the structure. In addition, surface seepage erupts along the northern side of the containment dike. The hydraulic gradient north of the site, however, is just slightly increased by the additional recharge. The amount of area subject to ground-water evapotranspiration exhibits minor increases with respect to conditions portrayed in Figure 46.

The steady-state ground-water budget resulting from the simulation of the 50-ft (15-m) saturated thickness is given in Table 19. The rate of recharge is increased by about 3.7 times over the natural case in Table 17 in response to water losses from the impoundment. The constant-head flux rate into the study area, chiefly as underflow from the east and south, decreases over 2 percent as local gradients become somewhat flatter. The most significant change in the budget is the four-fold increase in the rate of ground-water evapotranspiration versus the natural state. With a relatively constant head elevation of 1189 inside the structure, evapotranspiration comprises 83 percent of all discharges compared to a 55-percent share under undisturbed conditions. Base flow to perennial surface drainage, represented by the constant-head discharge, increases by approximately 7 percent over the natural regime but only by about 0.5 percent over the rate existing with a 25-ft (7.6-m) saturated waste thickness.

TABLE 19. Steady-state ground-water budget for the waste-containment area with a natural-soil bottom and 50 ft of saturated waste within the disposal structure.

	Rates (cfs)	
<b>SOURCES:</b>		
Areal recharge		
- Impoundment	0.3120	
- Other Areas	0.1301	
	<u>0.4421</u>	0.4421
Constant-head		0.0512
	Total	0.4933
<b>DISCHARGES:</b>		
Evapotranspiration		0.4112
Constant-head		0.0821
	Total	0.4933

The reader is reminded that these simulations are based on several worst-case assumptions and the effects shown in figures 46 and 47 and reported in tables 18 and 19 are probably of greater magnitude and extent than will occur if the wastes are placed directly on the natural soils within the containment structure. One shortfall of the recharge method adopted for the simulations is the steady-state assumption treating the waste pile as an infinite source of water with a constant phreatic level. This infinite-source characterization is satisfactory while the site is active and the tailings slurry is continuously discharged into the impoundment.

After filling is completed and the structure is capped, however, the water level within it is expected to fall, causing the seepage losses to gradually decline to a rate approaching that of natural recharge through the structure's surface. This is a transient phenomenon not treatable with the model in its present steady-state form. These limitations point to the need for cautious interpretation of the simulative results.

#### Containment Structure - Saprolite Bottom Seal

The second case studied with the simulator was the effect of lining the bottom of the disposal structure with a layer of compacted saprolite to reduce water loss and protect ground-water quality. The major difference between this case and the preceding one is the lower hydraulic conductivity of the saprolite with respect to the tailings which gives rise to considerations of unsaturated flow. Laboratory measurements on samples of compacted saprolite from the mine area were made by Soil Testing Services of Wisconsin (1972b) in anticipation of using the material for the dike core. The resulting conductivities ranged from  $7.1 \times 10^{-5}$  to  $0.173$  ft/d ( $2.5 \times 10^{-8}$  to  $6.1 \times 10^{-5}$  cm/s) with a mean value on the order of  $9.6 \times 10^{-3}$  ft/d ( $3.4 \times 10^{-6}$  cm/s). The mean conductivity is less than half the value assumed for the surficial soils in the previous simulation and is about 75 times lower than the average conductivity of the glacial till underlying the

soil, which is 0.71 ft/d ( $2.5 \times 10^{-4}$  cm/s). The laboratory measurements assumed the samples were compacted to approximately the same density as the dike core would be and should be verified by field studies on the finished liner material. It is clear that the low-permeability liner will be the agent controlling seepage from the impoundment under these circumstances.

It is difficult to ascertain in advance what hydrologic consequences will stem from using a saprolite liner beneath the waste. The surficial soils will be skinned from the area to provide a smoother and more stable base for the liner, possibly exposing the more transmissive glacial deposits in the process. The contrast in hydraulic conductivity between the liner and the soil beneath it would then be more pronounced. Seepage from the structure may not saturate the underlying soil in this case and flow at steady state would be due to gravity alone under a vertical gradient. This scenario is quite possible beneath the western part of the containment structure where the free-water surface is comparatively deep.

On the other hand, the water table in the eastern half of the structure location is generally within 2 to 4 ft (0.6 to 1.2 m) of the land surface and may be at the surface in areas now occupied by wetlands. A low rate of seepage through the liner may be sufficient to raise the phreatic surface to or above the liner's base in this area, creating a saturated system similar to that presumed in the previous simulation in which resistance to lateral flow within the underlying

soil significantly affects seepage rates at steady state. There is thus the possibility that a liner will create a complex flow system dominated by unsaturated flow to the west and saturated conditions beneath the liner to the east.

Assessing if, when, and where the two sets of conditions outlined above will occur requires information that is presently nonexistent. Much of the analysis is dependent on the preparation of the liner base and on the final hydraulic conductivity of the liner material. In addition, soils information required to study unsaturated flow conditions affecting the rate and degree of mounding is not available. As shown in the following paragraphs, the use of assumptions that are presently unsubstantiated by real data and the inability of the model to deal with unsaturated flow conditions reduces the simulation of the liner and its effects to a hypothetical exercise with largely unsatisfactory results. For later transient work, better simulative results may be achievable using options in the model for combined artesian/water-table systems. The waste/aquifer system may undergo conversion from water-table to confined conditions in some areas as a consequence of the mounding, and the concomitant build-up of artesian pressure below the liner might be successfully simulated if appropriate storativities and specific yields can be determined. For present purposes, the lined impoundment was simulated in a manner similar to the previous case.

Extending the analysis made for the preceding simulation, the capillary fringe, at its deepest point, may be no more than

5 ft (1.5 m) below a low-permeability liner placed on the land surface. In much of the eastern part of the impoundment site, the water table and the capillary fringe may be in direct contact with the liner at the time the saprolite is put into place. It was arbitrarily assumed that the water table will rise to the base of the liner in areas where the initial water table is within 5 ft (1.5 m) of the surface. This depth places the capillary fringe very close to the bottom of the saprolite layer. The area in which this condition is met consists of the nodes in row 13, columns 16 through 18, and in row 14, columns 15 through 18 of Figure 44 (this area is also shown in Figure 48). The average depth to the water table at the remaining nodes to the west within the impoundment boundaries ranges from 6 to 10 ft (1.6 to 3 m) so the top of the capillary fringe there is farther below the liner. This approach presumes the liner will transmit water at a rate sufficient to raise the water table or the capillary fringe to at least the base of the liner throughout all of the eastern area. The system there would then be analogous to an aquifer confined by an overlying semi-permeable aquitard composed of the compacted saprolite. The hydraulic conductivity of the waste material will be sufficiently low to assist in retarding seepage and must be taken into account along with the liner. Equation 50 can be modified to yield a weighted average of the vertical seepage rate from the surface of the tailings pond to the bottom of the liner (Bouwer, 1982):

$$V_1 = K_1 K_t \left( \frac{h_2 + b_1 - h_1}{b_1 K_t + b_t K_1} \right) \quad (51)$$

where  $V_1$  is the average seepage rate ( $Lt^{-1}$ ),  $K_1$  and  $K_t$  are the respective conductivities of the liner and waste materials,  $b_1$  and  $b_t$  are the respective thicknesses of the liner and wastes,  $h_2$  is the head difference across the saturated waste pile (its saturated thickness plus the depth of ponding on its surface), and  $h_1$  is the pressure head at the base of the liner. When the water level at the liner's base (the head when the foundation soils first reach saturation) is coincident with the land surface,  $h_1$  is zero as in the previous simulation.

Average initial seepage rates were computed for various liner thicknesses using Equation 51, an average tailings conductivity of 0.022 ft/d ( $7.8 \times 10^{-6}$  cm/s), an average saturated liner conductivity of  $9.3 \times 10^{-3}$  ft/d ( $3.4 \times 10^{-6}$  cm/s), and saturated waste accumulations of 25 and 50 ft (7.6 and 15 m). The results of the calculations are listed in Table 20. These initial rates approximate the flux when the rising water table first encounters the base of the liner and the gage pressure beneath the liner is zero. The rates are independent of the hydraulic properties of the foundation soils and are valid if the liner and wastes restrict seepage to a rate less than the hydraulic conductivity of the soils. Since no build-up of hydraulic head beneath the liner was taken into



TABLE 20. Estimated initial seepage rates for various combinations of liner and waste thicknesses computed with Equation 51 for saturated conditions.

<u>Waste Thickness (ft)</u>	<u>Liner Thickness (ft)</u>	<u>Seepage Rate (ft/d)</u>
25	2	0.020
	3	0.019
	5	0.018
50	2	0.021
	3	0.020
	5	0.020

$$K_1 = 0.0096 \text{ ft/d}; K_t = 0.022 \text{ ft/d}$$

account, the initial rates are conservatively large.

The argument presented for the previous simulation regarding the application of Equation 50 to the bottom of the impoundment is equally valid for Equation 51. This equation was thus applied to the eastern part of the structure's bottom (where saturated conditions are assumed) to find a volumetric seepage rate. From the earlier assumption defining the areas of unsaturated versus saturated conditions, the area of saturation beneath the eastern part of the impoundment would encompass approximately 38 acres (15 ha). For a 5-ft (1.5-m) clay liner with 25 ft (7.6 m) of saturated waste above it, an initial volumetric seepage flux of about 0.34 cfs ( $0.0096 \text{ m}^3/\text{s}$ ) is computed. This rate is equivalent to 153 gpm and is less than 40 percent of the initial rate computed for an unlined impoundment with the same accumulation

of waste. The difference, however, is due to the smaller area rather than to the retarding effects of the liner.

The liner may restrict flow to the degree that the best estimate of the water-loss rate in the western part of the site is the unsaturated hydraulic conductivity of the foundation soils. This is significantly different from the presumed situation to the east since the unsaturated conductivity is much less than saturated  $K$ 's, especially if negative pressure heads are maintained below the air-entry threshold. Data deficiencies, however, prevent an estimate of unsaturated conductivity of the foundation soils in that area. It may be assumed with some confidence, though, that the conductivity would be very small in relation to the rate of water loss through the saturated foundation soils that would presumably exist farther east. Recharge rates through the western part of the liner were consequently approximated as zero.

It is likely that an increase in fluid pressure beneath the eastern part of the liner would elevate the potentiometric surface above the original land surface. The head levels are not known beforehand and cannot be determined explicitly with the model. The increased heads, however, are the direct result of the resistance to flow offered by the receiving soils below the liner and the initial seepage rate computed above would eventually decrease to a steady-state rate as the pressure climbed toward an equilibrium level. An upper bound on the steady-state flux rate can therefore be found by assuming that the resistance to lateral flow through the saturated

foundation soils to the east will control the seepage (McWhorter and Nelson, 1979).

The amount of speculation regarding actual site conditions and the number of unverified assumptions invoked to treat the liner do not justify a rigorous examination of several variations of this case. Consequently, this simulation can only be considered demonstrative. The simulation was done for the single case of a 25-ft (7.6-m) accumulation of saturated tailings and waste rock and a 5-ft (1.5-m) sapro-lite liner using an initial seepage rate of 0.018 ft/d ( $6.4 \times 10^{-6}$  cm/s) from Table 20. Since it was assumed that no seepage will occur through the western portion of the impoundment, this area was treated as if there was no containment structure above it. As far as the model was concerned, only the eastern nodes comprised the impoundment.

The initial seepage rate produces simulated heads as much as 80 ft (24 m) above the phreatic surface within the tailings in the eastern part of the structure. The seepage rate existing at equilibrium when the loss of water is controlled by the foundation soils was found by repeatedly lowering the recharge rate until computed heads approximated the phreatic line at an elevation of 1163. Convergence to a solution was achieved after 25 iterations with a B' of 0.4.

The head distribution shown in Figure 48 results from the assumptions stated earlier and the recharge-adjustment method. The pattern of water-table contours differs little from that of Figure 45 except for evidence of some ground-

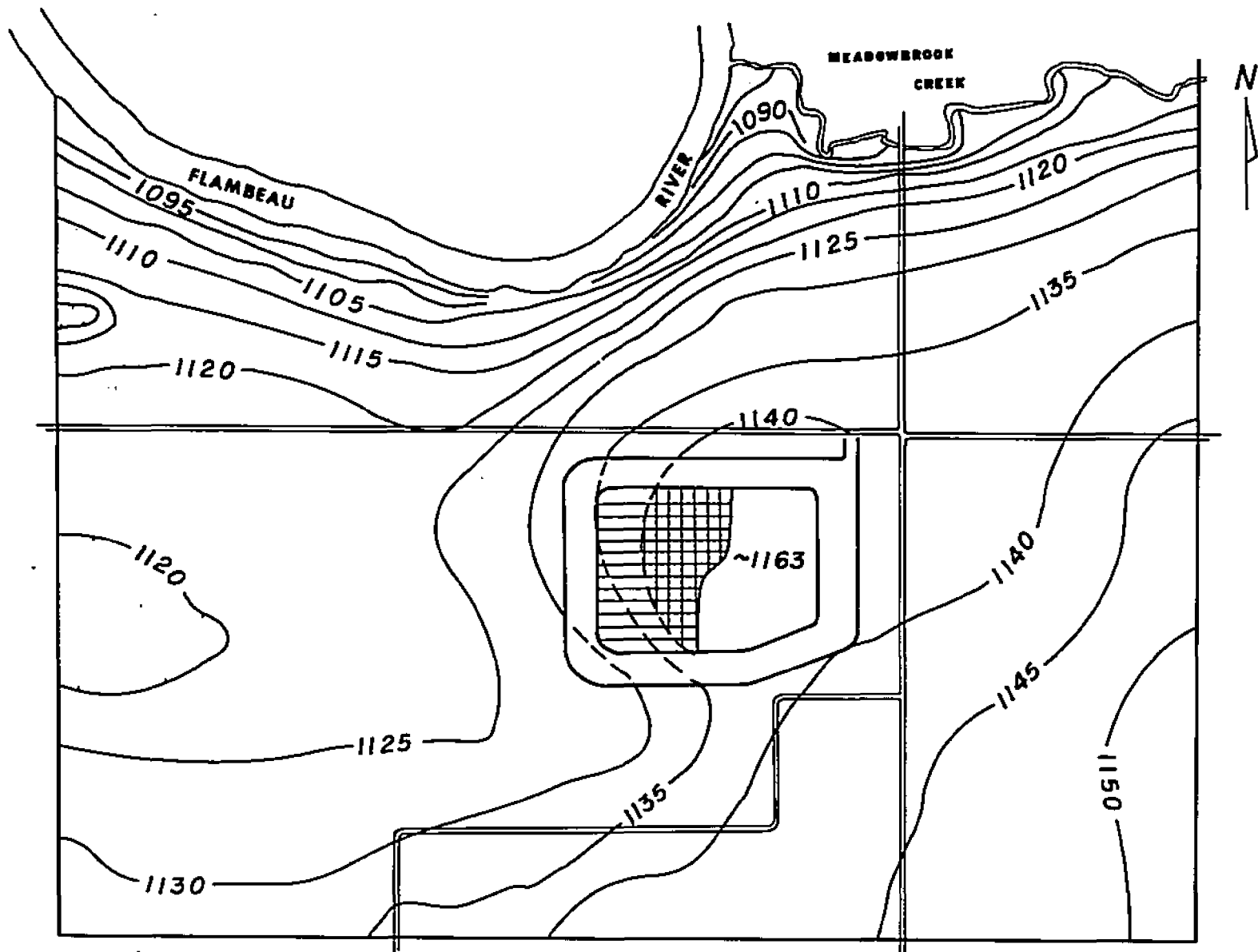


FIGURE 48. Simulated steady-state head distribution in the waste-containment area for a lined impoundment with 25 ft of saturated waste; unsaturated conditions are assumed in the patterned part of the site (the vertical lines show the westward migration of the groundwater mound).

water mounding along the northern side of the containment structure. The total seepage flux necessary to maintain the water table at 1163 within the impoundment is 0.081 cfs (0.0023 m<sup>3</sup>/s), which is about 36 gpm. This rate of water loss is about half that for the corresponding unlined case; it is probably conservatively large because the actual effects of the liner in the eastern part of the site are not included. The only liner effect explicitly assumed is its prevention of saturated conditions to the west.

Several difficulties became apparent during the simulation. The seepage rate needed to maintain a water level of 1163 inside the containment structure forces the ground-water to the west, saturating soils beneath all but the extreme west end of the impoundment. Attempting to represent this additional area of saturation in the model pushes it still farther west. This process can be repeated in a "leap-frog" cycle that culminates in the saturation of the entire soil zone beneath the liner. The simulation then becomes identical to the previous case which assumes that only the foundation soils control the steady-state rate of seepage through the entire bottom area of the structure. It is doubtful that this would be the case. Without a transient analysis of unsaturated flow characteristics of the area, it cannot be determined if the apparent westward migration of the saturated soil zone is a possible real occurrence or is a function of the way the system is represented in the model. Intuition says the liner will be sufficiently impervious to prevent the total saturation of

soils beneath it, especially at the west end of the structure. Consequently, it appears that the representation of the liner in the model, as described earlier, is not appropriate. The mounding phenomenon must be studied analytically using principles of unsaturated flow so that accurate rates of ground-water flow and mounding may be determined. Pertinent methodology for conducting such an analysis is provided in McWhorter and Nelson (1979) and Bower (1982), though their techniques depend on the availability of the proper soils data.

Because of the hypothetical nature of this simulation and the large amount of uncertainty associated with it, no attempt was made to analyze the ground-water budget or the effects on the distribution of vapor-discharge areas. It can be assumed, however, that the effects from the lined impoundment will be much less than those indicated by the earlier simulation for the 25-ft (7.6-m) accumulation of saturated waste on a natural soil bottom.

## CHAPTER X

### CONCLUDING REMARKS

#### Summary of Study and Findings

In 1970 Kennecott Minerals Company announced the discovery of a 4- to 6-million ton massive copper/zinc sulfide body southwest of Ladysmith in Rusk County, northwest Wisconsin. Called the Flambeau deposit because of its proximity to the Flambeau River, the steeply dipping, tabular ore body is imbedded within a linear belt of Middle Precambrian metavolcanics which extends eastward to the Michigan border.

Kennecott plans to mine the deposit through two 11-year phases of surface and deep mining, respectively. To assist in mine management and hydrologic-impact evaluation, the company authorized by development of digital models of the groundwater flow systems in the vicinities of the proposed mine and a 156-acre tailings disposal impoundment 1.2 miles to the south. The chief motivations for the authorization were the ability of computer models to predict the effects of different mining activities on the flow systems and the ease with which this type of model can be modified to account for new information and changing site conditions.

Ground water within the project area occurs primarily within the voids of the Pleistocene glacial deposits and a thin sequence of Upper Cambrian sandstone that overlies the dissected Precambrian surface. The study was thus limited

to these sediments. After an analysis of the surface-drainage system, climatological information, and a large body of subsurface data from on-site exploratory drilling and testing, a detailed hydrologic budget of the area was constructed and the hydraulic characteristics of the flow systems were defined. Numerical models of the proposed mine and waste-containment areas were then constructed using the two-dimensional finite-difference code of the U. S. Geological Survey (Trescott and others, 1976) which was modified to improve its applicability to the problems. The flow systems were modeled as single-layer unconfined aquifers with the Flambeau River as the major ground-water sink in the area. Steady-state calibration of the models consisted of adjusting initial hydraulic conductivities to achieve a reasonable match between the measured water-table surface and the hydraulic-head distributions generated by the models. Excellent matches were obtained in both cases. Limitations in data restricted all subsequent simulative work to the steady-state case.

Simulations of the mine pit were carried out for two major cases, the large 55-acre open pit originally proposed and a smaller direct-ship pit. The large pit was first simulated under conditions representing an interior drainage-collection system of sumps, ditches, and pumps. This set of conditions proved difficult to characterize in the model because of the anticipated development of a seepage face in the side-walls of the excavation above the Precambrian contact. Several representations were tried unsuccessfully before a method



employing a high hydraulic conductivity to represent the pit interior was devised and used successfully. The resulting simulations for pit geometries at 3, 4, and 11 years show a progressively enlarging cone of depression surrounding the excavation with induced infiltration eastward from the Flambeau River. The eastward expansion of the cone was effectively halted by the fine-grained glacial material. Steady-state rates of seepage into the pit for the three geometries were predicted at 45, 31, and 36 gpm, respectively.

Another water-control option investigated is encircling the large pit with a low-permeability slurry-trench cutoff wall. Simulations of this case using the final pit geometry indicate the wall will act as a subsurface dam, impounding ground water on its up-gradient (east) side while causing head losses west and northwest of the pit. The simulated head changes of largest magnitude (-8 and +14 ft) were restricted to within several hundred feet of the slurry wall.

The direct-ship pit is an alternative to the large surface mine and involves constructing a smaller pit to remove ore rich enough to be transported directly to a smelting facility. This smaller pit was simulated for the cases of an internal collection system, a slurry wall, and the use of dewatering wells to control seepage. The first two cases yield simulative results qualitatively similar to the corresponding simulations of the large pit. The predicted steady-state seepage rate into the internally drained direct-ship pit was 25 gpm. The simulation using dewatering

wells was generally less definitive because of the restriction to steady-state conditions. The final well-location scheme determined through trial-and-error consisted of 10 wells with a combined pumping rate of less than 17 gpm. The low discharge rate suggests that dewatering methods more suited for low-transmissivity soils would be more effective than large-diameter wells.

Simulations of the waste-containment impoundment were generally not as satisfactory as the pit predictions due to data and model limitations. In particular, conditions in this area are such that unsaturated flow in soils above the water table and beneath the structure must be considered to confidently predict its effects on the hydrologic regime. In the three simulations performed, seepage from the structure was represented by increasing the rate of areal recharge at appropriate nodes. The first case assumed that tailings and waste rock would be placed directly on the original land surface within the structure. The predicted rate of water loss at steady state was 72 gpm for an accumulation of 25 ft of saturated waste. Simulated water losses for a 50-ft accumulation of waste were roughly double this rate. Both simulations produced slight ground-water mounding around the disposal structure, especially to the north. The second case, in particular, was characterized by surface seepage along the outer base of the containment dike.

The final simulation called for lining the impoundment with compacted saprolite to reduce seepage and offer additional water-quality protection. This simulation was the

least satisfactory because of the prominent role that unsaturated flow would play under these circumstances. A simulation was attempted by assuming a 25-ft accumulation of saturated waste, a 5-ft saprolite liner, and that soils beneath the western part of the site where the water table is deeper would remain unsaturated. The resulting steady-state seepage rate predicted by the model was 36 gpm with mounding effects most evident on the north side of the structure.

#### Realization of Study Objectives

All of the pertinent objectives set forth in Chapter I were (or will be) addressed in some fashion during the course of the study, though several can be more completely satisfied through additional work as described later. The objectives were 1) to refine and interpret all existing geologic and hydrogeologic information, 2) to use the data to construct computer models of the flow systems at the two study areas for predicting adverse effects on local hydrologic regimes, 3) to test, if necessary, the effectiveness of remedial measures in abating adverse impacts of the mining operation, and 4) to determine what types of additional data are needed to improve the reliability of the models and where data-collection efforts should be concentrated. The first two of these goals were explicitly satisfied in the preceding chapters; the remaining two are considered below.

### Testing of Remedial Methods

The objective of testing the suitability of engineering solutions to hydrologic problems stemming from the operation was contingent on the results of the model simulations. In the author's judgment, none of the simulations suggest that problems not controllable through routine engineering practices will occur. In fact, the effects indicated by the simulations may not require any overt control measures because of their relatively small magnitude. In most cases, engineering techniques that are likely to be used to address minor problems, such as improvements in surface drainage, are not representable in the models anyway. Given these factors, the testing of remedial methods was deemed unnecessary.

It is possible that revised versions of the models based on better physical data could predict less favorable outcomes, although worst-case assumptions were routinely adopted during the study if doubt existed regarding the reliability of available data. However, in all predictive studies, even those with more complete data bases, some uncertainty exists concerning the simulative results. Hence, a prudent strategy is to satisfy the information gaps cited later and then refining the models accordingly. If subsequent simulations with the improved models still indicate a manageable degree of hydrologic disturbance by the mining operation, the only recourses that may be necessary (exclusive of water-quality concerns) are those aimed at improving working conditions and monitoring capabilities in affected areas.

### Recommendations for Additional Data

Several noteworthy deficiencies in the information presently available were detected during the investigation. Some of these were described in preceding chapters when knowledge of the deficiencies was required to justify certain assumptions or characterizations used in the models. Most of the data gaps would probably have been filled during early site investigations if a modeling study had been anticipated at that time. Specific deficiencies are detailed below.

1. Since the study areas are characterized as unconfined flow systems, better definition of the Precambrian surface at both sites is necessary to accurately represent the aquifer bottoms. This is especially true north and east of the pit location and in virtually every direction from the waste-containment structure.
2. The surficial geology in both areas should be defined more precisely. This recommendation is particularly crucial for the area east of the waste impoundment and the area between the structure and the Flambeau River where the northward and eastward extent of persistent outwash zones is presently unknown. The character of glacial deposits near the Flambeau River at both sites and east of the mine pit (including the area east of Highway 27) must also be delineated. Reliable descriptions of materials near the river will permit the interaction between it and the underlying outwash aquifer to be more clearly known.
3. Measurements of water levels in areas distant from the mine pit and containment structure are necessary for better calibration of the models. The lack of reliable

static water levels is most pronounced to the east of each site, including the area east of Highway 27. Similarly, water-level data near the Flambeau River could shed light on head relationships between the river and the outwash aquifer. Given the enormous hydrologic influence of the Flambeau, this information should be given a high priority. Attention must be given to the proper construction of any new observation wells so that problems encountered with existing wells can be avoided.

4. The hydraulic properties of the unconsolidated materials and the Cambrian sandstone at each study area should be measured through a series of carefully designed and executed pumping tests of suitable duration. In addition to providing better initial information for the models, the storativities (or specific yields) from the tests are needed for transient simulations. Pumping tests would also provide the nonsteady phenomena for verifying the transient models.
5. The representation of the Flambeau River in the models can be greatly improved if data from pumping tests near the river can be used to estimate the hydraulic conductivity of the river bed. If the bed's thickness can be determined or estimated in some manner, the river can be treated in the more realistic fashion described in chapters VIII and IX.
6. The total flow system at the southern study area may be treated better in three dimensions with the two major outwash zones comprising individual aquifers separated by an intervening aquitard of glacial till. If a three-dimensional model of the disposal area is contemplated, the transmissivities, storativities, and hydraulic-head distribution of each aquifer must be obtained through pumping tests and piezometer installations. These ac-

tivities, of course, should be preceded by a study to determine if the additional effort required for a three-dimensional approach will result in a corresponding increase in benefits.

7. Deficiencies most apparent in the simulations of the waste impoundment were of data needed to analyze the unsaturated flow system above the water table. Information critical for this analysis are reliable estimates of the hydraulic conductivity of the finished liner material, the tailings/waste-rock mixture, and the soils that will underlie the structure. In addition, data describing soil porosities, volumetric water contents, and negative pressure heads are needed.

#### Comments on Transient Simulations

Nonsteady flow occurs when the magnitudes and directions of velocity vectors vary with time at any point within the flow domain. Therefore, the effects of the mining operation can be traced through time only by conducting transient simulations of the flow systems. Nonsteady flow through saturated porous media is described in two dimensions by Equation 40 on page 170.

To simulate transient behavior with the U. S. G. S. model (Trescott and others, 1976), the data and several parameters used in the steady-state runs need only slight modification. Referring to the list of inputs at the end of Chapter VII, items 5, 10, and 11 must be changed to reflect the time and storage-parameter requirements of Equation 40. The storativity or specific yield satisfying item 5 is obtained from the

pumping tests described in the preceding section. Items 10 and 11 satisfy the transient model's need for time information and refer to the length of the simulation period and the number of discrete steps into which the time dimension is divided, respectively. To insure that transient effects are not already occurring at the start of a nonsteady simulation, the initial heads should consist of the steady-state configuration. This decreases the probability of solution instabilities and insures that transient effects computed by the model result only from the stresses that are specified.

Transient simulations, as stated in Chapter VIII, can be used to further refine the parameter distribution determined through steady-state calibration. This verification process consists of using the model to reproduce some real transient event with a known head distribution such as a pumping test. Additional parameter adjustment is usually necessary to meet this objective, though the refinements should not appreciably affect the steady-state solution.



## REFERENCES CITED

- Appel, C. A. 1976. A note on computing finite-difference interblock transmissivities. *Water Res. Res.* 12(3): 561-563.
- Bair, E. S. 1980. Numerical simulation of the hydrologic effects of open-pit anthracite mining. Ph.D. Thesis, The Pennsylvania State Univ., 273 p.
- Bair, E. S., and R. R. Parizek. 1981. Numerical simulation of potentiometric surface changes caused by a proposed open-pit anthracite mine. *Ground Water* 19(2): 190-200.
- Barnes, H. H. 1967. Roughness characteristics of natural channels. U. S. Geol. Surv. Water Sup. Paper 1849, 213 p.
- Bloyd, R. M. 1975. Summary appraisals of the nation's groundwater resources - Upper Mississippi region. U. S. Geol. Surv. Prof. Paper 813-B, 22 p.
- Borman, R. G. 1971a. Preliminary map of probable well yields from glacial deposits in Wisconsin. U. S. Geol. Surv. Open-file Rep., Madison.
- Borman, R. G. 1971b. Preliminary map of probable well yields from bedrock in Wisconsin. U. S. Geol. Surv. Open-file Rep., Madison.
- Bouwer, H. 1978. *Groundwater hydrology*. McGraw-Hill Book Co., New York, 480 p.
- Bouwer, H. 1982. Design considerations for earth linings for seepage control. *Ground Water* 20(5): 531-537.
- Bredehoeft, J. D., and G. F. Pinder. 1970. Digital analysis of areal flow in multiaquifer ground-water systems: A quasi 3-D model. *Water Res. Res.* 6(3): 883-888.
- Cahow, A. C. 1973. Geomorphology of the proposed Flambeau mine area. Unpubl. consult. rep. to Bear Creek Mining Co., 12 p.
- Cedergren, H. R. 1967. *Seepage, drainage, and flow nets*. John Wiley and Sons, New York, 489 p.
- Chow, V. T., ed. 1964. *Handbook of applied hydrology*. McGraw-Hill Book Co., New York.
- City of Ladysmith. 1982. Misc. data provided by the Water Dept. through the Flambeau Mining Co.

- Cooley, R. L. 1977. A method of estimating parameters and assessing reliability for models of steady state groundwater flow 1, Theory and numerical properties. *Water Res. Res.* 13(2): 318-324.
- Cooley, R. L. 1979. A method of estimating parameters and assessing reliability for models of steady state groundwater flow 2, Application of statistical analysis. *Water Res. Res.* 15(3): 603-617.
- Cooper, H. H., and C. E. Jacob. 1946. A generalized graphical method for evaluating formation constants and summarizing well field history. *Amer. Geophys. Union Trans.* 27: 526-534.
- Corbett, D. M., and others. 1945. Stream-gaging procedures. U. S. Geol. Surv. Water Sup. Paper 888, 245 p.
- Dettinger, M. D., and J. L. Wilson. 1981. First-order analysis of uncertainty in numerical models of groundwater flow, Part 1: Mathematical development. *Water Res. Res.* 17(1): 149-161.
- Devaul, R. W. 1975. Map of probable well yields of wells in the sand-and-gravel aquifer, Wisconsin. *Wisc. Geol. and Natural History Surv.*, Madison.
- DeWiest, R. J. M. 1965. *Geohydrology*. John Wiley and Sons, New York, 336 p.
- Dove, G. D. 1961. A hydrologic study of the valley-fill deposits in the Venice area, Ohio. Ohio Dept. of Natural Res. Tech. Rep. No. 4.
- Dutton, C. E., and R. F. Bradley. 1970. Map of northern Wisconsin showing areal geology of Precambrian rocks. U. S. Geol. Surv. Misc. Geologic Map I-631, Sheet 3.
- Dutton, C. E. 1971. Volcanic-sedimentary belts and sulfide occurrences in Wisconsin. U. S. Geol. Surv. Prof. Paper 750-B, pp. 96-100.
- Dutton, C. E. 1976. Precambrian geology. In "Mineral and water resources of Wisconsin". U. S. Geol. Surv. and Wisc. Geol. and Natural History Surv., Rep. to Committee on Interior and Insular Affairs. U. S. Govt. Print. Off., pp. 11-22.
- Faust, C. R., L. R. Silka, and J. W. Mercer. 1981. Computer modeling and ground-water protection. *Ground Water* 19(4): 362-365.
- Fetter, C. W. 1980. *Applied hydrogeology*. Charles E. Merrill Publ. Co., Columbus, Ohio, 488 p.

- Fetter, C. W. 1981. Determination of the direction of groundwater flow. *Ground Water Monitoring Review* 1(3): 28-31.
- Fenn, D. G., K. J. Hanley, and T. V. DeGeare. 1975. Use of the water balance method for predicting leachate generation from solid waste disposal sites. U. S. EPA/530/SW-168, 40 p.
- Flambeau Mining Corp. 1973. Unpubl. streamflow and water-level records from the Flambeau project area.
- Flambeau Mining Co. 1976. Mining permit application for mining the Flambeau copper deposit, Rusk County, Wisconsin. submitted to Wisc. Dept. of Natural Res.
- Freeze, R. A., and J. A. Cherry. 1979. *Groundwater*. Prentice-Hall, Englewood Cliffs, New Jersey, 604 p.
- Gray, D. M. 1970. *Handbook on the principles of hydrology*. Water Inform. Ctr., Huntington, New York.
- Hadley, D. W., and J. H. Pelham. 1976. Glacial deposits of Wisconsin: Sand and gravel resource potential. *Wisc. Geol. and Natural History Surv.*, Madison.
- Harder, A. H., and W. J. Drescher. 1954. Ground-water conditions in southwest Langlade County, Wisconsin. U. S. Geol. Surv. Water Sup. Paper 1294, 39 p.
- Harshbarger, J. W. 1971. Results of low capacity pumping tests, Flambeau project. Memo to N. Lutz dated Sept. 8. Records of Flambeau Mining Corp.
- Hendry, M. J. 1982. Hydraulic conductivity of a glacial till in Alberta. *Ground Water* 20(2): 162-169.
- Hotchkiss, W. O., E. F. Bean, and O. W. Wheelwright. 1915. Mineral land classification. *Wisc. Geol. and Natural History Surv. Bull.* 44, 377 p.
- IECO, Inc. 1960. Report on tailings pond site investigation, Hayden, Arizona. Unpubl. consult. rep. to Ray Mines, Kennecott Copper Corp.
- INTERA, Inc. 1983. Water quality evaluation for lower White-water Creek, Lake 1, and the tailings pile, Hurley, New Mexico. Draft consult. rep. to Chino Mines Div., Kennecott Minerals Co.
- Kitching, R., Shearer, T. R., and S. L. Shedlock. 1977. Recharge to Bunter sandstone determined from lysimeters. *J. Hydrol.* 33: 217-232.

- LaBerge, G. L., and M. G. Mudrey. 1979. Status report - Stratigraphic framework of the Wisconsin Middle Precambrian. Wisc. Geol. and Natural History Surv. Rep. 79-1, 22 p.
- Larson, S. P., and P. C. Trescott. 1977. Solution of water-table and anisotropic flow problems by using the strongly implicit procedure. U. S. Geol. Surv. J. Research 5(6): 815-821.
- Lohman, S. W. 1972. Ground-water hydraulics. U. S. Geol. Surv. Prof. Paper 708, 70 p.
- Lovell, R. E., L. Duckstein, and C. C. Kisiel. 1972. Use of subjective information in estimation of aquifer parameters. Water Res. Res. 8(3): 680-690.
- Martin, L. 1916. The physical geography of Wisconsin. Wisc. Geol. and Natural History Surv. Bull 36, 549 p.
- Martinson, A. H. 1970. Interim soil survey, Town of Flambeau and the north half of Grant, Rusk County, Wisconsin. USDA, Soil Conserv. Serv., 39 p.
- May, E. R. 1971. Soil investigation, proposed waste disposal area, Section 21, Grant Township, Wisconsin. Internal staff rep., Bear Creek Mining Co., 16 p.
- May, E. R. 1973a. Overburden reinterpretation, mine site, Flambeau development. Internal staff rep., Bear Creek Mining Co.
- May, E. R. 1973b. Argillic alteration west of Flambeau River. Memo to N. Lutz dated March 28. Records of Flambeau Mining Corp.
- May, E. R. 1977. Flambeau - A Precambrian supergene enriched massive sulfide deposit. Geoscience Wisconsin 1: 1-26.
- McElwee, C. D. 1982. Sensitivity analysis and the ground-water inverse problem. Ground Water 20(6): 723-735.
- McWhorter, D. B., and J. D. Nelson. 1979. Unsaturated flow beneath tailings impoundments. J. Amer. Soc. Civil Eng. 105(GTII): 1317-1334.
- McWhorter, D. B., and D. K. Sunada. 1977. Ground-water hydrology and hydraulics. Water Res. Publs., Fort Collins, Colo., 290 p.
- Mercer, J. W., and C. R. Faust. 1981. Ground-water modeling. National Water Well Assoc., Worthington, Ohio, 60 p.

- Motts, W. S., and R. W. Heeley. 1973. Wetlands and ground water. In "A guide to important characteristics and values of freshwater wetlands in the northeast", J. S. Larson, ed. Univ. of Mass. Water Resources Research Ctr. Publ. No. 31, pp. 5-8.
- Mudrey, M. G. 1979. The massive sulfide occurrences in Wisconsin. Wisc. Geol. and Natural History Surv. Misc. Paper 79-2, 20 p.
- Myers, P. E. 1974. Precambrian geology of the Eau Claire region, Wisconsin. Annual Tri-State Geol. Field. Conf. 38th: 1-3.
- National Oceanic and Atmospheric Admin. 1981. Climatological data: Annual summary, Wisconsin, 1980. U. S. Dept. Commerce, National Climatic Ctr., vol. 85, no. 13, 19 p.
- Neuman, S. P. 1973. Calibration of distributed parameter groundwater flow models viewed as a multiple-objective decision process under uncertainty. Water Res. Res. 9(4): 1006-1021.
- Novitzki, R. P. 1979. An introduction to Wisconsin wetlands: Plants, hydrology and soils. Wisc. Geol. and Natural History Surv., 19 p.
- O'Brien, A. L., and W. S. Motts. 1980. Hydrogeologic evaluation of wetland basins for land use planning. Water Res. Bull. 16(5): 785-789.
- Passavant, C. R. 1971. Observation well test pumping program, January 5-13, 1971. Internal staff rep., Great Lakes Exploration Co., 32 p.
- Paull, R. K., and R. A. Paull. 1980. Field guide, Wisconsin and upper Michigan. Kendall-Hunt Publ. Co., Dubuque, Iowa.
- Paydirt. Kennecott teamwork discovered Flambeau copper deposit, opened new district. Oct. 1979, p. 58-59.
- Pinder, G. F., and J. D. Bredehoeft. 1968. Application of the digital computer for aquifer evaluation. Water Res. Res. 4(5): 1069-1093.
- Prickett, T. A., and C. G. Lonquist. 1971. Selected digital computer techniques for groundwater resource evaluation. Ill. State Water Surv. Bull. 55, 62 p.
- Prudic, D. E. 1982. Hydraulic conductivity of a fine-grained till, Cattaraugus County, New York, Ground Water 20(2): 194-204.

- Remson, I., C. A. Appel, and R. A. Webster. 1965. Ground-water models solved by digital computer. *J. Hydraulics Div., ASCE, HY3*, pp. 133-147.
- Remson, I., G. M. Hornberger, and F. J. Molz. 1971. *Numerical methods in subsurface hydrology*. Wiley-Interscience, New York, 389 p.
- Rushton, K. R., and S. C. Redshaw. 1979. *Seepage and ground-water flow*. Wiley and Sons, New York, 339 p.
- Rushton, K. R., and C. Ward. 1979. The estimation of ground-water recharge. *J. Hydrol.* 41: 345-361.
- Sather, L. M., S. I. Jones, and C. W. Threinen. 1971. *Surface water resources of Rusk County*. Wisc. Dept. of Natural Res., Madison, 97 p.
- Schwenk, C. G. 1977. Discovery of the Flambeau deposit, Rusk County, Wisconsin: A geophysical case history. *Geoscience Wisconsin* 1: 27-42.
- Shedlock, R. J. 1981. U. S. Geol. Surv., Indianapolis. Personal communication.
- Sims, P. K. 1976. Presidential address - Precambrian tectonics and mineral deposits, Lake Superior region. *Econ. Geol.* 71(6): 1092-1118.
- Singh, V. P. 1977. Criterion to choose step length for some numerical methods used in hydrology. *J. Hydrol.* 33: 287-299.
- Soil Conservation Service. 1972. *Soil considerations for waste disposal in Indiana*. USDA, Indianapolis.
- Soil Testing Services of Wisconsin. 1972a. Part I, Proposed Flambeau project, Ladysmith, Wisconsin. Unpubl. consult. rep. to Great Lakes Exploration Co.
- Soil Testing Services of Wisconsin. 1972b. Part II, Proposed Flambeau project, Ladysmith, Wisconsin. Unpubl. consult. rep. to Great Lakes Exploration Co.
- Soil Testing Services of Wisconsin. 1973. Proposed mine development, Bear Creek Mining Co., Ladysmith, Wisconsin. Unpubl. consult. rep. to Bear Creek Mining Co.
- Soil Testing Services of Wisconsin. 1975. Proposed ore process plant, Flambeau Mining Corp., Ladysmith, Wisconsin. Unpubl. consult. rep. to Kennecott Copper Co.

- Soil Testing Services of Wisconsin. 1976a. Utilization of overburden, Flambeau open pit mine, Flambeau Mining Corp., Ladysmith, Wisconsin. Unpubl. consult. rep. to Flambeau Mining Corp.
- Soil Testing Services of Wisconsin. 1976b. Phase II, Sub-surface exploration, proposed ore process plant, Flambeau Mining Corp., Ladysmith, Wisconsin. Unpubl. consult. rep. to Kennecott Copper Co.
- Soil Testing Services of Wisconsin. 1976c. Gravel pit design. Unpubl. consult. rep. to Flambeau Mining Corp.
- Sokolov, A. A., and T. G. Chapman, eds. 1974. Methods for water balance computations, An international guide for research and practice. The Unesco Press, Paris, 127 p.
- Stacey, J. S., B. R. Doe, L. T. Silves, and R. E. Zartman. 1976. Plumbo Tectonics IIA, Precambrian massive sulfide deposits. U. S. Geol. Surv., Denver.
- Stallman, R. W. 1956. Numerical analysis of regional water levels to define aquifer hydrology. Amer. Geophys. Union Trans. 37(4): 451-460.
- Stone, H. K. 1968. Iterative solution of implicit approximations of multidimensional partial differential equations. Soc. Industrial Appl. Math., J. Numerical Analysis 5(3): 530-558.
- Summers, W. K. 1972. Specific capacities of wells in crystalline rocks. Ground Water 10(6): 37-47.
- Tanner, C. B., and W. L. Pelton. 1960. Potential evapotranspiration estimates by the approximate energy balance method of Penman. J Geophys. Res. 65(19): 3391-3413.
- Theis, C. V. 1935. The relation between lowering of the piezometric surface and the rate and duration of discharge of a well using groundwater storage. Amer. Geophys. Union Trans. 2: 519-524.
- Thomas, R. G. 1973. Groundwater models. Food and Agricult. Organiz. of the United Nations Paper 21, 192 p.
- Thorntwaite, C. W., H. G. Wilm, and others. 1944. Report of the committee on transpiration and evaporation, 1943-1944. Amer. Geophys. Union Trans 25, Part V: 683-693.
- Thorntwaite, C. W., and J. R. Mather. 1955. The water balance. Drexel Instit. of Technol., Lab. of Climatology, Publs. in Climatology 8(1).

- Thorntwaite, C. W., and J. R. Mather. 1957. Instructions and tables for computed potential evapotranspiration and the water balance. Drexel Instit. of Technol., Lab. of Climatology, Publs. in Climatology 10(3): 184-311.
- Trescott, P. C. 1975. Documentation of finite-difference model for simulation of three-dimensional ground-water flow. U. S. Geol. Surv. Open-file Rep. 75-438.
- Trescott, P. C., and S. P. Larson. 1976. Supplement to Open-file Rep. 75-438. U. S. Geol. Surv. Open-file Rep. 76-591, 21 p.
- Trescott, P. C., G. F. Pinder, and S. P. Larson. 1976. Finite-difference model for aquifer simulation in two dimensions with results of numerical experiments. U. S. Geol. Surv. Techniques of Water Res. Invest., Book 7, Chap. C1, 116 p.
- Trescott, P. C., and S. P. Larson. 1977. Solution of 3-dimensional groundwater flow equations using the strongly implicit procedure. J. Hydrol. 45: 49-60.
- Trewartha, G. T. 1968. An introduction to climate. McGraw-Hill Book Co., New York, 408 p.
- Trexler, B. D. 1983. Kennecott Minerals Co., Salt Lake City, Personal communication.
- U. S. Bureau of Reclamation. 1977. Groundwater manual. U. S. Govt. Print. Off., 480 p.
- U. S. Environmental Data Service. 1968. Climatic atlas of the United States. U. S. Dept. of Commerce, Environ. Sciences Serv. Adm.
- U. S. Geological Survey. 1977. Physical basin characteristics for hydrologic analysis. Chapter 7 of National Handbook of Recommended Methods for Water-Data Collection, 38 p.
- Walton, W. C. 1965. Groundwater recharge and runoff in Illinois. Ill. State Water Surv. Rep. of Invest. 48.
- Walton, W. C. 1970. Groundwater resource evaluation. McGraw-Hill Book Co., New York, 664 p.
- W. A. Wahler and Assocs. 1974. Evaluation of mill tailings disposal practices and potential dam stability problems in southwestern U. S., Kennecott Copper Corp.'s Magna tailings dam, Magna, Utah. Unpubl. consult. rep. to U. S. Bureau of Mines, vol. 3, Chap. II.



- Wang, H. F., and M. P. Anderson. 1982. Introduction to ground-water modeling. W. H. Freeman and Co., San Francisco, 237 p.
- Williams, R. E., and R. N. Farvolden. 1967. The influence of joints on the movement of ground water through glacial till. *J. Hydrol.* 5: 163-170.
- Williams, R. E. 1968. Flow of ground water adjacent to small, closed basins in glacial till. *Water Res. Res.* 4(4): 777-783.
- Wisconsin Department of Natural Resources, Bureau of Environmental Impact. 1975. Preliminary environmental report for the proposed Flambeau Mining Corporation copper mine, Rusk County, Wisconsin, 161 p.
- Wisconsin Statistical Reporting Service. 1967. Wisconsin weather: Causes, variations, and effects.
- Xanthakos, P. P. 1979. Slurry walls. McGraw-Hill Book Co., New York, 622 p.
- Young, H. L., and S. M. Hindall. 1972. Water resources of Wisconsin - Chippewa River basin. U. S. Geol. Surv. Hydrologic Atlas HA-386.

A P P E N D I X I

Unified Soil Classification  
and  
Descriptions of Common Soil Types  
near the Flambeau Mine Site

TABLE A1-1. Unified Soil Classification.

MAJOR DIVISIONS			LETTER SYMBOL	TYPICAL DESCRIPTIONS
<b>COARSE GRAINED SOILS</b>  More than 50% of material is <b>LARGER</b> than no. 200 sieve size	<b>GRAVEL AND GRAVELLY SOILS</b>  More than 50% of coarse fraction <b>RETAINED</b> on no. 4 sieve	<b>CLEAN GRAVELS</b> <i>(Little or no fines)</i>	GW	Well-graded gravels, gravel-sand mixtures, little or no fines
			GP	Poorly-graded gravels, gravel-sand mixtures, little or no fines
		<b>GRAVELS WITH FINES</b> <i>(Appreciable amount of fines)</i>	GM	Silty gravels, gravel-sand-silt mixtures
			GC	Clayey gravels, gravel-sand-silt mixtures
	<b>SAND AND SANDY SOILS</b>  More than 50% of coarse fraction <b>PASSING</b> no. 4 sieve	<b>CLEAN SAND</b> <i>(Little or no fines)</i>	SW	Well-graded sands, gravelly sands, little or no fines
			SP	Poorly-graded sands, gravelly sands, little or no fines
		<b>SANDS WITH FINES</b> <i>(Appreciable amount of fines)</i>	SM	Silty sands, sand-silt mixtures
			SC	Clayey sands, sand-clay mixtures
<b>FINE GRAINED SOILS</b>  More than 50% of material is <b>SMALLER</b> than no. 200 sieve size	<b>SILTS AND CLAYS</b>  Liquid Limit <u>LESS</u> than 50	ML	Inorganic silts and very fine sands, rock flour, silty or clayey fine sands or clayey silts with slight plasticity	
		CL	Inorganic clays of low to medium plasticity, gravelly clays, sandy clays, silty clays, lean clays	
		OL	Organic silts and organic silty clays of low plasticity	
	<b>SILTS AND CLAYS</b>  Liquid Limit <u>GREATER</u> than 50	MH	Inorganic silts, micaceous or diatomaceous fine sand or silty soils	
		CH	Inorganic clays of high plasticity, fat clays	
		OH	Organic clays of medium to high plasticity, Organic silts	
<b>HIGHLY ORGANIC SOILS</b>			PT	Peat, humus, swamp soils with high organic contents

NOTE: Dual symbols are used to indicate borderline soil classifications.

Common soil types on the Flambeau Project Area (Martinson, 1970); refer to Figure 9 on page 46.

Onamia Loam (OL) - a well-drained loamy soil developed over rapidly permeable sand and gravel outwash; it occurs over the western half of the pit area and continues northward, encompassing and extending beyond the gravel pits; the soil is typically 20 to 40 ins (51 to 102 cm) thick and has moderate to moderately rapid hydraulic conductivity (Table A1-2) which increases with depth.

Brill Silt Loam (Br) - a moderately well-drained soil underlain by rapidly permeable sand and gravel at 24 to 36 ins (61 to 91 cm); the soil occupies nearly level to gently sloping areas (0 to 6 percent slopes) south and northeast of the pit perimeter, as well as the southern and east-central part of the pit location; it includes a moderate amount of cobble-size rocks and is characterized by a moderate conductivity.

Chetek Sandy Loam (Ch) - a well-drained soil occurring at the southwest end of the pit location; it is developed on outwash sand and gravel of small stream terraces, is 12 to 20 ins (30 to 51 cm) thick, and has moderately rapid conductivity which increases with depth.

Poskin Silt Loam (Po) - this soil mantles the northeast end of the proposed pit; it is a somewhat poorly drained material 36 to 50 ins (91 to 127 cm) thick developed over rapidly permeable outwash sand with some gravel; it is characterized by a seasonal high water table 1 to 3 ft (0.3 to 0.9 m) deep within the sand and gravel and moderate to moderately slow conductivities.

Auburndale and Almena Silt Loams (Au and Am) - Almena soils occur on low, broad interstream ridges; Auburndale soils are typically found at the bases of slopes of Almena soils in broad depressional areas, adjacent to streams, and at

heads of drainage areas; these similar soils are somewhat poorly to poorly drained, are typically greater than 30 ins (76 cm) thick, and are developed on nearly level to gently sloping till plains (0 to 6 percent slopes) from loamy tills; they occur south and east of the mine location in the area of the ore-processing plant; the Auburndale soil has slow conductivities, a seasonal high water table, and is subject to ponding; the Almena soil is characterized by moderate to moderately slow conductivities.

TABLE A1-2. Soil permeability classes of the Soil Conservation Service and their metric equivalents (from Soil Conservation Serv., 1972).

PERMEABILITY CLASS		RATES
Very Slow	<0.06 in/hr	<4.2 X 10 <sup>-5</sup> cm/s
Slow	0.06 to 0.2	4.2 X 10 <sup>-5</sup> to 1.4 X 10 <sup>-4</sup>
Moderately Slow	0.2 to 0.6	1.4 X 10 <sup>-4</sup> to 4.2 X 10 <sup>-4</sup>
Moderate	0.6 to 2.0	4.2 X 10 <sup>-4</sup> to 1.4 X 10 <sup>-3</sup>
Moderately Rapid	2.0 to 6.0	1.4 X 10 <sup>-3</sup> to 4.2 X 10 <sup>-3</sup>
Rapid	6.0 to 20.0	4.2 X 10 <sup>-3</sup> to 1.4 X 10 <sup>-2</sup>
Very Rapid	>20.0	>1.4 X 10 <sup>-2</sup>

A P P E N D I X    I I

General Hydrologic Budget

and

Estimates of Natural Ground-Water Recharge

TABLE A2-1. Calculation of potential evapotranspiration for the Flambeau project area using the method of Thornthwaite and Mather (1957).

	J	F	M	A	M	J	J	A	S	O	N	D	
Av. Temp. (°C)	-13.0	-9.5	-2.5	6.2	13.0	17.4	20.2	18.6	13.8	8.4	-0.4	-7.8	
Heat Index	0	0	0	1.39	4.25	6.61	8.28	7.31	4.65	2.19	0	0	34.68 <sup>1</sup>
PET <sub>ua</sub>	0	0	0	1.0	2.1	2.9	3.4	3.1	2.3	1.4	0	0	
Corr. Factor	0	0	0	33.9	38.4	38.7	39.3	36.3	31.2	28.2	0	0	
PET	0	0	0	34	81	112	134	113	72	39	0	0	585 mm

<sup>1</sup> Temperature-efficiency index (TE in Eq. 6, page 88)

EXPLANATION OF ABBREVIATIONS:

PET<sub>ua</sub> - Unadjusted daily potential evapotranspiration

PET - Potential evapotranspiration adjusted for month and day length (latitude)

C<sub>RO</sub> - Runoff coefficient (RO = runoff)

ST - Soil-moisture storage or moisture retained after a given amount of accumulated potential water loss or gain

ΔST - Change in soil-moisture storage

AET - Actual evapotranspiration (AET = PET + I - ΔST when I < 0; I = N - PET); AET is assumed to equal 0 when the average monthly temperature is less than 0°C.

TABLE A2-2. Hydrologic budget for a silt-loam soil with pasture conditions at the Flambeau mine site. All quantities are in millimeters unless noted otherwise.

	J	F	M	A	M	J	J	A	S	O	N	D	
PET <sup>1</sup>	0	0	0	34	81	112	134	113	72	39	0	0	585
Precip.	25	20	43	63	92	126	108	102	94	56	41	29	799
C <sub>RO</sub>	.35	.35	.30	.25	.25	.25	.25	.25	.25	.25	.30	.35	
Runoff	9	7	13	16	23	32	27	26	24	14	12	10	213
P-RO = N	16	13	30	47	69	94	81	76	70	42	29	19	586
N-PET = I	10	13	30	13	-12	-18	-53	-37	-2	3	29	19	
$\Sigma(I < 0)$				0	-12	-30	-83	-120	-122				
ST	214	227	250	250	238	222	178	154	153	156	185	204	
$\Delta$ ST	+10	+13	+30	0	-12	-16	-44	-24	-1	+3	+29	+19	
AET	0	0	0	34	81	110	125	100	71	39	0	0	560
Percolation <sup>2</sup>	6	0	0	13	0	0	0	0	0	0	0	0	19 <sup>3</sup>

<sup>1</sup> From Table A2-1

<sup>2</sup> Percolation = n -  $\Delta$ ST - AET

<sup>3</sup>19 mm = 0.75 ins



TABLE A2-3. Hydrologic budget for a silt-loam soil the wooded conditions at the Flambeau mine site. All quantities are in millimeters unless noted otherwise.

	J	F	M	A	M	J	J	A	S	O	N	D	
PET <sup>1</sup>	0	0	0	34	81	112	134	113	72	39	0	0	585
Precip.	25	20	43	63	92	126	108	102	94	56	41	29	799
C <sub>RO</sub>	.30	.30	.28	.23	.23	.23	.23	.23	.23	.23	.28	.30	
Runoff	8	6	12	14	21	29	25	23	22	13	11	9	193
P-RO = N	17	14	31	49	71	97	83	79	72	43	30	20	606
N-PET = I	17	14	31	15	-10	-15	-51	-34	0	4	30	20	
$\Sigma(I < 0)$				0	-10	-25	-76	-110					
ST	374	388	400	400	390	376	330	303	303	307	337	357	
$\Delta$ ST	+17	+14	+12	0	-10	-14	-46	-27	0	+4	+30	+20	
AET	0	0	0	34	81	111	129	106	72	39	0	0	572
Percolation	0	0	19	15	0	0	0	0	0	0	0	0	34 <sup>2</sup>

<sup>1</sup> From Table A2-1

<sup>2</sup> 34 mm = 1.34 ins

TABLE A2-4. Hydrologic budget for a fine sandy loam soil with pasture conditions at the Flambeau mine site. All quantities are in millimeters unless noted otherwise.

	J	F	M	A	M	J	J	A	S	O	N	D	
PET <sup>1</sup>	0	0	0	34	81	112	134	113	72	39	0	0	585
Precip.	25	20	43	63	92	126	108	102	94	56	41	29	799
C <sub>RO</sub>	.14	.14	.14	.12	.12	.12	.12	.12	.12	.12	.13	.14	
Runoff	4	3	6	8	12	15	13	12	11	7	5	4	100
P-RO = N	21	17	37	55	80	111	95	90	83	49	36	25	699
N-PET = I	21	17	37	21	-1	-1	-39	-23	11	10	36	25	
$\Sigma(I < 0)$				0	-1	-2	-41	-64					
ST	150	150	150	150	149	148	113	97	108	118	150	150	
AST	0	0	0	0	-1	-1	-35	-16	+11	+10	+32	0	
AET	0	0	0	34	81	112	130	106	72	39	0	0	574
Percolation	21	17	37	21	0	0	0	0	0	0	4	25	125 <sup>2</sup>

<sup>1</sup> From Table A2-1

<sup>2</sup> 125 mm = 4.9 ins

TABLE A2-5. Hydrologic budget for a fine sandy loam soil with wooded conditions at the Flambeau mine site. All quantities are in millimeters unless noted otherwise.

	J	F	M	A	M	J	J	A	S	O	N	D	
PET <sup>1</sup>	0	0	0	34	81	112	134	113	72	39	0	0	585
Precip.	25	20	43	63	92	126	108	102	94	56	41	29	799
C <sub>RO</sub>	.12	.12	.11	.10	.10	.10	.10	.10	.10	.10	.11	.12	
Runoff	3	2	5	6	9	13	11	10	9	6	5	3	82
P-RO = N	22	18	38	57	83	113	97	92	85	50	36	26	717
N-PET = I	22	18	38	23	2	1	-37	-21	13	11	36	26	
I (I < 0)						0	-37	-58					
ST	300	300	300	300	300	300	265	247	260	271	300	300	
ΔST	0	0	0	0	0	0	-35	-18	+13	+11	+29	0	
AET	0	0	0	34	81	112	132	110	72	39	0	0	580
Percolation	22	18	38	23	2	1	0	0	0	0	7	26	137 <sup>2</sup>

<sup>1</sup> From Table A2-1

<sup>2</sup> 137 mm = 5.4 ins

A P P E N D I X I I I

Estimates of  
Transmissivity and Hydraulic Conductivity  
from Soil-Boring Logs

TABLE A3-1. Mean transmissivities and hydraulic conductivities for the total saturated vertical sections at the boreholes indicated (see pages 127 to 128 in text).

<u>BORING</u>	<u>TRANSMISSIVITY</u>	<u>HYDR. CONDUCTIVITY</u>
ST9-1 <sup>1</sup>	$1.17 \times 10^{-3}$ ft <sup>2</sup> /s	$1.60 \times 10^{-5}$ ft/s
2	$2.28 \times 10^{-3}$	$3.12 \times 10^{-5}$
3	$1.54 \times 10^{-3}$	$2.20 \times 10^{-5}$
4	$6.16 \times 10^{-4}$	$1.50 \times 10^{-5}$
5	$4.78 \times 10^{-4}$	$1.33 \times 10^{-5}$
6	$1.16 \times 10^{-3}$	$3.14 \times 10^{-5}$
7	$1.93 \times 10^{-3}$	$4.02 \times 10^{-5}$
12	$5.06 \times 10^{-4}$	$1.01 \times 10^{-5}$
13	$1.20 \times 10^{-3}$	$2.07 \times 10^{-5}$
17	$1.94 \times 10^{-3}$	$4.73 \times 10^{-5}$
18	$3.33 \times 10^{-4}$	$2.22 \times 10^{-5}$
19	$5.63 \times 10^{-3}$	$1.88 \times 10^{-4}$
20	$8.60 \times 10^{-4}$	$2.61 \times 10^{-5}$
21	$5.23 \times 10^{-4}$	$1.11 \times 10^{-5}$
22	$9.24 \times 10^{-4}$	$2.31 \times 10^{-5}$
23	$1.30 \times 10^{-3}$	$3.33 \times 10^{-5}$
24	$6.62 \times 10^{-4}$	$1.95 \times 10^{-5}$
25	$1.11 \times 10^{-4}$	$6.94 \times 10^{-6}$
26	$2.32 \times 10^{-4}$	$4.83 \times 10^{-6}$
27B	$2.79 \times 10^{-3}$	$1.64 \times 10^{-4}$
28B	$1.21 \times 10^{-4}$	$1.01 \times 10^{-5}$
29	$1.24 \times 10^{-5}$	$1.77 \times 10^{-6}$
33	$1.01 \times 10^{-4}$	$1.94 \times 10^{-6}$
57	$1.28 \times 10^{-2}$	$3.12 \times 10^{-4}$
58	$1.20 \times 10^{-2}$	$2.73 \times 10^{-4}$
59	$2.79 \times 10^{-3}$	$5.94 \times 10^{-5}$
60	$1.43 \times 10^{-2}$	$2.75 \times 10^{-4}$
61	$7.60 \times 10^{-3}$	$1.62 \times 10^{-4}$
63	$1.44 \times 10^{-3}$	$2.77 \times 10^{-5}$
64	$7.24 \times 10^{-4}$	$1.81 \times 10^{-5}$

65	$1.06 \times 10^{-3} \text{ ft}^2/\text{s}$	$2.52 \times 10^{-5} \text{ ft/s}$
66	$2.41 \times 10^{-3}$	$3.65 \times 10^{-5}$
67	$8.36 \times 10^{-4}$	$1.47 \times 10^{-5}$

---

<sup>1</sup> Boring locations shown on Plate 1

VITA

NAME: James M. King

BIRTH: May 6, 1953  
Port Clinton, OH

EDUCATION: A.B. Geology 1975  
Wittenberg University  
Springfield, OH

M.S. Hydrogeology 1977  
University of Toledo  
Toledo, OH

Ph.D. Hydrogeology 1983  
Indiana University  
Bloomington, IN

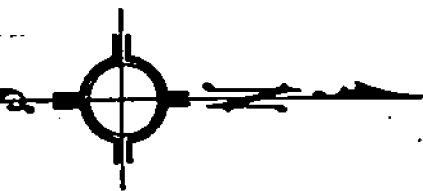
EMPLOYMENT: Indiana State Board of Health  
Division of Sanitary Engineering  
Indianapolis, IN  
1977-79

Residuals Management Services Corp.  
Indianapolis, IN  
1979-80

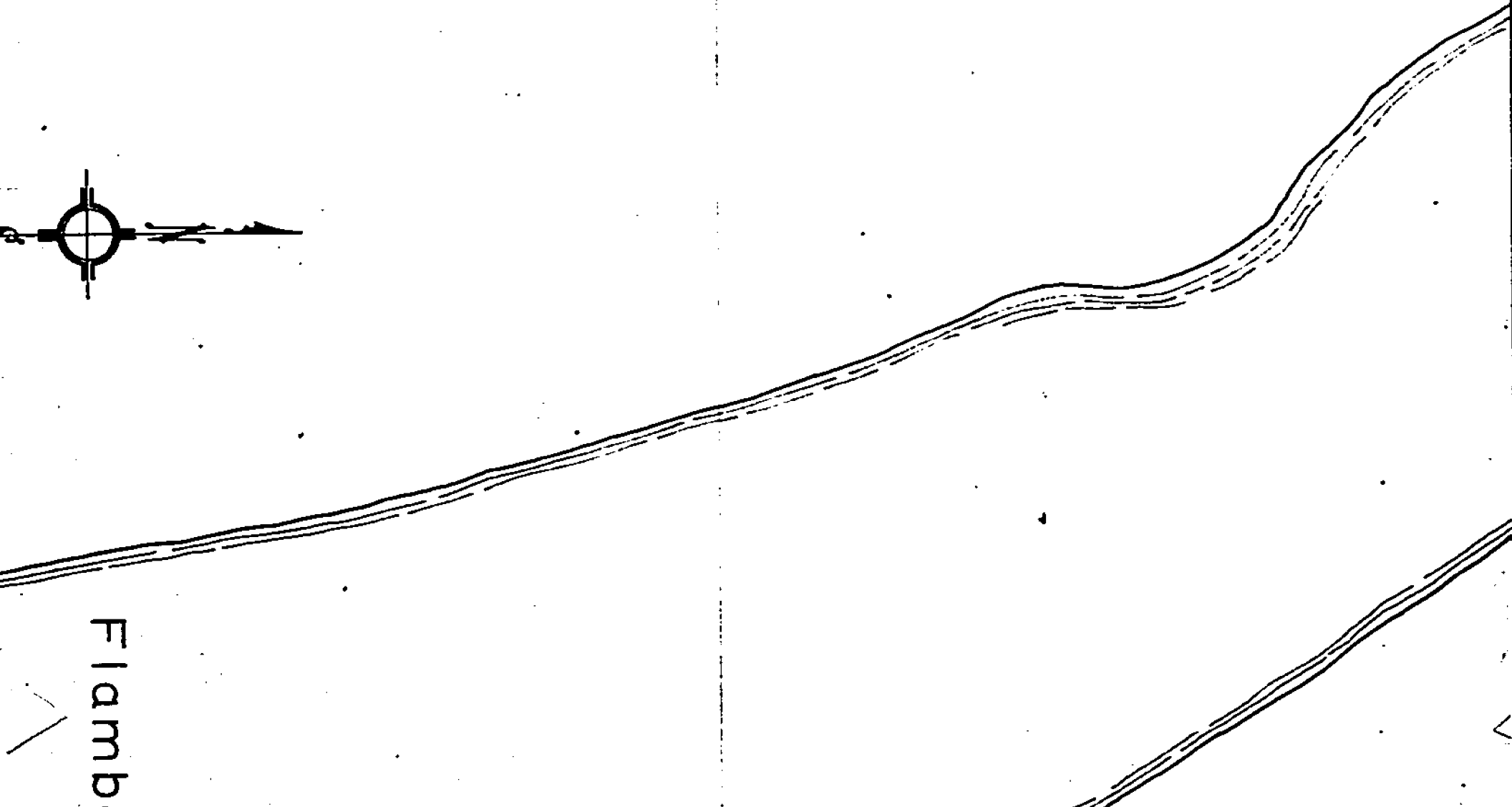
Consulting hydrogeologist  
Bloomington, IN  
1980-present

42,000 N

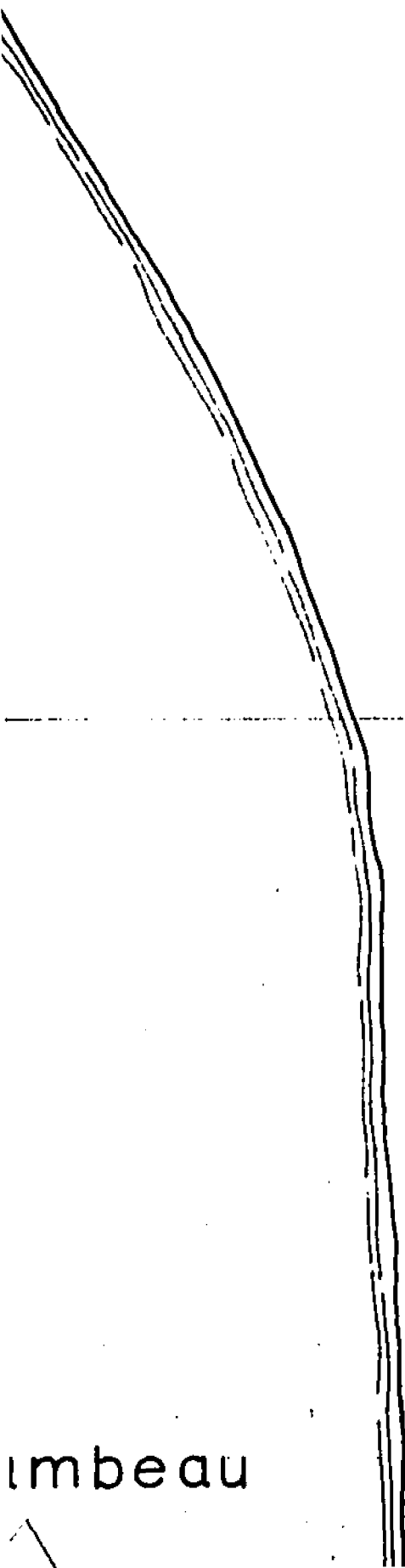
37,000 E



Flamb







imbeau

38,000

17  
O

15  
O



16  
O

13  
O

12  
O



10

15

40,000 E

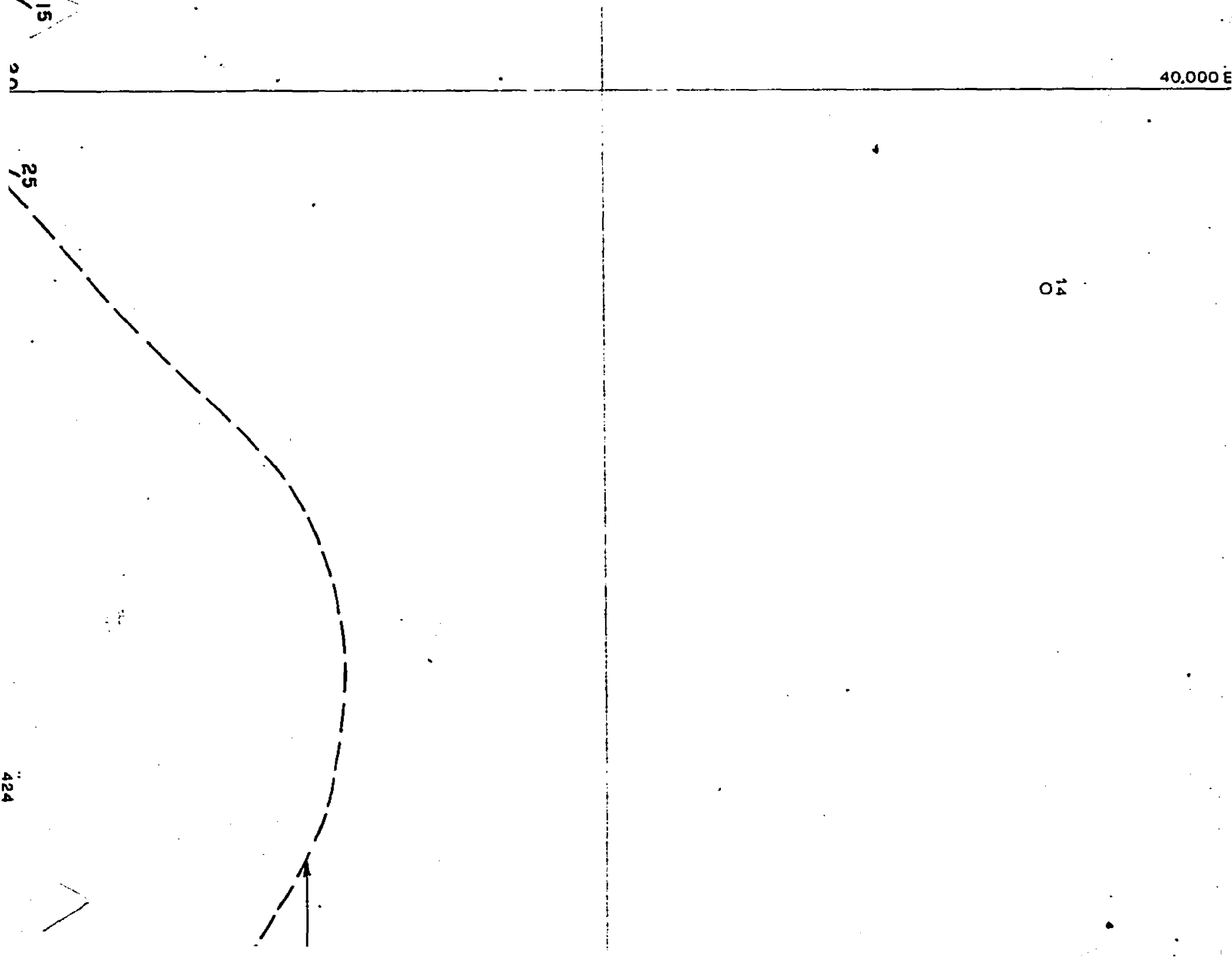
14

25

15

20

424

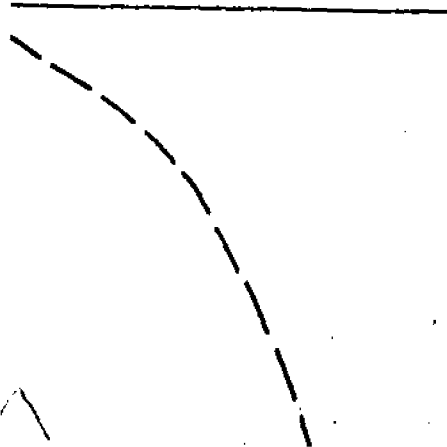


41.000 E

42.000

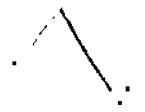
Pit Perimeter

F-3

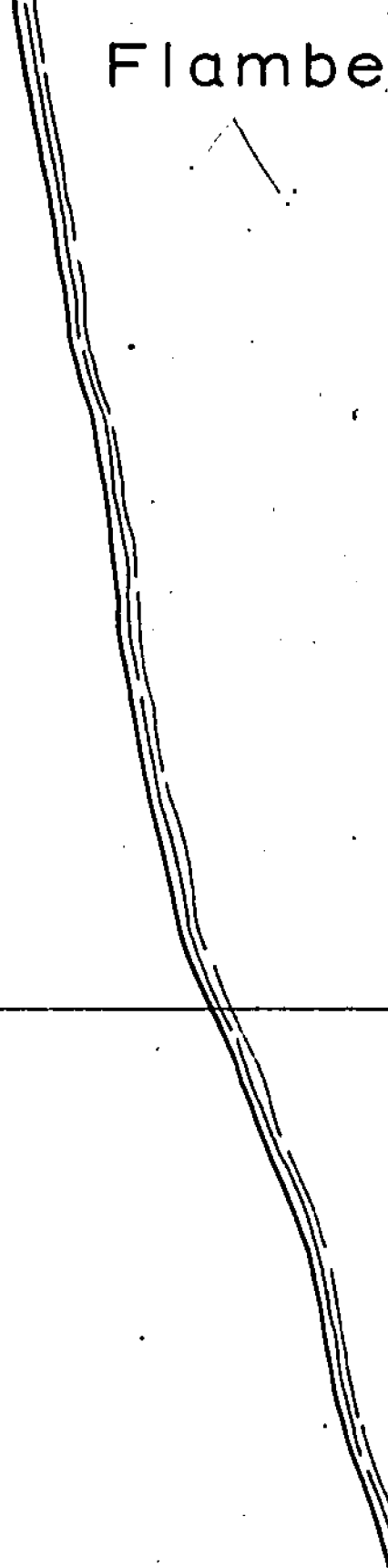


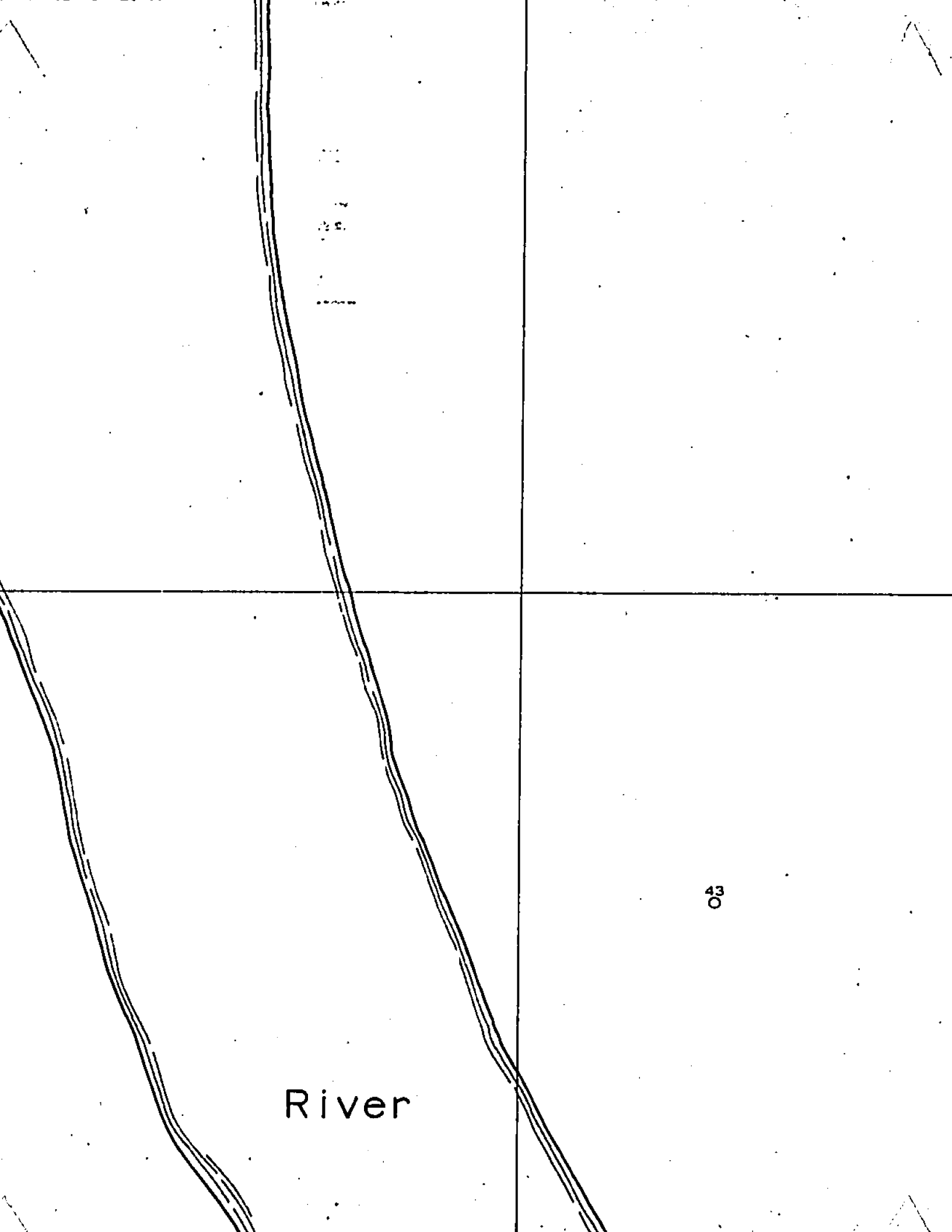


Flambe



41,000 N.





River

43

11  
O

10  
O

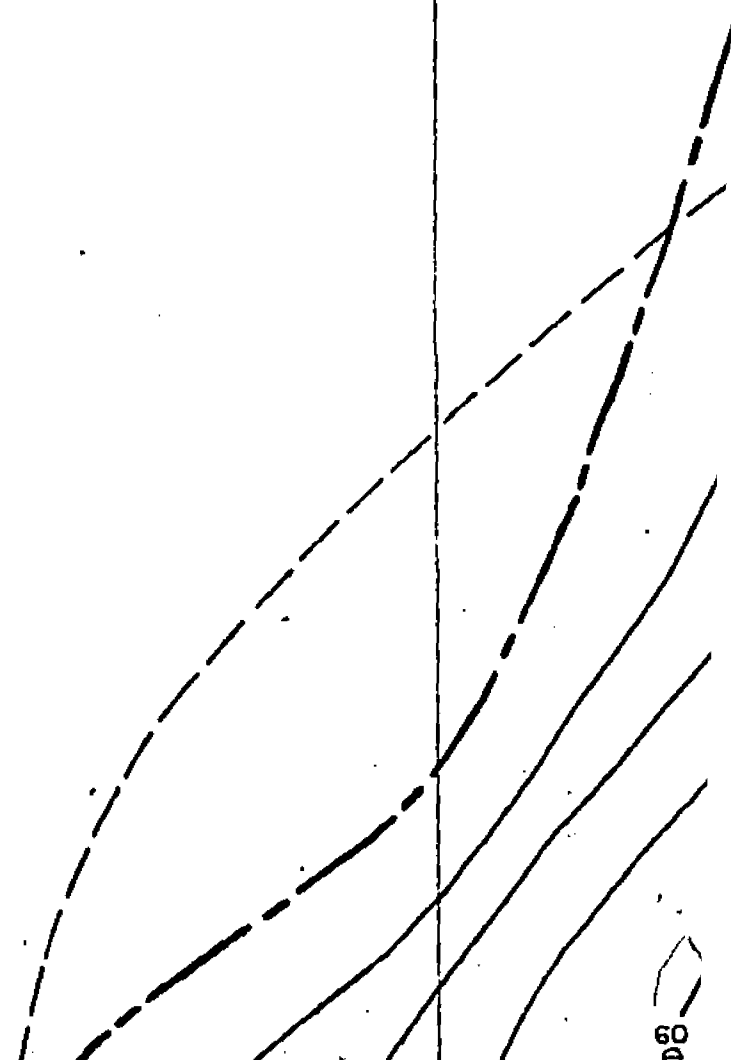
34  
O

019  
O

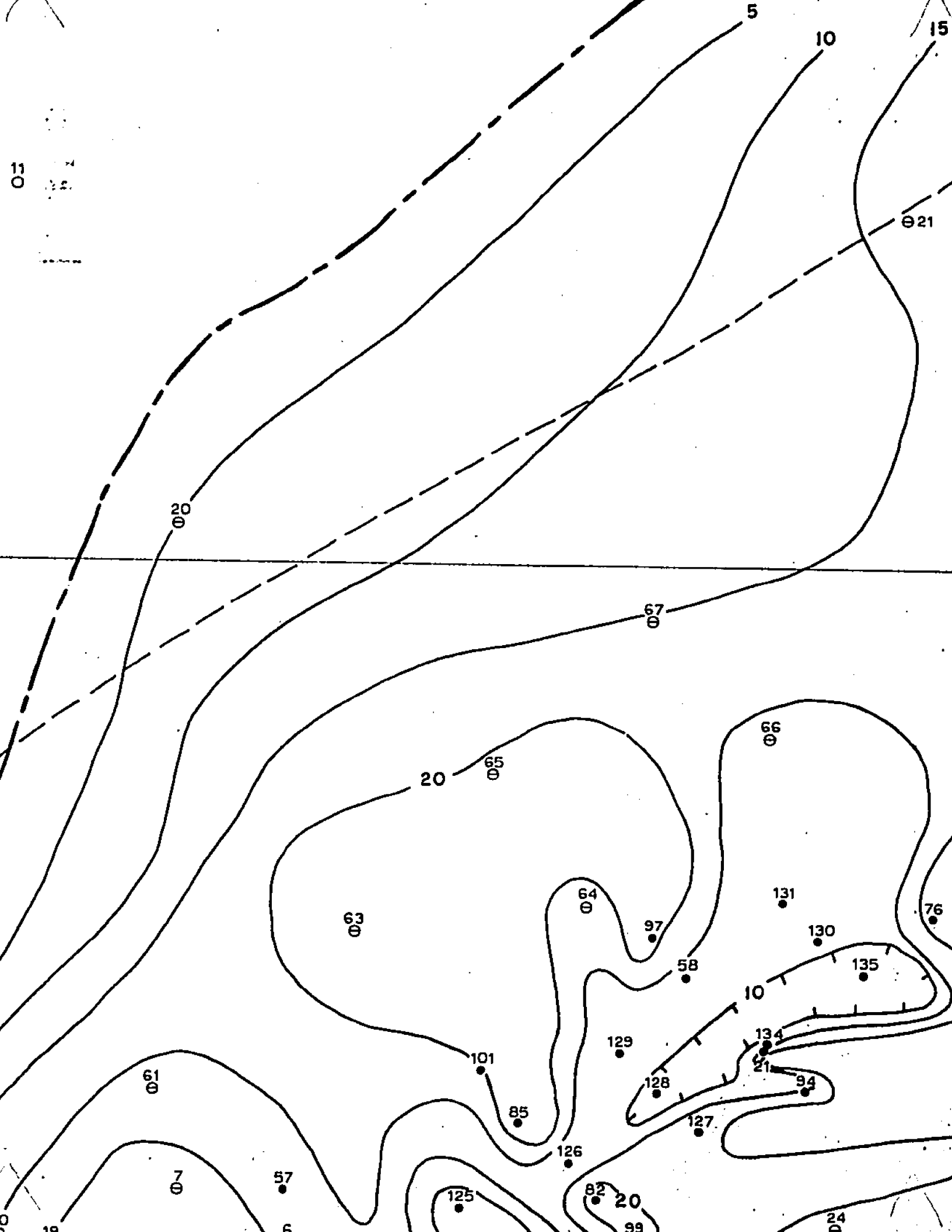
29  
O

42  
O

06  
O







11  
O

20  
O

5

10

15

21  
O

67  
O

20

65  
O

66  
O

63  
O

64  
O

131

76

130

135

10

58

129

134

21

94

101

128

127

61  
O

85

126

7  
O

57

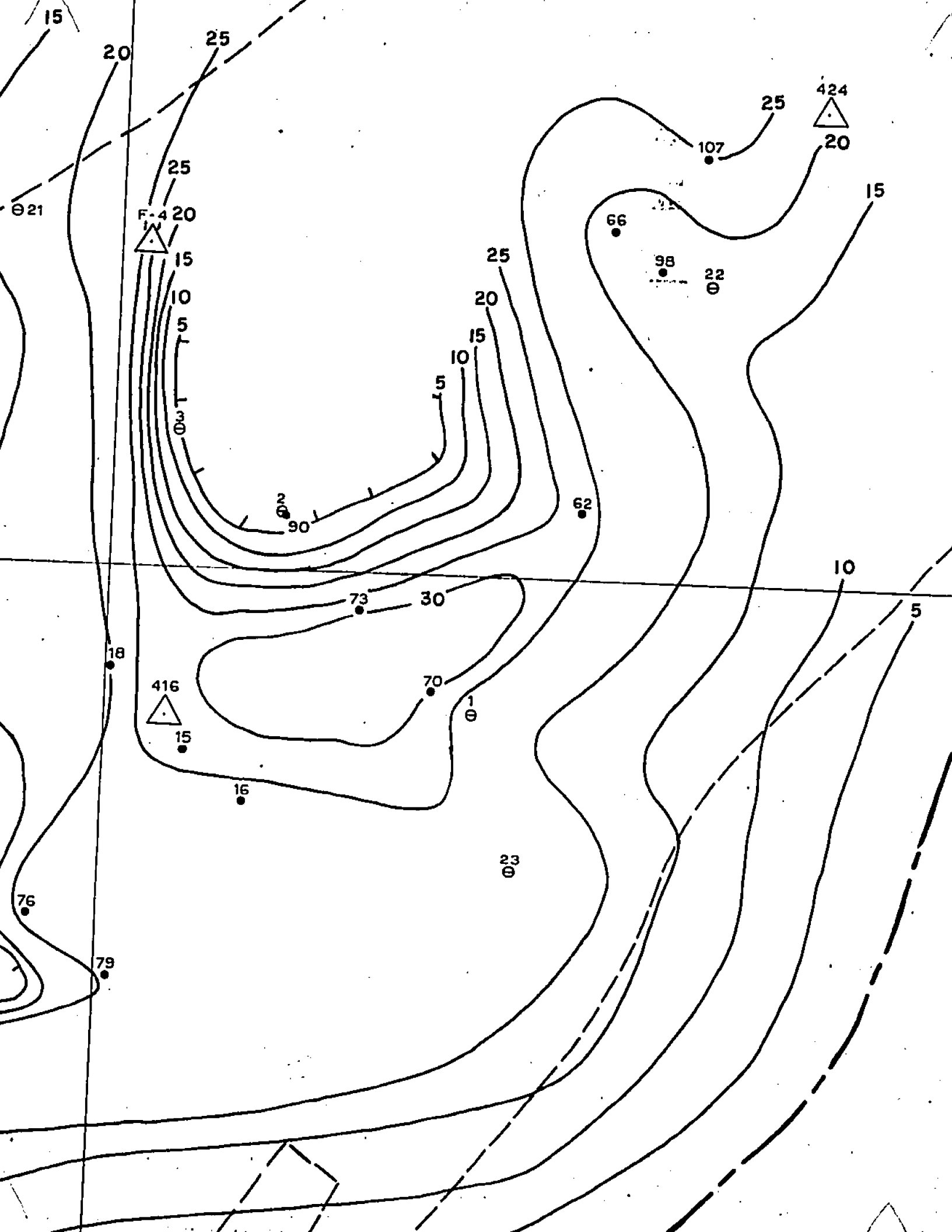
125

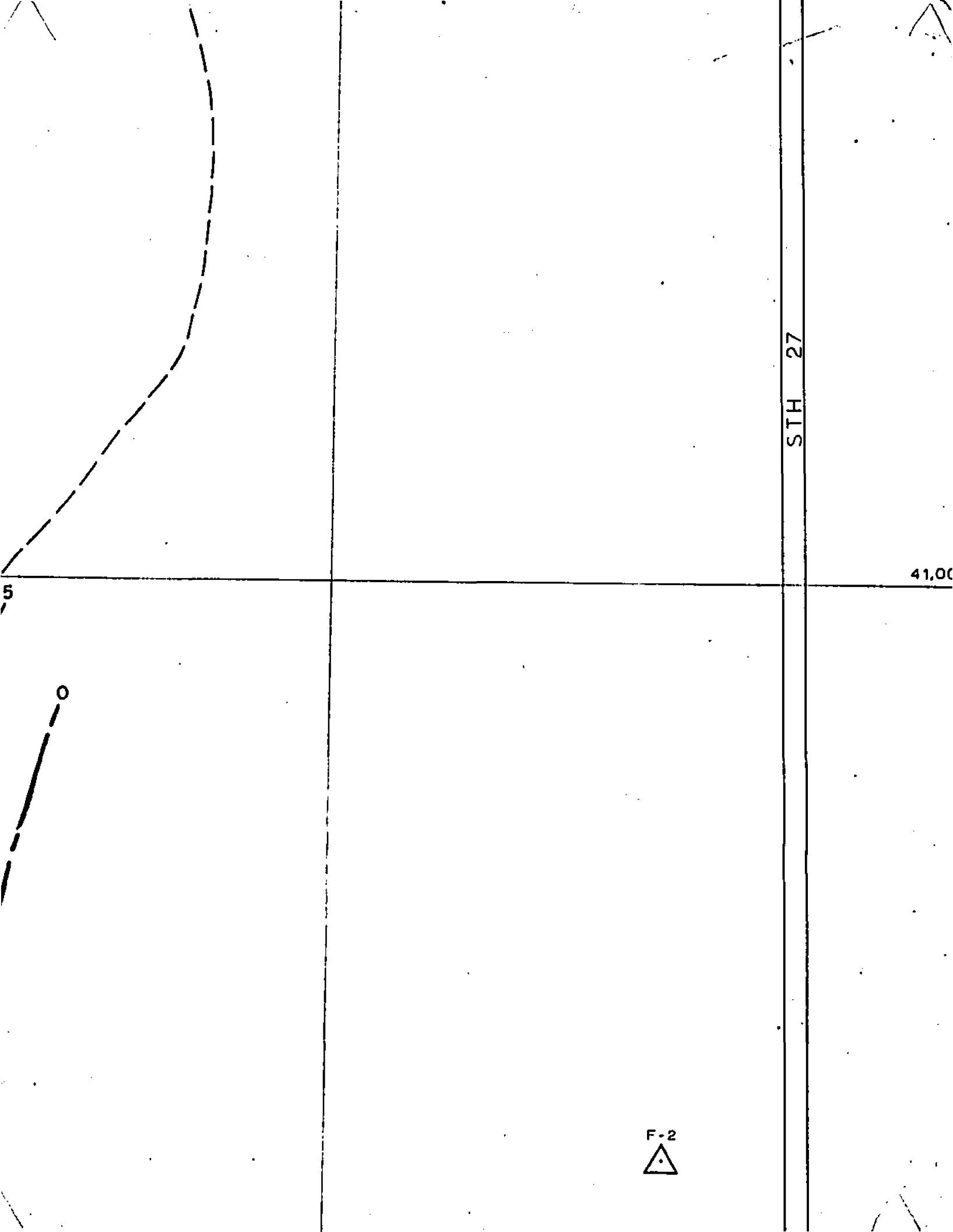
82

20

99

04





STH 27

41.00

F-2  


40,000 N

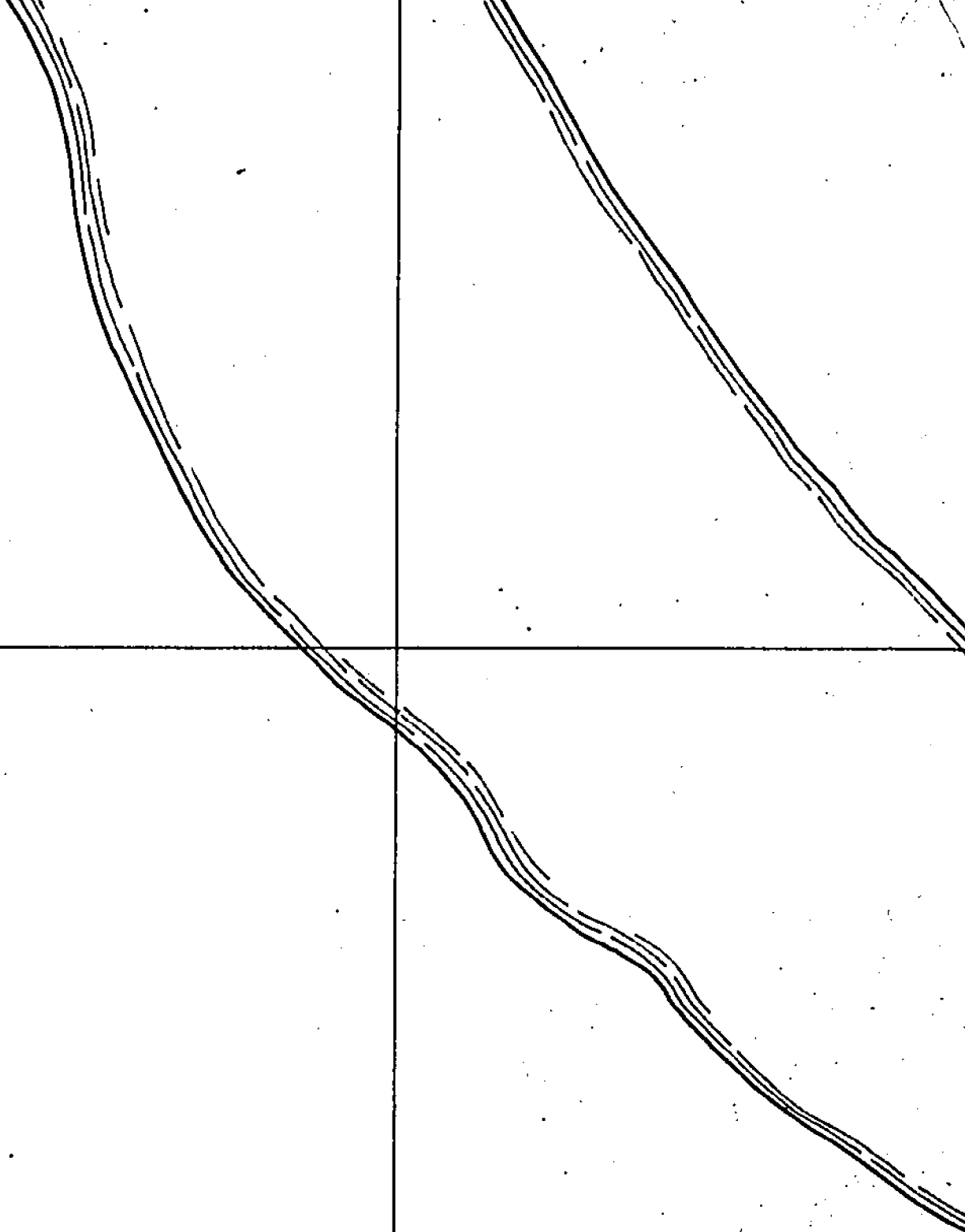
## LEGEND

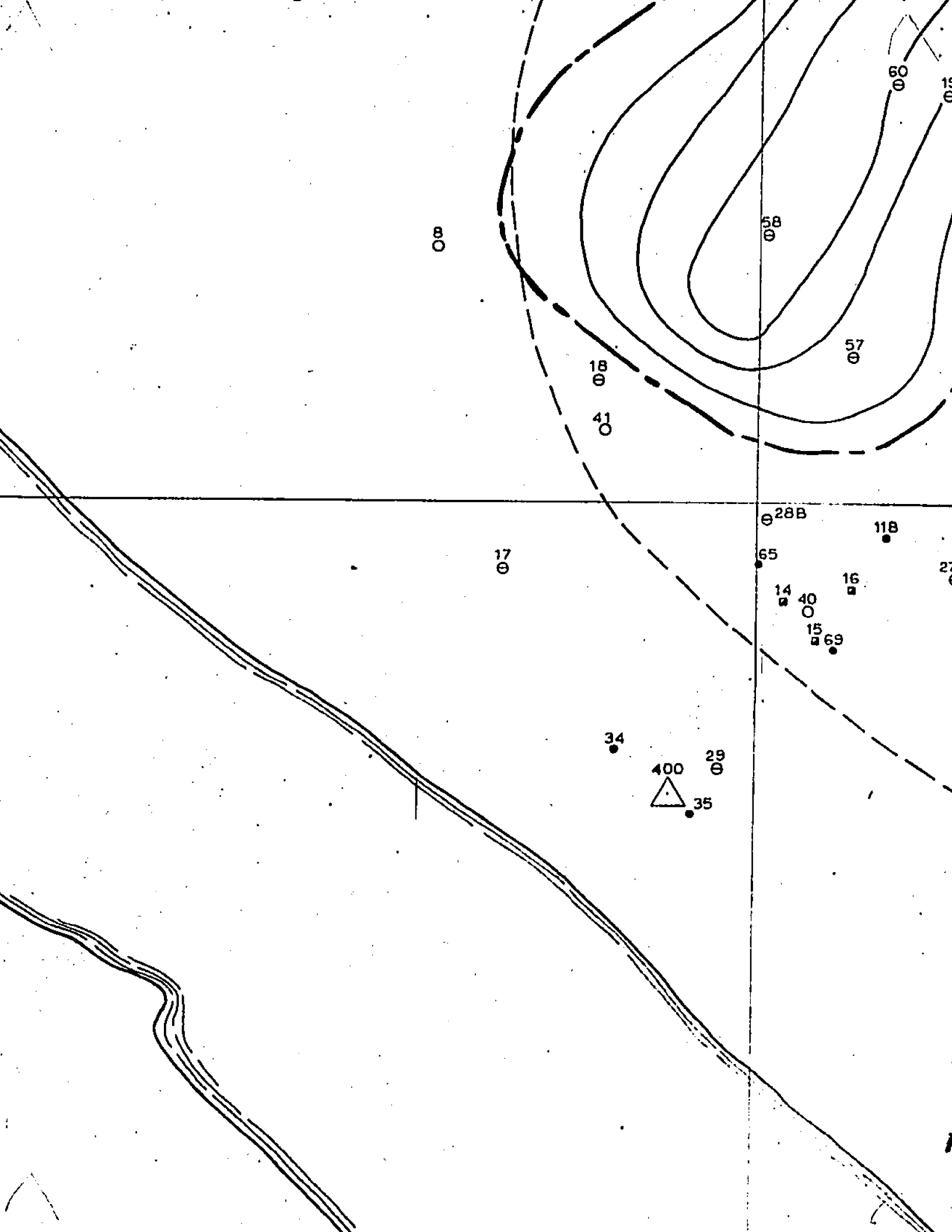
- Diamond Drill Hole
- Observation Water Well
- ⊖ Soil Test Hole
- Soil Test Pit
- Massive Sulfide > 50%
- — — — — 0 (zero) Contour

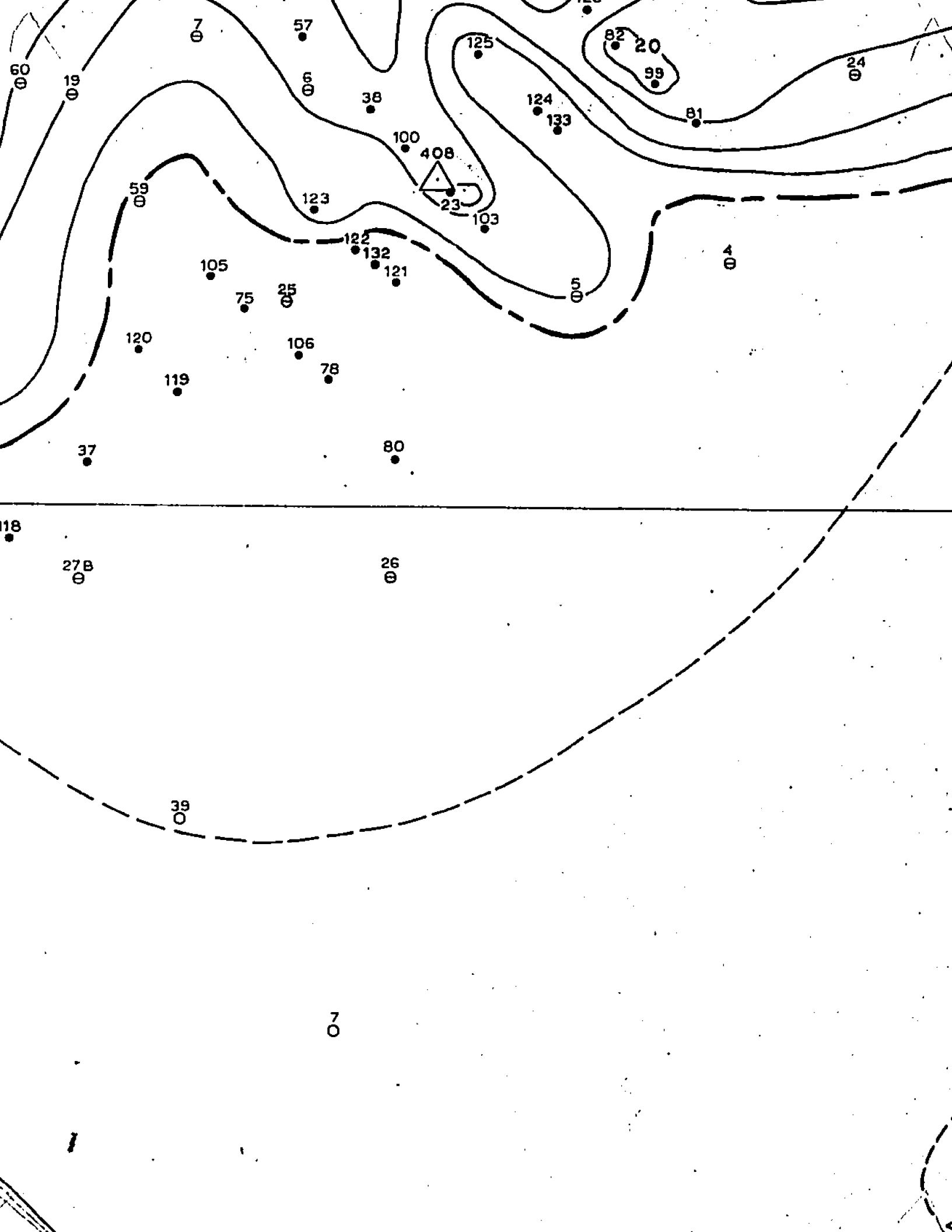
ND

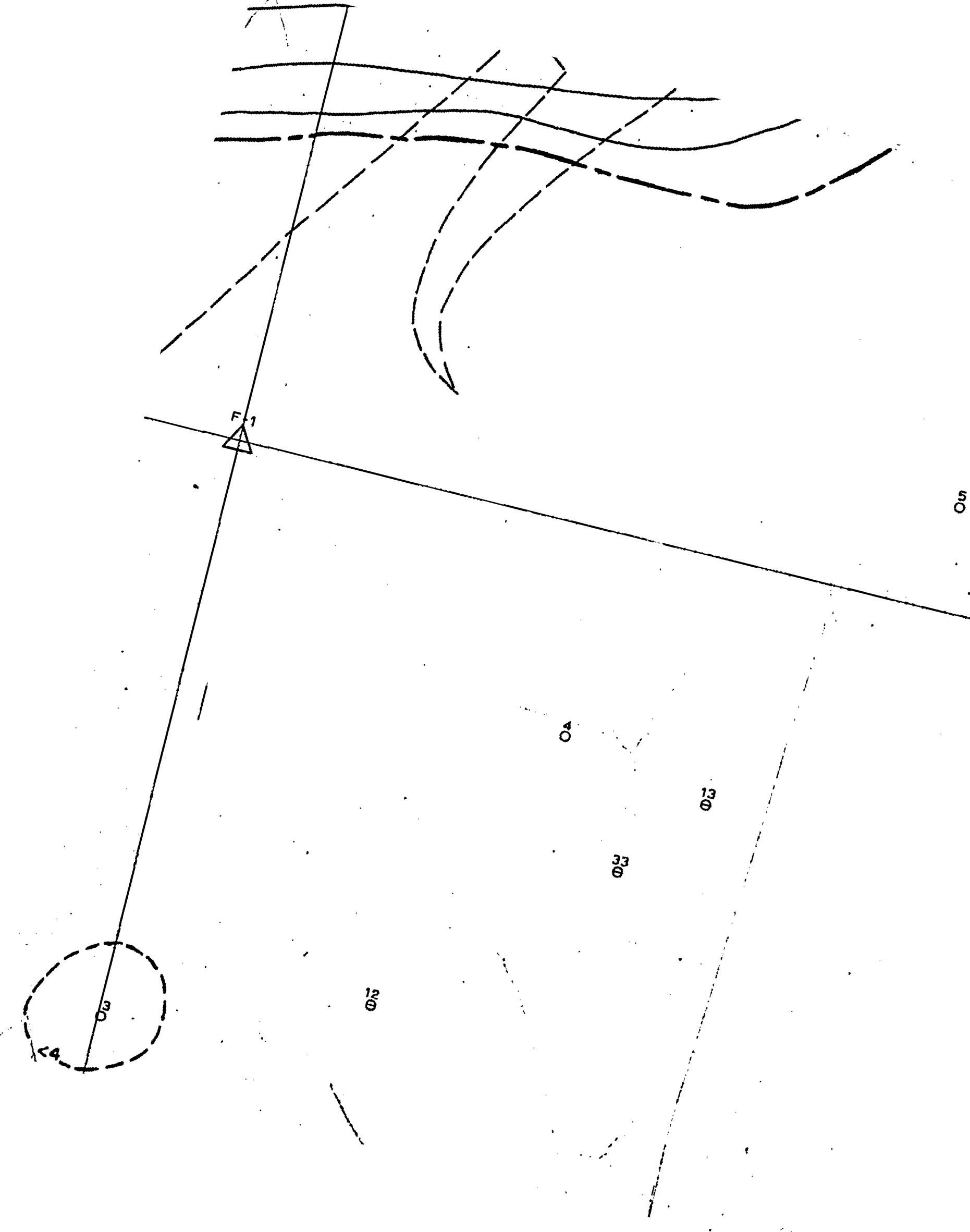
Well

50%









F1

O5

O4

O13

O33

12  
O

O6

4



06

0

40,000

40,000 N

# LEGEND

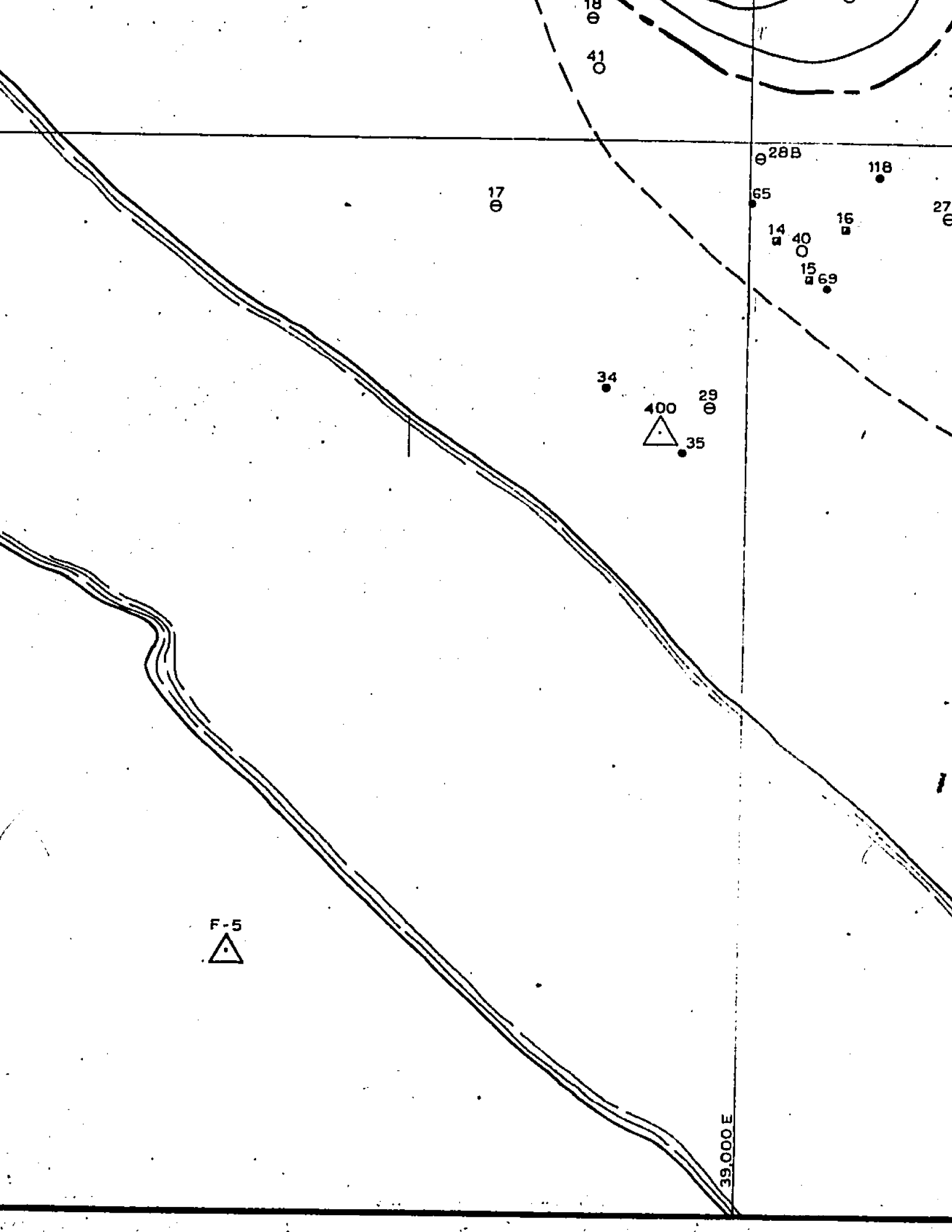
- Diamond Drill Hole
- o Observation Water Well
- e Soil Test Hole
- Soil Test Pit
- Massive Sulfide > 50%
- — — — — 0 (zero) contour

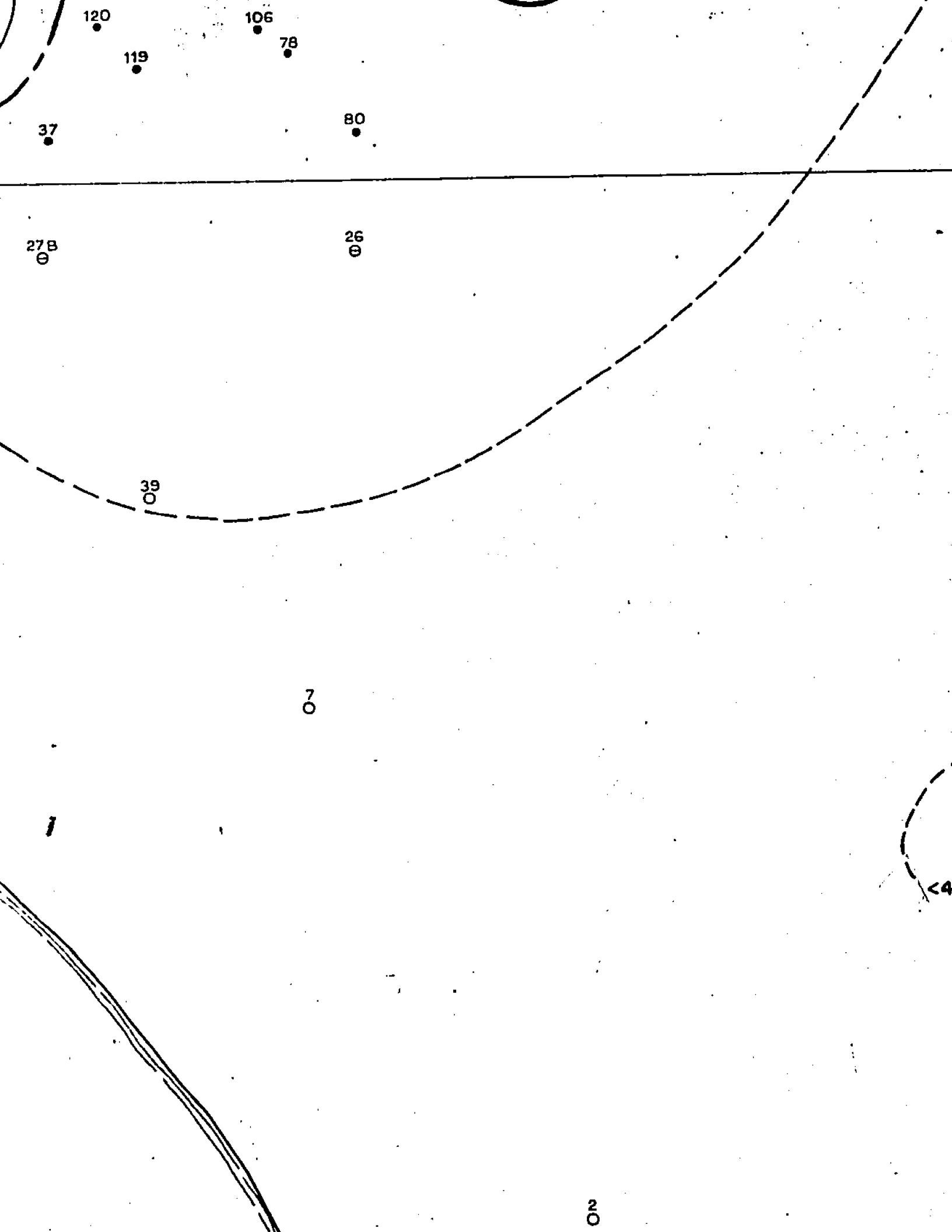
37,000 E

Modified from May, 1976 (unpubl.)

38,000 E







120

106

78

119

80

37

27B  
⊖

26  
⊖

39  
○

7  
○

1

4

2  
○

no

F-1



40

13

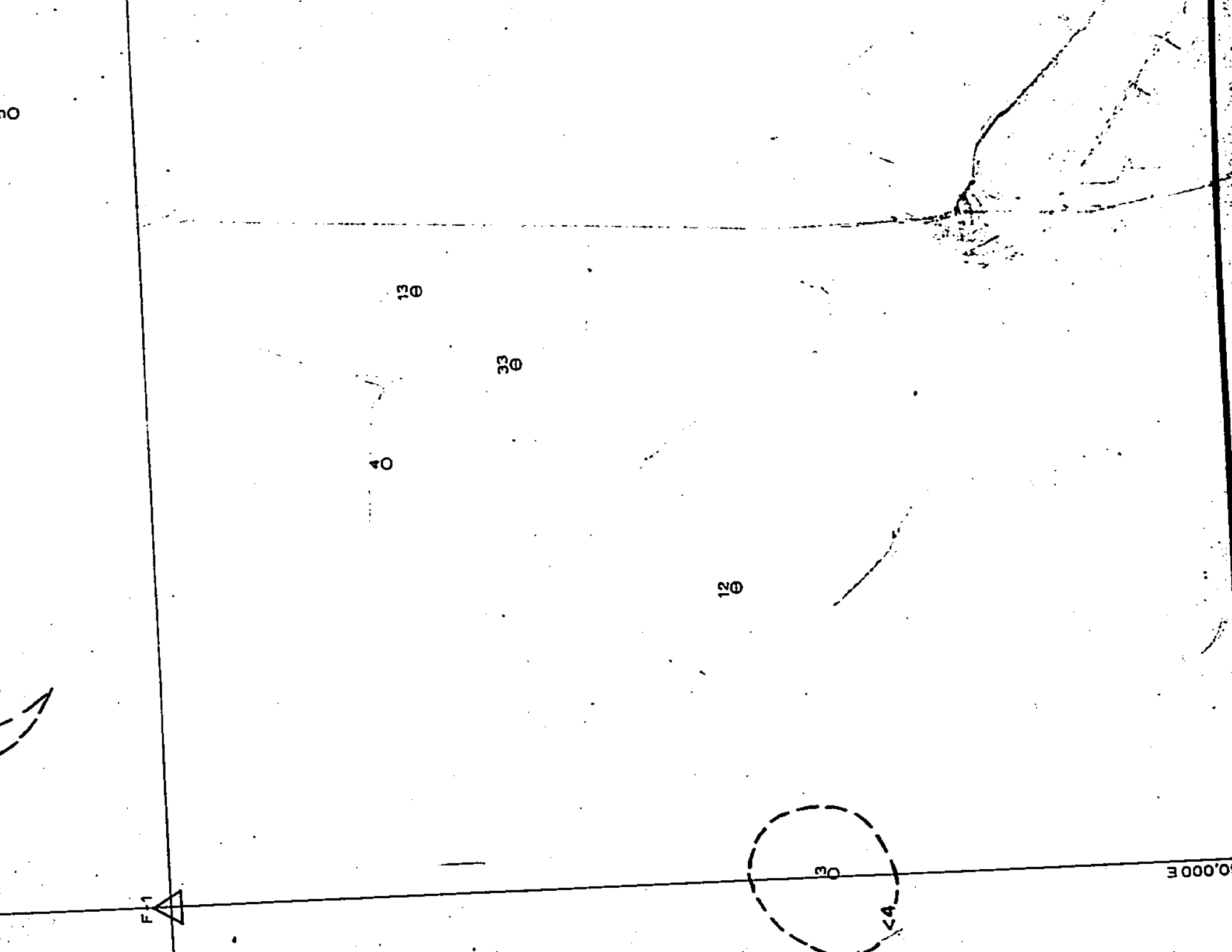
33

13

30

44

0,000E



41,000 E

**PLATE 1**

<b>FLAMBEAU MINING CORP.</b>		
<b>ISOPACHS</b>		
<b>CAMBRIAN <sup>of</sup> SANDSTONE</b>		
<b>SCALE: 1" = 100'</b>	<b>CONTOUR INTERVAL: 5 ft.</b>	<b>REVISIONS</b>
	<b>DATA BY: ERM, EJ, JK</b>	
<b>DATE: NOV. 1981</b>		
<b>DRAWN BY: GLB</b>		<b>FILE</b>





37,000 E

42,000 N



Flambe



38.000 E

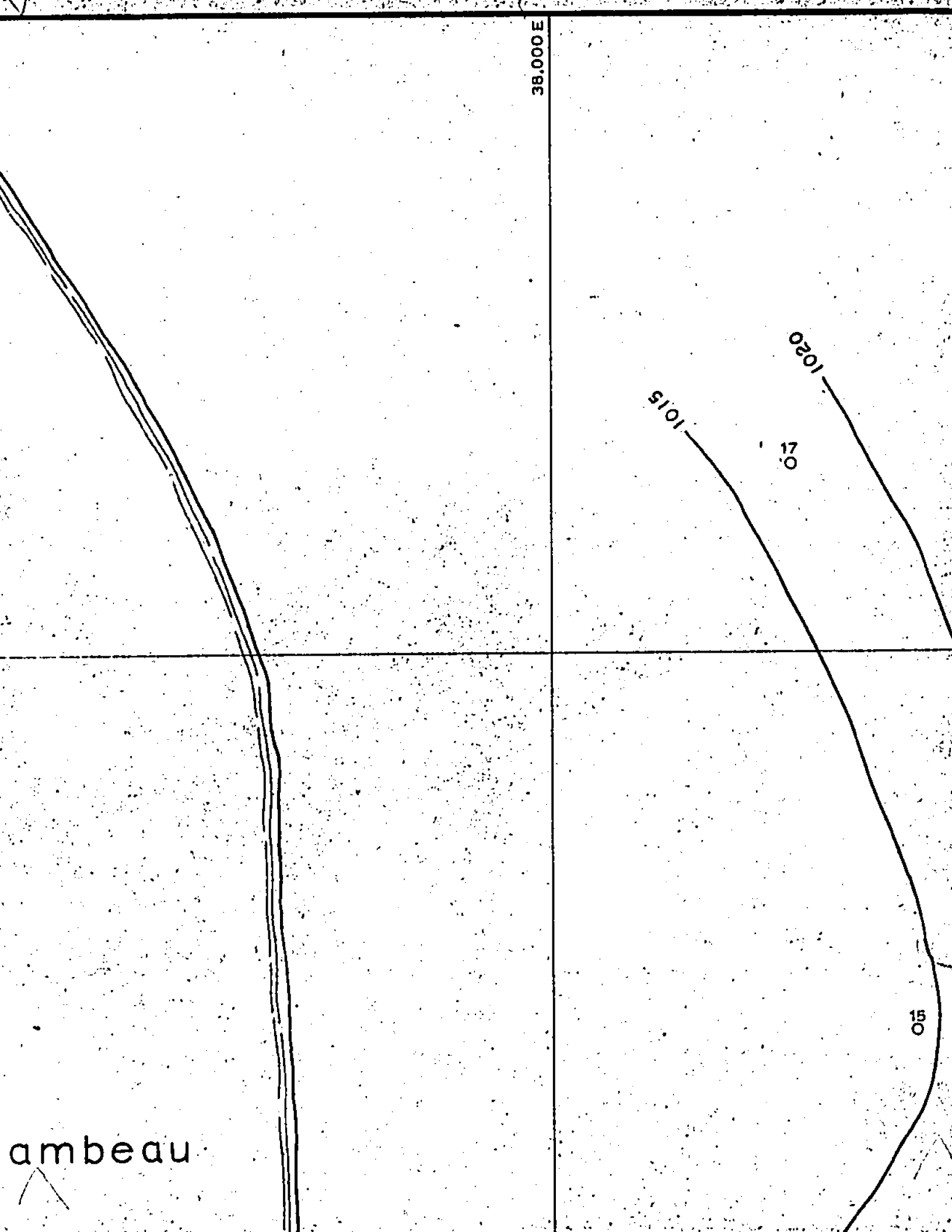
1015

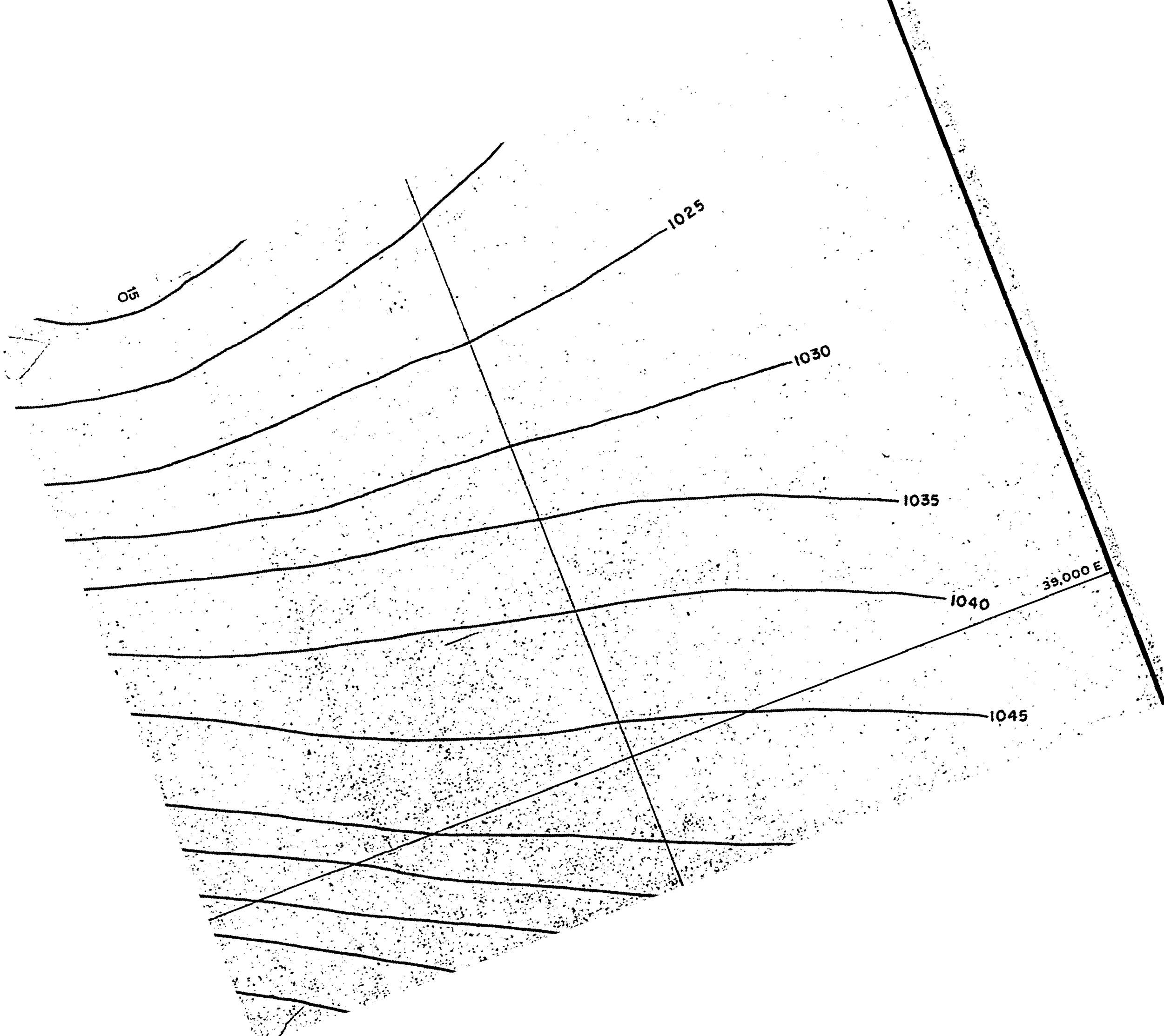
1020

170

015

ambeau





05

1025

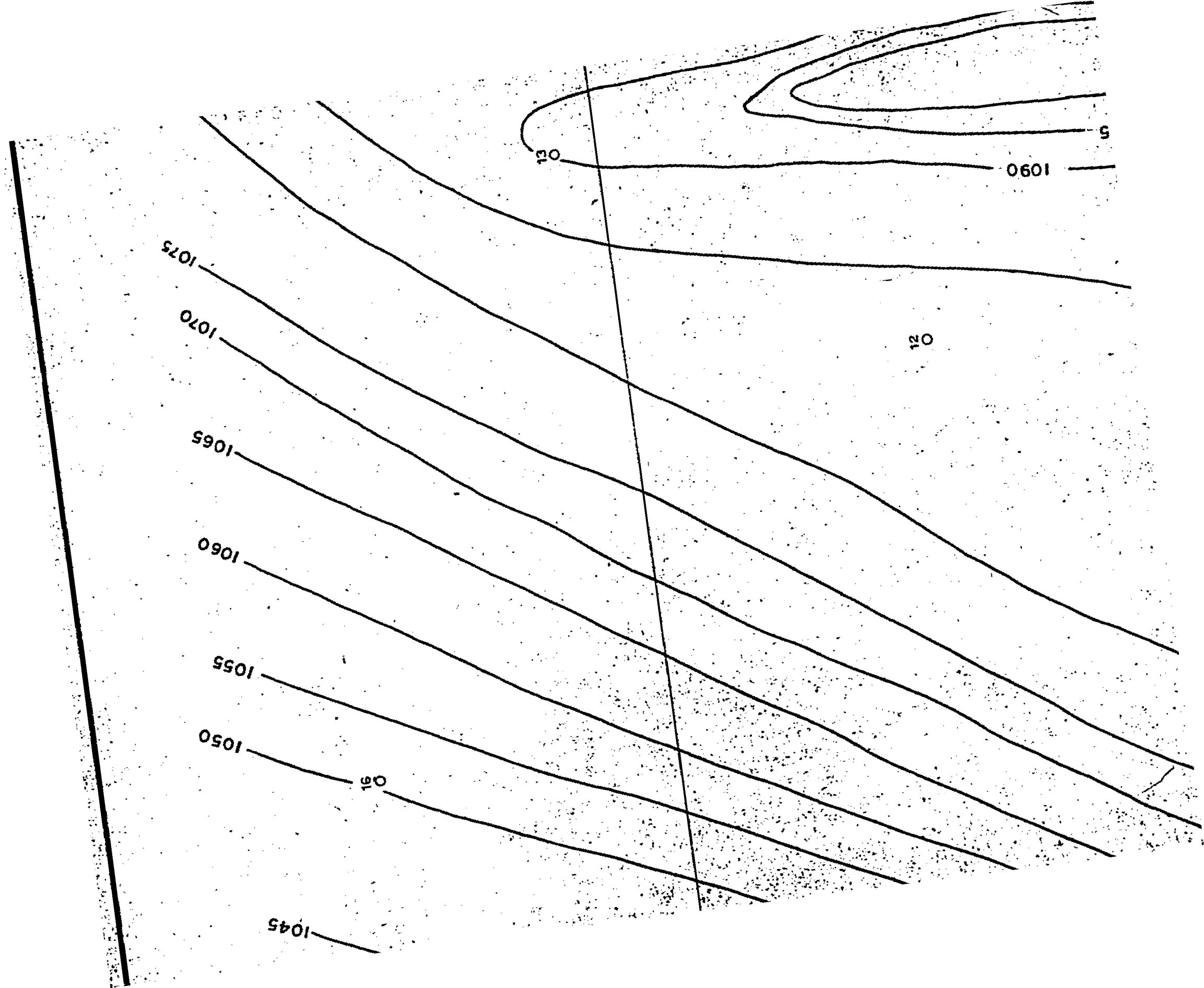
1030

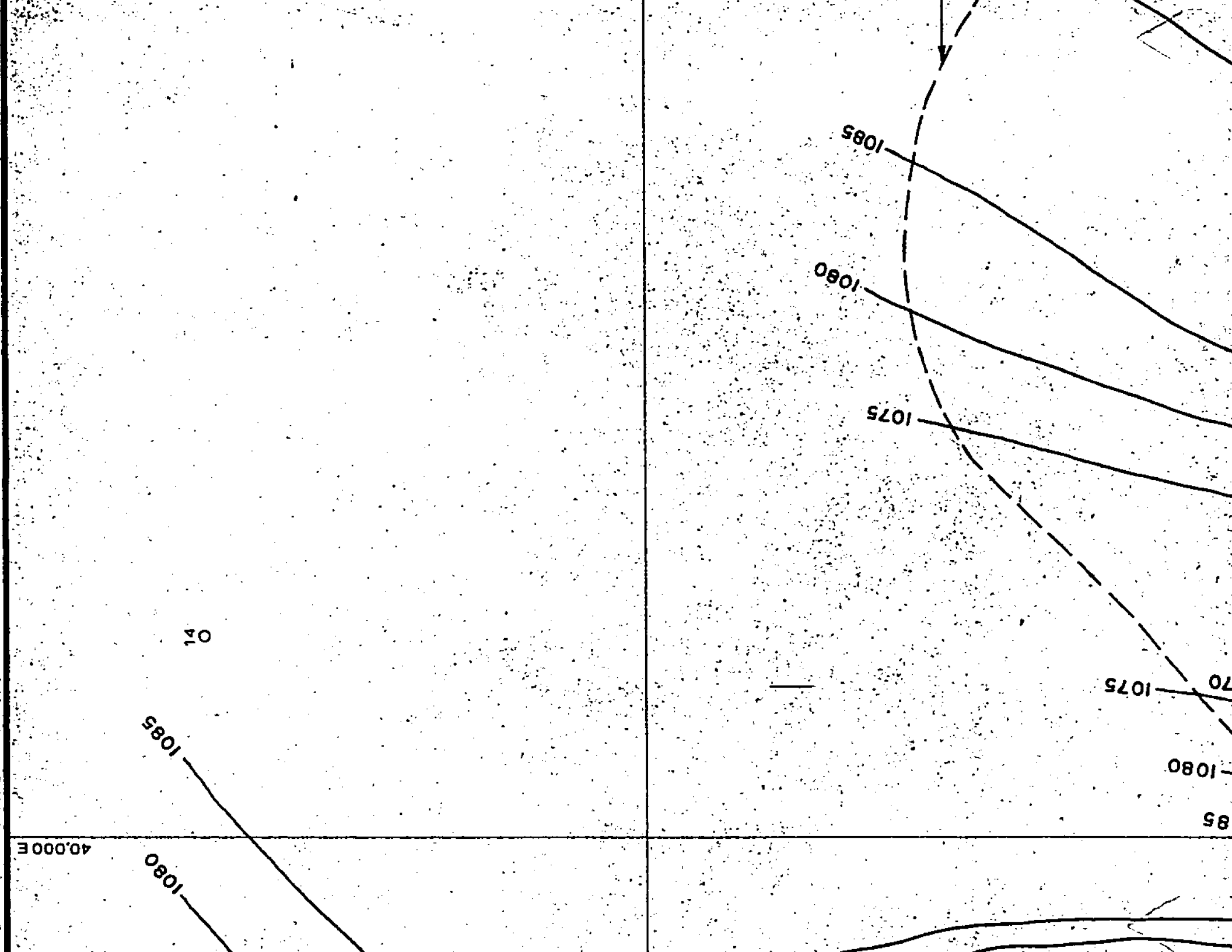
1035

1040

1045

39,000 E

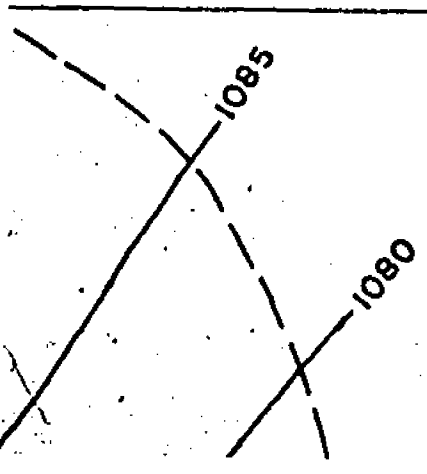




41,000 E

42.00

Pit Perimeter

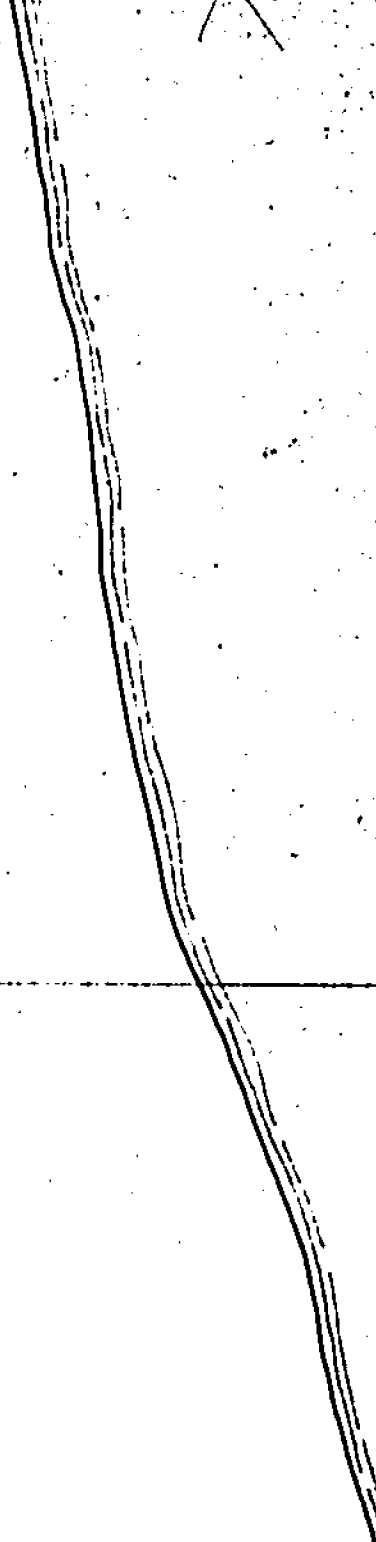


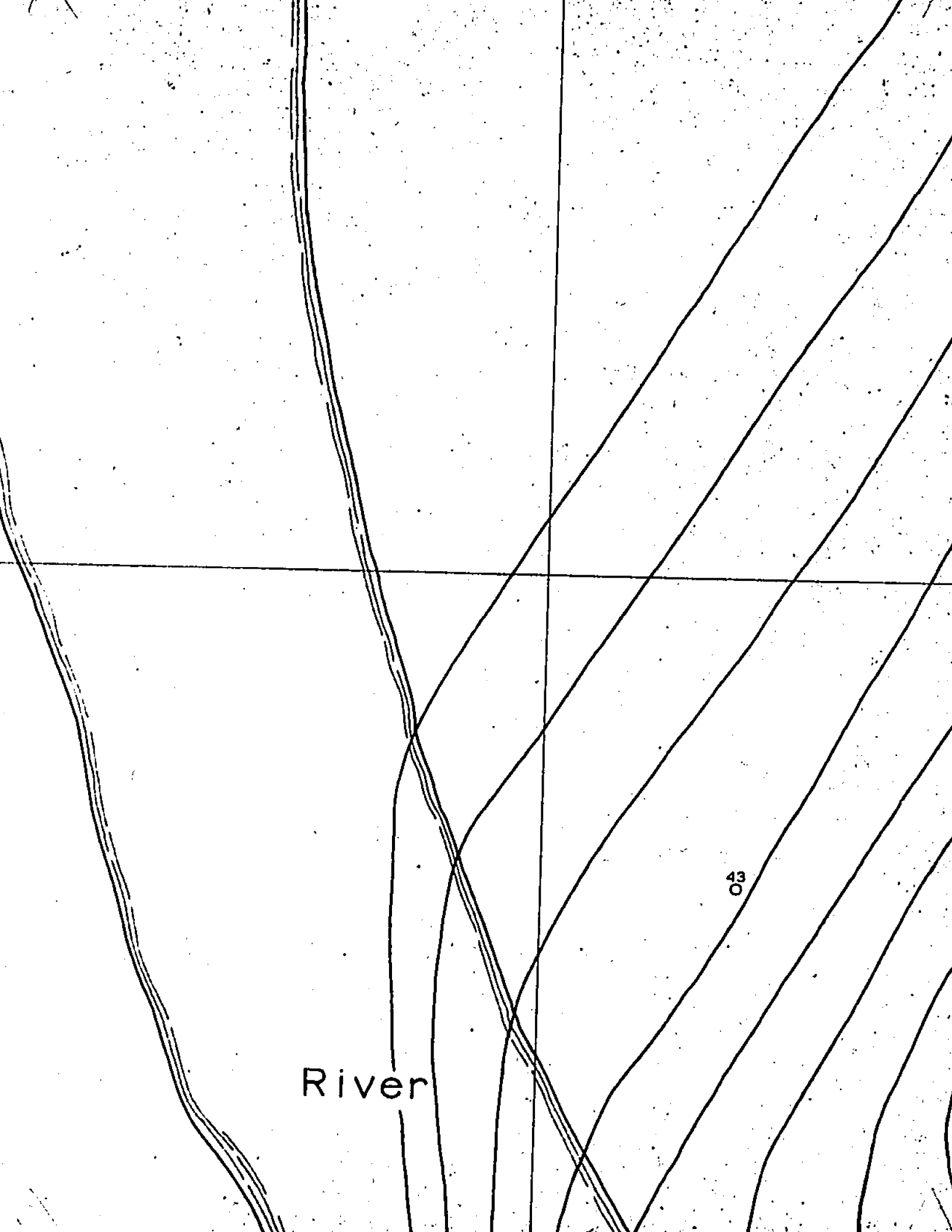
F-3



S

41,000 N

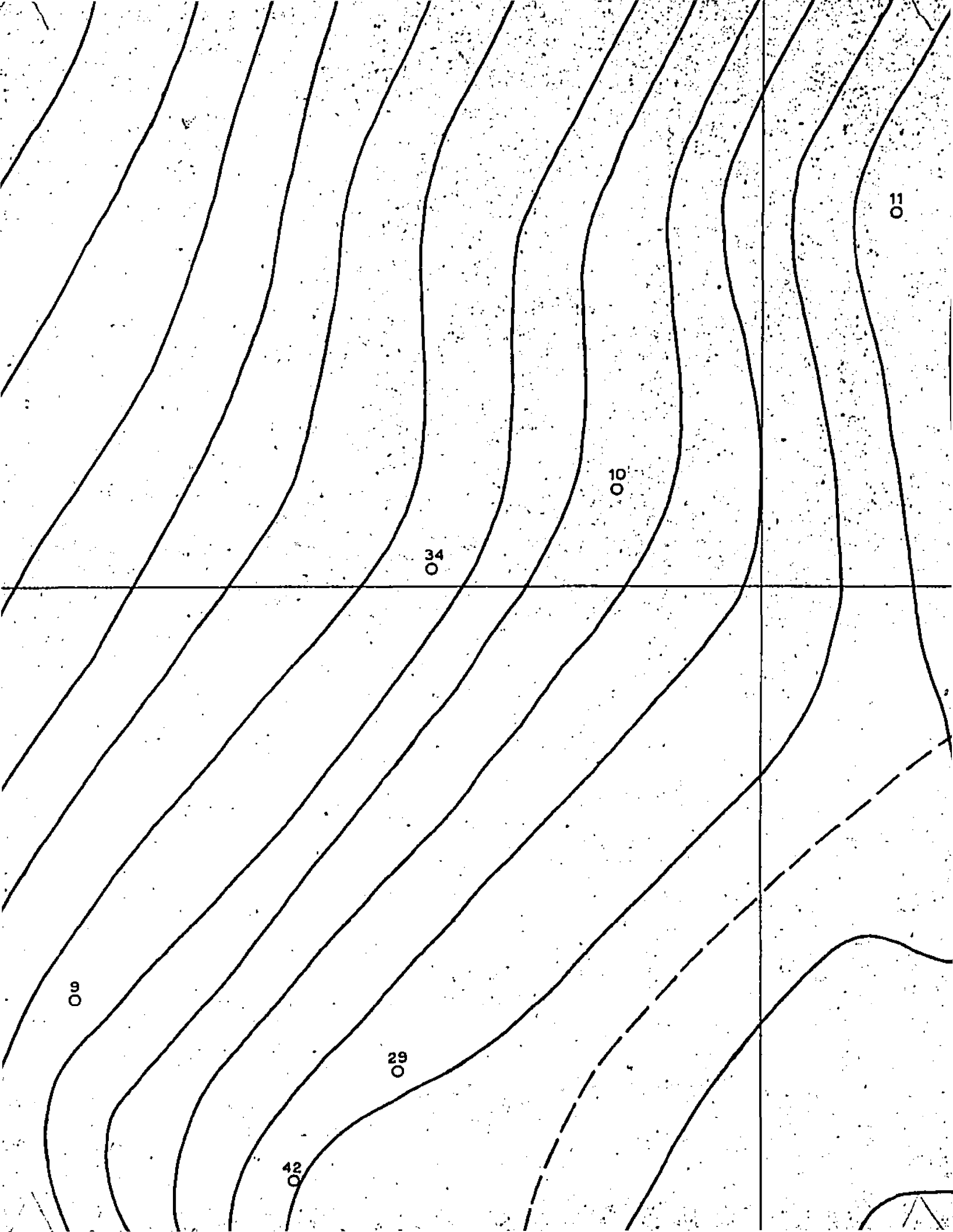




River

43  
O





11  
O

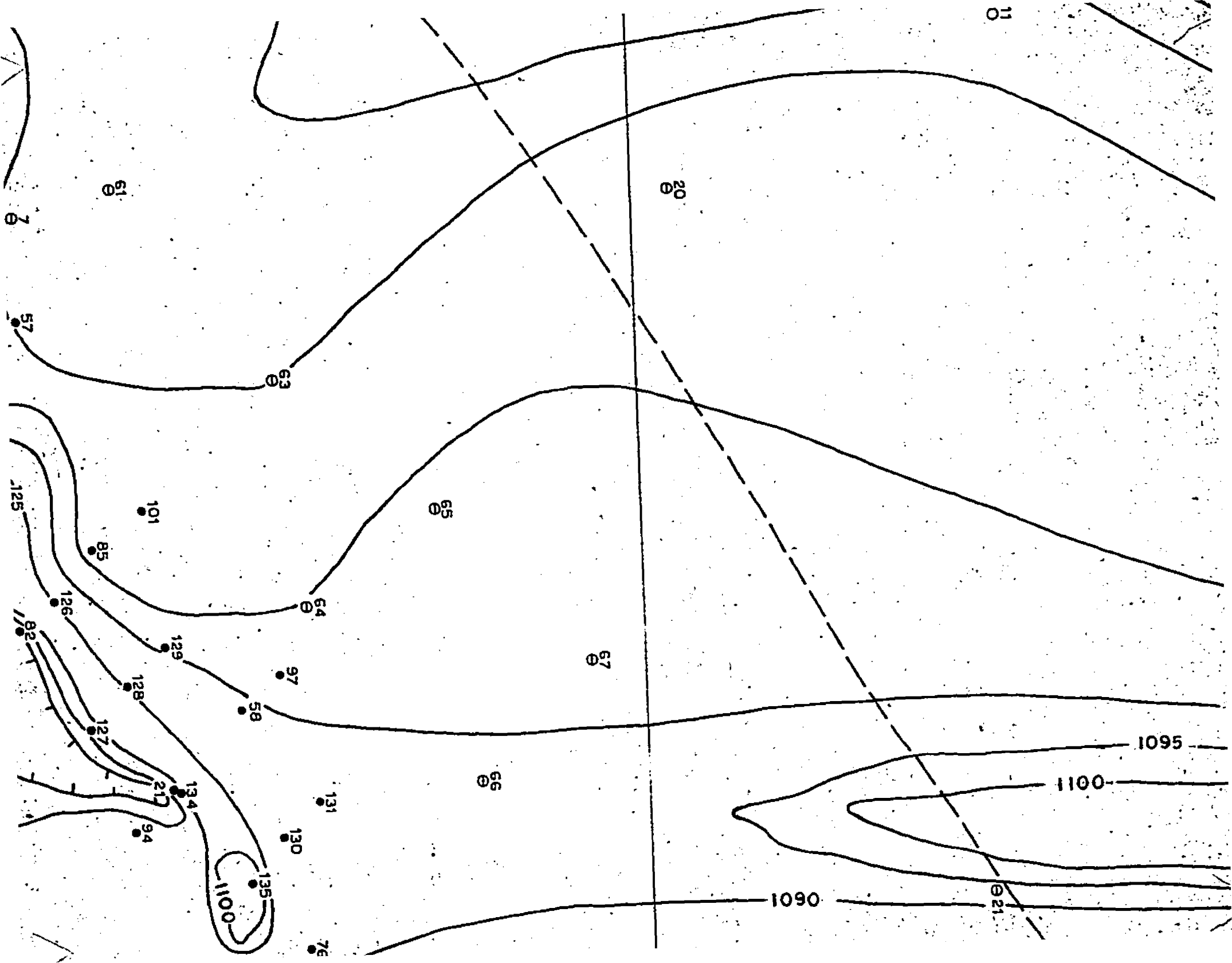
20  
O

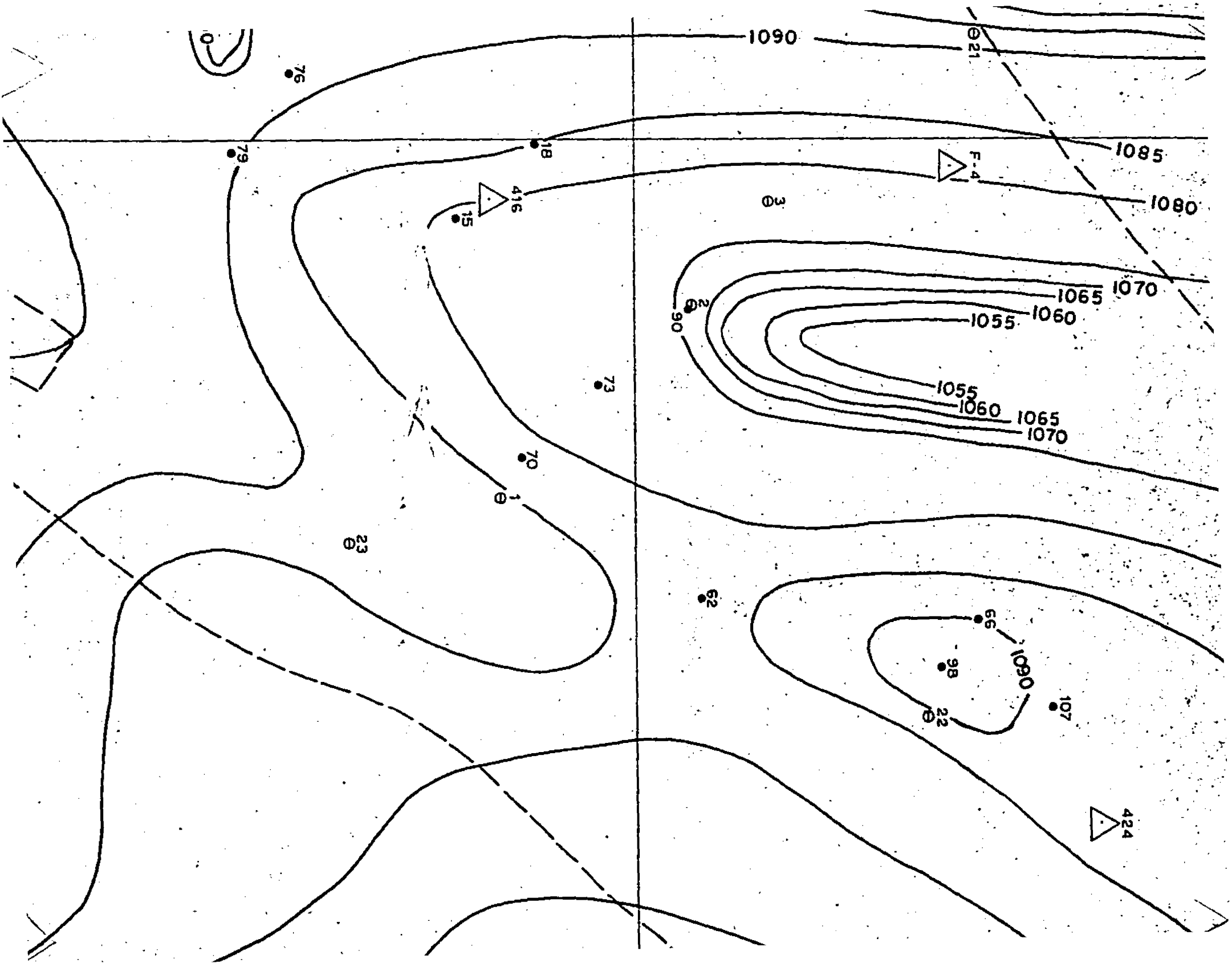
34  
O

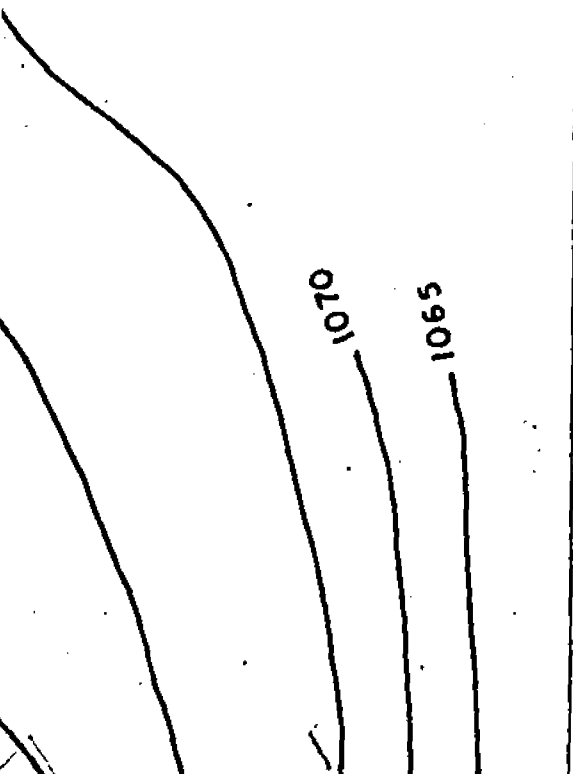
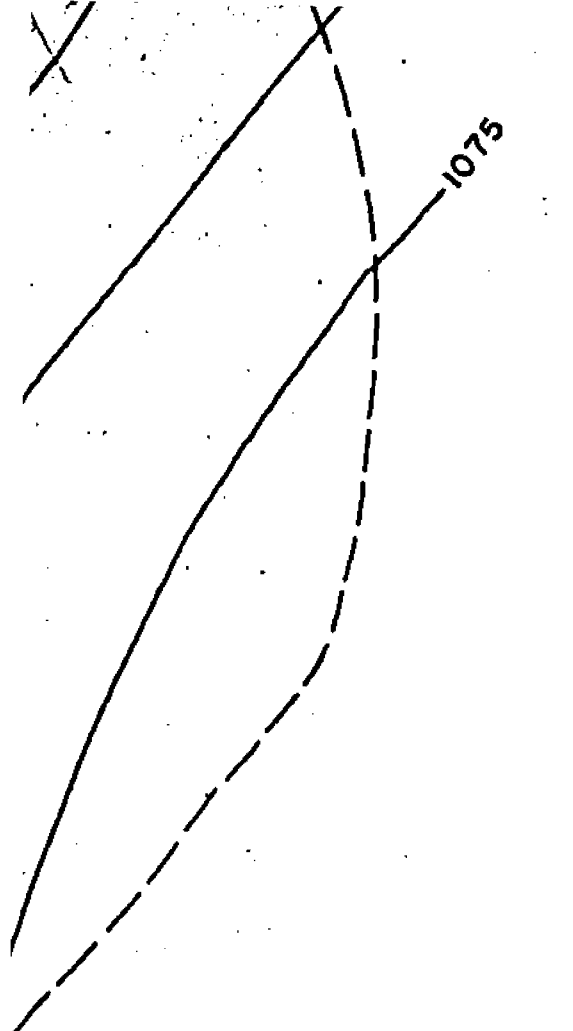
39  
O

29  
O

42  
O







STH 27

41.00

F-2



40,000N

## LEGEND

- Diamond Drill Hole
- Observation Water Well
- ⊖ Soil Test Hole
- Soil Test Pit
- ▨ Massive Lignite > 50%

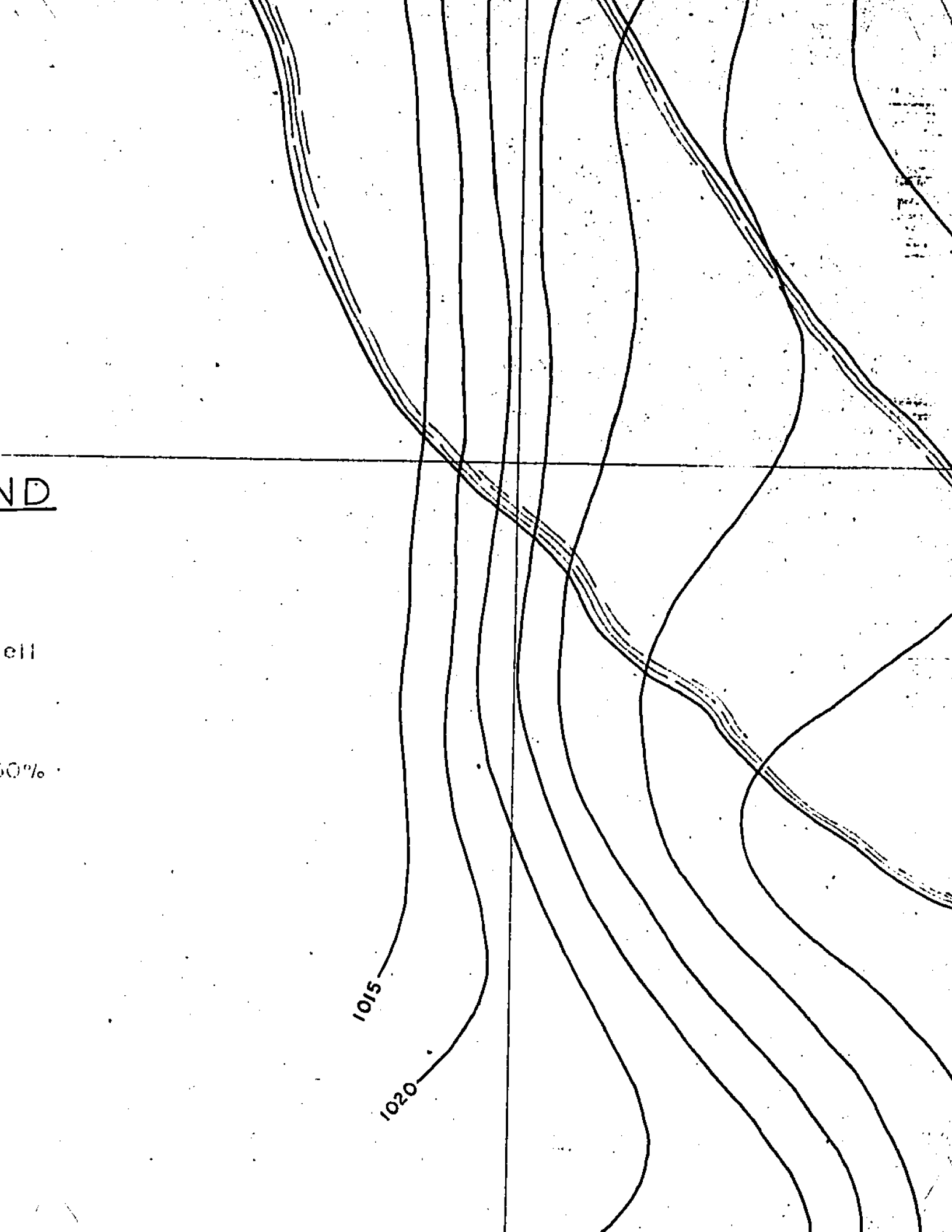
ND

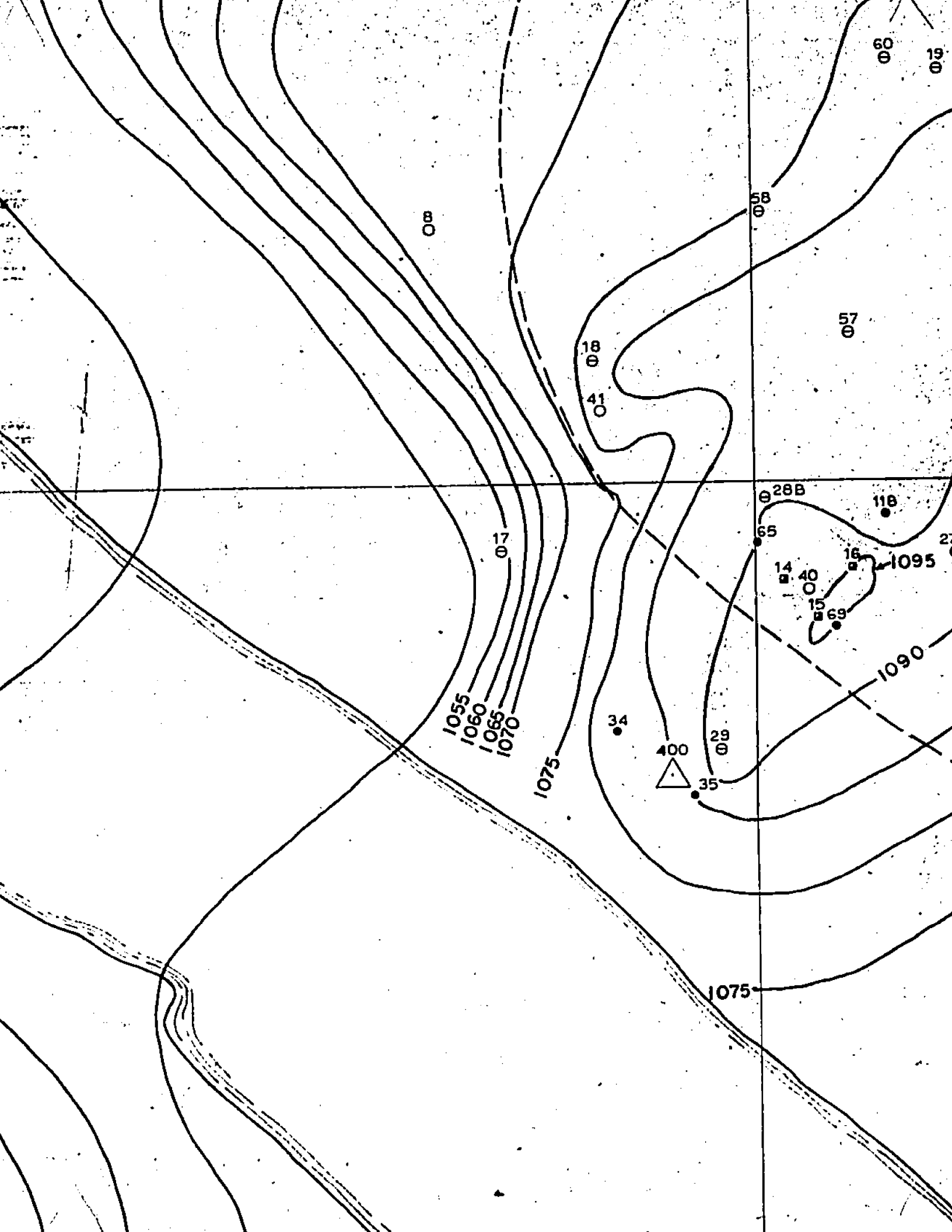
ell

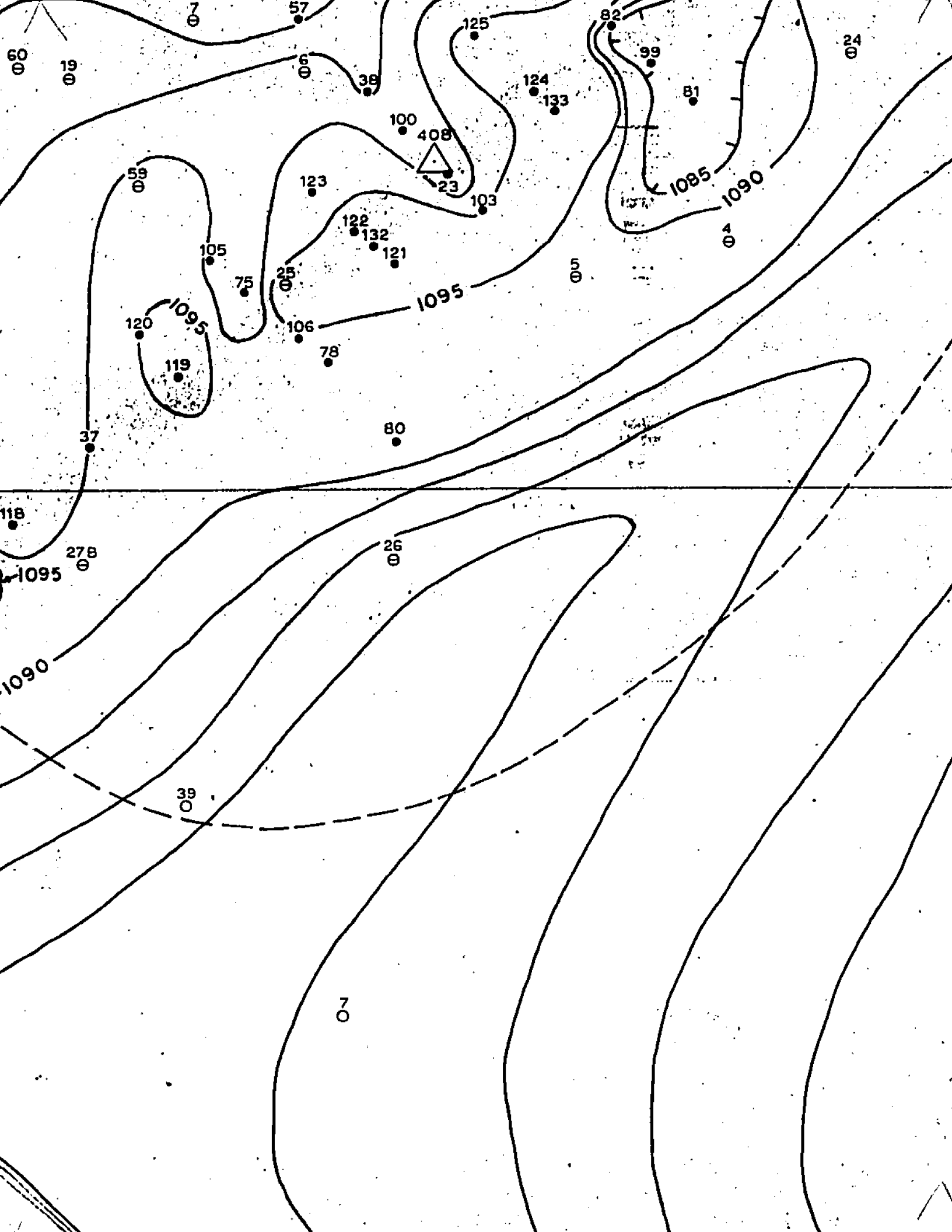
50%

1015

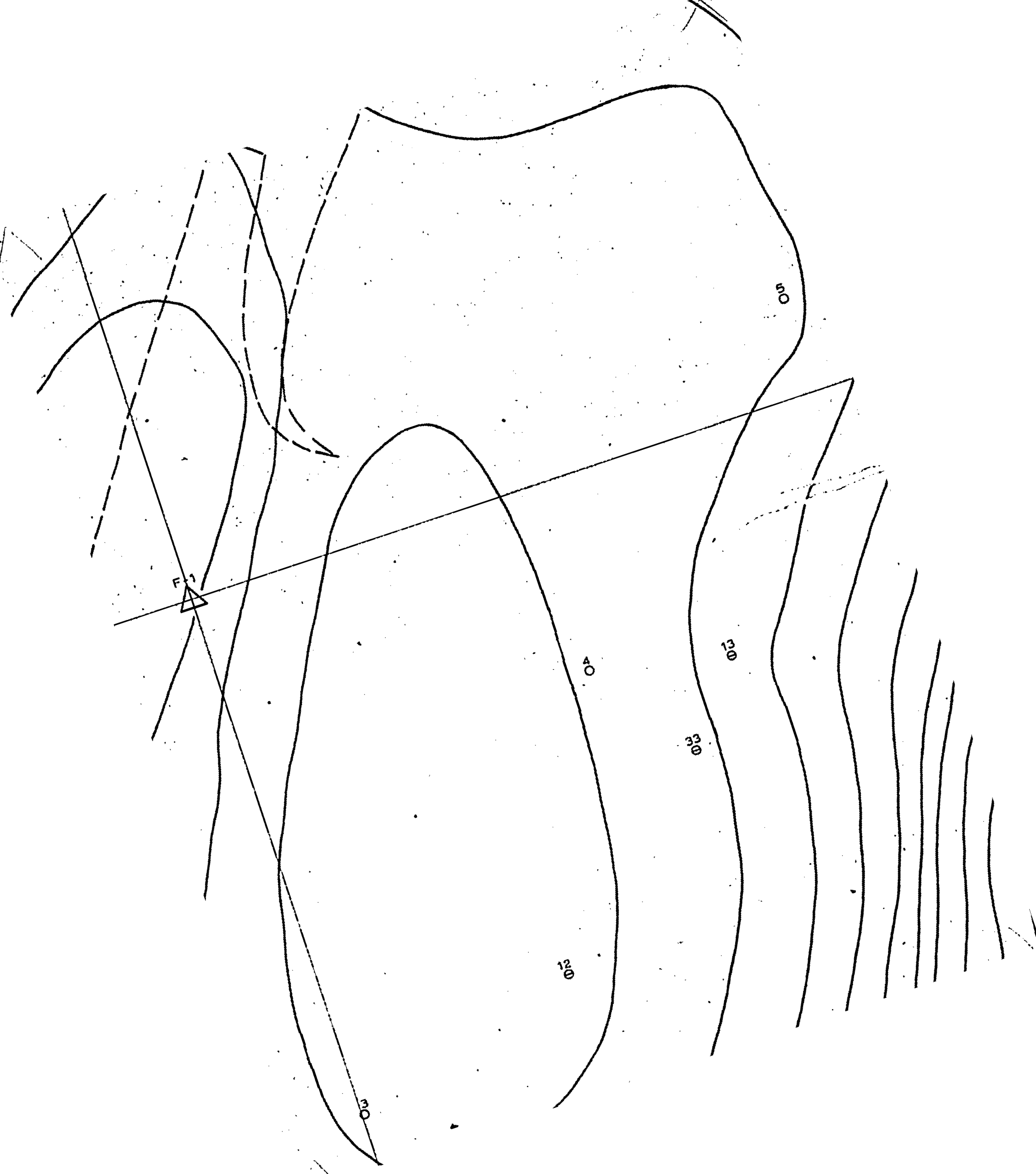
1020

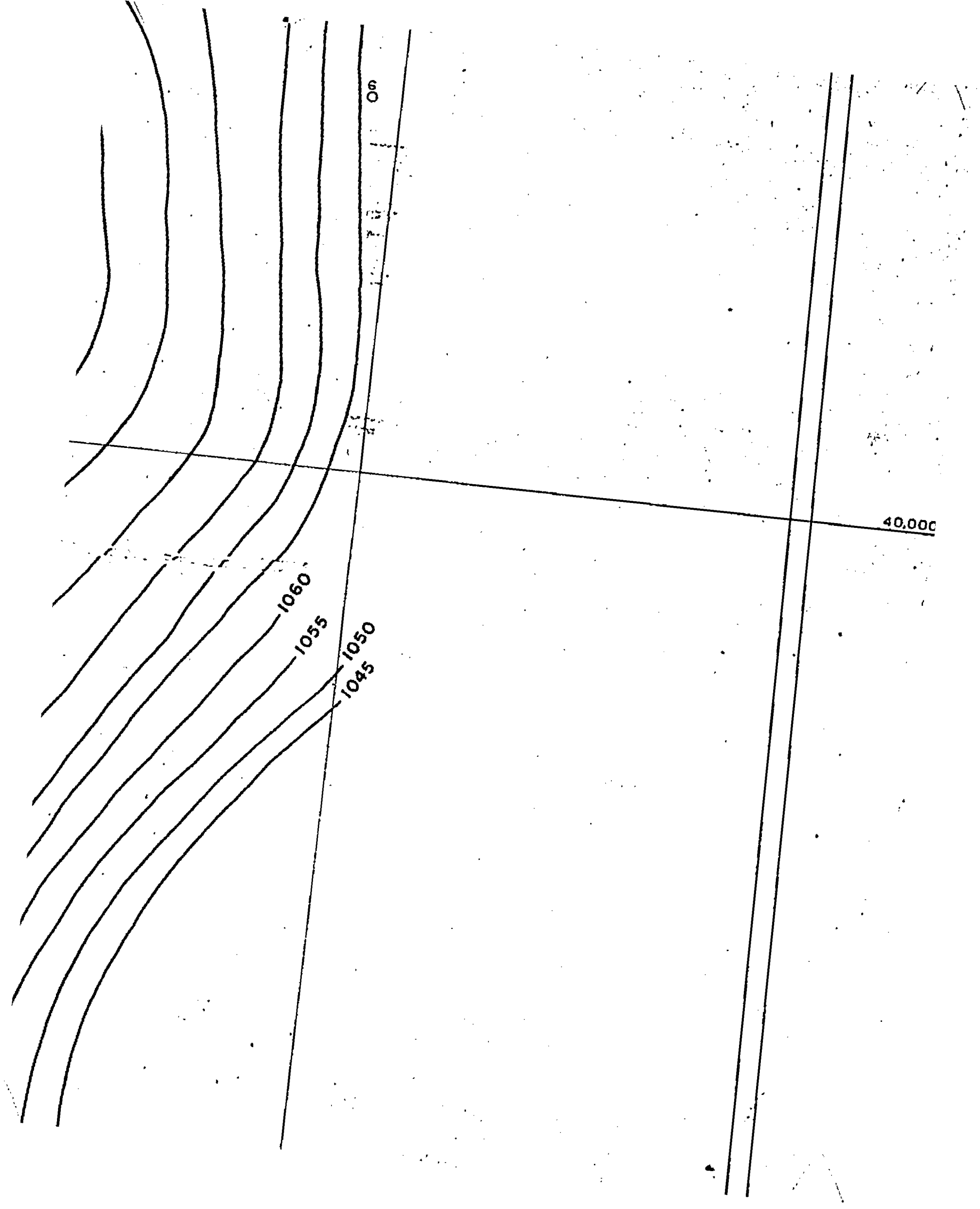












0m

1060

1055

1050  
1045

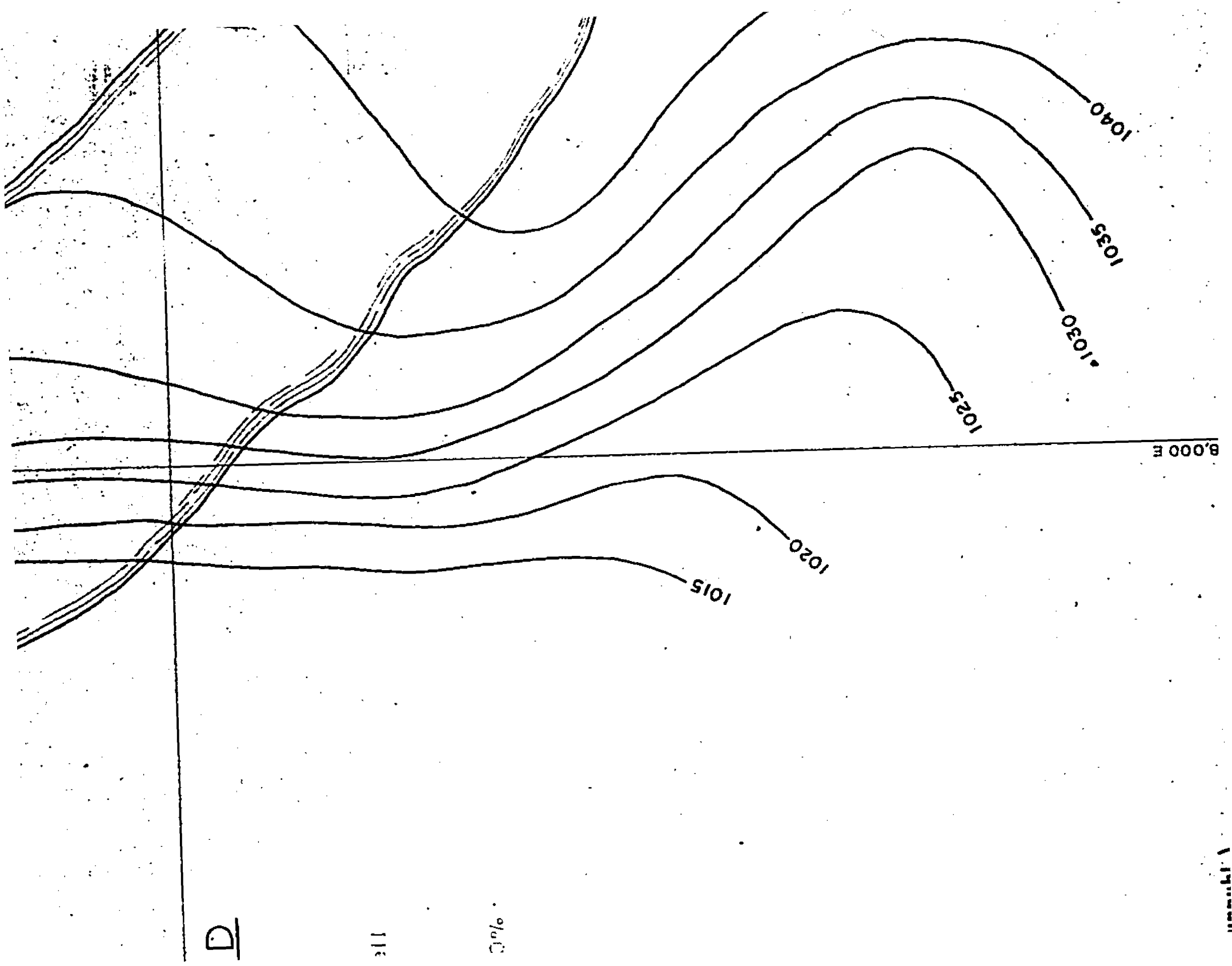
40,000

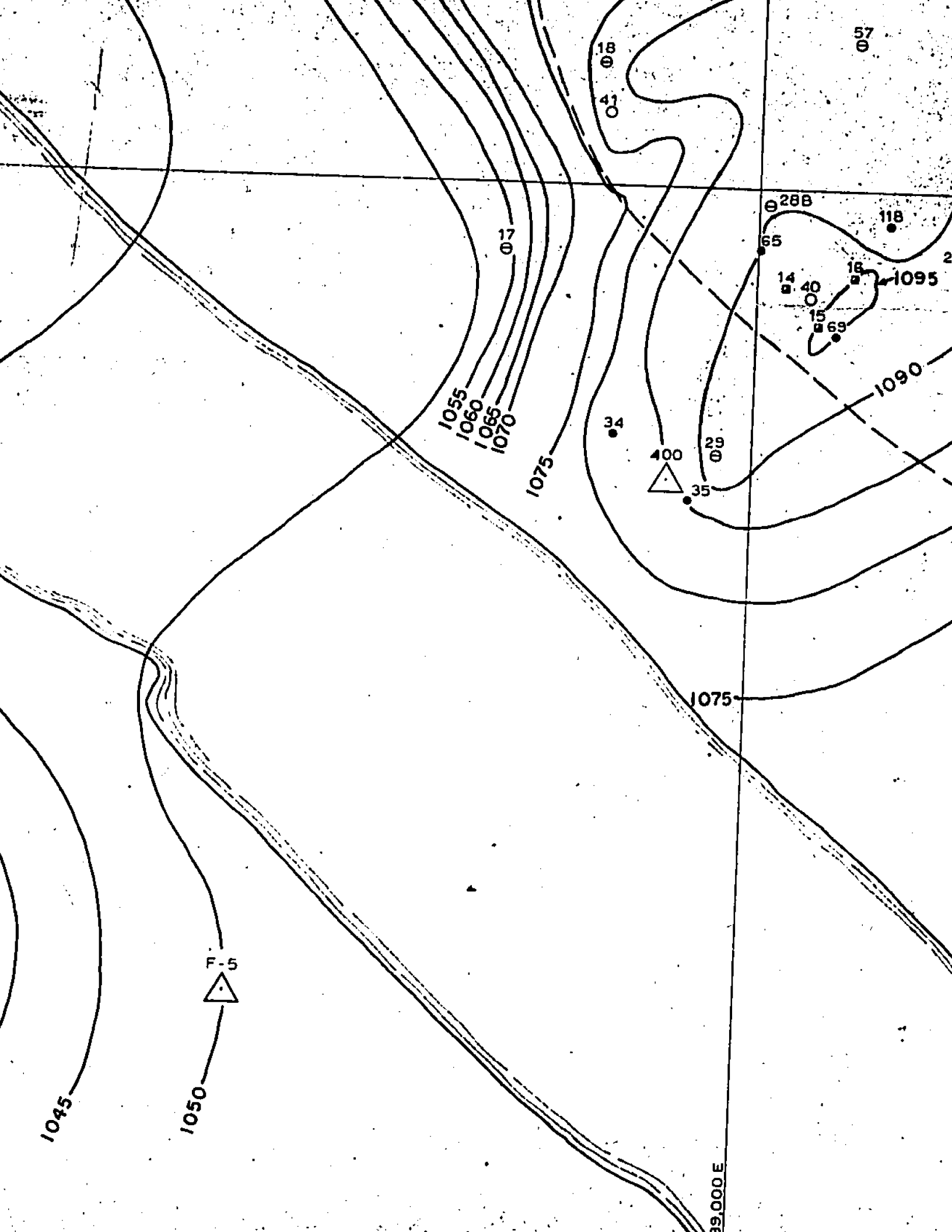
40,000 N

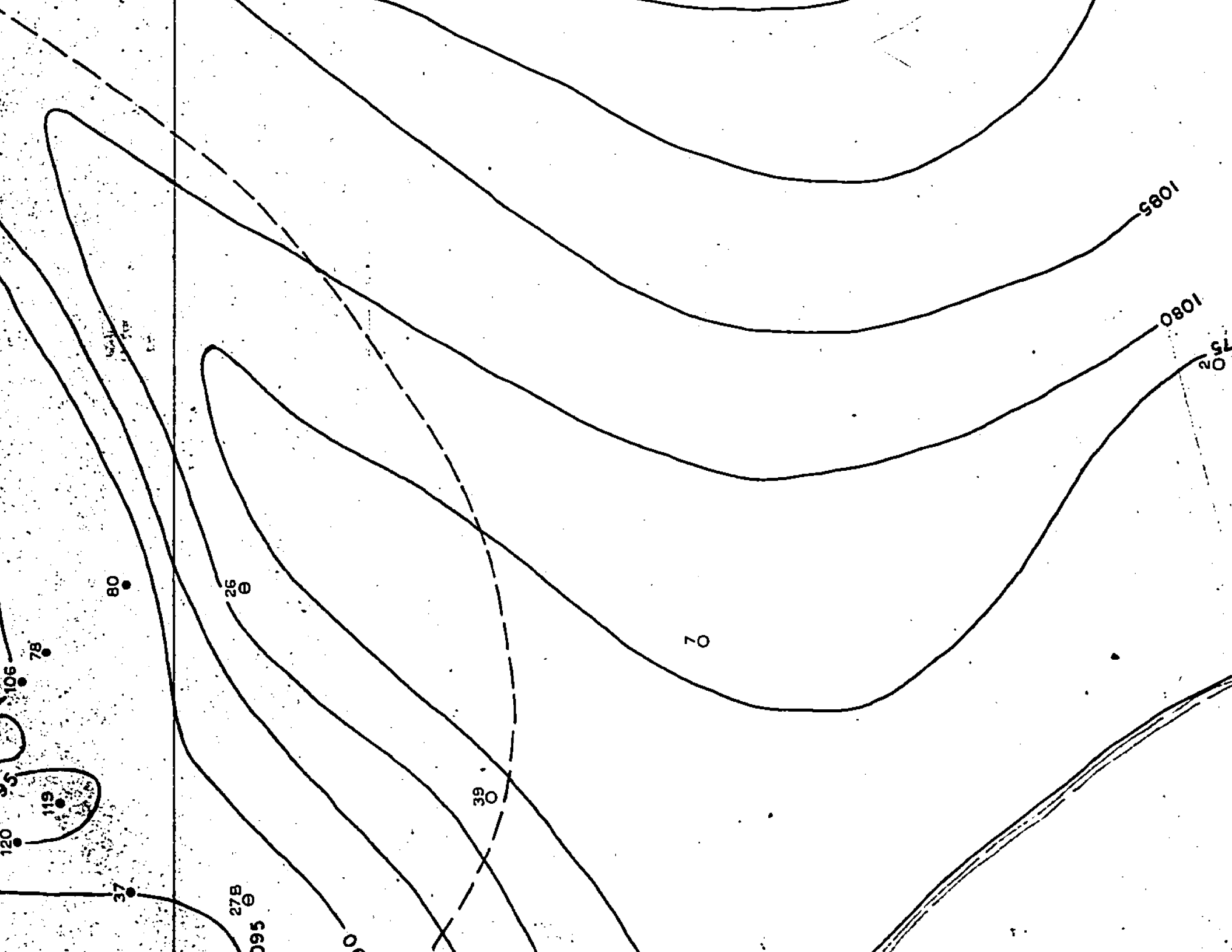
# LEGEND

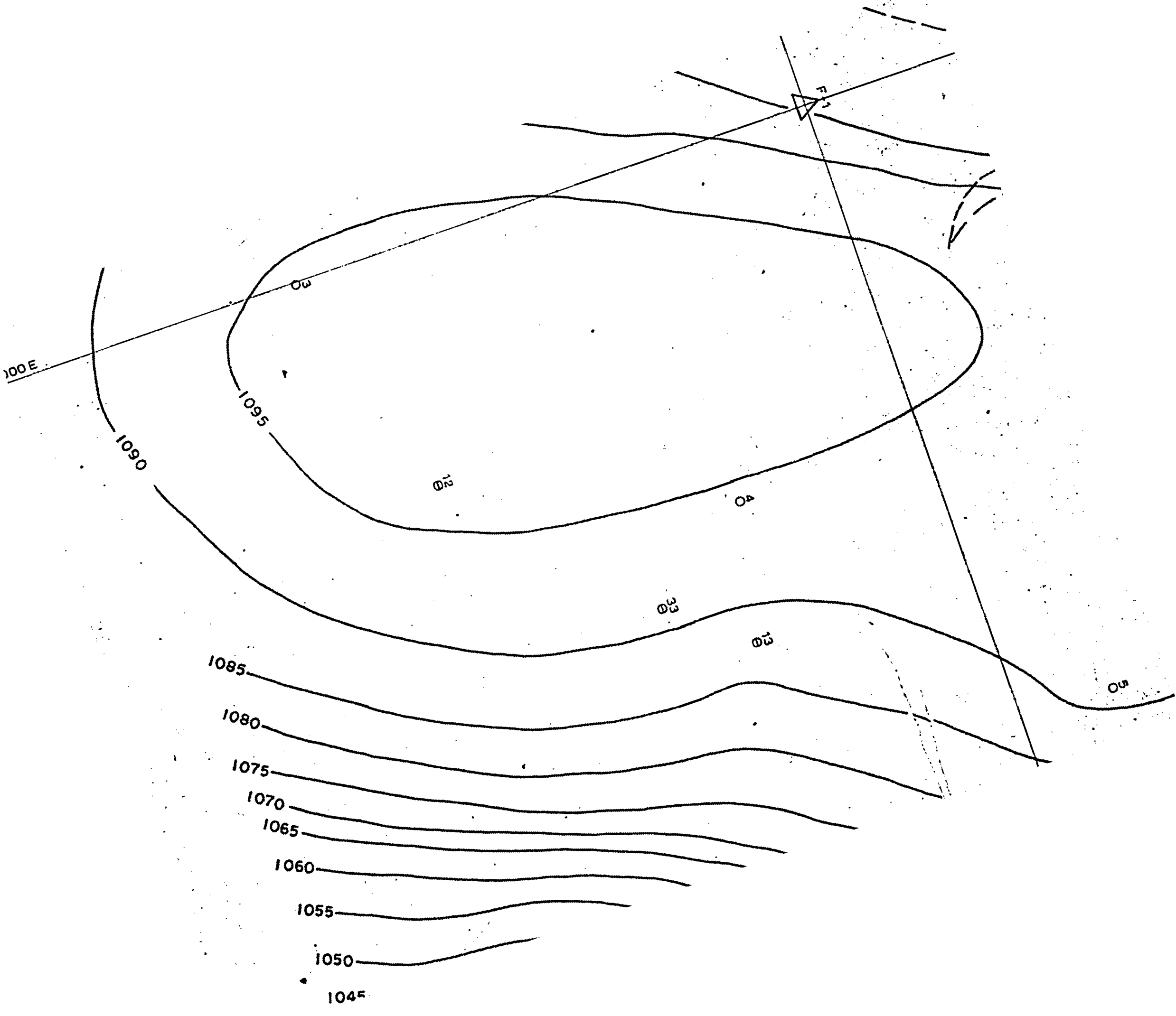
- Diamond Drill Hole
- Observation Water Well
- ⊖ Soil Test Hole
- Soil Test Pit
- ▒ Massive Saltside > 50%

7,000 E

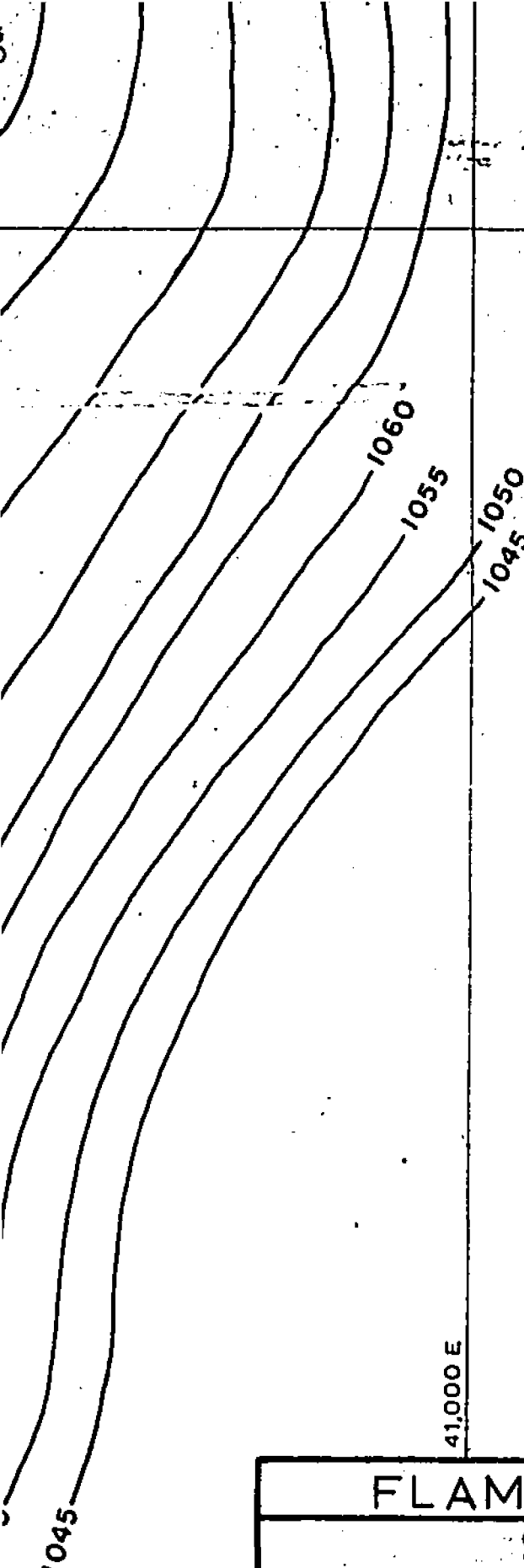








40.00



41,000 E

**PLATE 2**

**FLAMBEAU MINING CORP.**

**STRUCTURE CONTOURS  
on  
PRECAMBRIAN SURFACE**

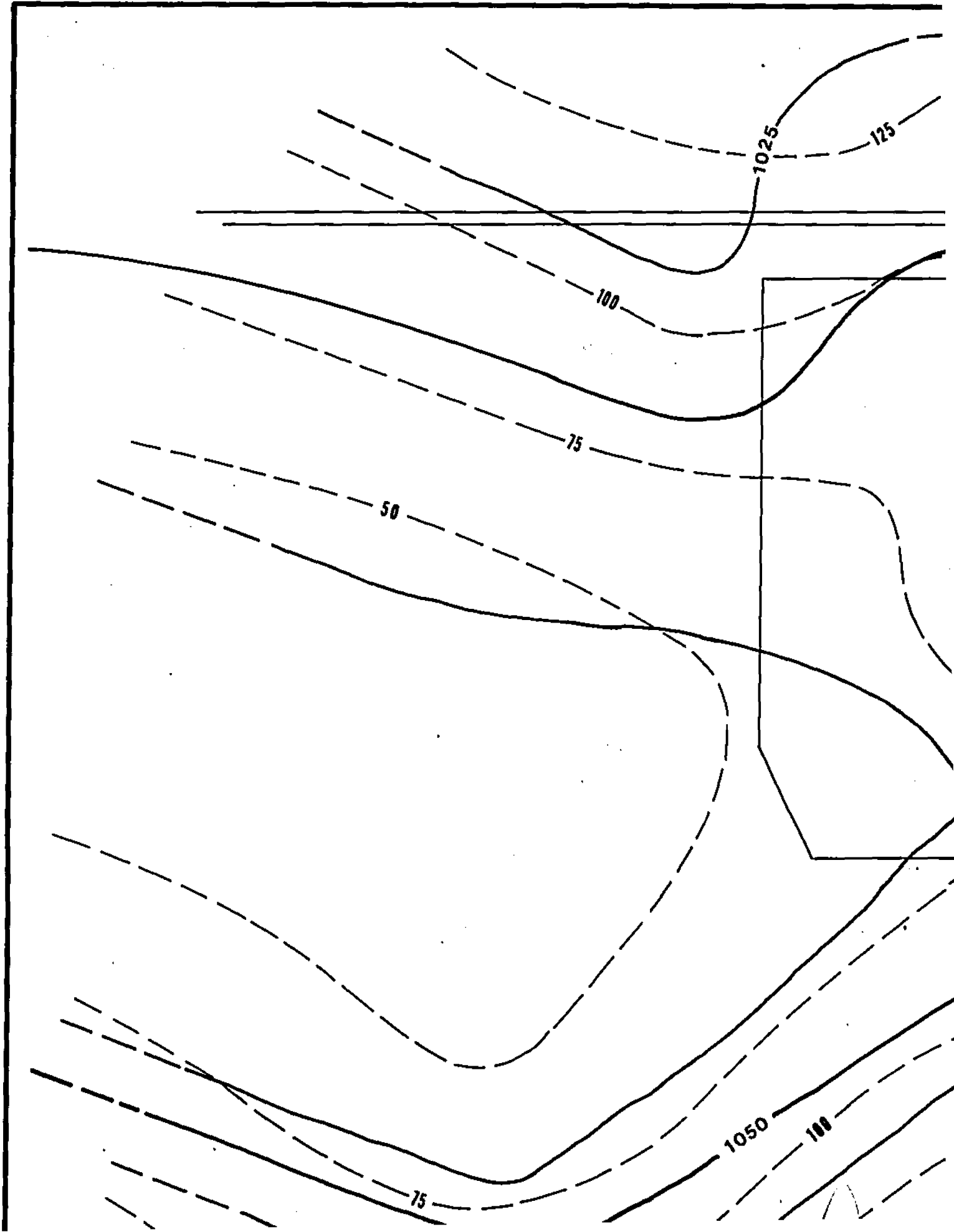
SCALE: 1" = 100'	CONTOUR INTERVAL: 5 ft.	REVISIONS:
------------------	-------------------------	------------

	DATA BY: ERM, EJ, JK	
--	----------------------	--

DATE: NOV. 1981		
-----------------	--	--

DRAWN BY: C.L.P.		FILE
------------------	--	------





P

1.2 MI TO MINE

C. R. P

waste - containment  
structure

27  
HWY

TILL ISOPACH

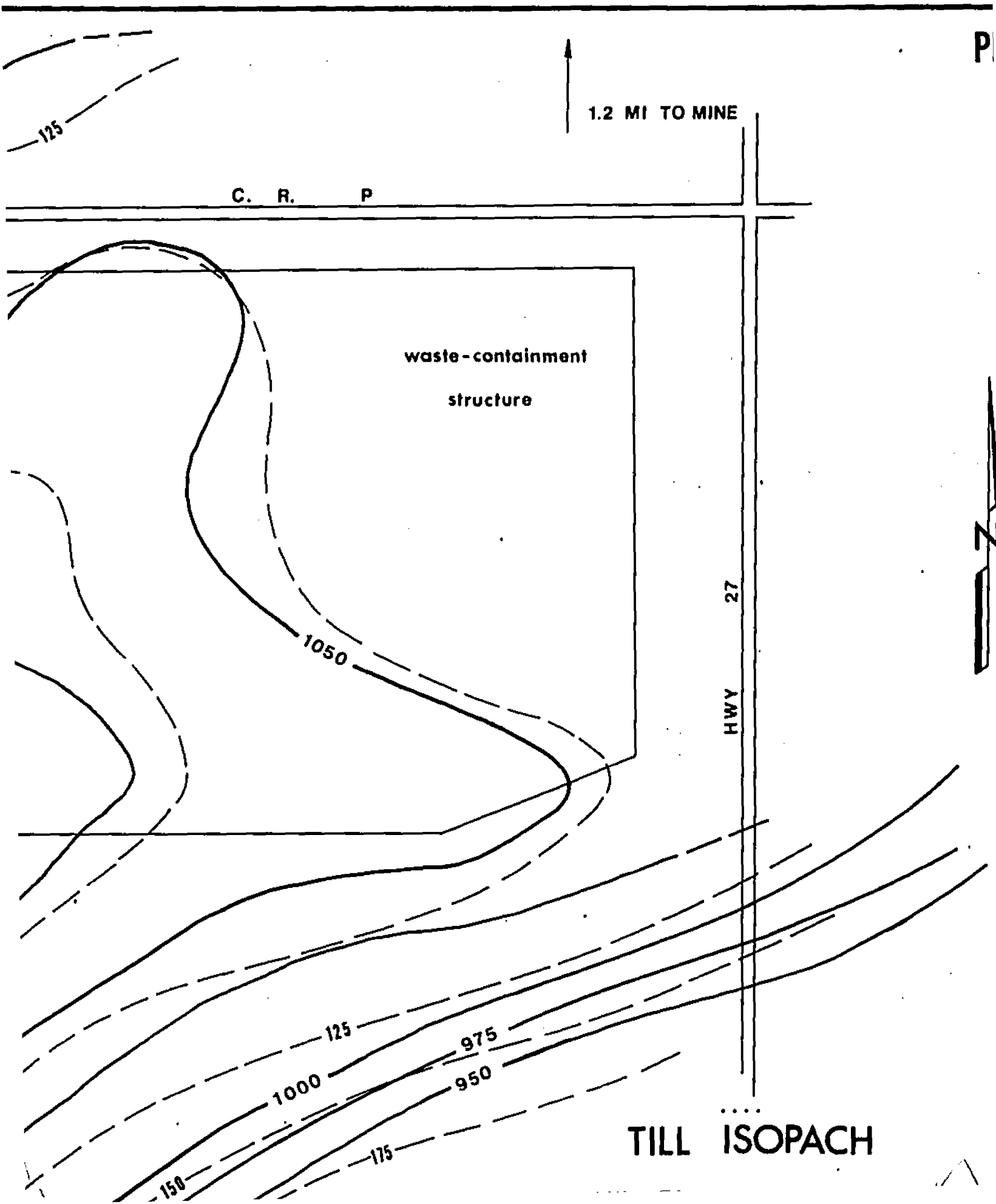


**PLATE 3**

↑  
1.2 MI TO MINE

R. P

waste - containment  
structure



27  
HWY

1050

125

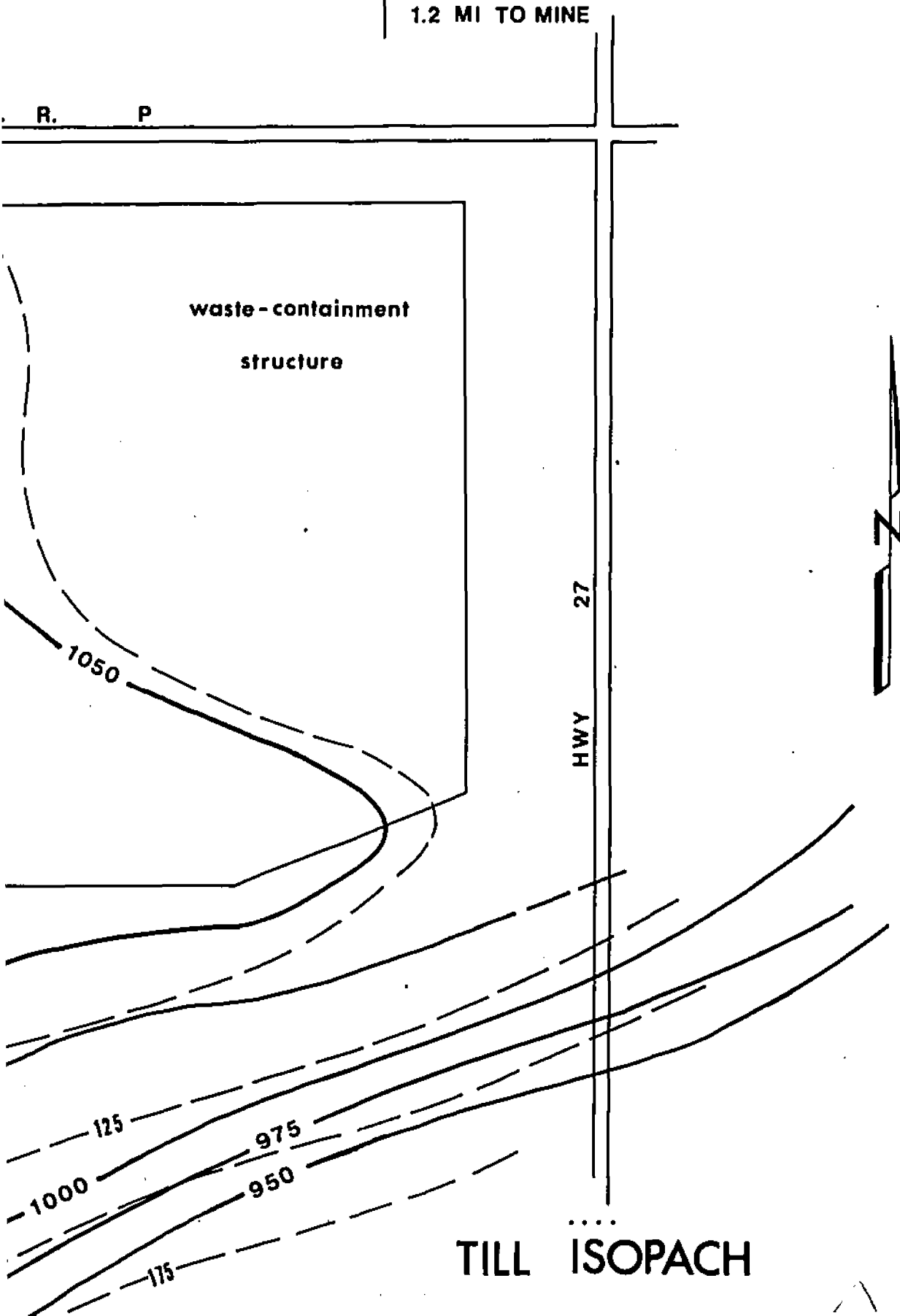
1000

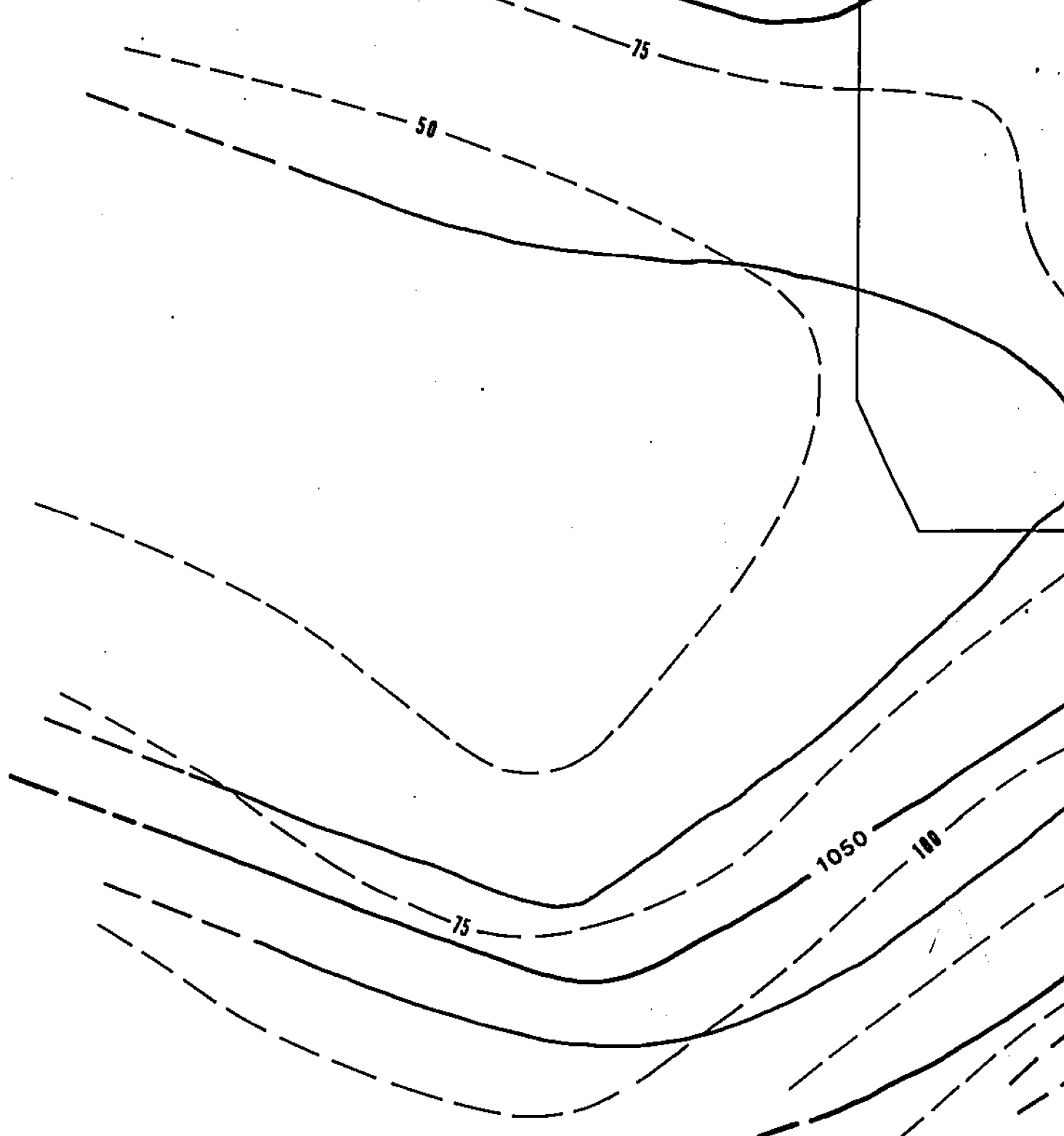
975

950

175

....  
**TILL ISOPACH**





**KEY**

—1050—

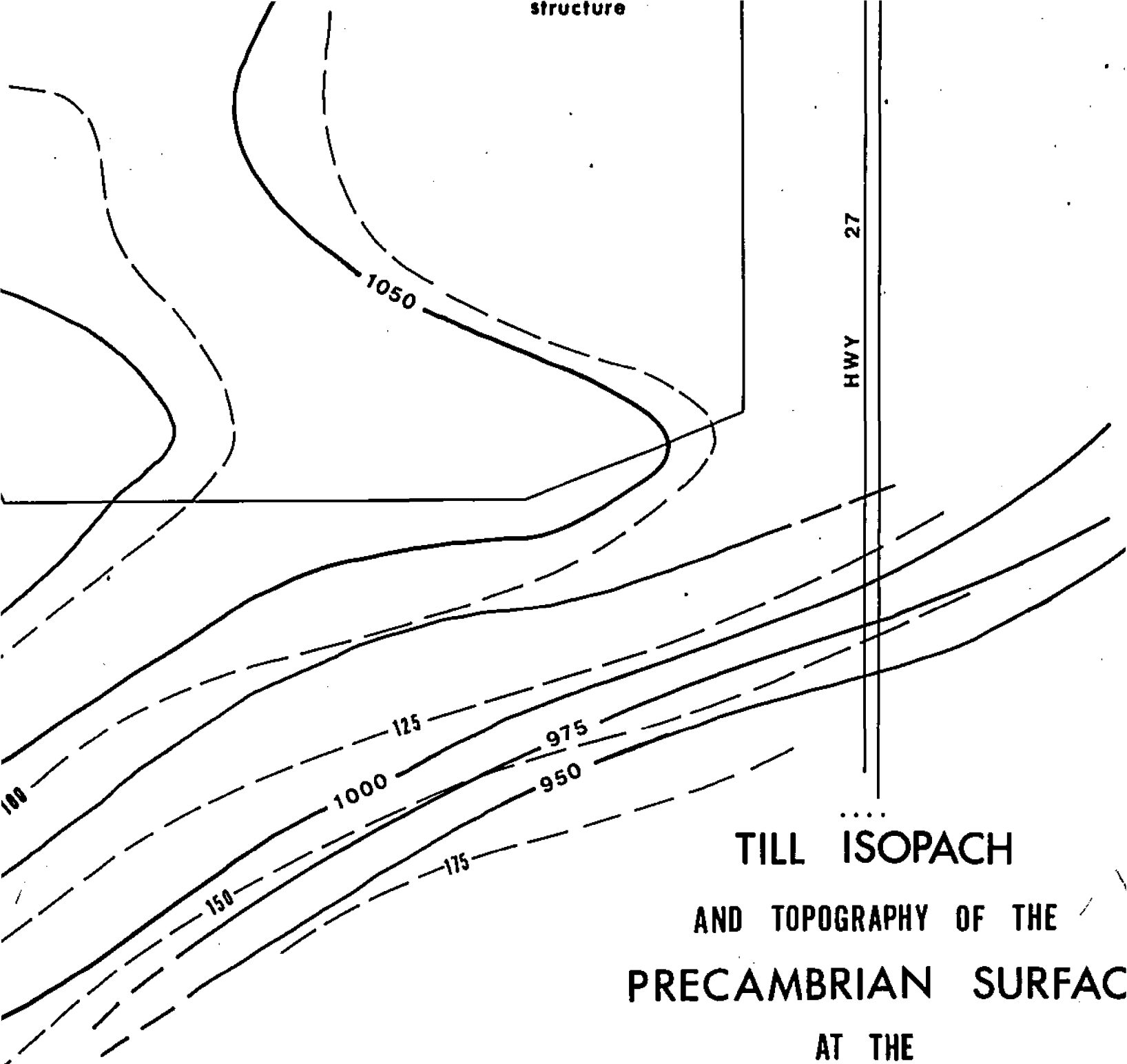
PRECAMBRIAN SURFACE

—75—

TILL THICKNESS

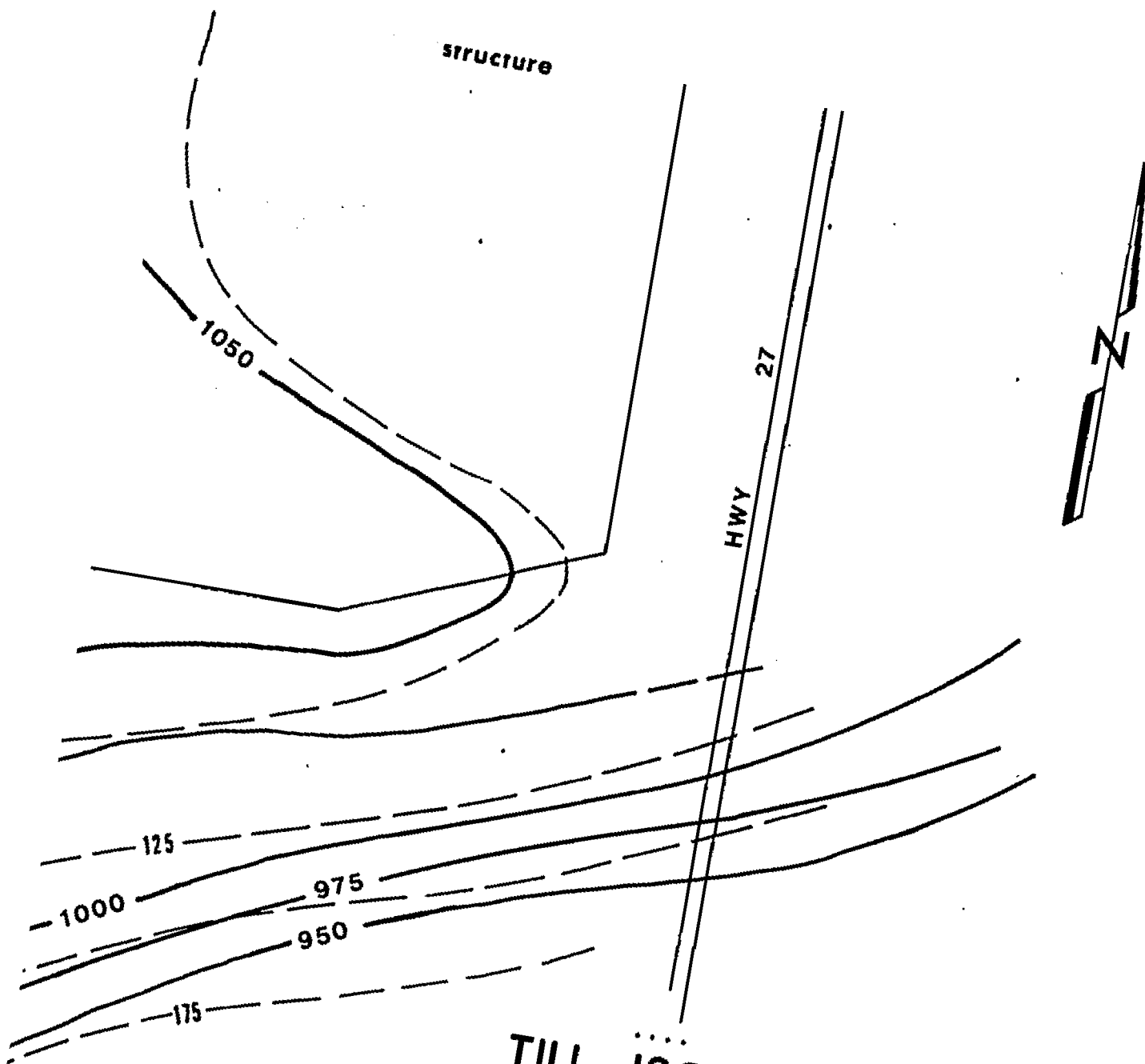
From unpubl. data, Flambeau Mining Corp.

structure



**TILL ISOPACH  
AND TOPOGRAPHY OF THE  
PRECAMBRIAN SURFACE  
AT THE  
WASTE-CONTAINMENT AREA,  
FLAMBEAU SITE**

0 500 ft  
Contour Interval = 25 ft.



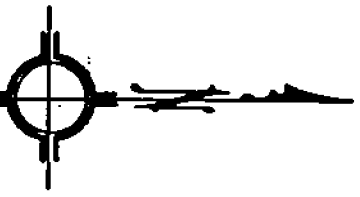
TILL ISOPACH  
AND TOPOGRAPHY OF THE  
PRECAMBRIAN SURFACE  
AT THE  
WASTE-CONTAINMENT AREA,  
FLAMBEAU SITE

0 500 ft  
Contour Interval = 25 ft

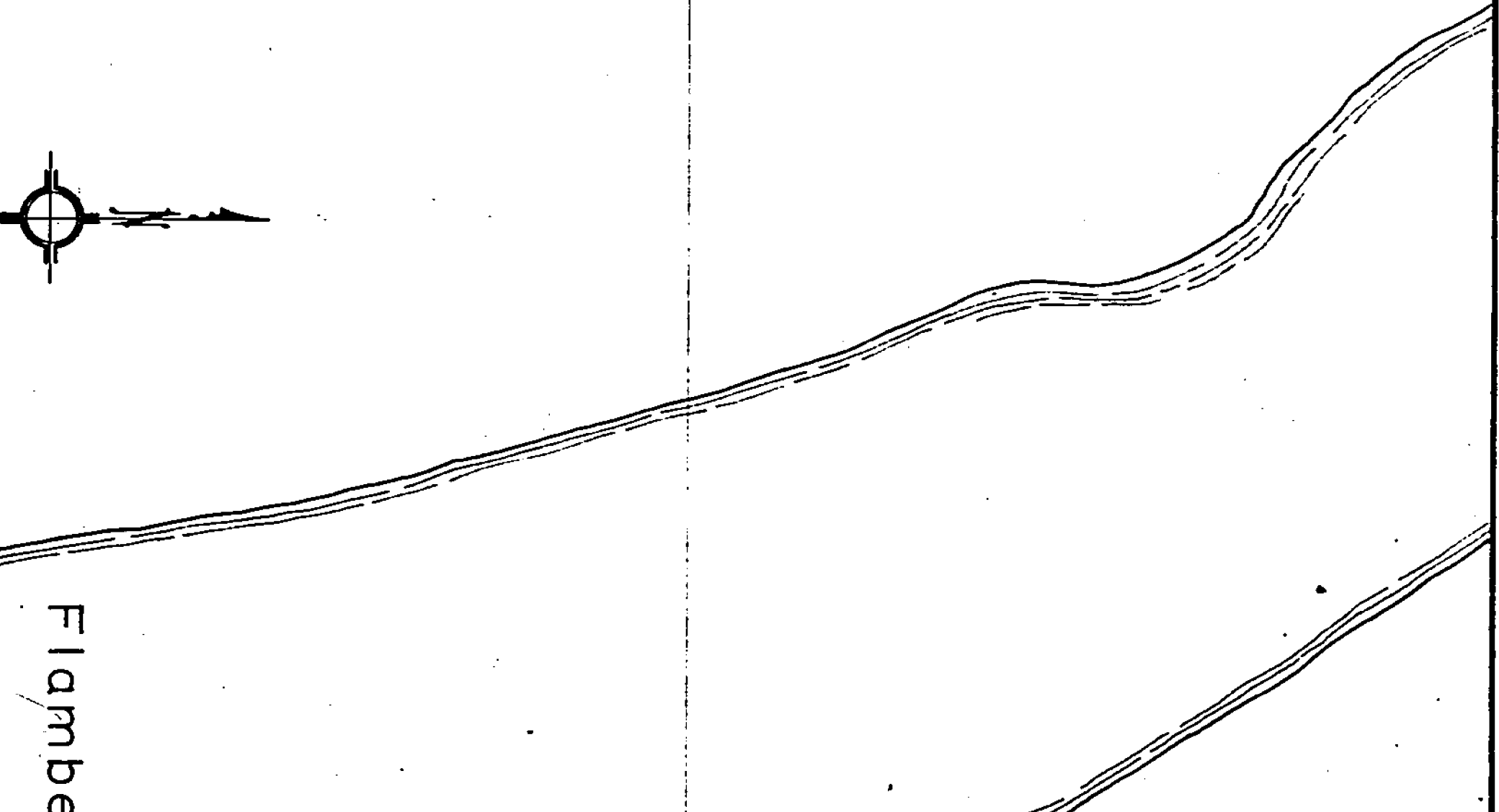
J. M. KING, 1982

37.000 E

42.000 N



Flambe

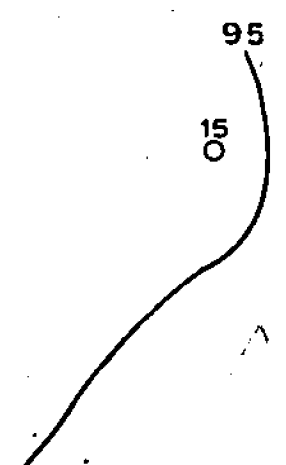
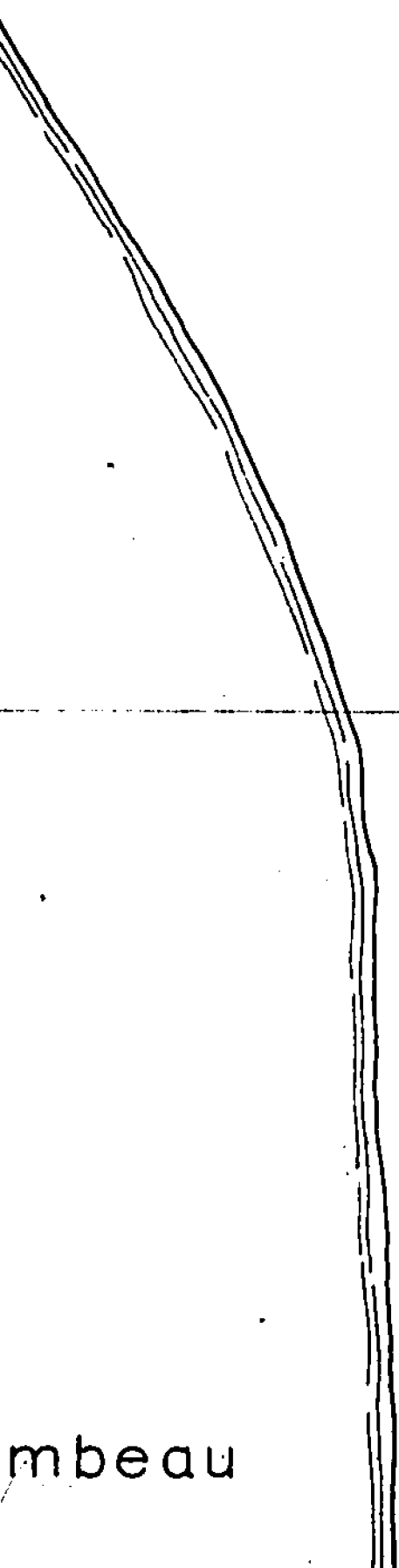


38.000 E

17  
O

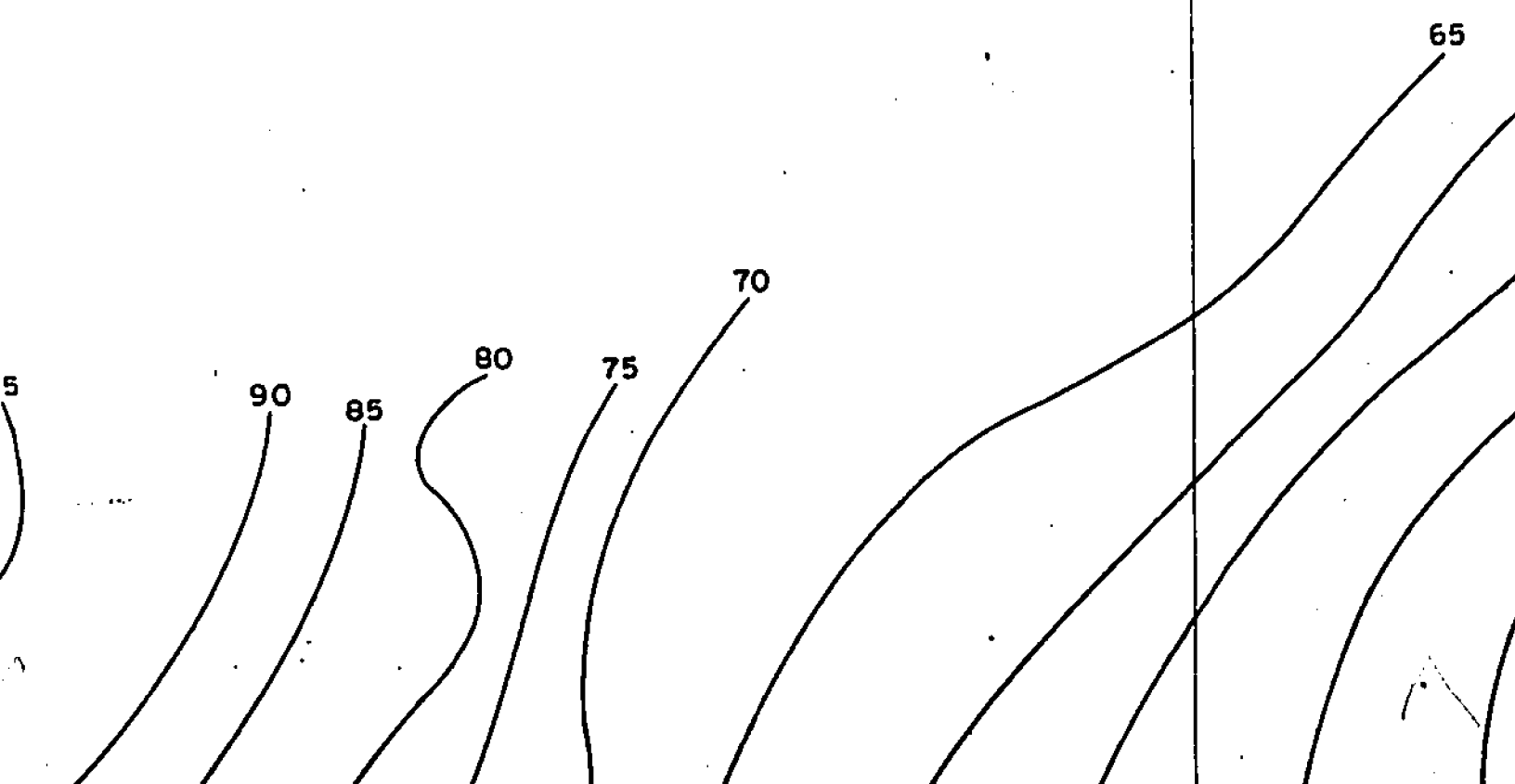
95  
15  
O

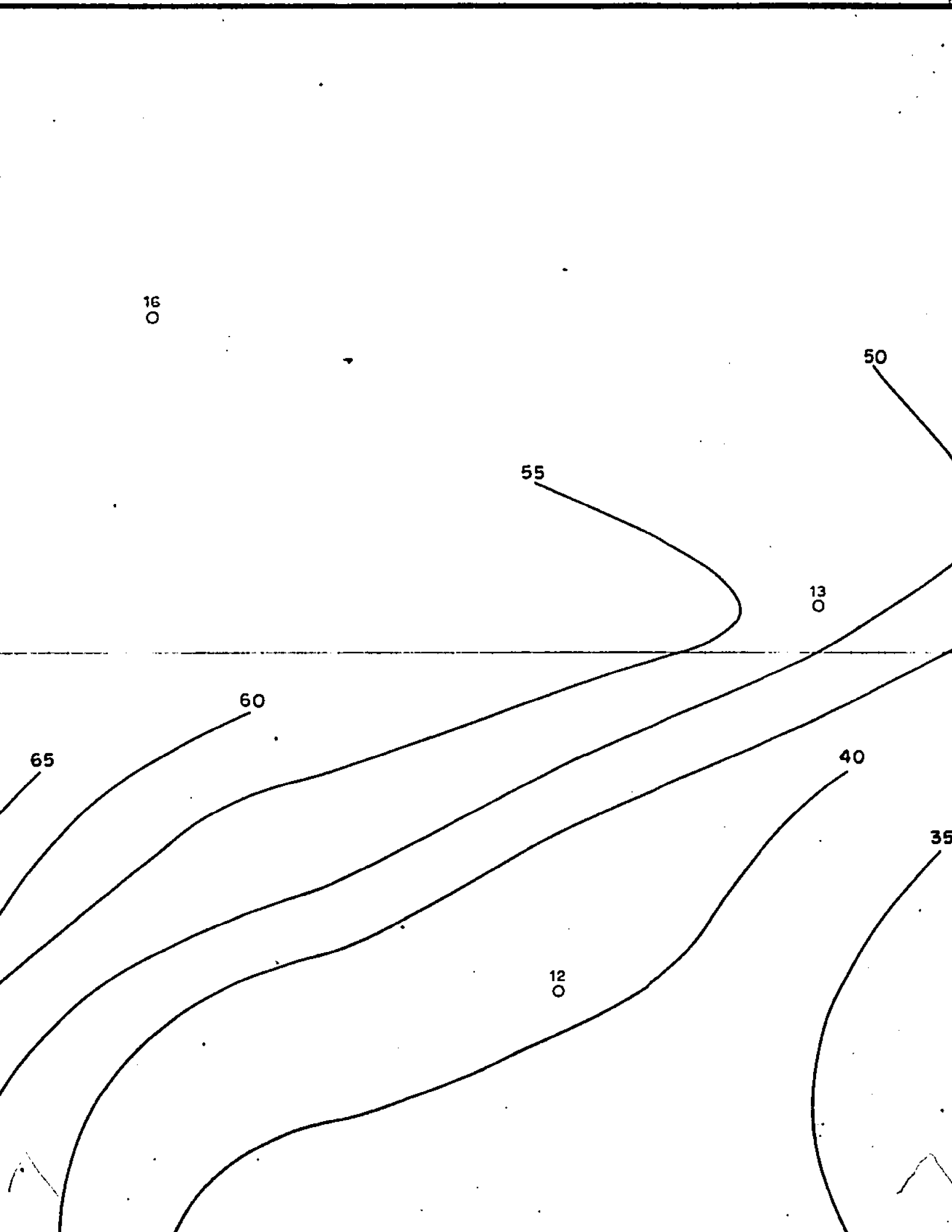
mbeau





39,000 E





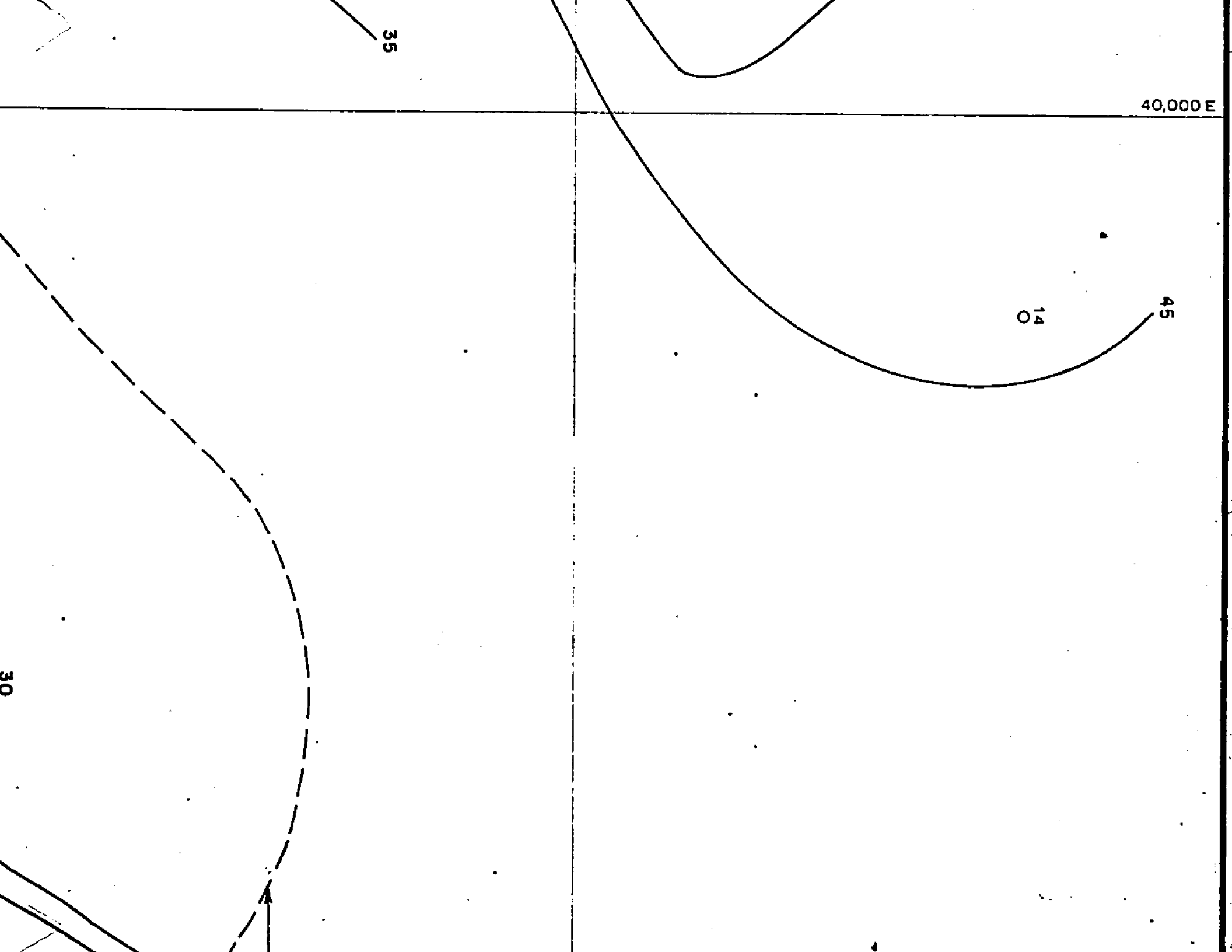
40,000 E

35

14

45

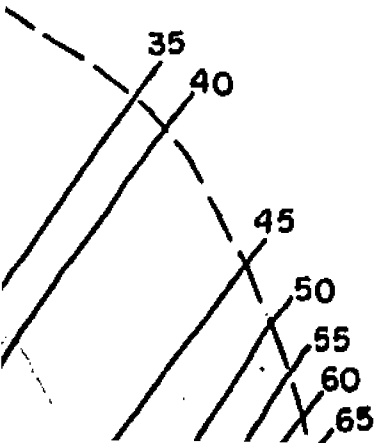
30



41,000 E

42,000

Pit Perimeter



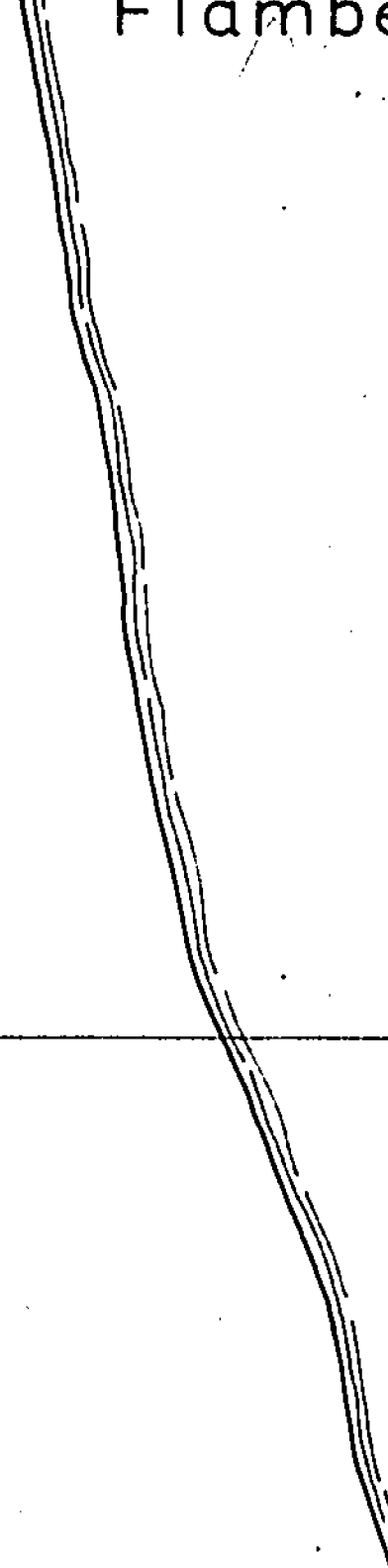
F-3



Flambe



41,000 N



mscua



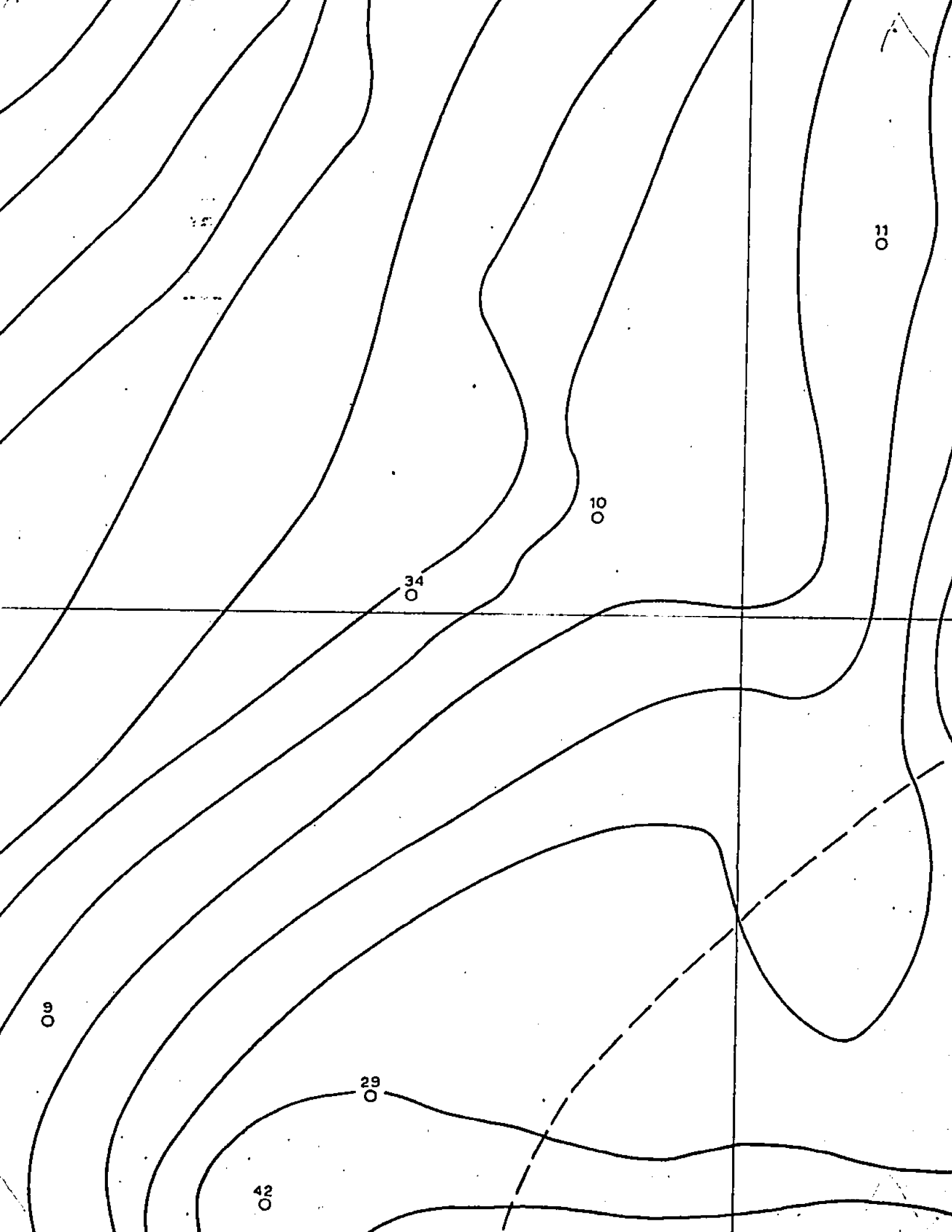
95

90

90

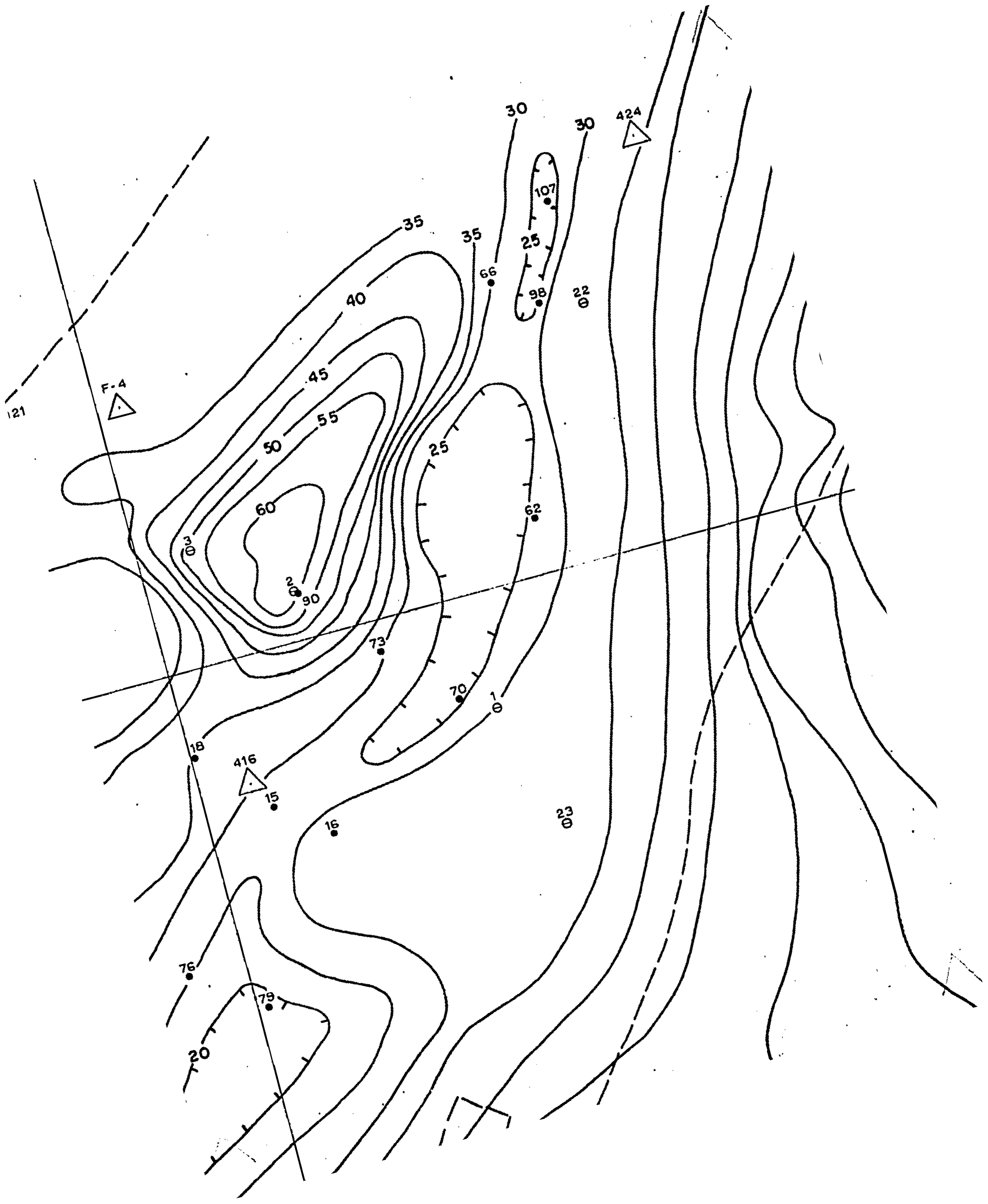
43  
O

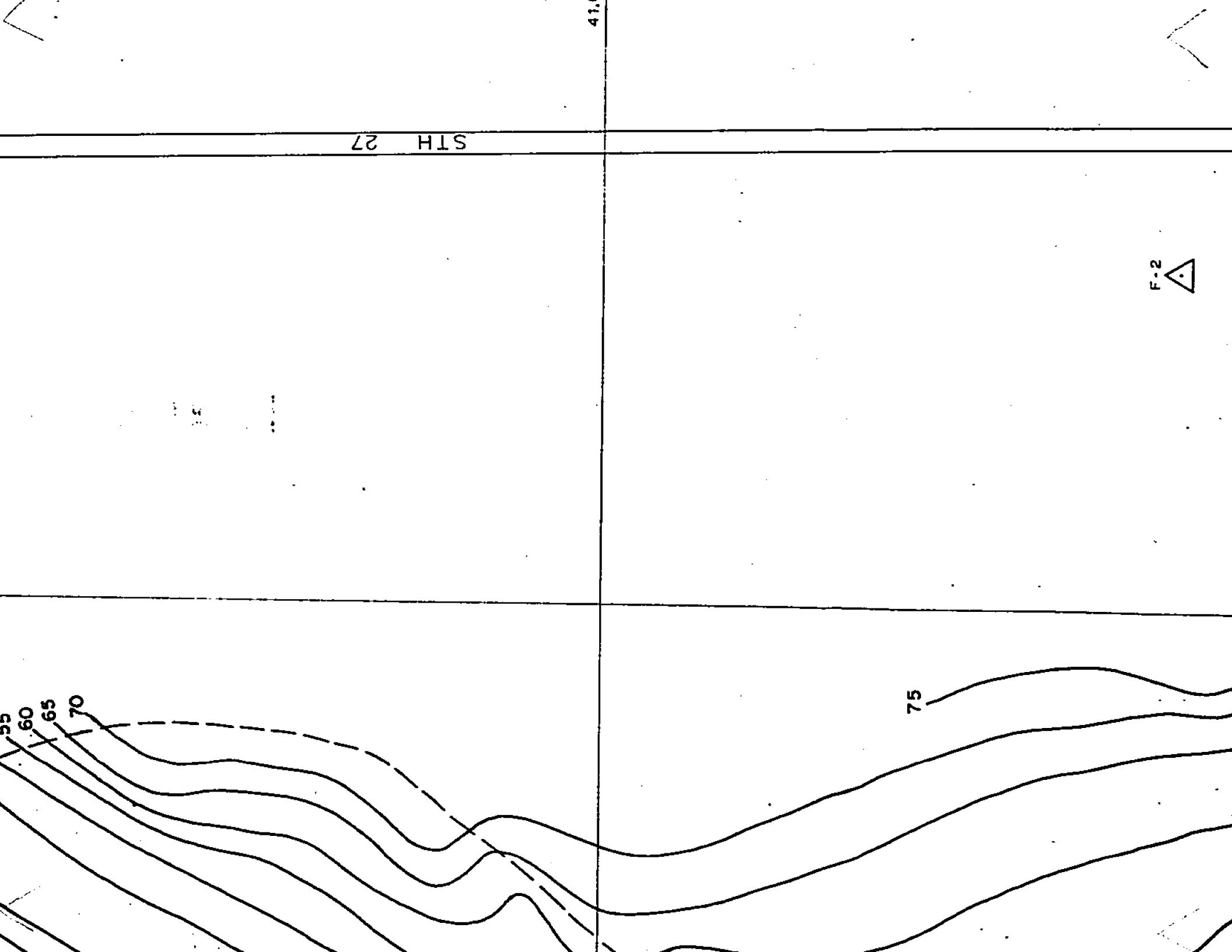
River







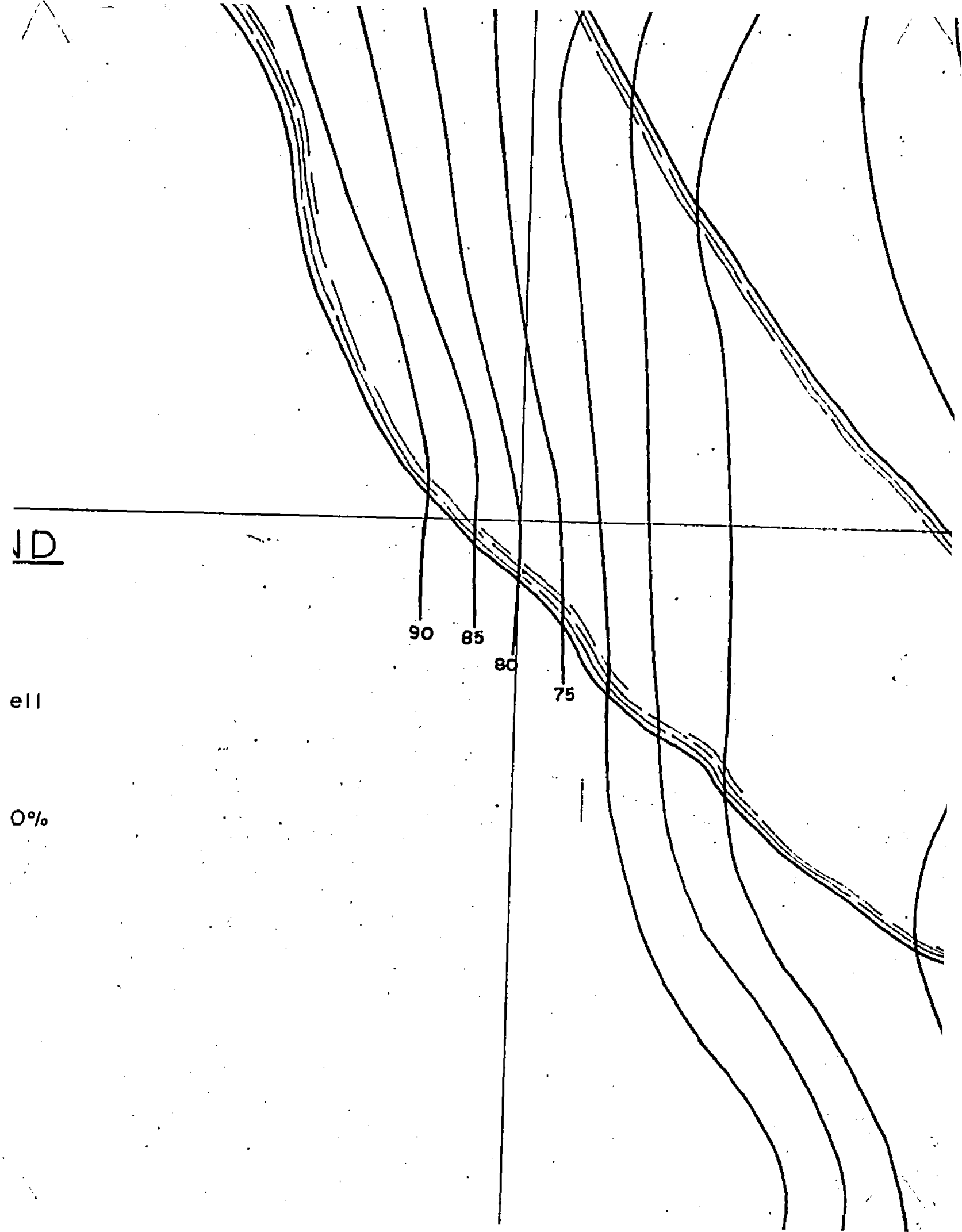




40,000 N

## LEGEND

- Diamond Drill Hole
- Observation Water Well
- ⊖ Soil Test Hole
- Soil Test Pit
- Massive Sulfide >50%



JD

90

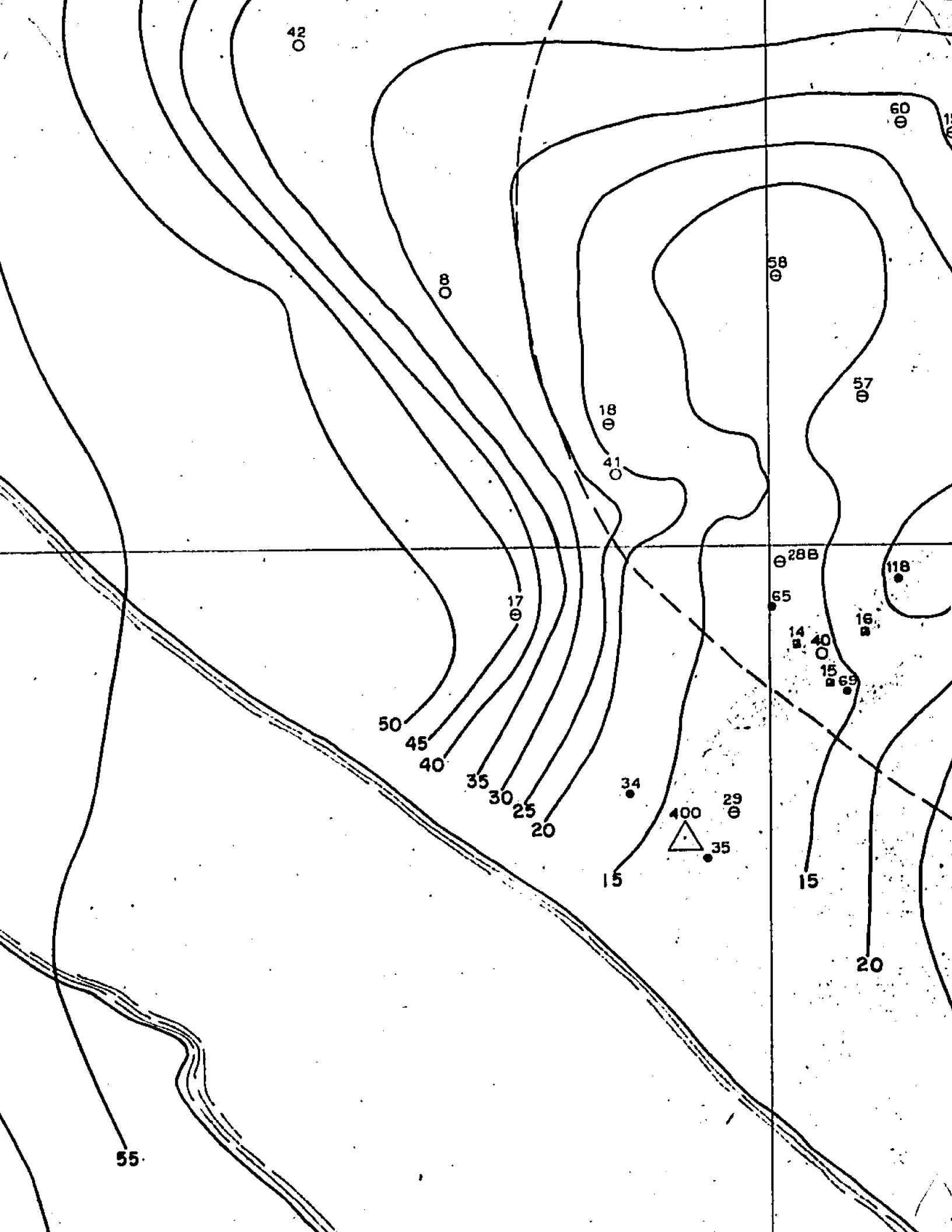
85

80

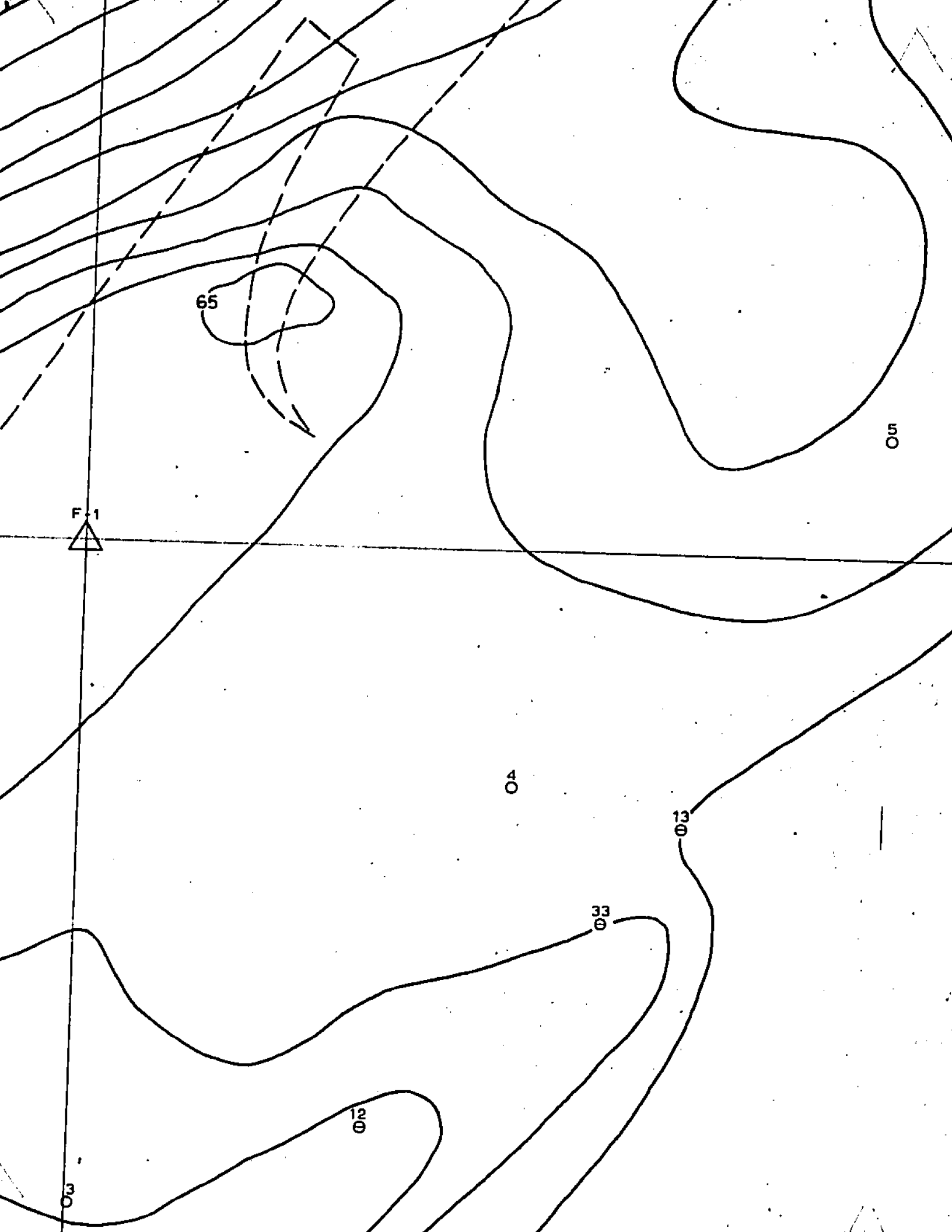
75

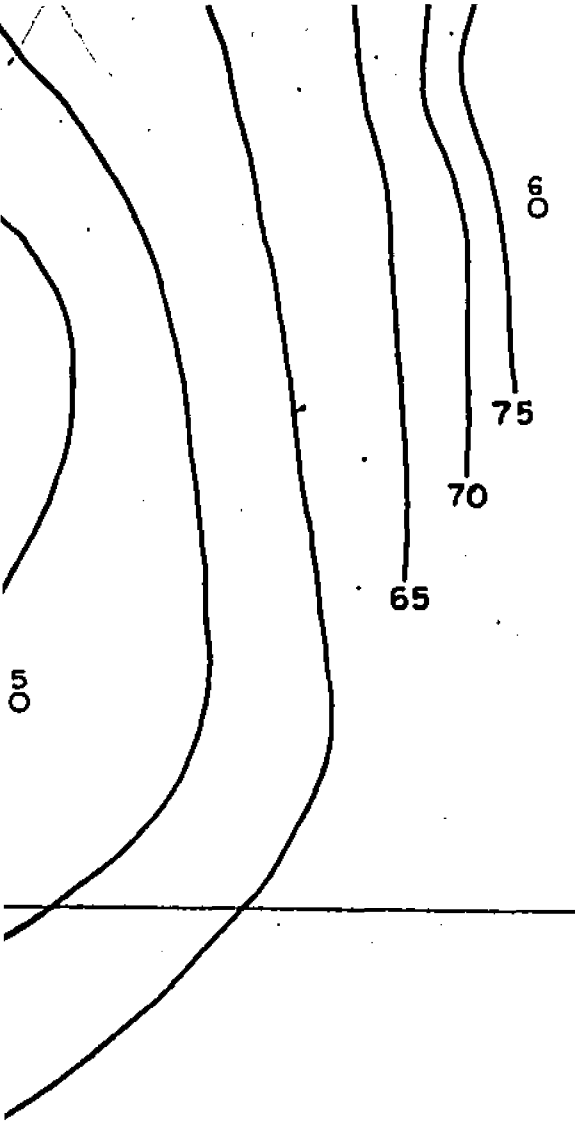
ell

0%









40.0



0,000 N

## LEGEND

- Diamond Drill Hole
- Observation Water Well
- ⊖ Soil Test Hole
- ▣ Soil Test Pit
- Massive Sulfide > 50%

0,000 E

1000 E

60

65

70

75

80

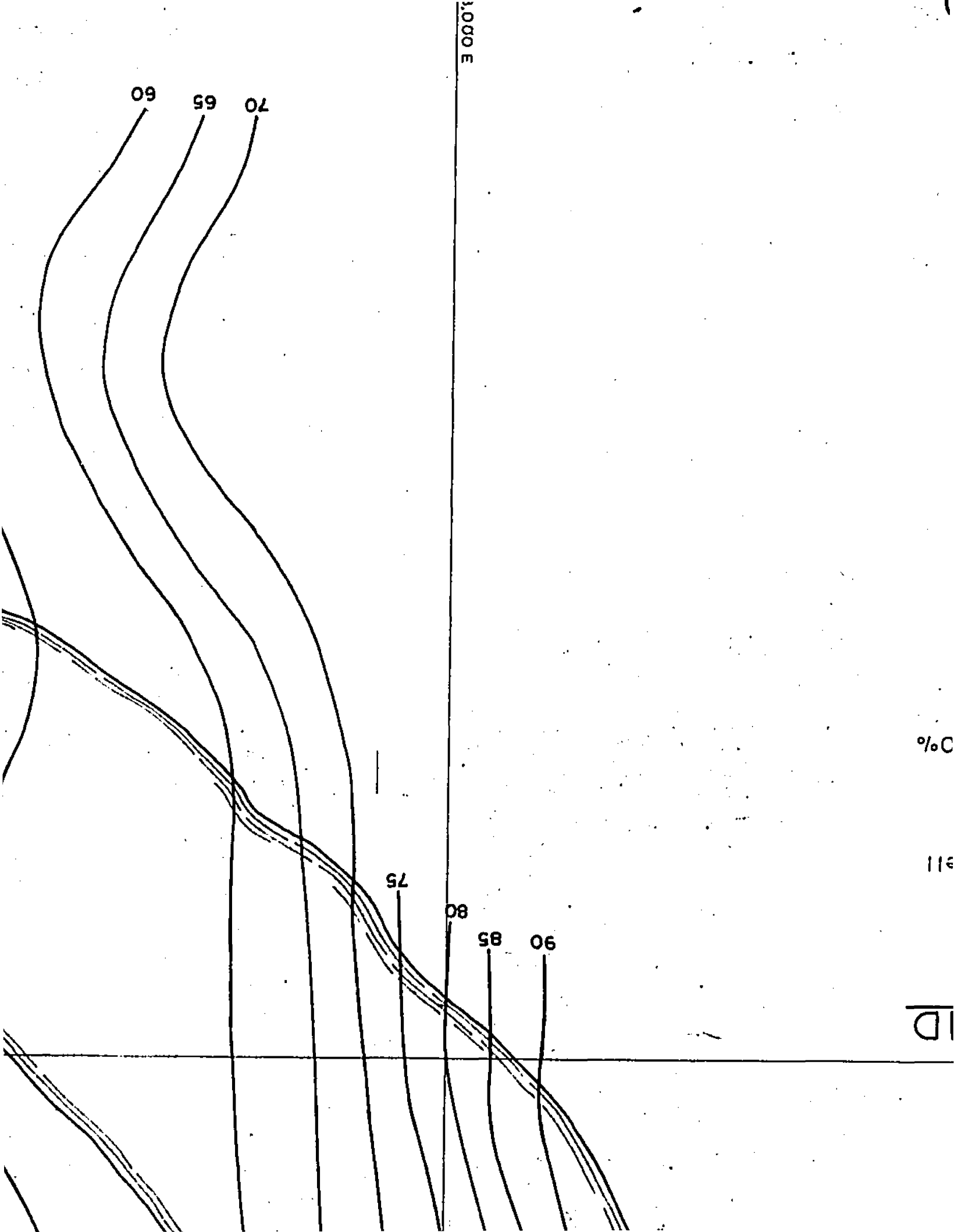
85

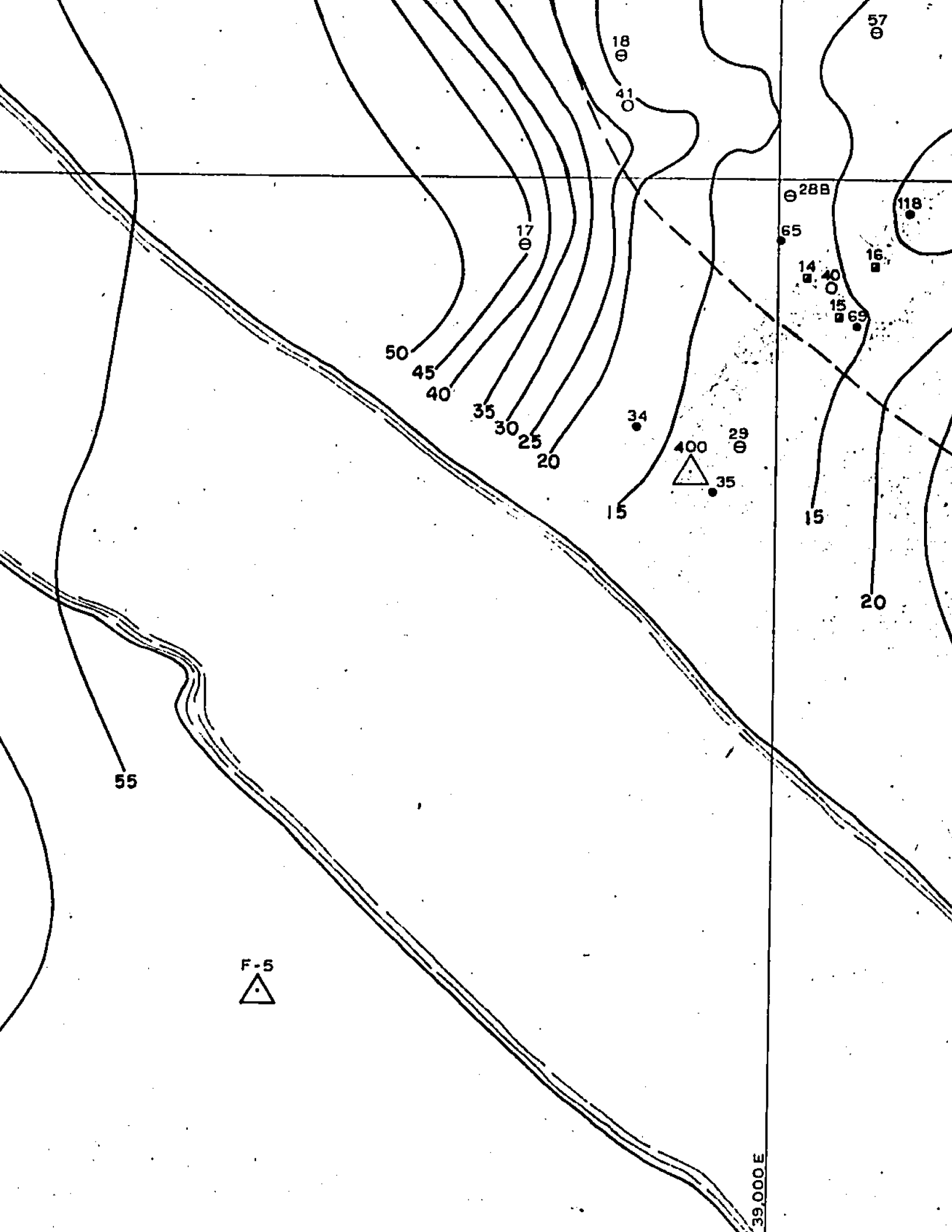
90

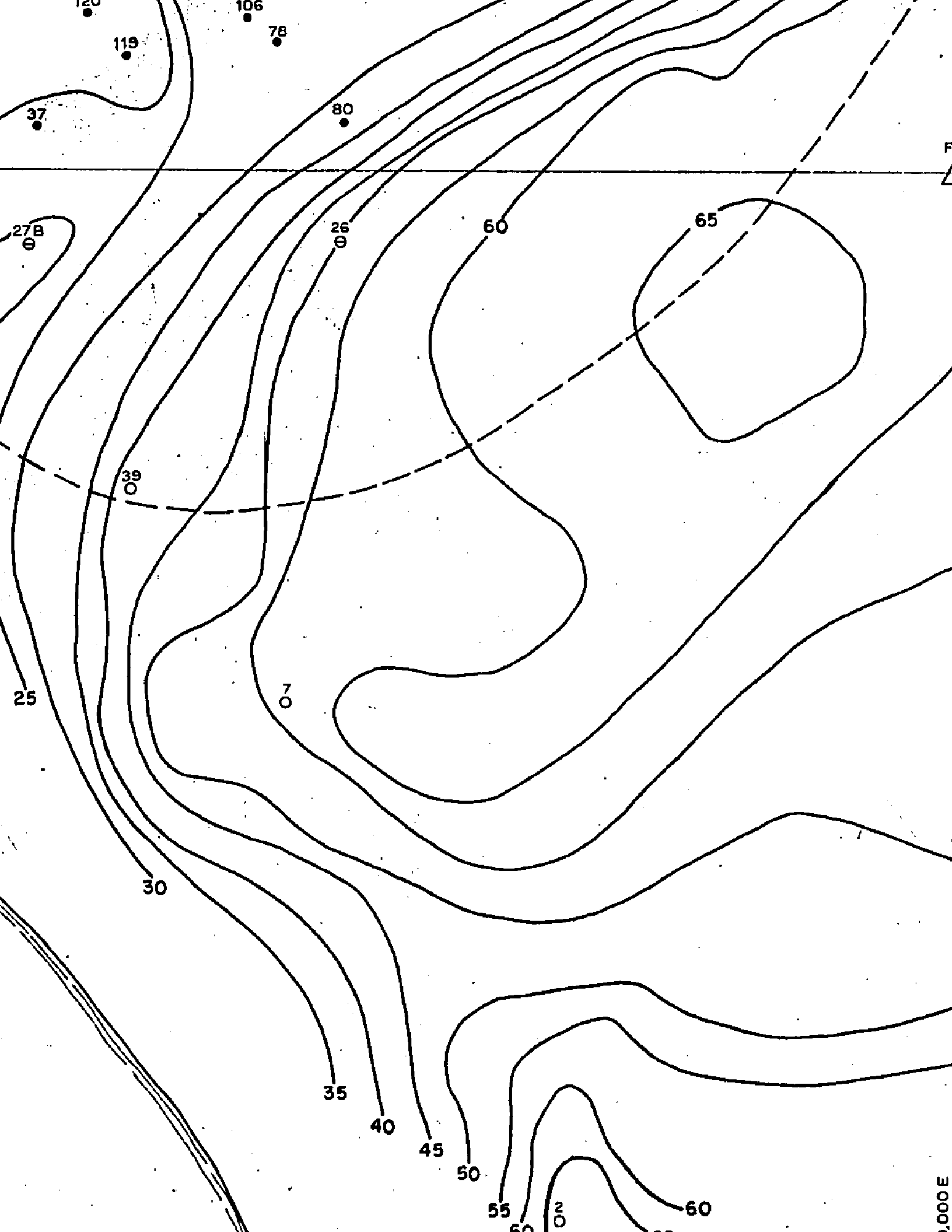
%C

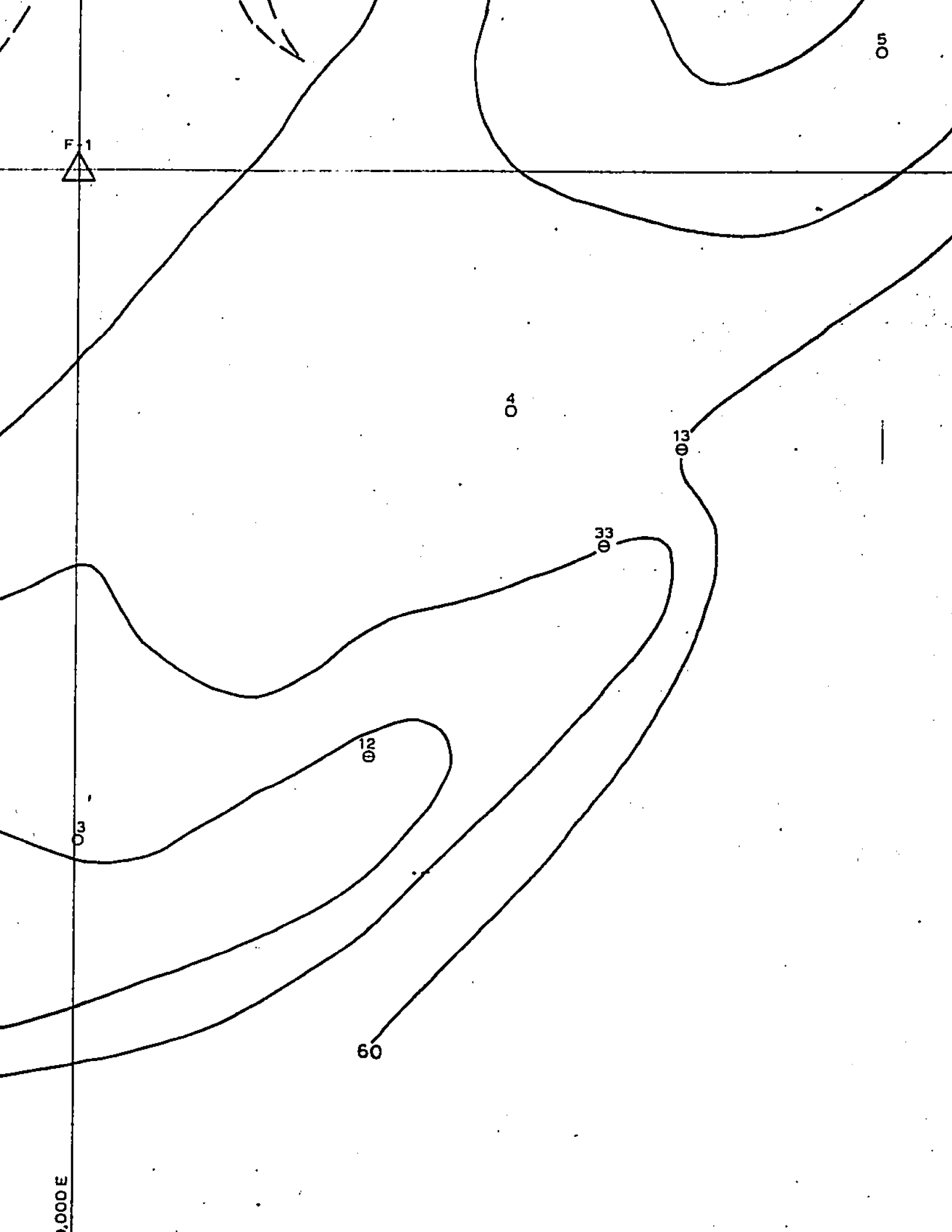
115

1D









F 1

05

04

13

33

12

03

60

1,000 E

40,000

41,000 E

**PLATE 4**

**FLAMBEAU MINING CORP.**

**ISOPACHS  
of  
SURFICIAL DEPOSITS**

**SCALE: 1" = 100'**

**CONTOUR INTERVAL: 5 ft.**

**REVISIONS**

**DATA BY: ERM, EJ, JK**

**DATE: NOV. 1981**

FLAMBEAU RIVER

17

57

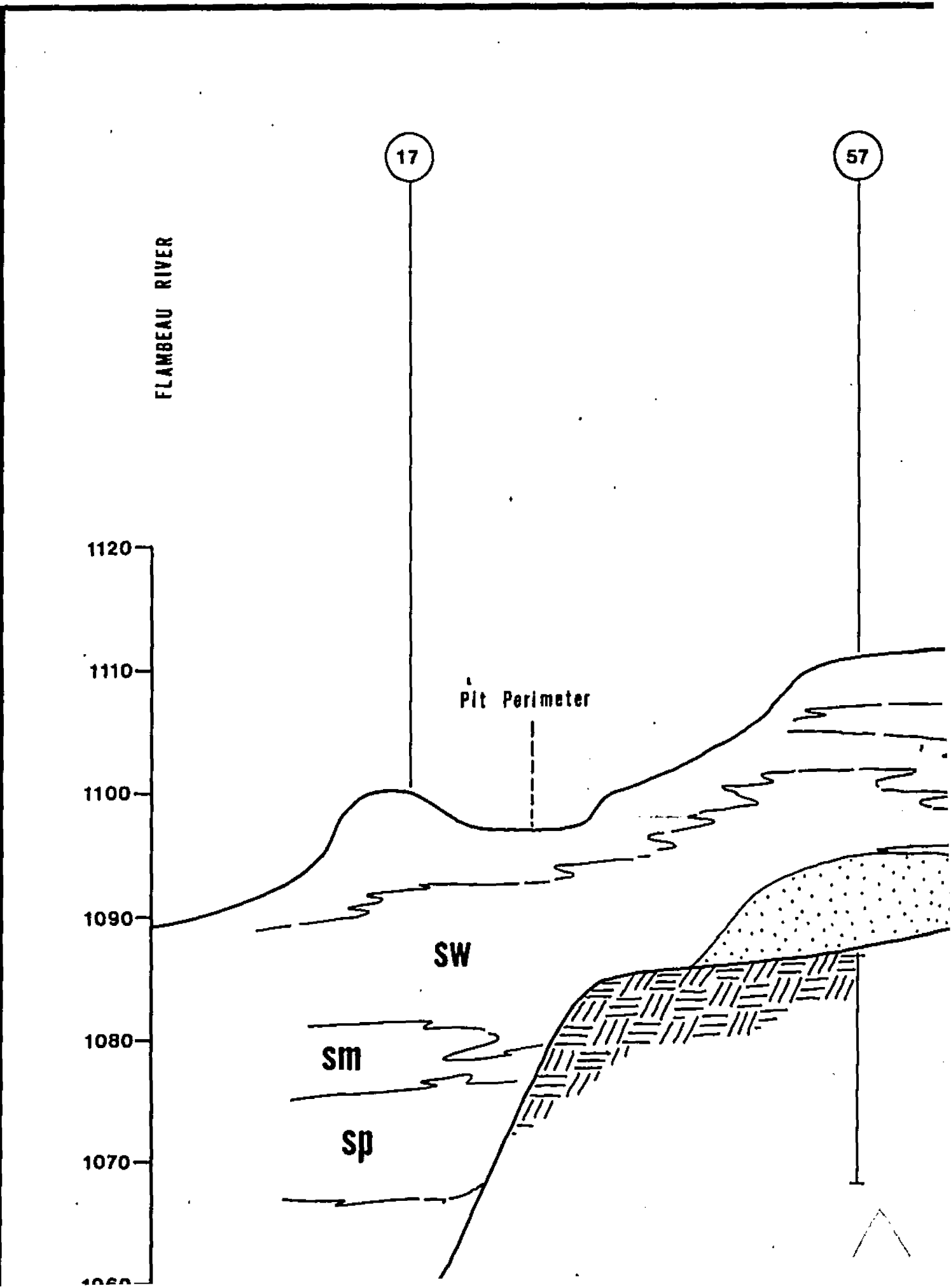
1120  
1110  
1100  
1090  
1080  
1070  
1060

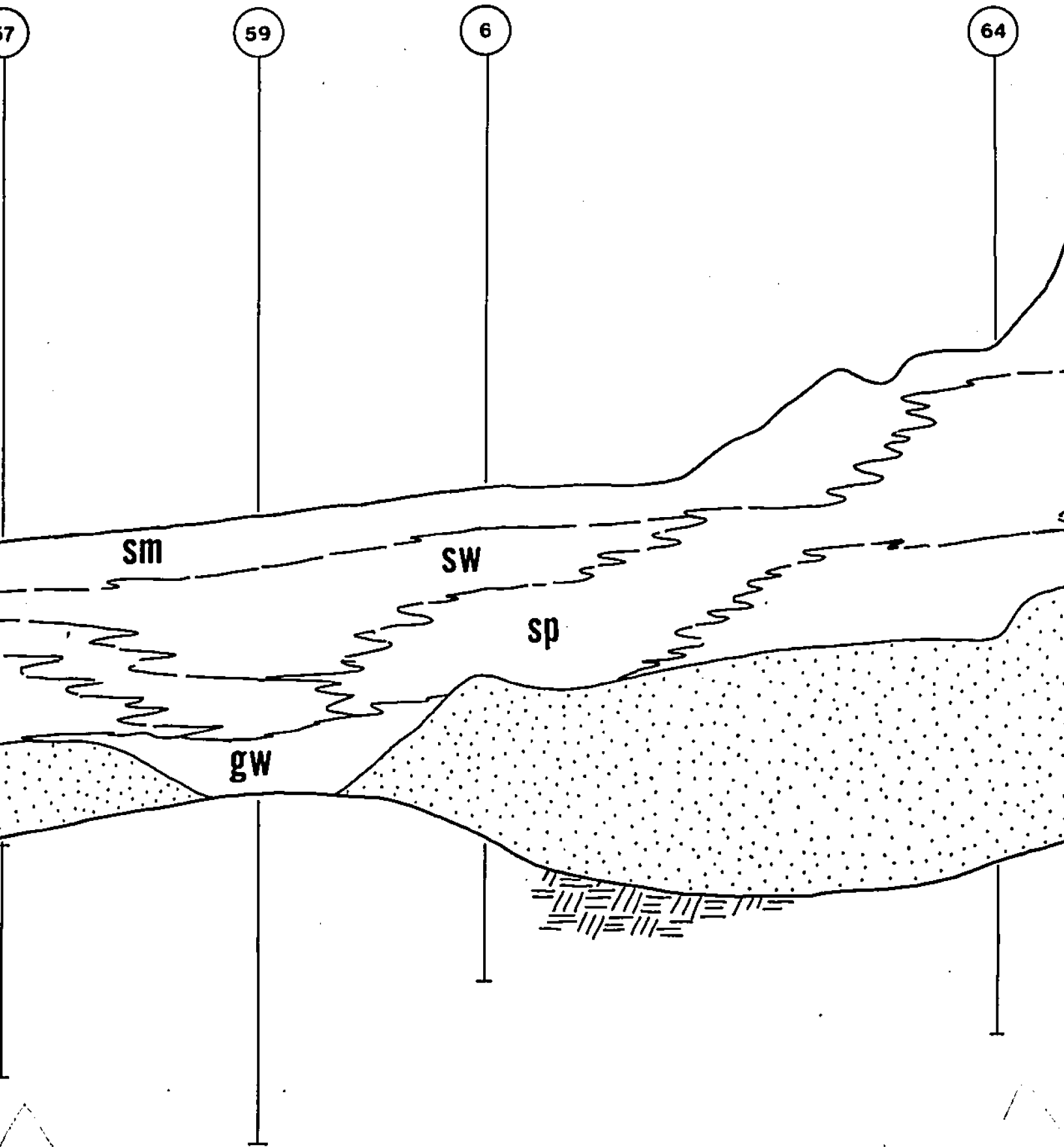
Pit Perimeter

SW

sm

sp



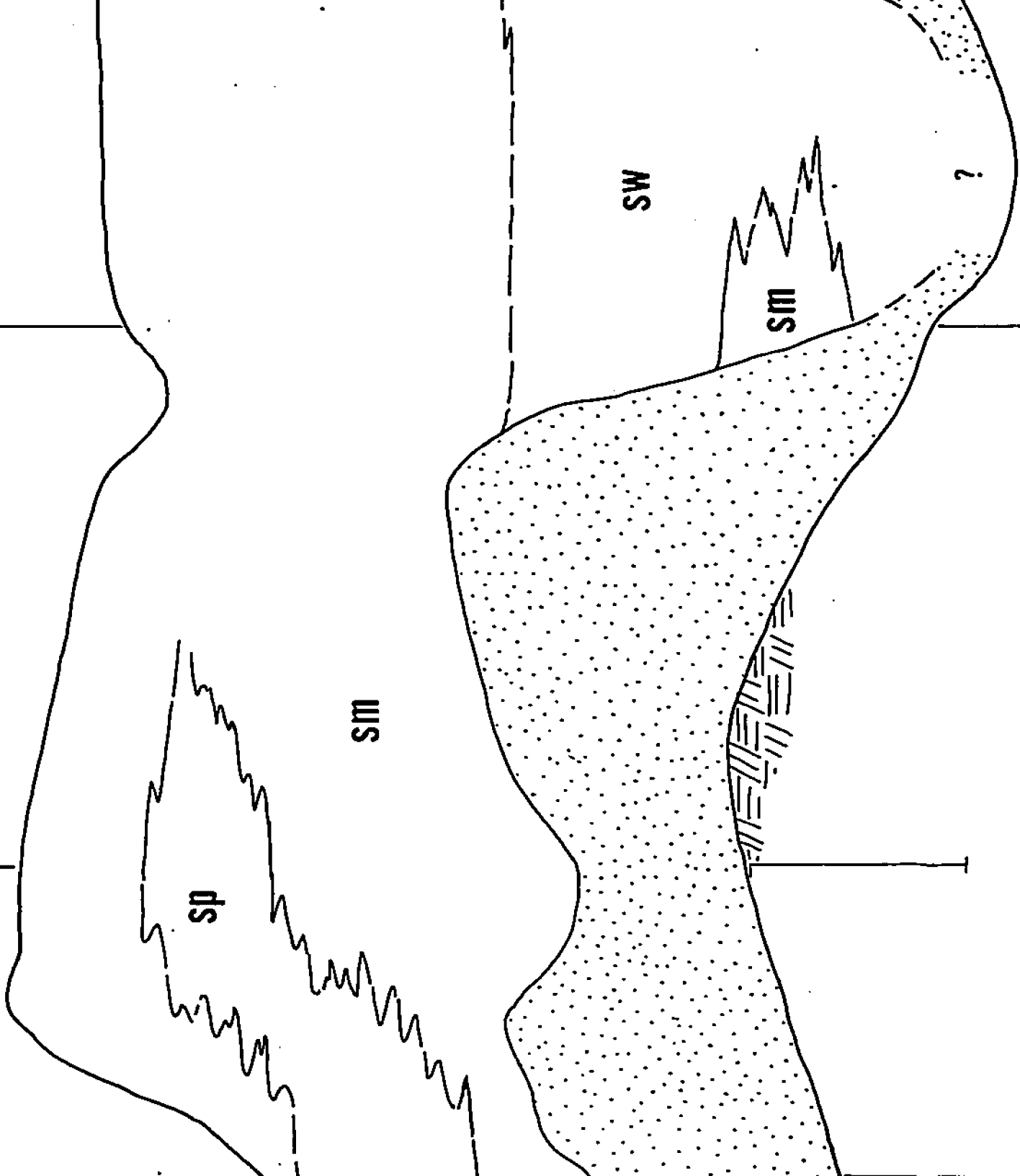




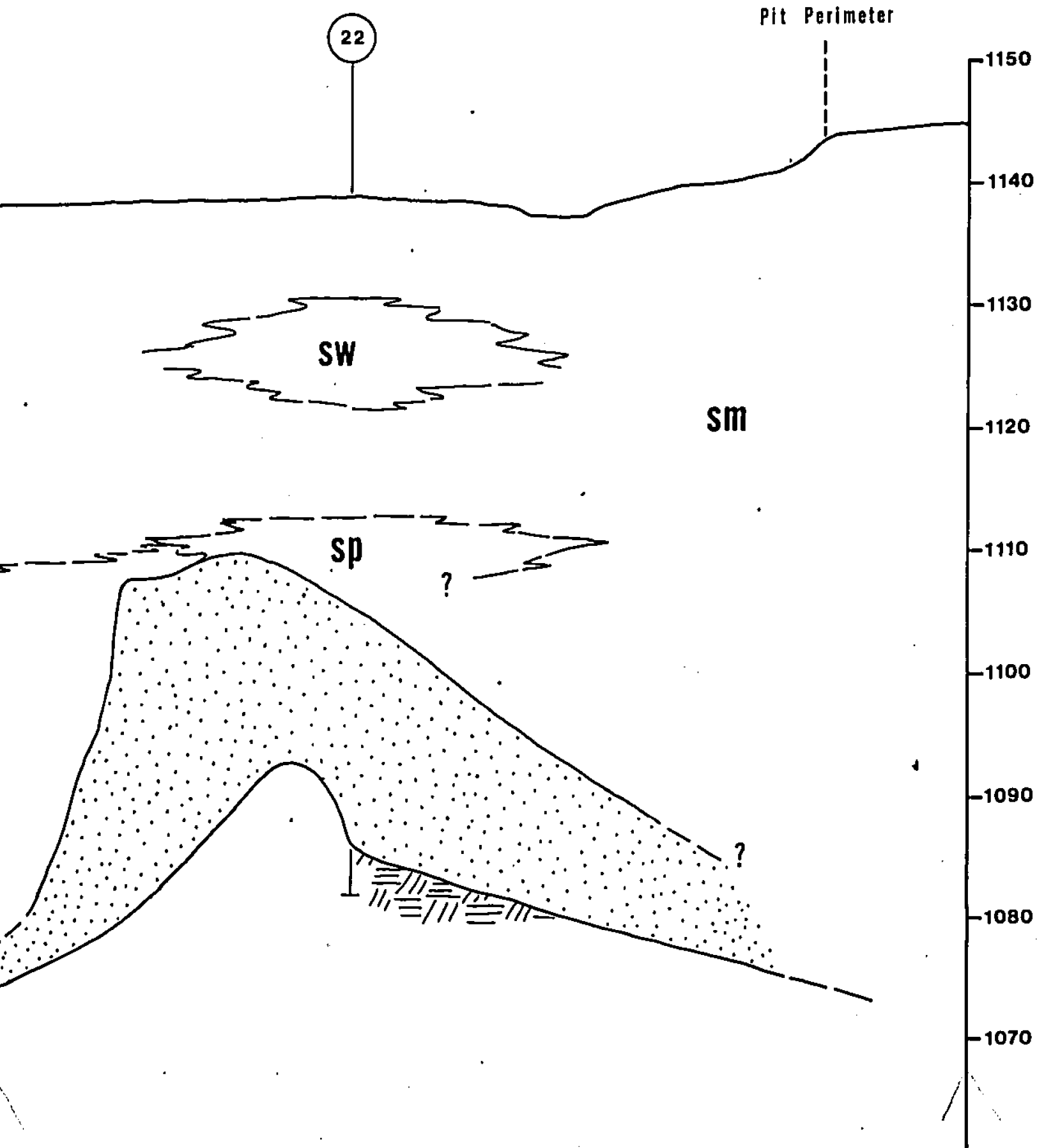
4

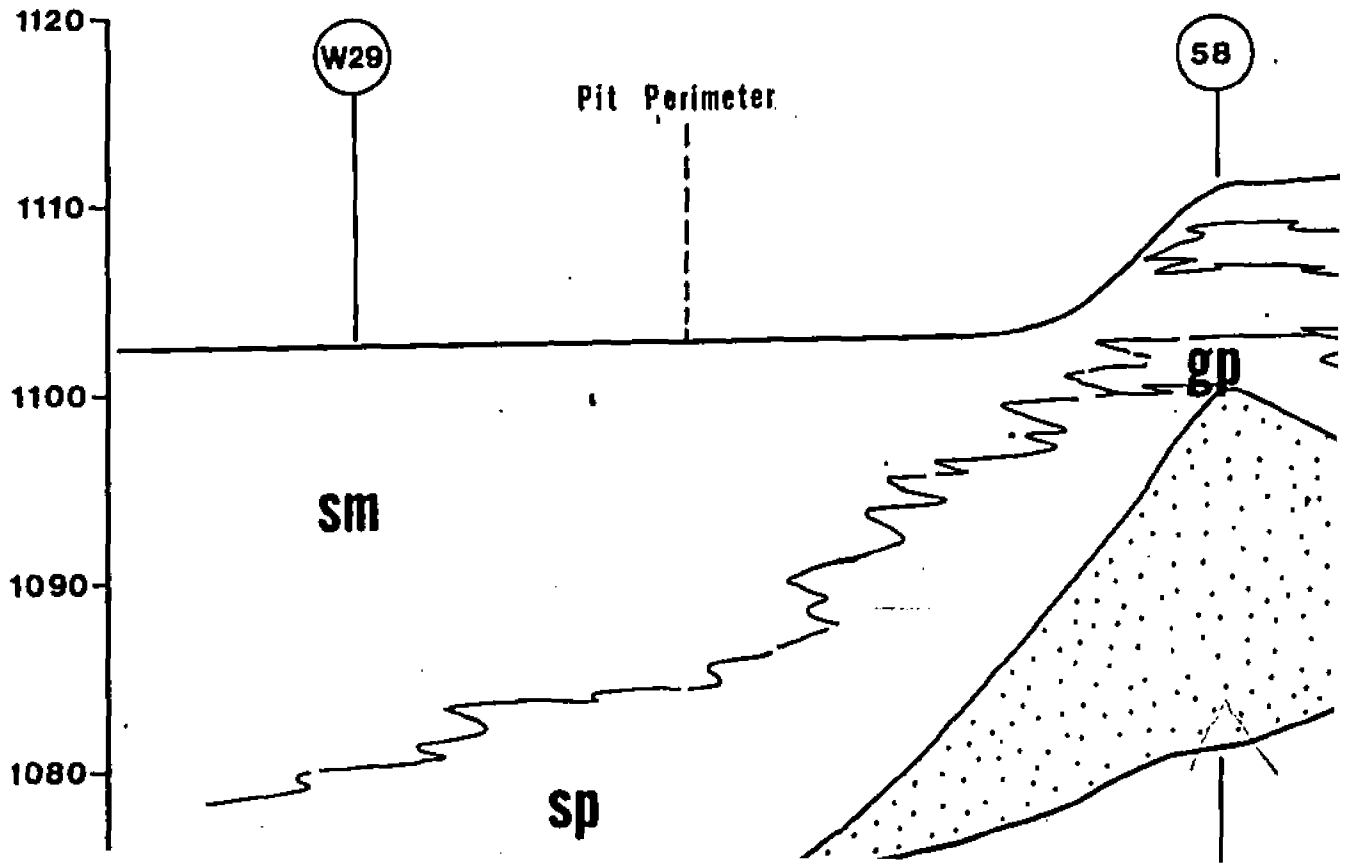
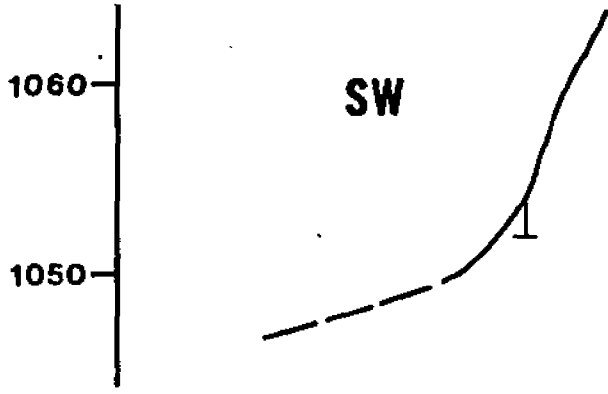
66

3

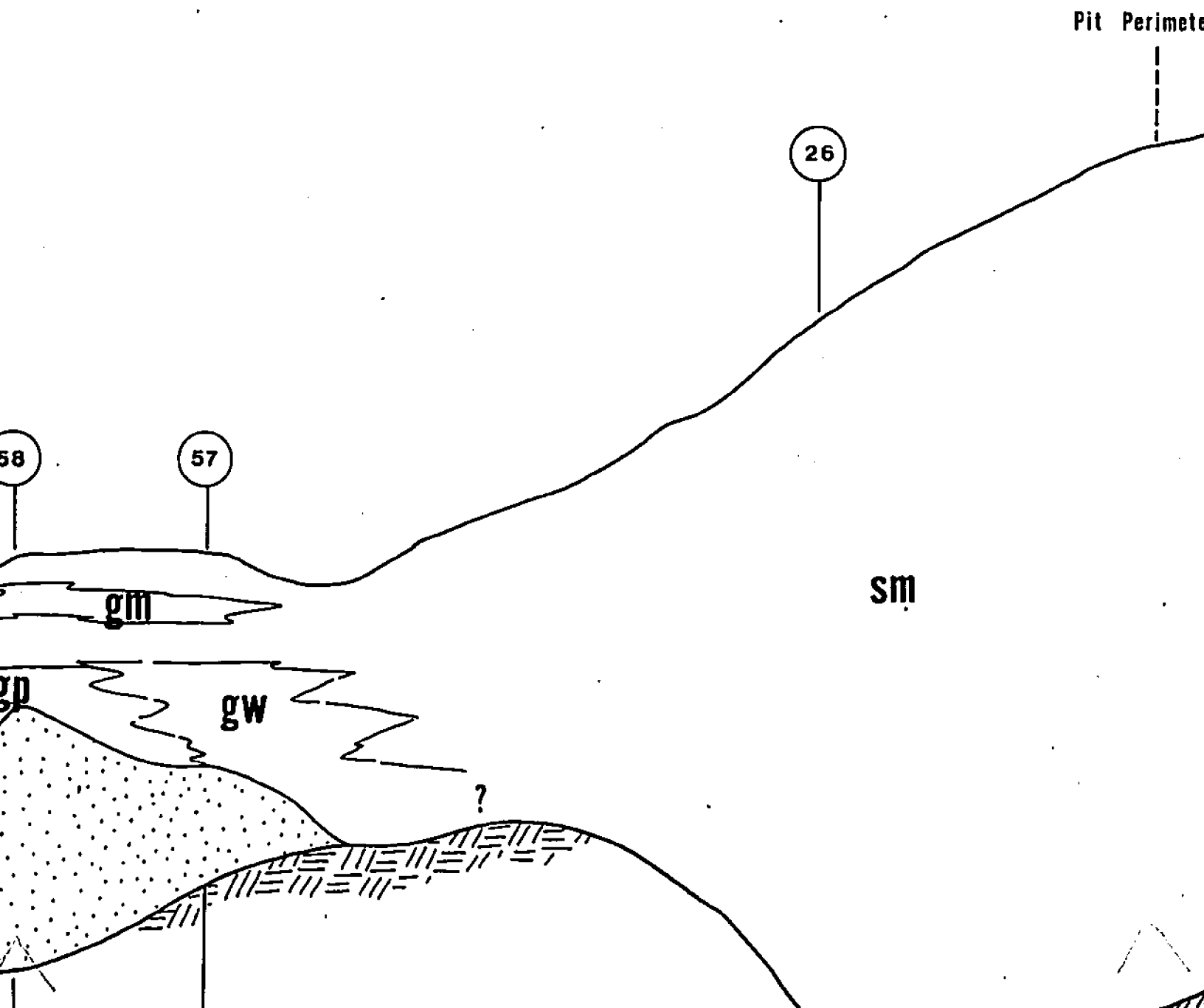


# PLATE





LONGITUDINAL SECTION A-A'



Perimeter

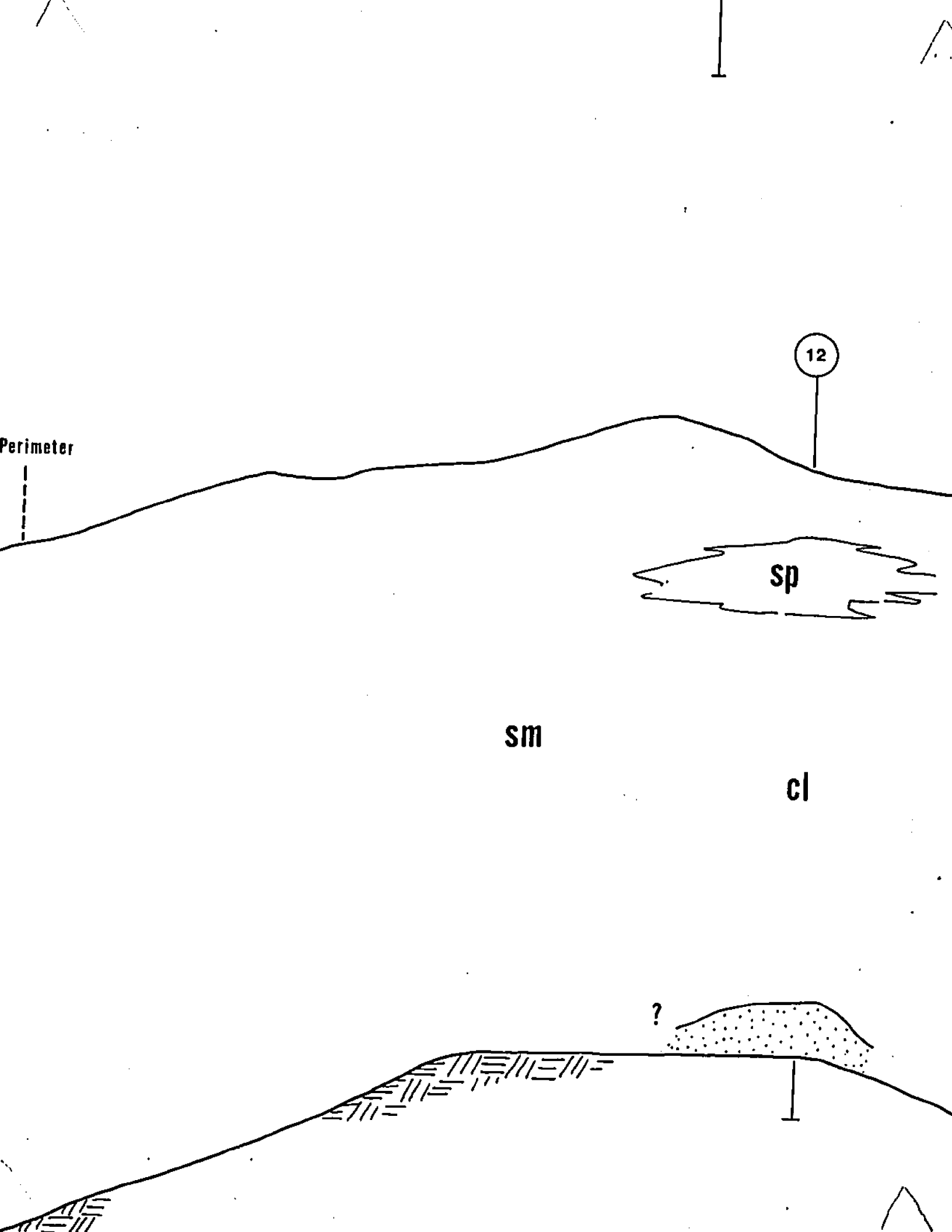
12

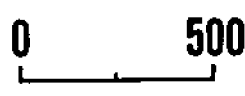
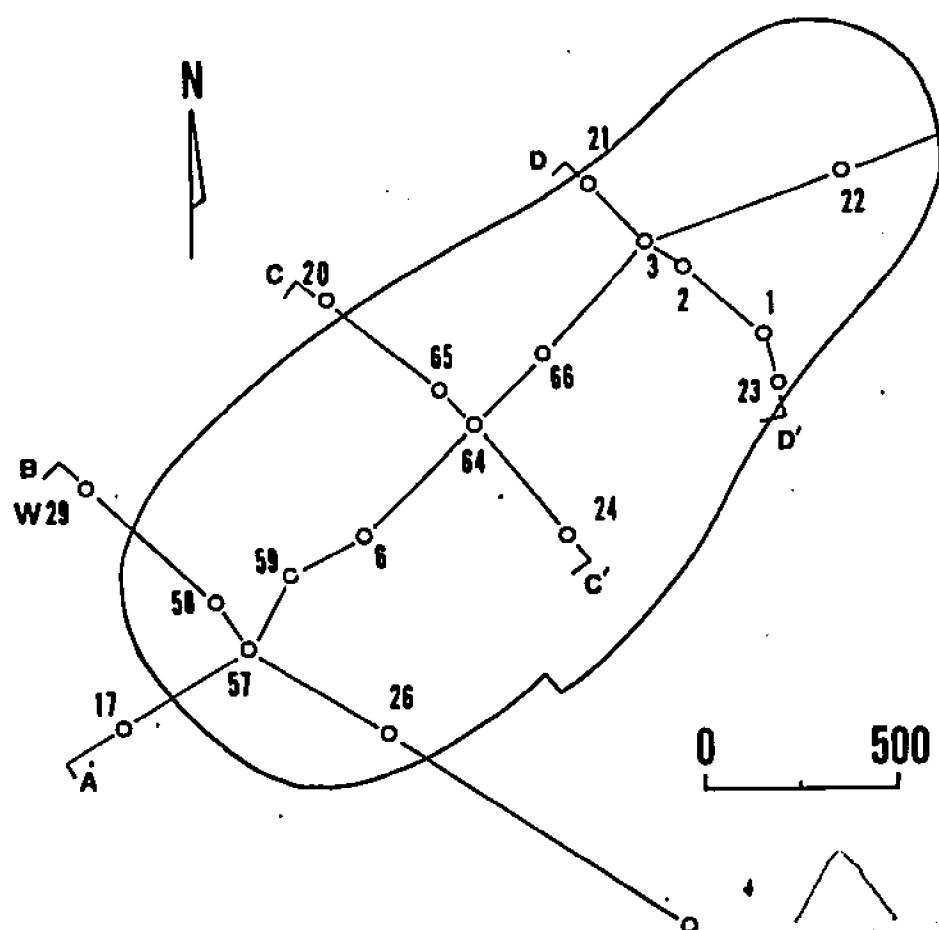
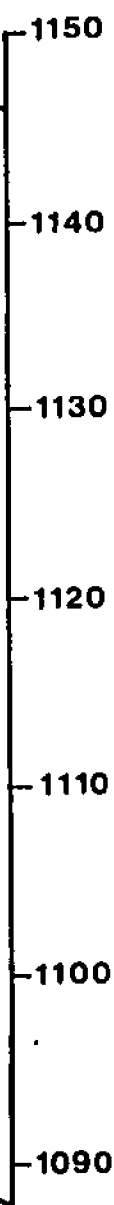
sp

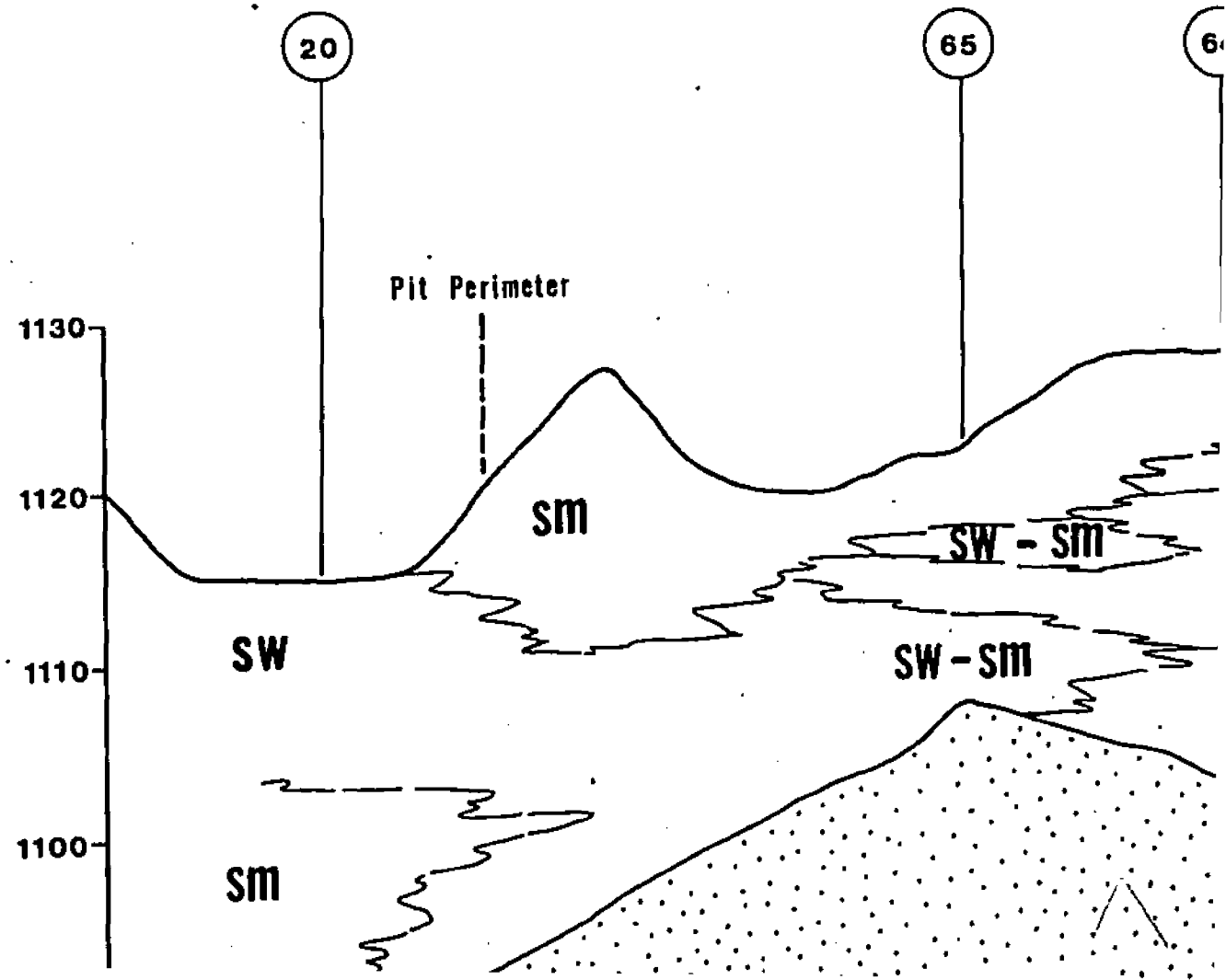
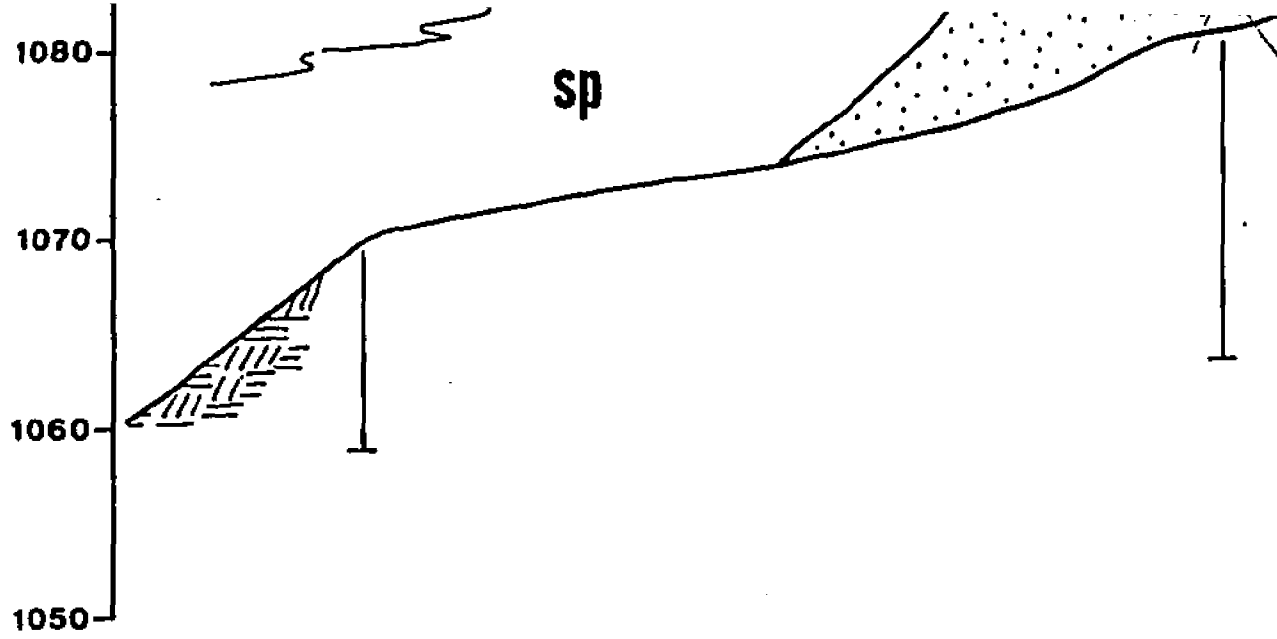
sm

cl

?

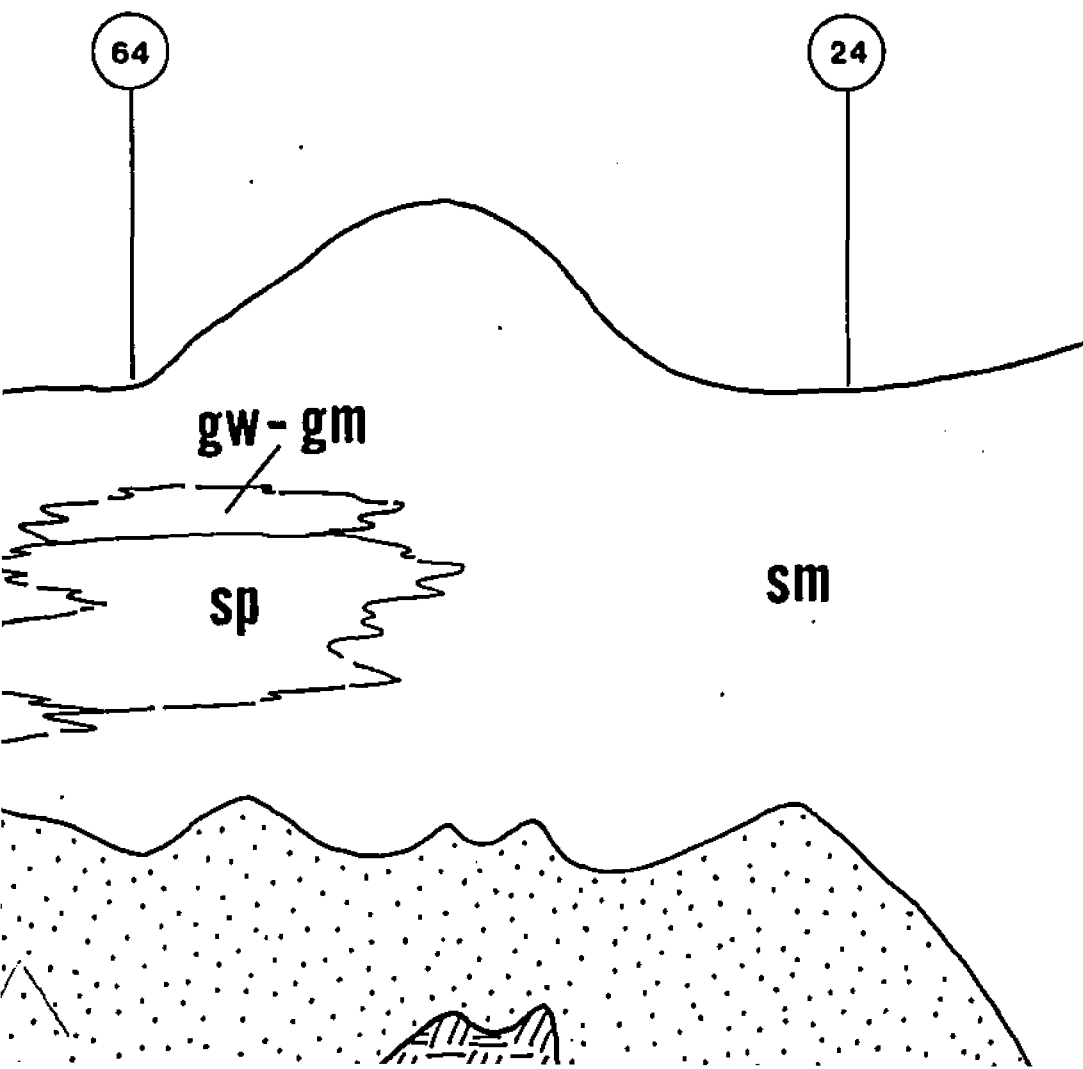




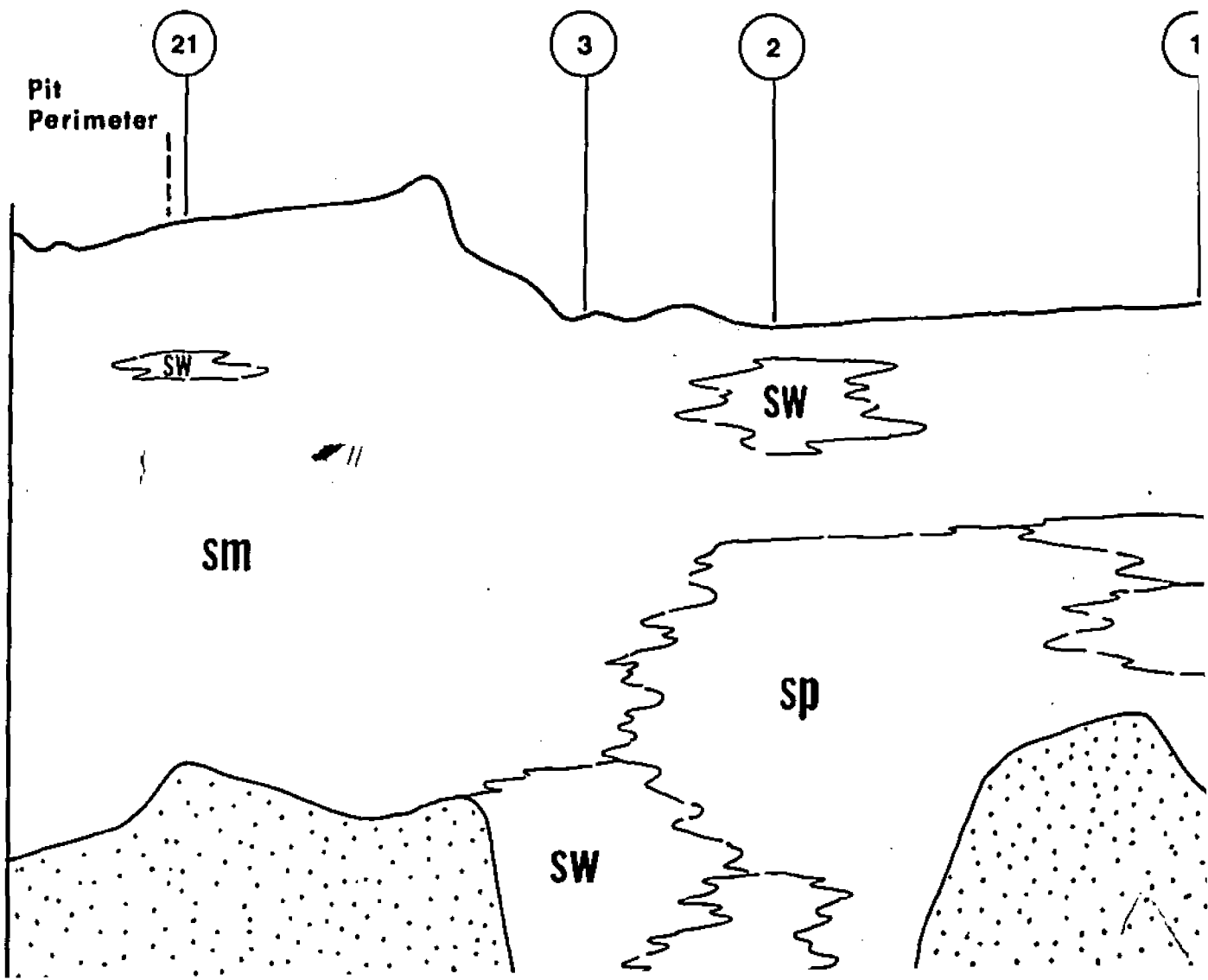




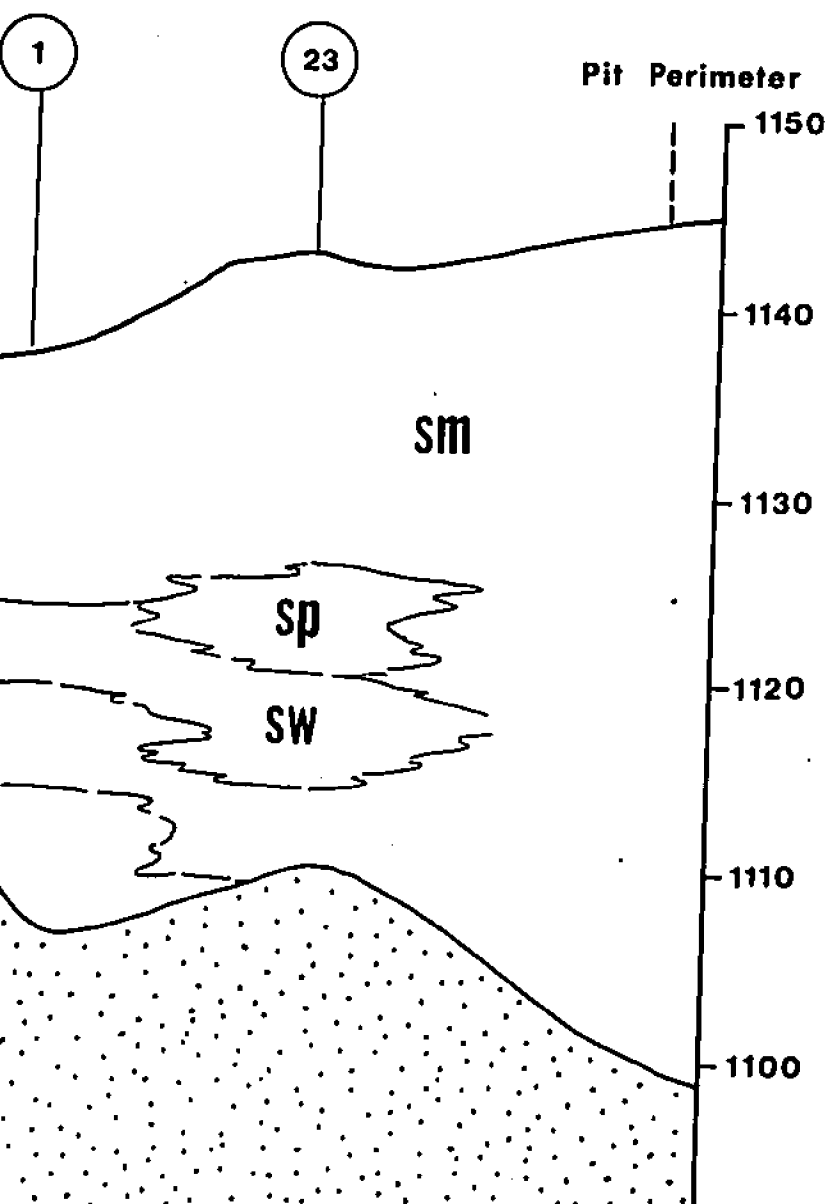
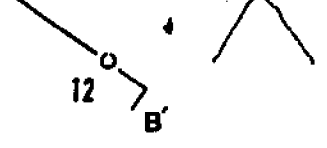
TRANSVERSE SECTION B-B'

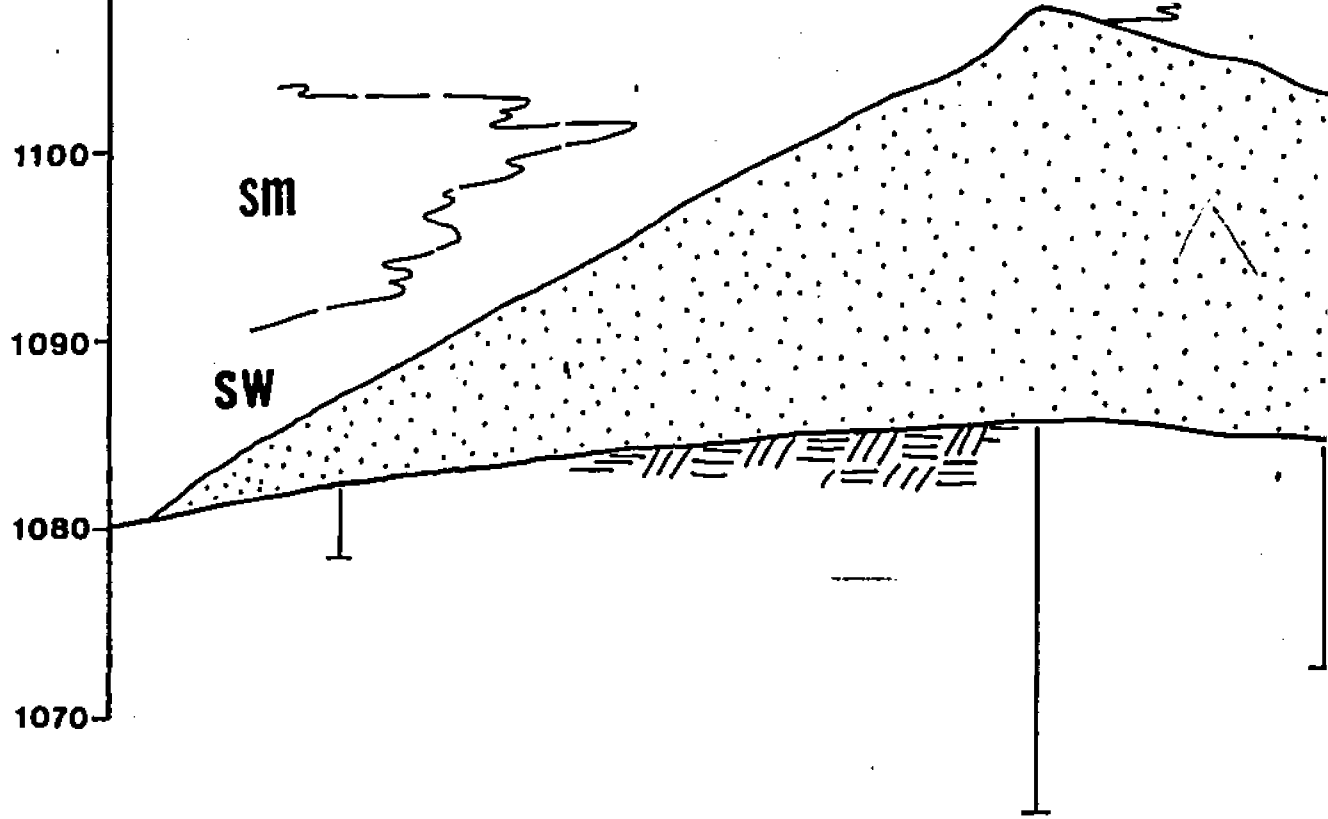






1080





**TRANSVERSE SECTION**

**KEY**



**SANDSTONE**



**SAPROLITE**

**CL**

**CLAY**

**SM**

**SILTY SAND**

**SW**

**GRADED SAND**

**(57)**

**BORING**

**SP**

**SORTED SAND, GRAVEL**

**GW**

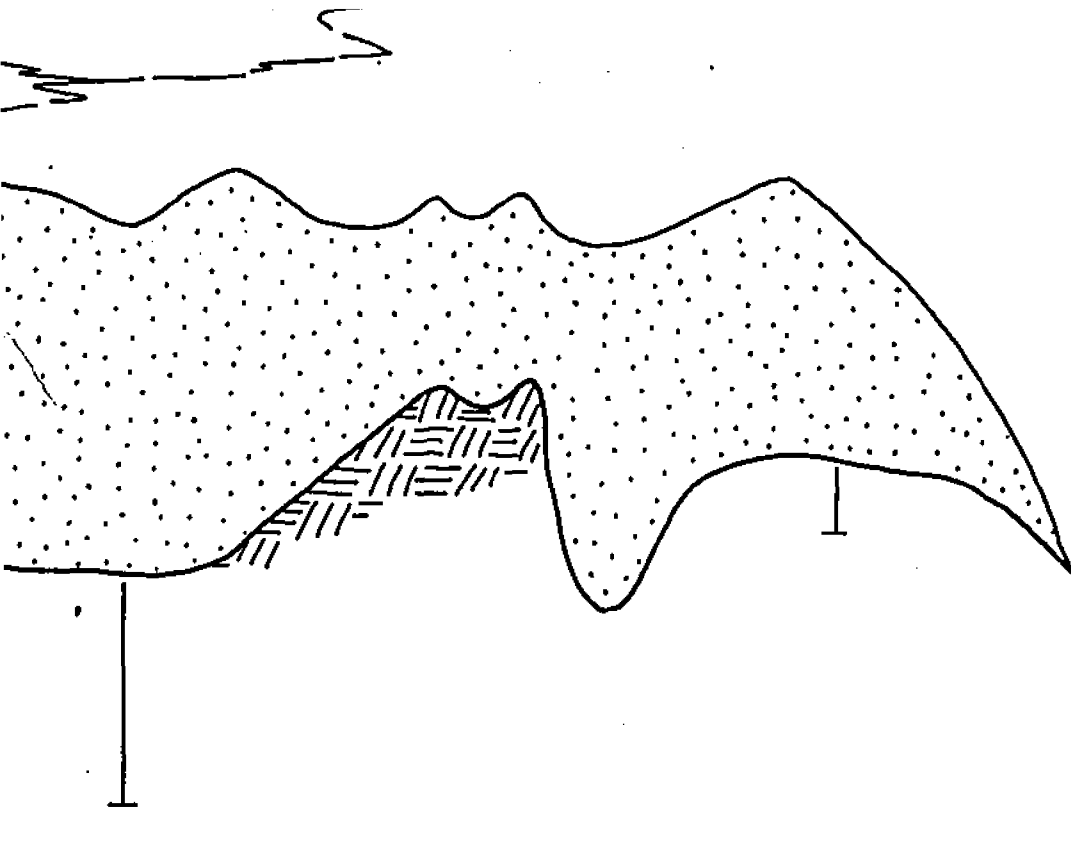
**GRADED GRAVEL, SAND**

**GM**

**SILTY GRAVEL**

**GP**

**SORTED GRAVEL, SAND**



SECTION C-C'

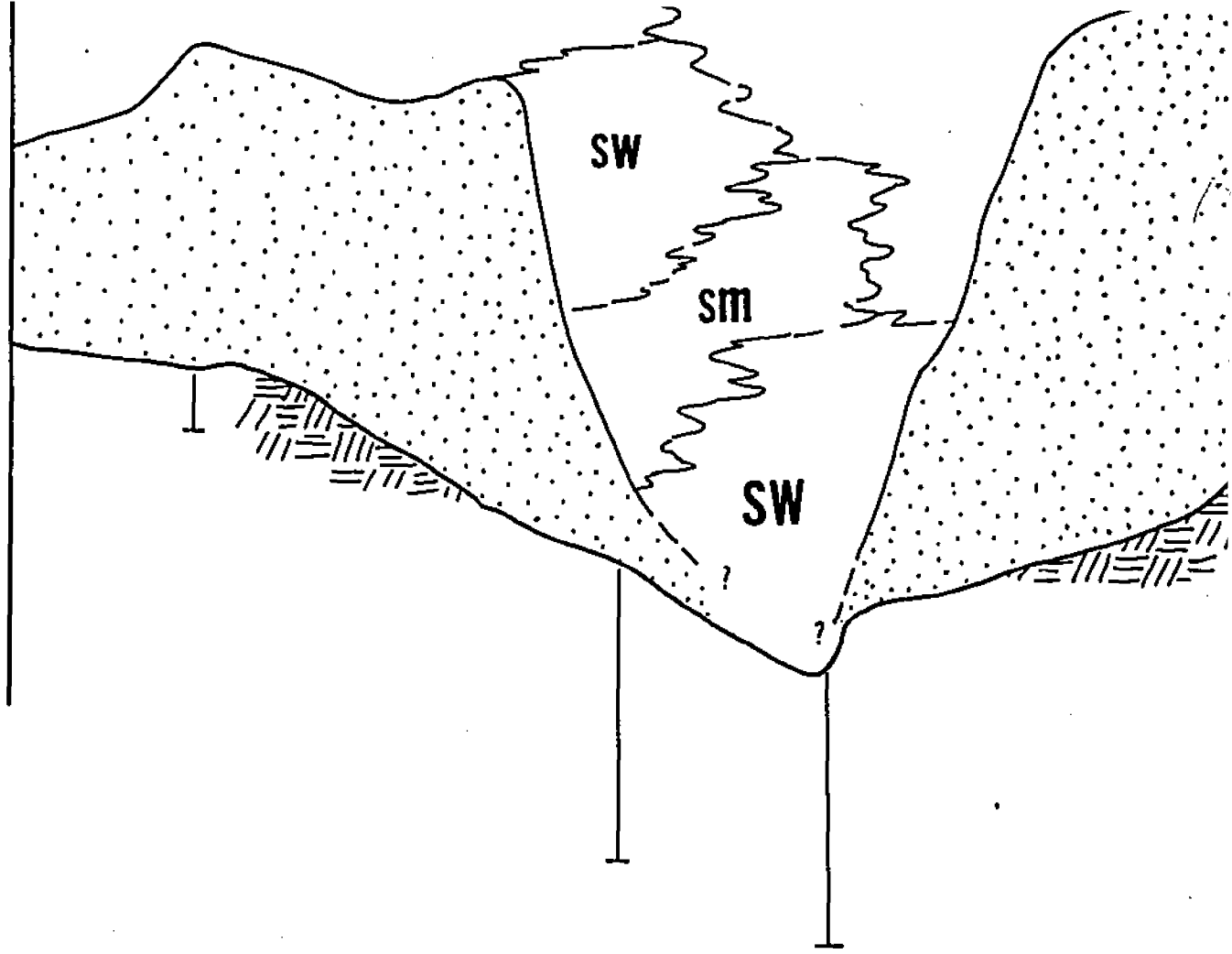
CLAY

BORING

ND

HORIZONTAL

1 IN = 100



TRANSVERSE    SECTION    D-D'

TOTAL SCALE:

= 100 FT

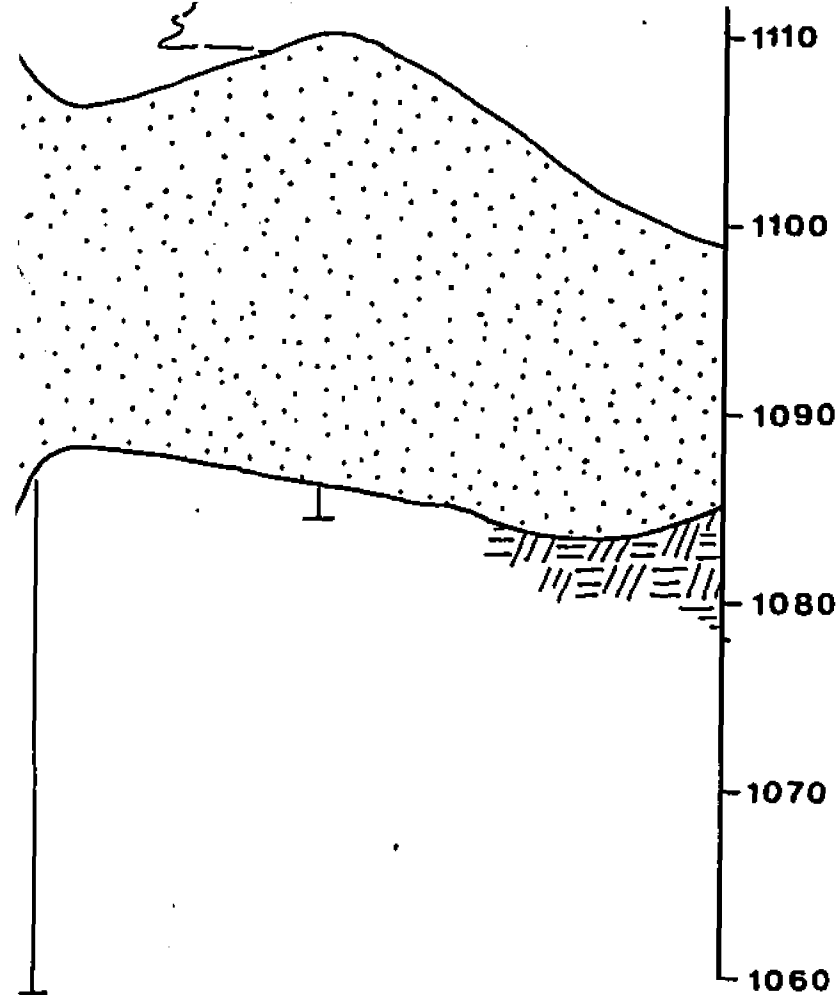
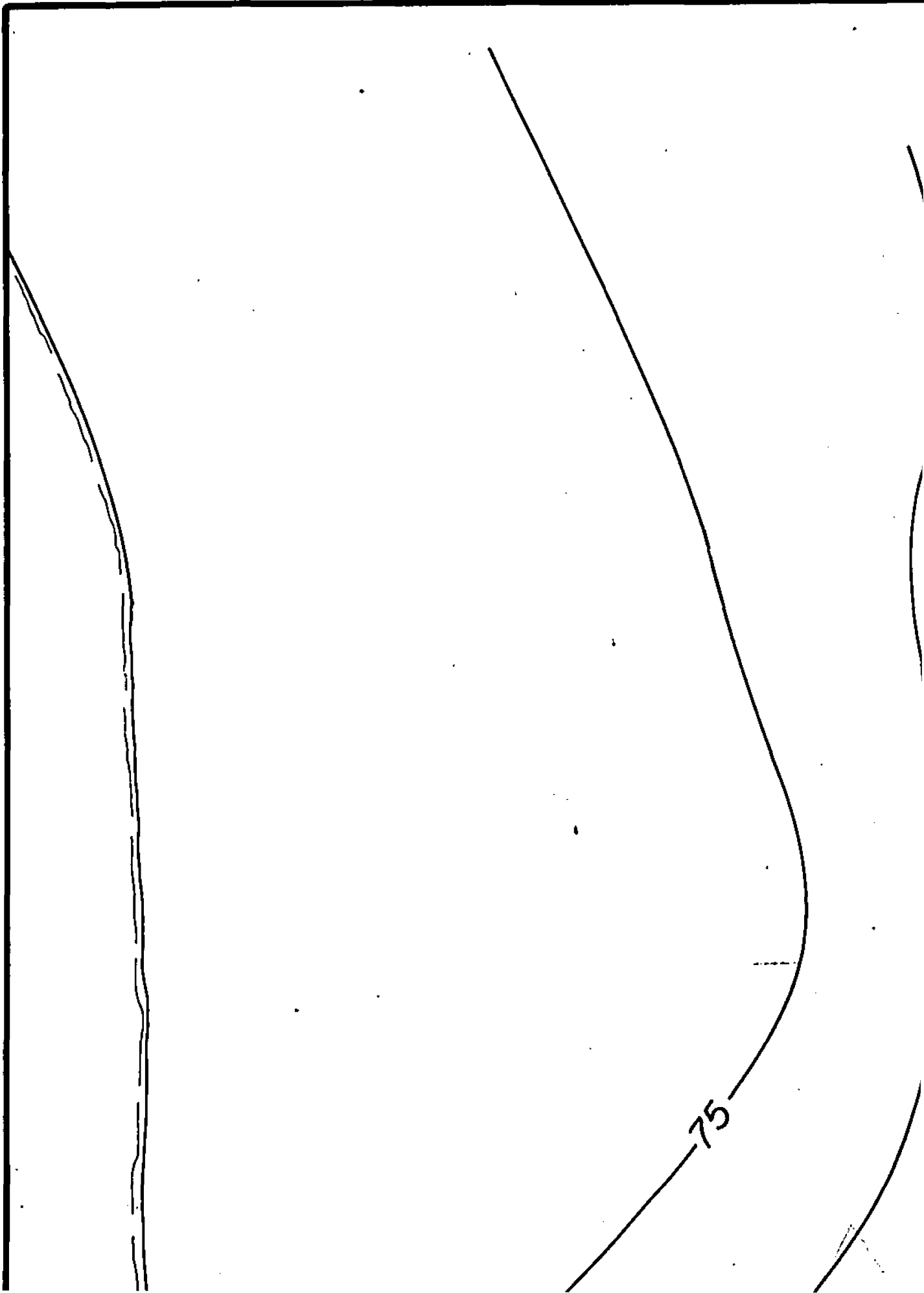


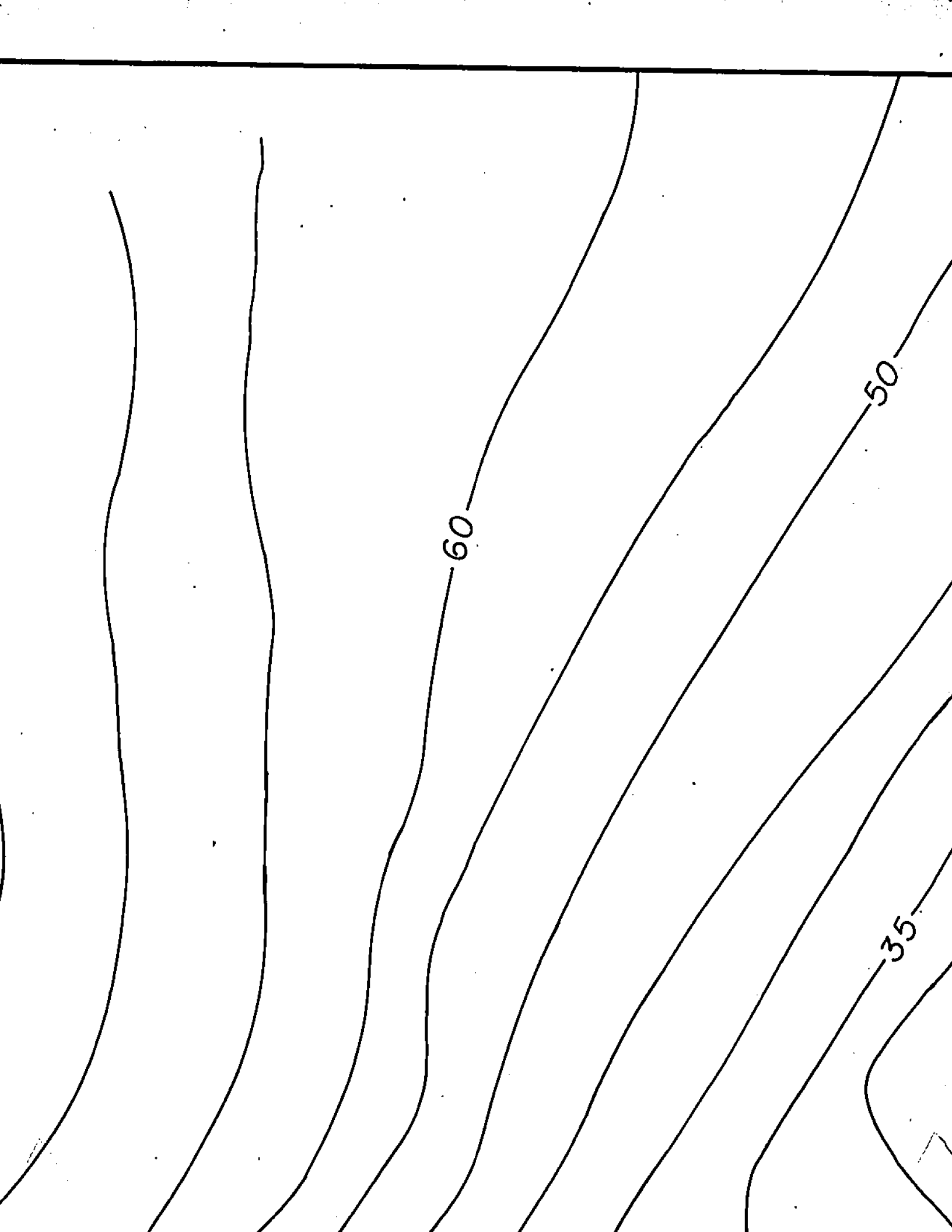
PLATE 5

GEOLOGIC CROSS SECTIONS  
PIT AREA - FLAMBEAU SITE

From unpubl. data, Flambeau Mining Corp.

J. M. King, 19



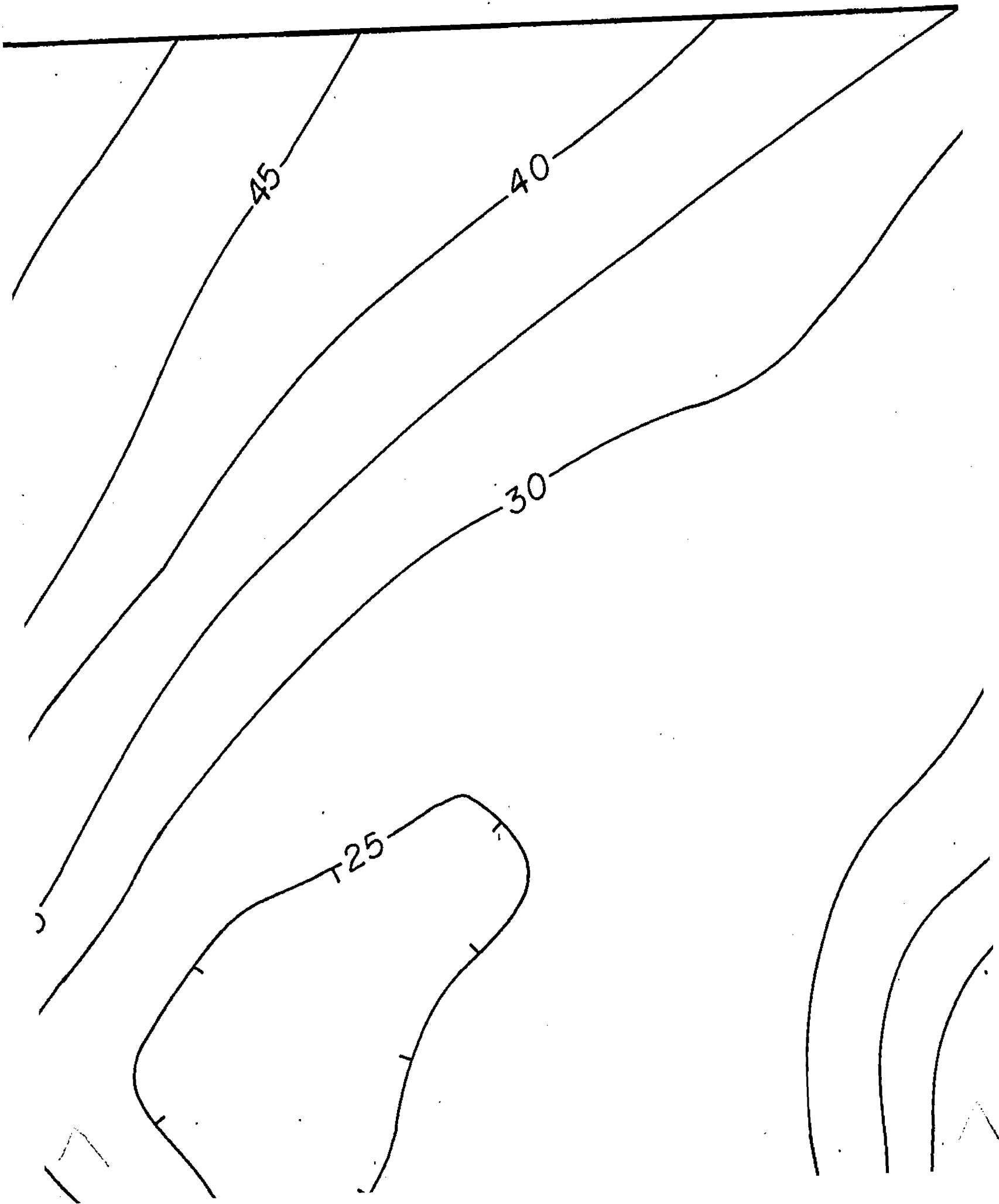


60

50

35





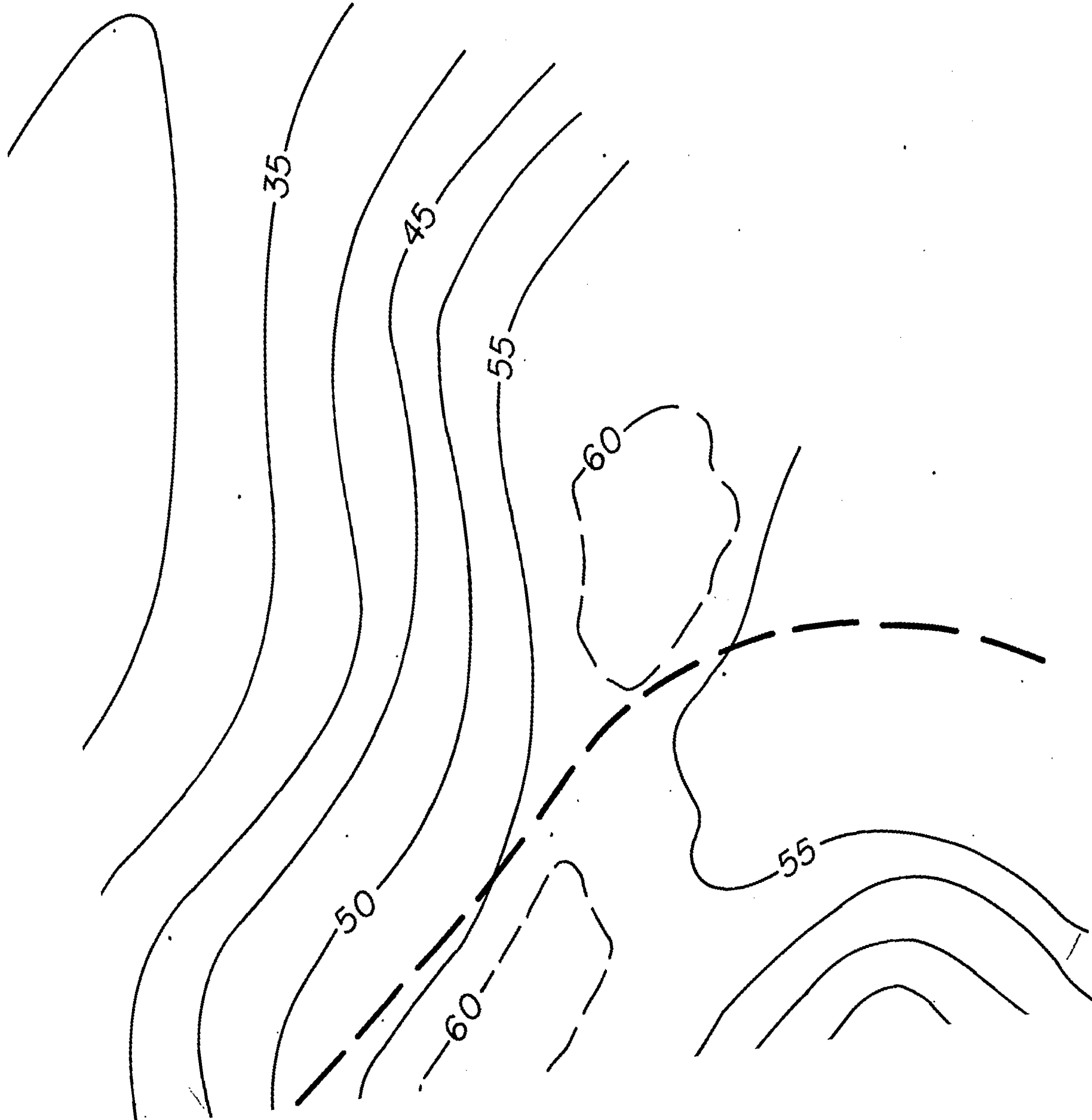
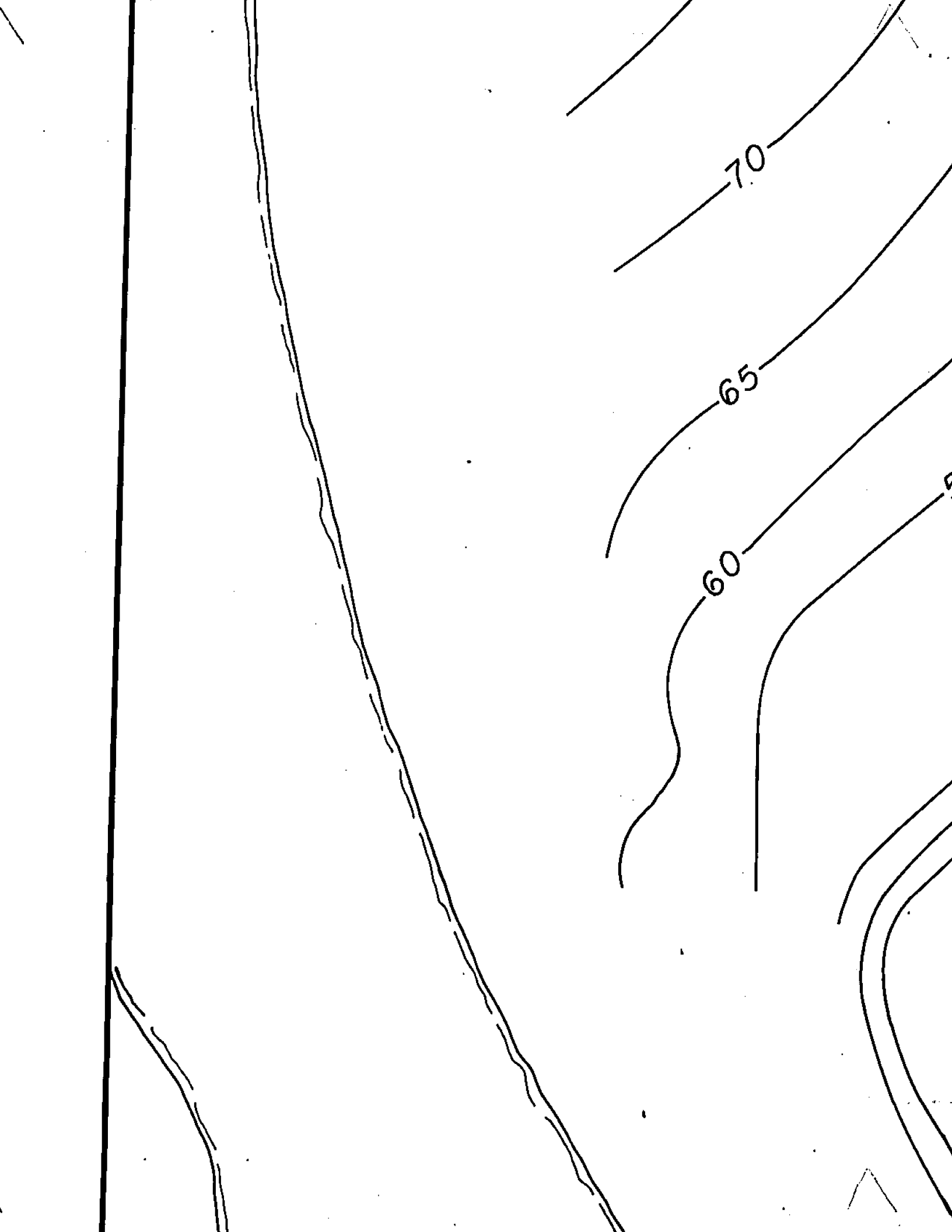
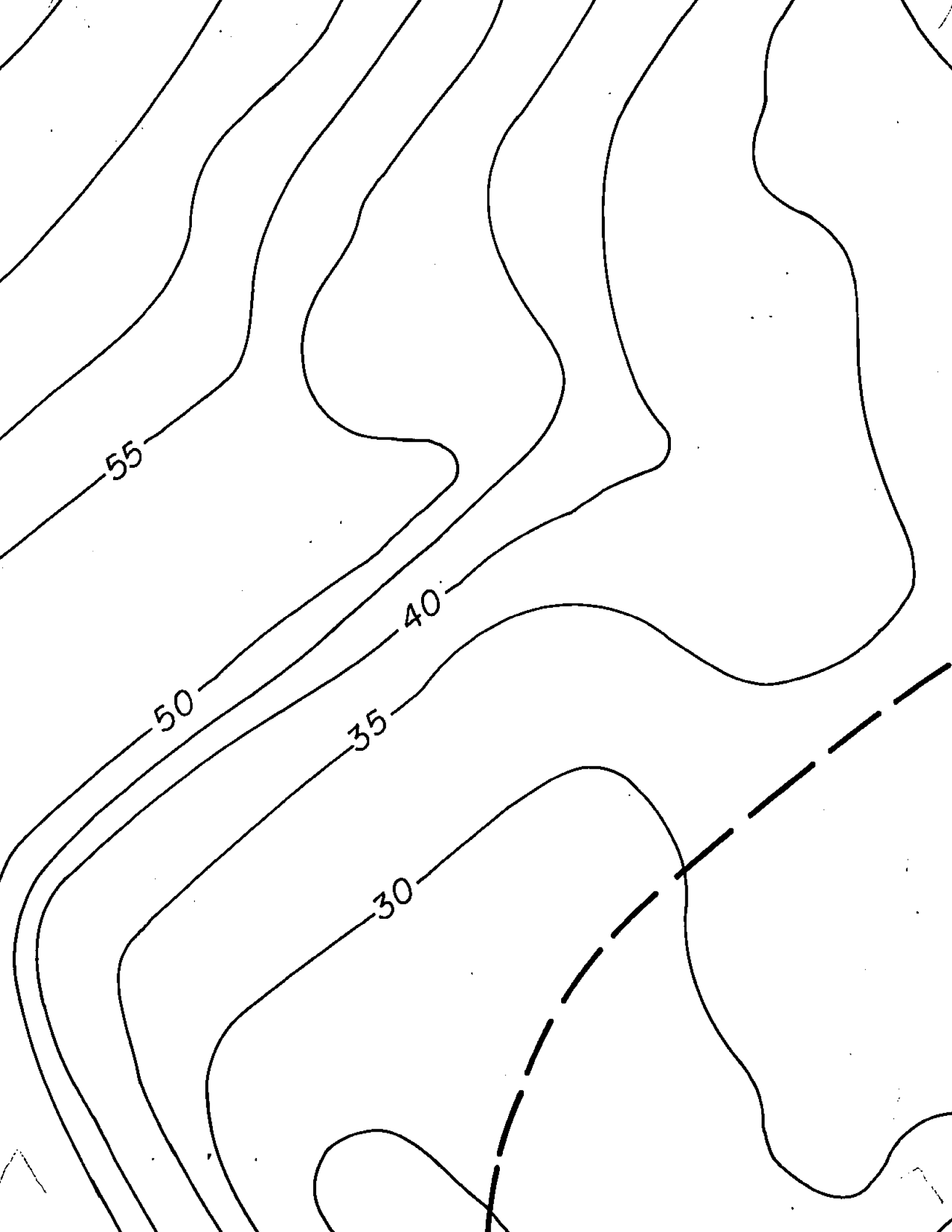


PLATE 6







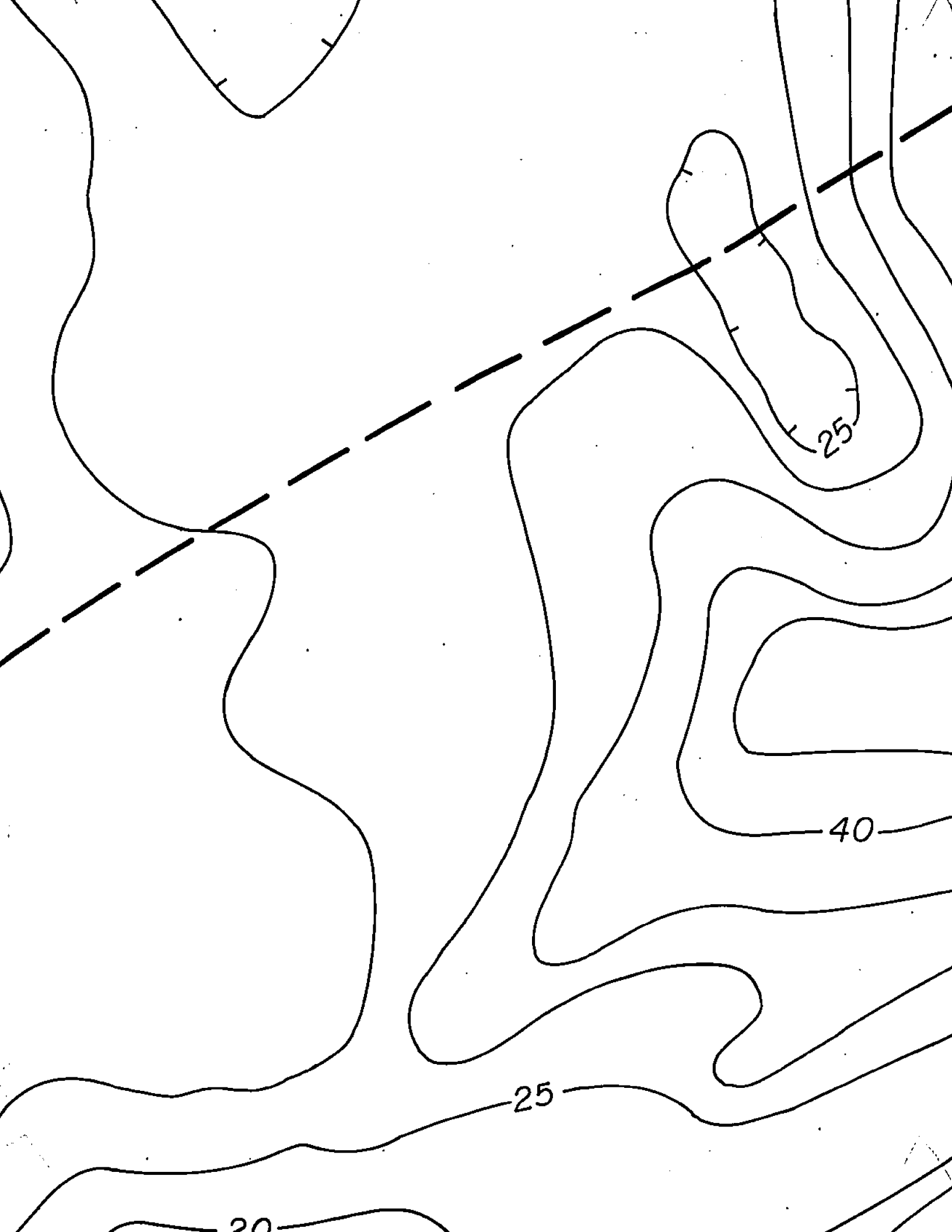
55

50

35

40

30

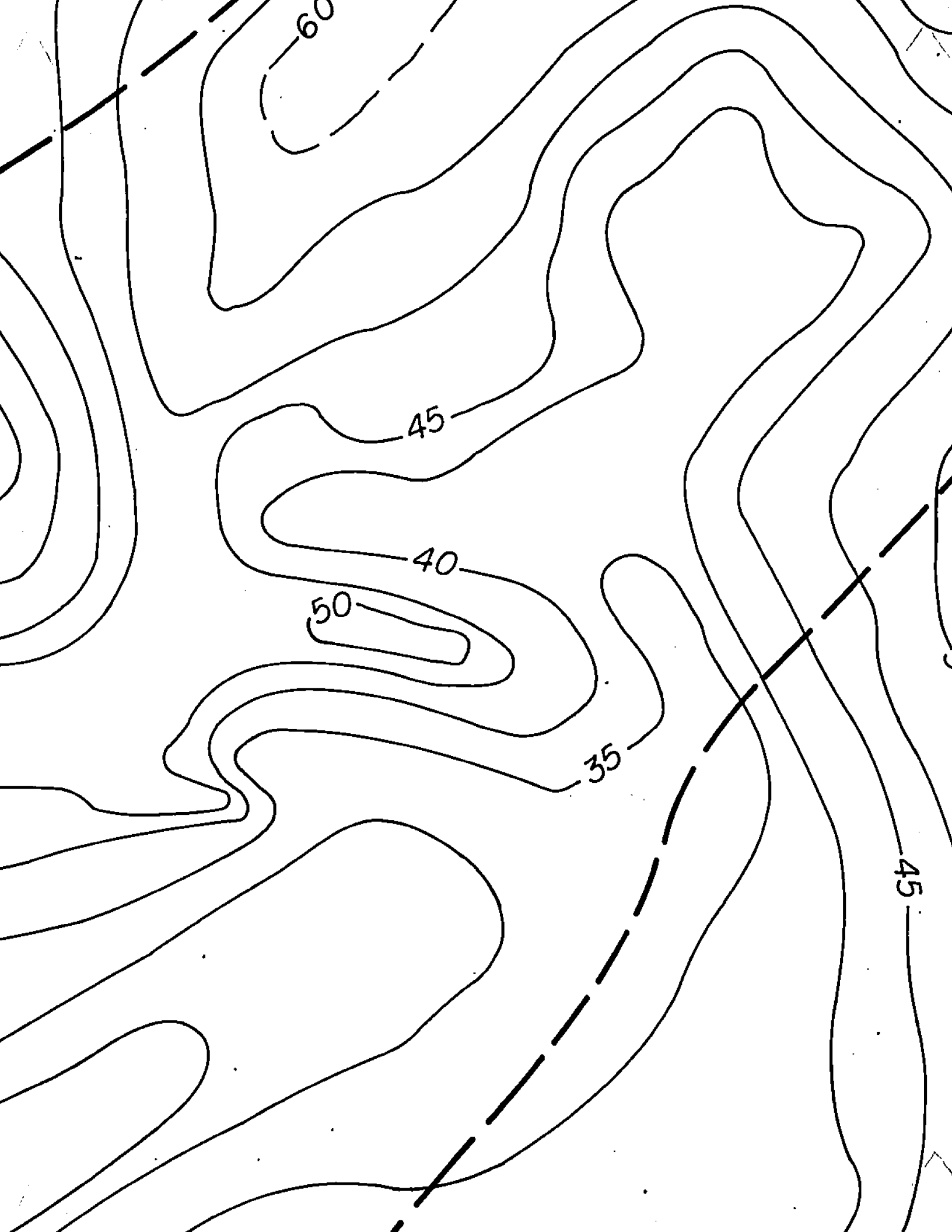


25

40

25

20



60

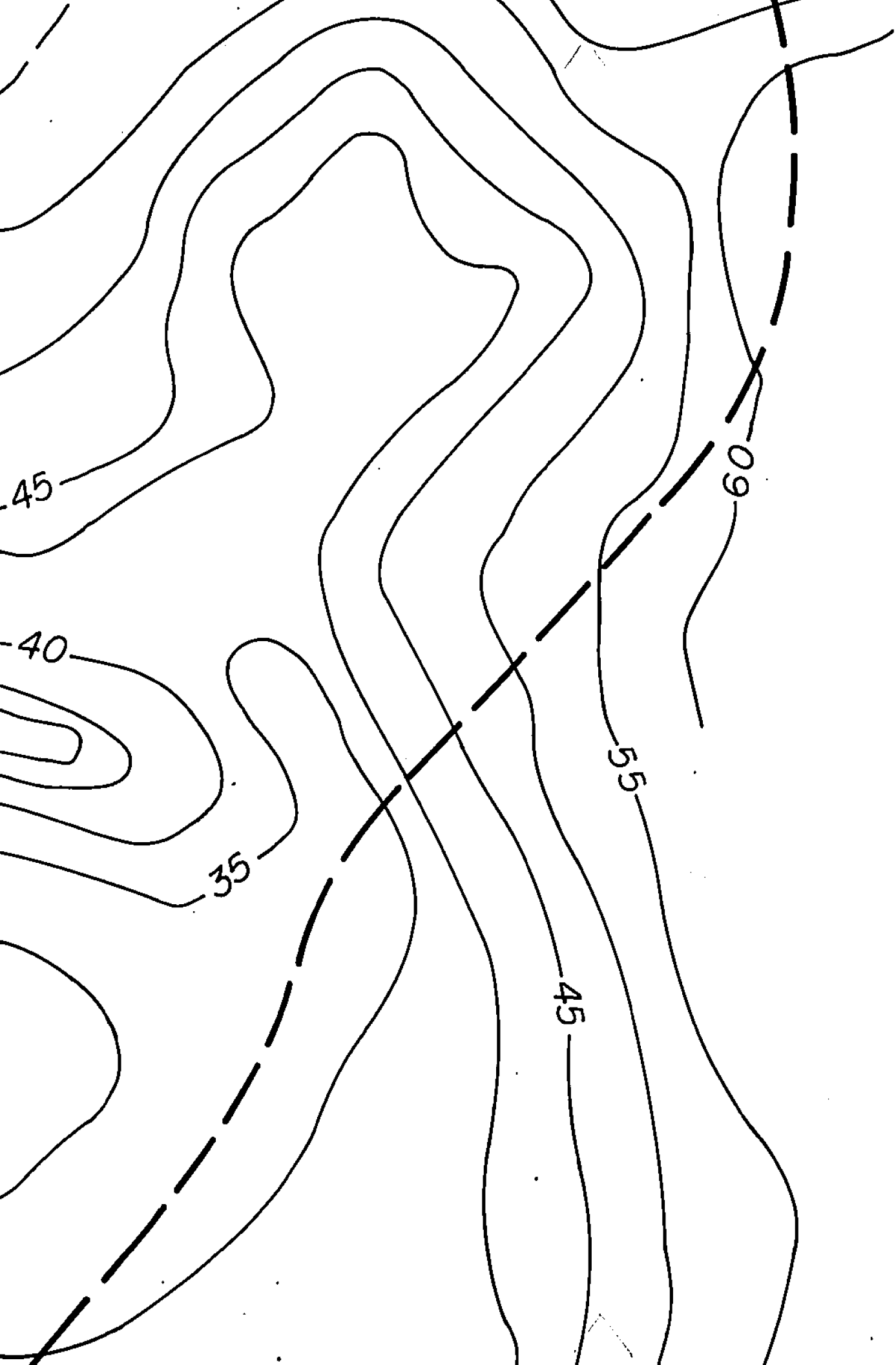
45

40

50

35

45

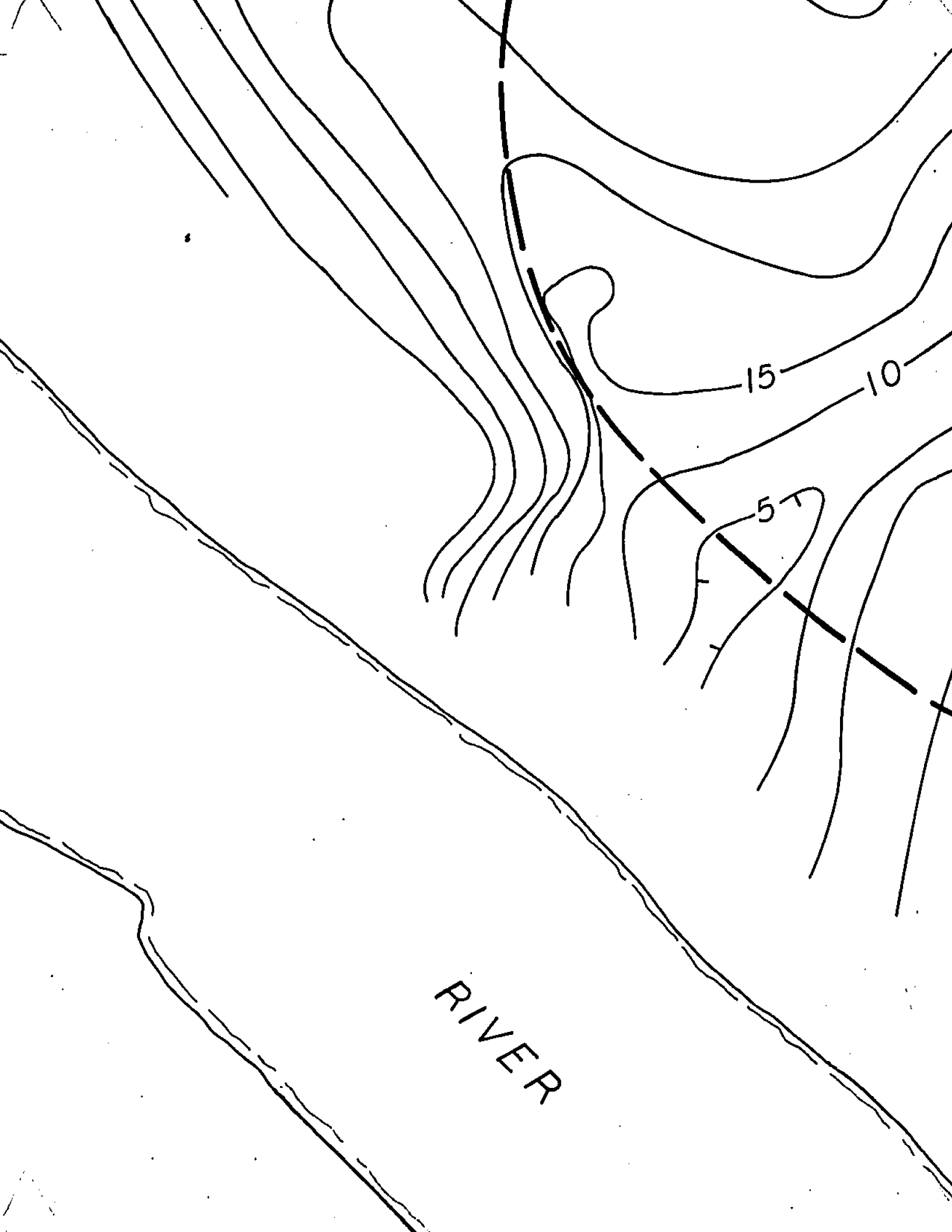




FLAMBEAU

N



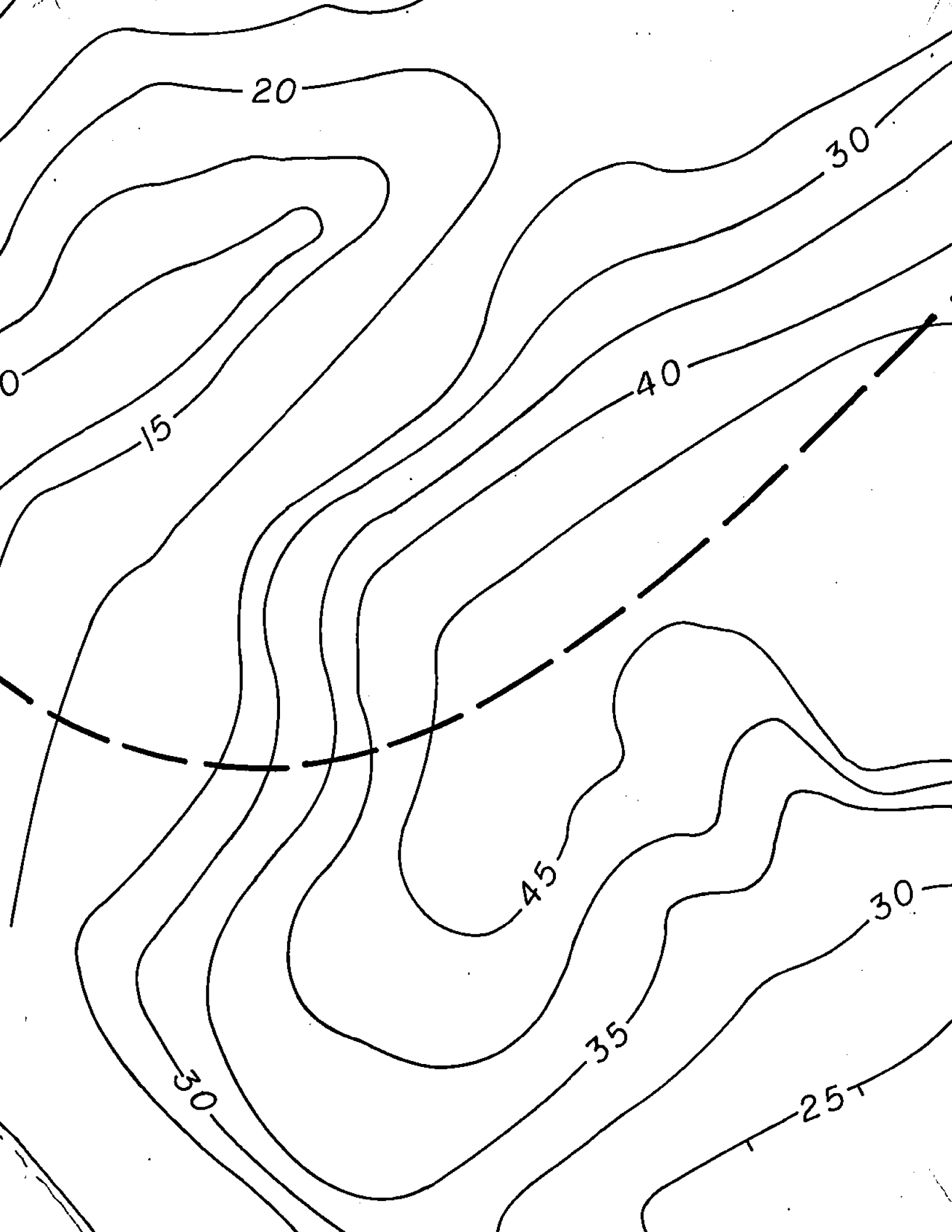


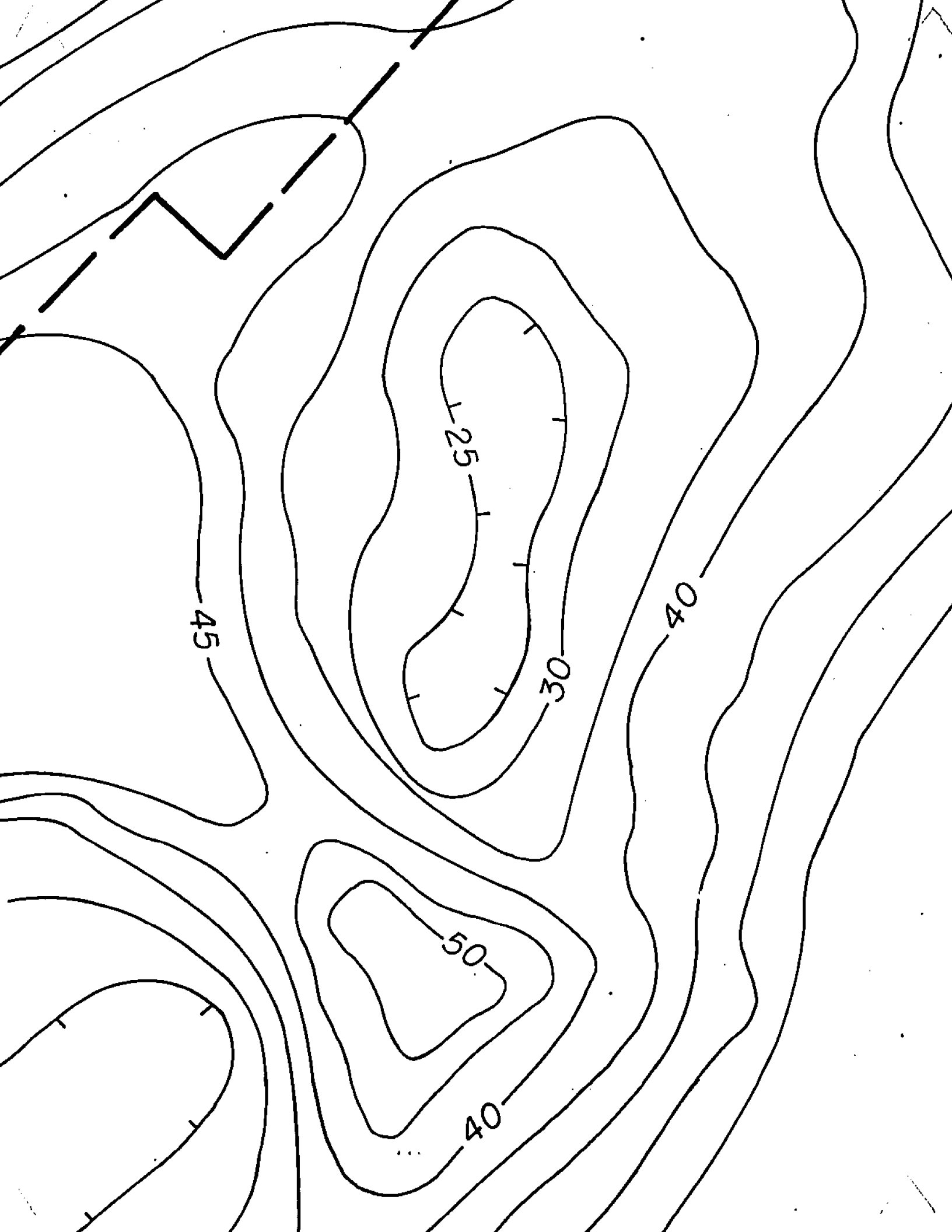
RIVER

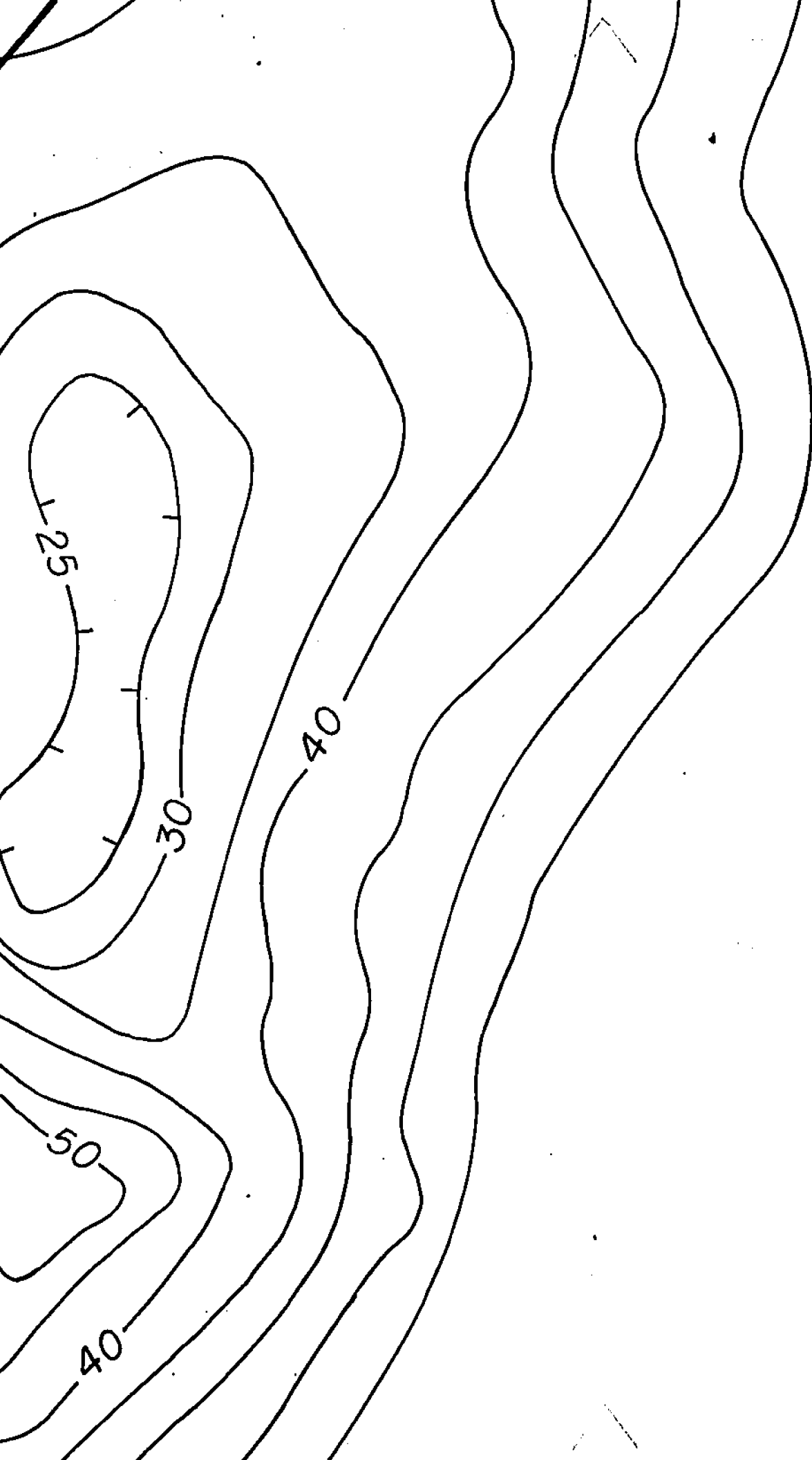
15

10

5







N



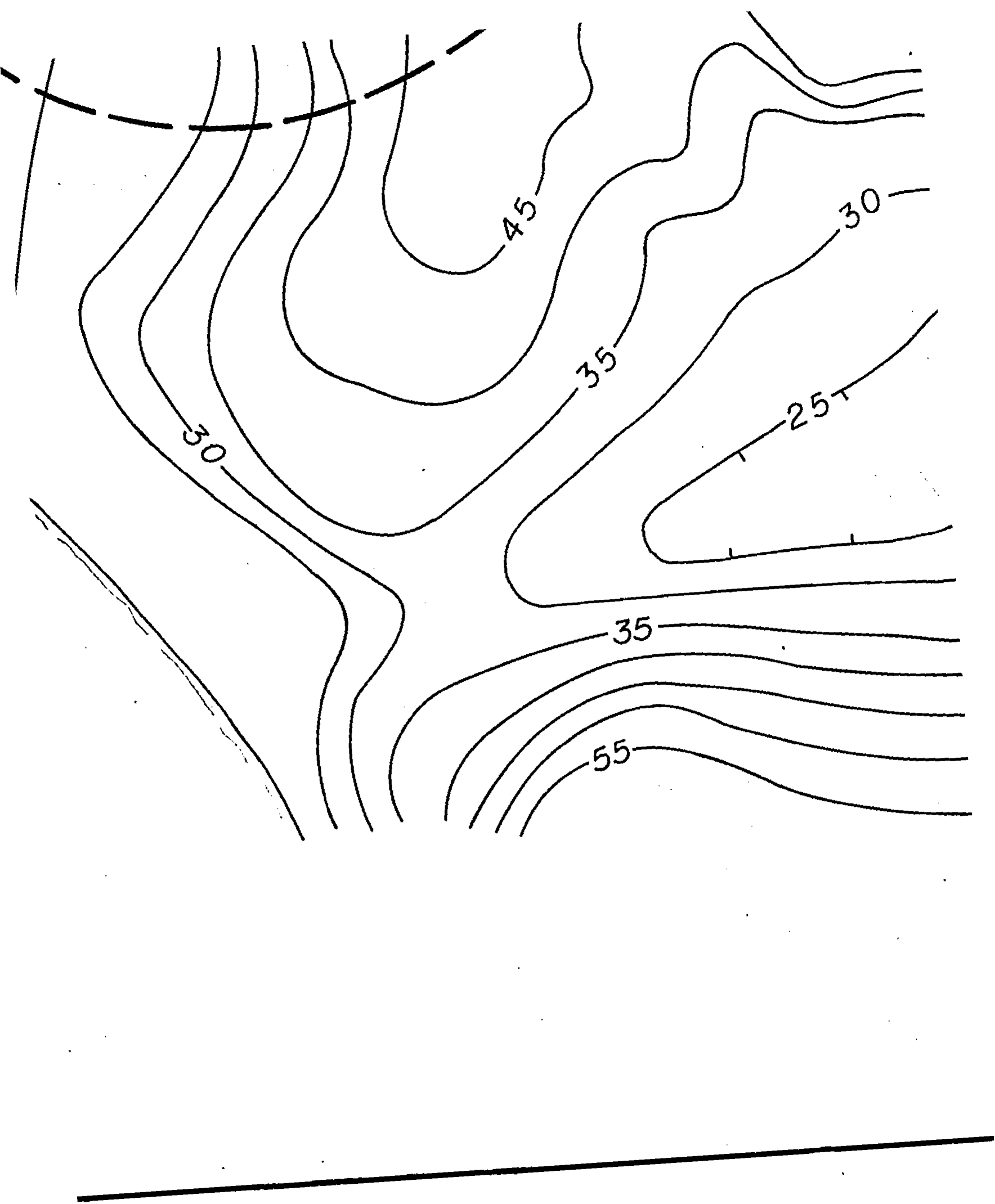
0 200 FT



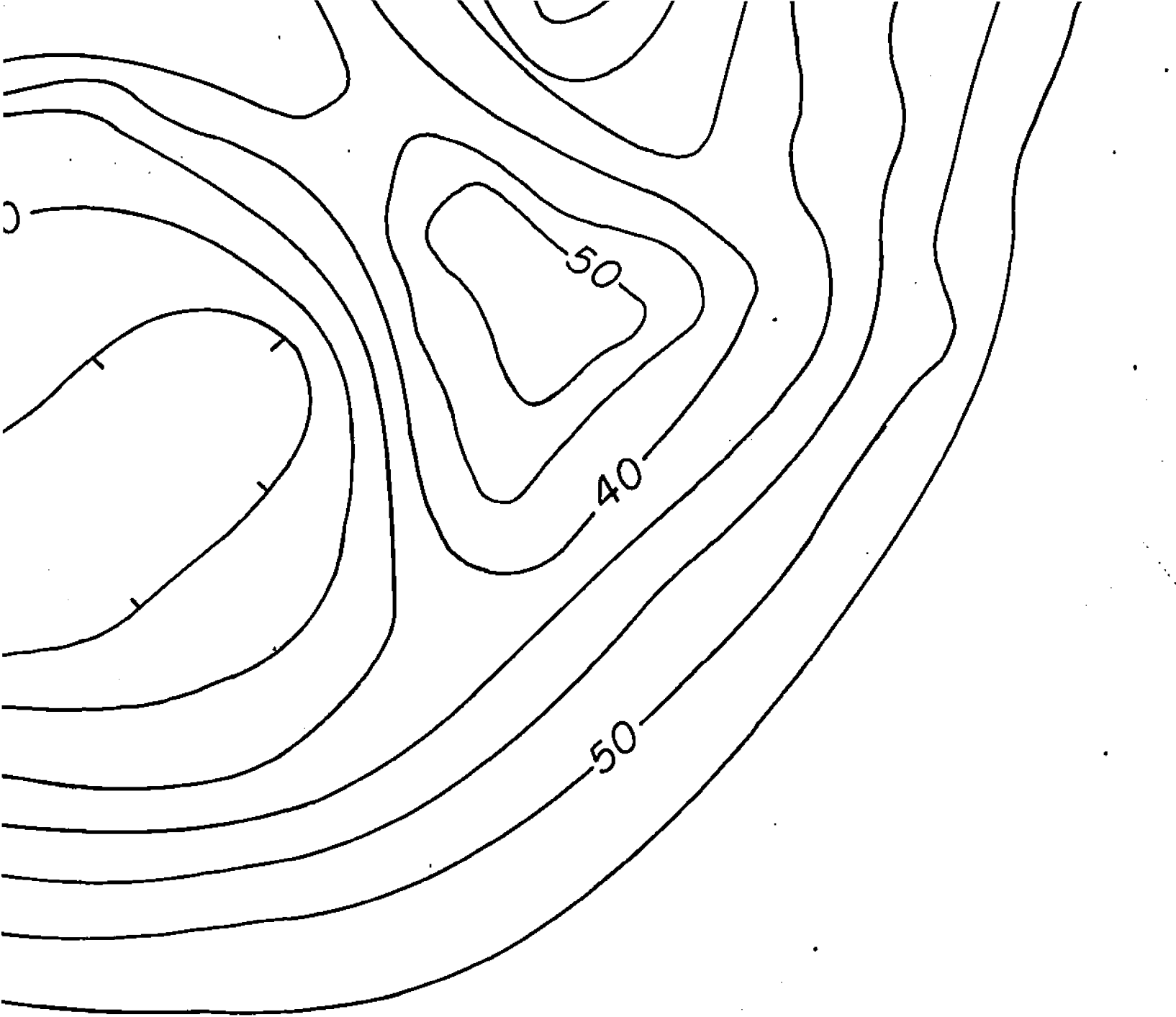
J. M. KING, 1983

A hand-drawn map of a river system. The river is depicted with two parallel lines, one solid and one dashed, representing the banks. The river flows from the top right towards the bottom left. In the center of the river, the word "RIVER" is written in a simple, uppercase font. The background is white, and there are some faint, curved lines in the top right corner, possibly representing terrain or another part of the map.

RIVER







PLATE

SATURATED

AT THE FLAMB

CONTOUR INT.  
= 5 FT

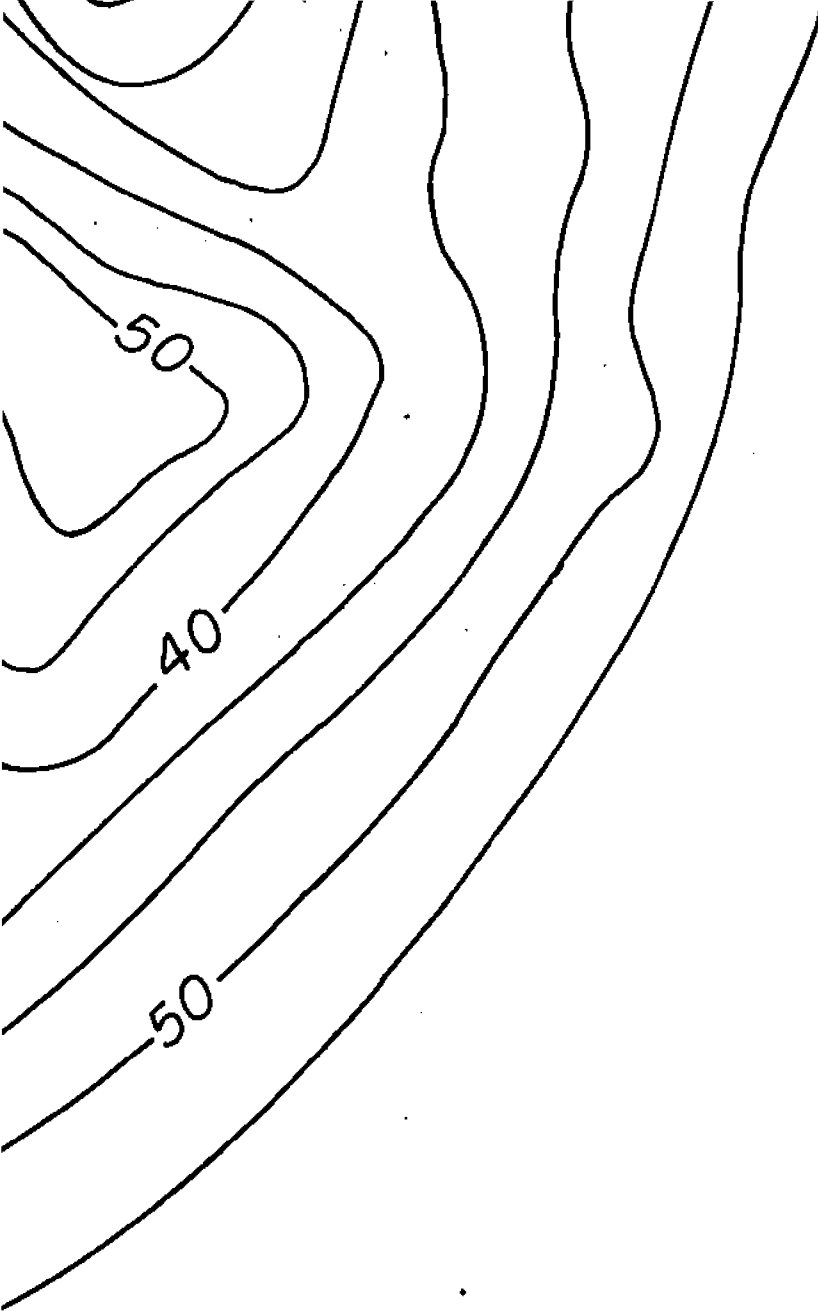


PLATE 6

SATURATED THICKNESS  
AT THE FLAMBEAU MINE  
CONTOUR INTERVAL  
= 5 FT